PREPARATION, CHARACTERISATION AND PROPERTIES OF THERMALLY-RESPONSIVE COPOLYMERS AND EMULSIONS

A Thesis Submitted Towards the Degree of

Doctor of Philosophy

by

Andrew Yew Chiang Koh

B.Sc. (Hons)

THE UNIVERSITY
OF ADELAIDE
AUSTRALIA

School of Chemistry and Physics

May 2003

TABLE OF CONTENTS

ABSTRACT

A number of poly(NIPAM-*co*-PEGMA) copolymers from different synthesis routes and varying molecular architectures were synthesised by free radical polymerisation of NIPAM (N-isopropylacrylamide) with PEGMA (polyethylene glycol methacrylate). Gel permeation chromatography (GPC) data indicated that the copolymers were polydisperse. This was attributed to the method of copolymerisation employed. Viscosity data showed that the onset of chain entanglement, c_p^*, for the copolymer was *ca.* 1 wt%. Turbidity measurements revealed that the lower critical solution temperature (LCST) for the copolymers is higher than that for poly(NIPAM). The monomer reactivity ratios were estimated at low conversions (*ca.* 5%) by using ^1H nuclear magnetic resonance (NMR) spectroscopy. By means of the Lewis-Mayo method, these values were estimated to be 1.05 and 0.63 for NIPAM and PEGMA, respectively.

Small-angle neutron scattering (SANS) data showed that the scattering profiles of the poly(NIPAM-*co*-PEGMA) copolymer in D_2O were temperature-dependent. At 25°C, the chains comprised of individual coils having a radius of gyration, R_g, of 8 nm and rods with a radius of 1 nm. At 36°C, aggregation of the coils led to the formation of copolymer micelles with an aggregate R_g of *ca.* 17 nm. Porod scattering was observed at 50°C and was attributed to the emergence of NIPAM-rich particles. The radius of the particles was estimated to 60 nm. Gaussian coils that were rich in PEGMA connected the particles through a diffuse shell. Particle precipitation caused further aggregation of the coils and R_g increased to 26 nm.

The copolymer prepared from the NIPAM-feed method and containing 86 mol% NIPAM was found to yield emulsions with optimum stability, whilst exhibiting thermally-induced gelation behaviour. The large droplet size of *ca.* 10 μm was comparable to related data reported

in the literature for emulsions stabilised with polymeric surfactants. Above 45°C, the viscosity of the emulsions increased dramatically. Visual inspection revealed gelation at these temperatures. This behaviour was reversible, in that cooling resulted in the gelled emulsion being able to flow again. Preliminary gelation studies showed that gelation occurred for emulsions containing volume fraction of oil, ϕ_o, higher than 0.1 and polymer concentration, c_p, greater than 1 wt%.

Steady shear rheological data indicated that the gelation concentration, c_{gel}, for the copolymer solutions was *ca.* 10 wt%. At 25°C, the samples behaved as viscous liquids, but became more elastic as temperature was increased. In the case of the emulsions, the dispersed phase droplets appeared to have the same qualitative effect on the rheological properties as a substantial increase in the copolymer concentration. Analysis of the oscillatory shear data using the Winter-Chambon gel point criteria indicated that samples containing ϕ_o = 0.3 and 0.5 had gelled above 50°C. No gelation behaviour was observed for the ϕ_o = 0 sample. Similar results were obtained when the copolymer concentration in the emulsions was varied. At 50°C, the elastic modulus for the 3.5 and 10 wt% samples were effectively independent of the frequency, indicating that the emulsions have gelled. In contrast, the emulsion containing 0.1 wt% copolymer showed no gelation behaviour. Heating/cooling cycles indicated that the rheological properties of the emulsions were not significantly affected by temperature-induced gelation.

A mechanism for temperature-induced gelation was proposed based on the data obtained. Above the LCST of the copolymer, bridging flocculation occurs due to the attractive nature of inter-chain interactions. The copolymer chains at one droplet surface may attach to other chains which are adsorbed on a second droplet. Gelation results when a critical concentration of oil droplets is exceeded which allows formation of the network, or a high enough copolymer concentration is present which spans the entire system. The oil droplets act as anchoring sites for

the copolymer and increase the number density of network links. Only copolymer adsorbed at the droplet surface need be involved in formation of the connected droplet network and gelation.

AUTHOR'S DECLARATION

This work contains no material which has been accepted for the award of any other degree or diploma in any university or other tertiary institution and, to the best of my knowledge and belief, contains no material previously published or written by another person, except where due reference is made in the thesis.

I give consent to this copy of my thesis, when deposited in the University Library, being available for loan and photocopying.

Andrew Yew Chiang Koh

School of Chemistry and Physics

The University of Adelaide

May, 2003

ACKNOWLEDGEMENTS

I would like to express my gratitude to my supervisor, Dr. Brian Saunders, for giving me the opportunity to be involved in this project with many challenges. Through this work, I have learned many indispensable pieces of knowledge of modern science. I am indebted to his scientific guidance and encouragement, which he has endlessly provided.

I am grateful to Dr. Clive Prestidge and Dr. Igor Ametov, at the Ian Wark Research Institute, University of South Australia, for their help and discussions, with regard to the rheological studies.

The author is grateful for the expertise and help of Dr. Stephen King at the ISIS facility, Rutherford Appleton Laboratory, Didcot, United Kingdom, in setting up the equipment to carry out the SANS experiments. Dr. Richard Heenan is thanked for his help with the FISH fitting and helpful discussions regarding the analysis of the SANS data.

I also wish to thank Dulux Australia for providing the GPC data.

There are several people at the University of Adelaide whose support and encouragement made this work possible. Dr. Louis Rendina is thanked for his help. The School of Chemistry and Physics is acknowledged for access to materials and equipments. I would like to thank Michael Shields and Emma Daly for creating a pleasant and innovative working environment in the laboratory.

I would like to thank the University of Adelaide for awarding me with an Overseas Postgraduate Research Scholarship.

Finally, warmest thanks I wish to owe to my parents and my friends, especially Shuk Yee, for standing by me through happy as well as miserable moments.

ABBREVIATIONS AND SYMBOLS

a	droplet radius
A_{11}	Hamaker constant of the dispersed phase
A_{22}	Hamaker constant of the continuous phase
A_{eff}	effective Hamaker constant
A_B	peak intensity of the methine protons of the isopropyl group and the oxyethylene protons closest to the carbonyl group at δ 4.0 ppm
A_c	consistency factor
A_C	peak intensity of the oxyethylene protons at δ 3.7 ppm
B_{inc}	incoherent background signal
c_{gel}	gelation concentration
c_l	concentration of liquid
c_p	concentration of polymer
c_p^*	critical overlap concentration of polymer
C	number of carbons of the hydrophobic segment of a surfactant
d_i	droplet diameter
d_h	hydrodynamic diameter
d_v	volume average diameter
$d\gamma/dt$	shear rate
D_0	Stokes-Einstein diffusion coefficient
E	number of EO units of a surfactant
f	applied frequency
f_x	mole fraction of monomer in reaction mixture
F_x	mole fraction of monomer in copolymer
g	acceleration due to gravity
G	shear modulus
G'	elastic modulus
G"	viscous modulus
h	Planck's constant
H	droplet separation

$I(q)$	differential scattering cross-section
k	Boltzman's constant
m	number of NIPAM segments per n
m_r	relative refractive index
M	molar mass
M_n	number average molecular mass
M_w	weight average molecular mass
n	number of PEGMA or MPEGMA segments
n_{pl}	power law index
N_A	Avogadro's number
PD	polydispersity
$P(q)$	form factor
q	scattering vector
R	gas constant
R_g	radius of gyration
R'	terminal group of EO unit
R^2	correlation coefficient
$S(q)$	interparticle factor
t	time
T	temperature
T_{gel}	gelation temperature
V_{tot}	total interaction energy
V_A	London dispersion interaction energy
V_A^c	critical attractive energy for flocculation to occur
V_R	repulsive interaction
V_S	steric interaction

Greek Symbols

χ	Flory-Huggins polymer-solvent interaction parameter
δ	chemical shift
δ_a	adsorbed layer thickness

δ_h	hydrodynamic thickness
δ_i	interfacial layer thickness
δ_m	minimum layer thickness required to keep droplets from flocculating
δ_p	phase difference in radians between the peak value of the stress and the peak value of the strain
ε	permittivity
ϕ	volume fraction
ϕ_{eff}	effective volume fraction
ϕ_i	volume fraction of droplets
ϕ_o	volume fraction of oil
ϕ_p	volume fraction of polymer
γ	strain
γ_{12}	interfacial tension between two liquids
η	viscosity of medium
η_{inh}	inherent viscosity
η_{red}	reduced viscosity
η_p	viscosity of polymer
η_l	viscosity of liquid
$[\eta]$	intrinsic viscosity
λ	wavelength
θ	fractional conversion
θ_s	scattering angle
ρ	density
σ	shear stress
τ	turbidity
ω_a	radial frequency
ζ	zeta

Abbreviations

AAc	acrylic acid
AIBN	2,2'-azobisisobutyronitrile

cmc	critical micelle concentration
DLVO	Deryagin, Landau, Verwey and Overbeek
EO	ethylene oxide
GPC	gel permeation chromatography
HEUR	hydrophobically modified urethane-ethoxylate
HLB	hydrophilic-lipophilic balance
Hz	hertz
LCST	lower critical solution temperature
mol%	mole percent
MPEGMA	polyethylene glycol methyl ether methacrylate
NMR	nuclear magnetic resonance
NIPAM	N-isopropylacrylamide
OD	optical density
O/W	oil-in-water
ppm	parts per million
PAANa	poly(sodium acrylate)
PCS	photon correlation spectroscopy
PD	polydispersity
PDMS	poly(dimethylsiloxane)
PEG	polyethylene glycol
PEGMA	polyethylene glycol methacrylate
PEO	polyethylene oxide
PMMA	polymethacrylic acid
PPO	polypropylene
SANS	small-angle neutron scattering
SDS	sodium dodecyl sulphate
t-OH	*tert*-butyl alcohol
TEMED	N, N, N', N'-tetramethylethylenediamine
THF	tetrahydrofuran
wt%	weight percent
W/O	water-in-oil

CHAPTER 1 INTRODUCTION

1.1 Polymers

A polymer is defined as a substance composed of long covalently-bonded molecules.[1] Polymers synthesised in the laboratory are made by reacting monomers under controlled conditions. Thus, monomers are the structural units that form polymers. When a single monomer type is concerned (*e.g.*, ethylene), the result is a homopolymer [*e.g.*, poly(ethylene)]. More complex polymers require two (or more) monomer types and are generally known as copolymers.

From the usage of natural polymeric materials, such as wood and horn, used by humans during prehistoric times to the large number of discoveries in the nineteenth century and more recently the advancement of current research in polymer science, polymers play a major role in our everyday lives. In 1839, Charles Goodyear showed that by heating natural rubber with sulphur, not only would the elastic properties of rubber be improved, but also its tackiness eliminated. The first fully synthetic polymer to be commercialised started in 1910 from Leo Baekeland's Bakelite phenol-formaldehyde resins. During this time numerous research was done to try and understand the physical and chemical properties of polymers. From his studies of the synthesis, structure and properties of poly(oxymethylene) and poly(styrene), Hermann Staudinger coined the word "macromolecule" to describe polymers. Improved understanding of polymer science and global demand have led to increased production of synthetic polymers [*e.g.*, nylon, poly(methyl methacrylate) and poly(vinyl chloride)] for commercial purposes over the years. For example, the total production of low-density poly(ethylene) and thermoset resins in the USA has tripled and doubled, respectively from 1969 to 1996.[2]

The large size of polymer molecules allows the accumulation of secondary intermolecular forces, which imparts strength and mechanical properties to the bulk materials. For example, above a certain concentration the formation of macromolecular associations between water-soluble polymer chains lead to thickening of the aqueous solution.[3] Polymers are widely used in many fields, including food, pharmaceutical and food emulsions, agriculture (*e.g.*, water treatment, soil stability, coal washing and oil recovery), ceramics, paper and ink technology, explosives and the textile industry. In most cases, these polymers are employed as stabilisers.[4]

For polymerisation to occur the monomer in question must be able to link between two (or more) other monomers by chemical reactions. In other words, a monomer must be bifunctional (or higher) through which each bonding site can be linked to other monomers to build the polymer chain.[5] This simple requirement allows different chemical reactions between monomers to occur during the polymerisation process.

1.1.1 Copolymers

Copolymers usually form when more than one monomer type is present in the polymerisation process. When only one type of monomer is present in the polymerisation reaction, the product is called a homopolymer. There are several types of copolymers, each depending on how the monomer units are arranged along the polymer chain (Table 1.1).

Random copolymers are copolymers in which the distribution of the two monomers in the polymer chain is essentially random, but influenced by the individual monomer reactivity ratio (later). On the other hand, alternating copolymers have the different monomers alternating

with one another along the polymer chain. The properties of these copolymers are somewhere in between to those of the corresponding homopolymers.

Block copolymers are made up of sequences or blocks of the same monomer type; effectively two homopolymer chains are joined together by a chemical linkage. Although block copolymers usually display properties characteristic of each of the constituent homopolymers, the chemical linkage prevents the homopolymer sequences from functioning independently of each other.

Table 1.1: Nomenclatures used for copolymers

Chain Structure	Copolymer Type	Nomenclature
-ABBABABABBBAB-	Random	Poly(A-*co*-B)
-ABABABABABABA-	Alternating	Poly(A-*alt*-B)
-AAAAAAABBBBBB-	Block	Poly(A-*b*-B)
-AAAAAAAAAAAAA- B B B B B B B B B B	Graft/comb	Poly(A-*g*-B)

In their simplest form graft copolymers are made up of homopolymer chains connected to a different homopolymer chain as side chains (Table 1.1). The side chains have different chemical structure to those of the main chain. Graft copolymers can be viewed as comb-like branched copolymers (since the side chains are typically shorter than the backbone) and are distinctly different to branched polymers, where the branches are the same as the main chain. Like block copolymers, graft copolymers usually display properties characteristic of each of the

constituent homopolymers. In the case where the main chain and the backbone are thermodynamically incompatible, the systems will be multiphase in the solid state. In solution, *e.g.*, when used to stabilise emulsions, the more hydrophobic segment will adsorb to the organic phase and the more hydrophilic part resides in the aqueous phase.

1.1.2 Polymer Synthesis

Two general types of chemical processes are available for the incorporation of monomers into a polymeric chain. These are referred to as step and chain polymerisations.[1] In step polymerisations, polymer chains are formed by the step-wise intermolecular condensation or addition of the reactive groups. Condensation reactions involve the elimination of a small molecule in the course of creating the new chemical bond. Reactions between monomer molecules and the reactive end of the growing polymer chain are the chemical features of chain polymerisation; the most common involves free radicals. Although the monomer concentration remains constant throughout the reaction, high degrees of polymerisation are achieved at low monomer conversions in chain polymerisation.

Free-radical polymerisation involves the growth of each polymer molecule by addition of a monomer to a terminal (or active) site. It is in fact a chain reaction; the polymer chain can be viewed as a growing entity. The reaction can be divided into three distinct stages: initiation, propagation and termination (Figure 1.1).

(a) Initiation

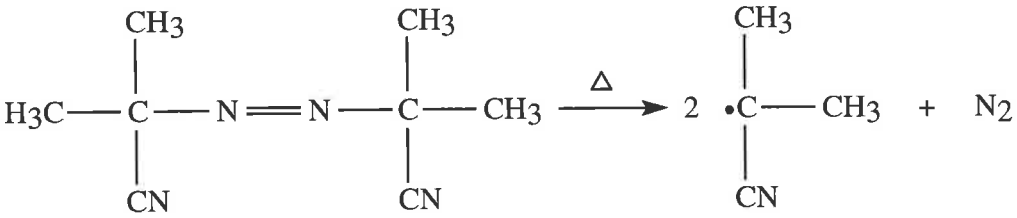

AIBN

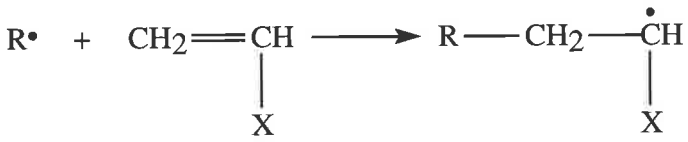

(b) Propagation

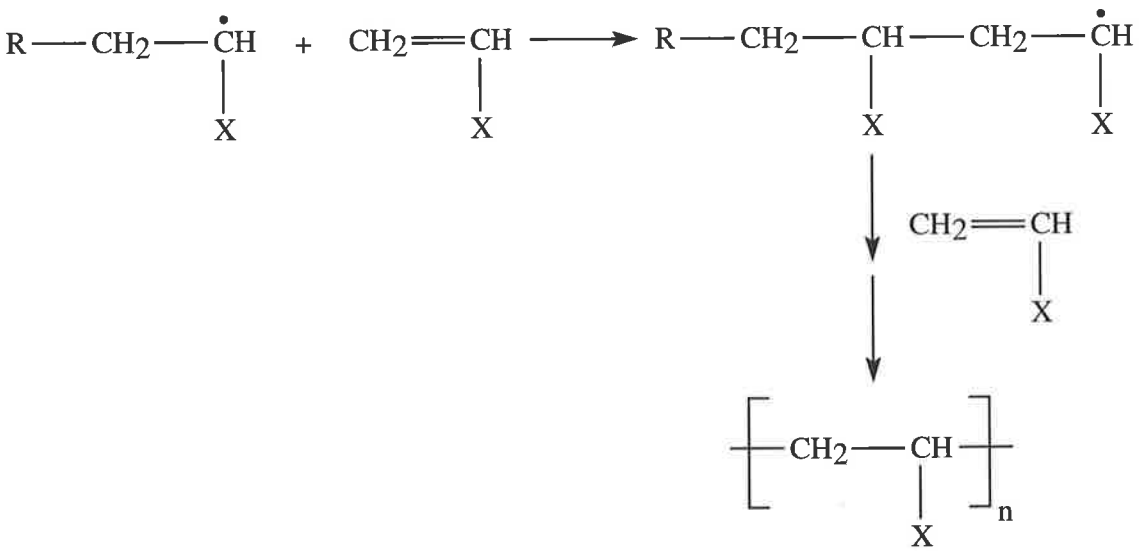

(c) Termination

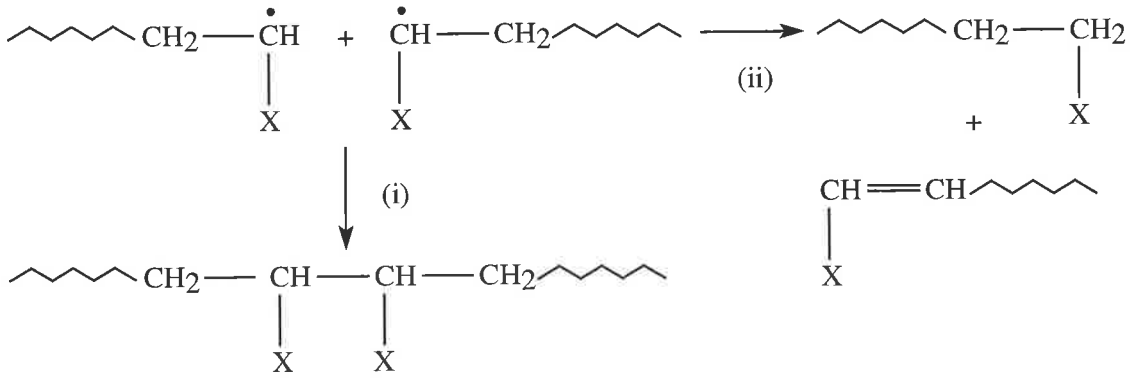

Figure 1.1: The three major steps in a free-radical polymerisation reaction; (a) initiation, (b) propagation and (c) termination. AIBN and R$^{\cdot}$ are the initiator and free radical, respectively. Termination mechanism involves combination (i) or disproportionation (ii).

The formation of a free-radical active centre (initiation) and occurs in two steps [Figure 1.1(a)]. The first step is the formation of free radicals from the initiator [*e.g.*, 2,2'-azobisisobutyronitrile (AIBN), benzoyl peroxide and hydrogen peroxides]. This may involve thermal decomposition, redox reactions or photo dissociation of the initiator. Initiation is completed when one of these free radicals is added to a molecule of monomer.

Chain propagation [Figure 1.1(b)] occurs rapidly by addition of monomer to the active centre to produce a linear polymer. The concentration of monomer will be high during early stages of the reaction. Thus, once a reactive site (initiation) has appeared in the system it can induce a large number of propagation reactions in a very short time. Low concentrations of initiator will give rise to fewer longer growing chains, while a high concentration will produce a large number of actively growing short chains.

Termination of the polymerisation reaction occurs in a number of ways: (i) bimolecular interactions of growing polymer chains; (ii) transfer of the active centre to another molecule; (iii) interaction with impurities or inhibitors. The most common mechanism of termination involving reaction between neighbouring chains is the first. Two routes are possible [Figure 1.1(c)]. Combination concerns two chains adding together at the radical ends to form a single long chain, while the abstraction of hydrogen from one end to produce two polymer chains (one containing a saturated group and the other without an unsaturated group) is known as disproportionation.

1.1.3 Copolymerisation

The polymerisation of two (or more) structurally different monomer types into the same polymer chain is known as copolymerisation. As mentioned before, these copolymers usually display better qualities compared to the parent homopolymers. In most cases, the reactivity of the monomers are different. This causes the sequence distribution of the repeat unit in the polymer chain to vary as the polymerisation progresses.

The composition of copolymers formed at a particular instance in time during polymerisation can be determined by using the terminal model. The rate constant for addition of each monomer to the growing chain is assumed to be dependent only upon the identity of the terminal monomer unit on which it is located. Thus, four propagation rate constants are required:[1]

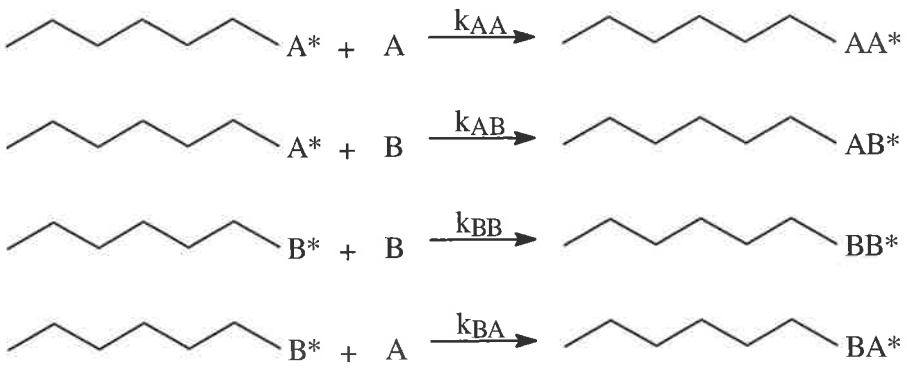

where A and B are the monomers and the asterisk represents the active centre (*e.g.*, an unpaired electron for free-radical polymerisation). Note that k_{AA} and k_{BB} are the rate constants for the homopropagation reactions, while k_{AB} and k_{BA} are the corresponding cross-propagation rate constants. According to this model the rates of monomer consumption are given by:[1]

$$-\frac{d[A]}{dt} = k_{AA}[A^*][A] + k_{BA}[B^*][A] \tag{1.1}$$

$$-\frac{d[B]}{dt} = k_{BB}[B^*][B] + k_{AB}[A^*][B] \tag{1.2}$$

where [A*] and [B*] are the total concentrations of propagating chains with terminal A-type and B-type active centres, respectively. Dividing Equation (1.2) into (1.1) and applying steady-state conditions to [A*] and [B*], *i.e.*, the rate of initiation equals the rate of termination, an expression for copolymer composition is obtained:

$$\frac{d[A]}{d[B]} = \frac{[A]}{[B]}\left(\frac{r_A[A]+[B]}{[A]+r_B[B]}\right) \tag{1.3}$$

where r_A and r_B are the respective monomer reactivity ratios. These are defined as:

$$r_A = \frac{k_{AA}}{k_{AB}} \quad \text{and} \quad r_B = \frac{k_{BB}}{k_{BA}} \tag{1.4}$$

Thus, the reactivity ratio is the ratio of the reactivity of the propagating species with its own monomer to the reactivity of the propagating species with the other monomer. Equation (1.3) gives the molar ratio of the A-type to B-type repeat units in the copolymer at any instance during the copolymerisation.

Usually the compositions are expressed as mole fractions. The mole fraction, f_A, of monomer A in the comonomer mixture of A and B is [A]/([A] + [B]) and that of monomer B is $f_B = 1 - f_A$. The mole fraction, F_A, of A-type repeat units in the copolymer formed at a particular instant in time is d[A]/(d[A] + d[B]) and that of B-type repeat units is $F_B = 1 - F_A$. Addition of unity to both sides of Equation (1.3) allows the Lewis-Mayo equation to be obtained:[6]

$$F_A = \frac{r_A f_A^{\,2} + f_A f_B}{r_A f_A^{\,2} + 2 f_A f_B + r_B f_B^{\,2}} \tag{1.5}$$

$$F_B = \frac{r_B f_B^{\,2} + f_A f_B}{r_A f_A^{\,2} + 2 f_A f_B + r_B f_B^{\,2}} \tag{1.6}$$

Equation (1.5) can be rearranged to give:[1]

$$Y = r_B + X r_A \tag{1.7}$$

where

$$X = \frac{f_A^{\,2}(F_A - 1)}{F_A(1 - f_A)^2} \quad \text{and} \quad Y = \frac{f_A(1 - 2F_A)}{F_A(1 - f_A)} \tag{1.8}$$

The dependence for several combinations of reactivity ratios that illustrate copolymerisations is shown in Figure 1.2. The probability of reaction for a particular monomer depends only on its more fraction when $r_A = r_B = 1$ [curve (a)]. Under these conditions, random copolymers are formed. When $r_A r_B = 1$, the copolymerisation is ideal since the relative rates at which the two monomers add into the growing chains are the same for both types of active centre. When $r_A = r_B = 0$, alternating copolymers of 1 : 1 composition are formed regardless of the feed composition [curve (b)]. When both r_A and r_B are less than or greater than 1, azeotropic copolymerisation occurs [curve (c)]. In most cases where the monomer reactivity is different, *e.g.*, $r_A > 1$, $r_B < 1$ (or vice versa) with $r_A r_B \neq 1$, there will be slight variation from ideal copolymerisation, with the curve moving towards copolymer compositions having more of the repeat units derived from the more reactive monomer [curve (d)].

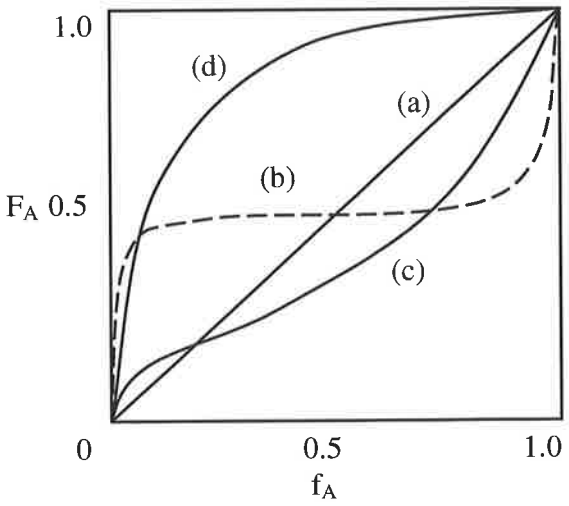

Figure 1.2: Copolymer composition, F_A, as a function of comonomer composition, f_A, for various reactivity ratio combinations; (a) $r_A = r_B = 1$, (b) $r_A = r_B = 0$, (c) $r_A < 1$, $r_B < 1$ and (d) $r_A > 1$, $r_B < 1$.[1]

It can be seen from Equation (1.5) that the copolymer composition is also governed by the comonomer composition in the feed. The more reactive monomer reacts preferentially and so is incorporated into the growing chain formed early in the reaction in a higher proportion than its initial mole fraction in the reaction mixture (*i.e.*, $F_A > f_A$ during early stages of the reaction). Since the concentration of the monomer changes as the reaction progresses, the composition of the copolymer will also vary with conversion. This results in a phenomenon known as copolymer composition drift and leads to the copolymer having a range of compositions. As the concentration of the more reactive monomer diminishes, the instantaneous composition of the growing chains becomes richer in the less reactive monomer.

1.1.4 Polymers in Solution

In order to obtain an improved understanding of polymer properties (*e.g.*, changes in physical and chemical properties of polymers when solution temperature is altered), characterisation and physical measurements of polymers are essential. Since most of these methods concern with polymers in dilute environment, the thermodynamics of polymers in solution will be discussed.

For polymers to mix with liquids, *i.e.*, for a polymer solution to form, under constant pressure, P, and temperature, T, the Gibbs free energy change of mixing, ΔG_m, must be negative in Equation (1.9):[1]

$$\Delta G_m = \Delta H_m - T\Delta S_m \tag{1.9}$$

where ΔH_m is the enthalpy of mixing and ΔS_m is the entropy of mixing.

1.1.4.1 Flory-Huggins Theory

The Flory-Huggins theory, which is based on a simple cubic lattice model, was introduced to predict the behaviour of polymers in solution (through ΔG_m). The entropy is calculated from the number of solvent-segment interactions, while the difference in interaction energy between the various combinations of polymer segments and solvent gives the enthalpy.

When using this theory a number of constrains need to be considered. These are as follow. Every lattice site must contain either a solvent molecule or a polymer segment and random mixing between solvent molecules and polymer segments occurs. In addition, solvent molecules and polymer segments will have the same size and shape. The probability that a site contains a solvent molecule is the solvent volume fraction. Finally, the polymer segment must form a chain on the lattice.

The Flory-Huggins polymer-solvent interaction parameter, χ, was introduced to identify polymer-solvent interactions. It can be expressed in the form:[1]

$$\chi = a_{FH} + \frac{b_{FH}}{T} \tag{1.10}$$

where a_{FH} and b_{FH} are temperature-independent quantities. The Flory-Huggins interaction parameter may be viewed as the sum of enthalpy, χ_H, and entropy, χ_S, components:

$$\chi = \chi_H + \chi_S \tag{1.11}$$

Note that χ is usually a measure of the solvent power.[5] As χ decreases, the solubility of the polymer increases (*i.e.*, good solvent), while increasing χ decreases polymer solubility (*i.e.*, bad

solvent). In the case of polymer solutions, $\chi > 0.5$ and < 0.5 results in poor and good solvency conditions, respectively. When $\chi = 0.5$, the polymer solution is in an ideal state (*i.e.*, in theta solvent).

Whilst the Flory-Huggins theory adequately describes the thermodynamic properties of polymer solutions, there are a few limitations to it. For example, it was assumed that on passing from the solid state into the solution, the flexibility of the polymer chains remains the same. This entropy change, which opposes the mixing of polymer and solvent, is not accounted for by the theory. Note that χ is found experimentally to depend upon the polymer concentration. Although the theory predicts that mixing should be favoured as temperature increases (since it is an entropically driven process), it has been found that many aqueous polymer solutions undergo phase separation as the temperature is increased to near the critical (or theta) point of the solvent. This phenomenon is associated with hydrogen bonds between hydrophilic portion of the polymer and water (later). The theory did not consider hydrogen bonds between solvent molecules.

1.1.4.2 Chain Conformation

In dilute solutions, the polymer chains have large number of degrees of freedom. The excess of space for the chains compared to the excluded volume allows the chains to take up some coil-like conformation. As the concentration increases, there comes a point where the volume of the coils just occupies the total volume of the system. The solution is considered semi-dilute at this stage. The concentration of polymer, c_p, at which this occurs is known as the critical overlap concentration and is denoted by c_p^*. Note that c_p^* represents the critical concentration at which the polymer chains begin to overlap. As the concentration increases even further, interactions between polymer chains begin to dominate, *e.g.*, chain overlap and entanglement, as

opposed to intramolecular interactions which start to diminish. The solution is known as concentrated when the local polymer concentration is representative of the system.[7] The concentration at which this occurs is denoted by c_p^{**}.

Clearly, the nature of the interactions between polymer and the solvent will affect the conformation the polymer chains adopt in solution. The radius of gyration, R_g, defined as the average distance of the segments from the centre of mass for a large number of polymer molecules, which is given by:[7]

$$R_g = \frac{I\sqrt{N}}{\sqrt{6}} \tag{1.12}$$

for a polymer containing N segments of length I, allows characterisation of polymer coils. For polymer in a good solvent, *i.e.*, the chains have a greater affinity for the solvent than itself, the chains will adopt a self-avoiding walk where:[8]

$$R_g \propto N^{0.6} \tag{1.13}$$

1.1.4.3 Phase Separation Behaviour

In most cases, increase in thermal energy on heating allows the solubility of the system in water to increase. However, a number of polymers in aqueous solution display the opposite behaviour. As the temperature increases beyond a certain point, commonly referred to as the lower critical solution temperature (LCST) or the phase transition temperature, the polymer chains collapse. Below the LCST the polymer is soluble in water; the chains are extended and surrounded by water molecules. But above the LCST, the polymer becomes insoluble and phase

separation occurs (Figure 1.3). Examples of polymers which undergo this type of phase transition include poly(N-isopropylacrylamide) [poly(NIPAM)] and other N-substituted acrylamides, poly(ethylene oxide) (PEO), poly(vinylmethylether) (PVME) and poly(2-ethyl oxazoline).[9,10]

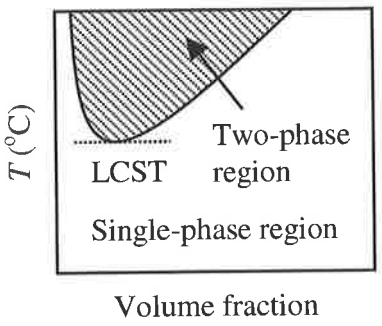

Figure 1.3: The two-phase region, characterised by the lower critical solution temperature (LCST), and a single-phase region across the temperature range are chemical features usually found in aqueous polymer solutions characterised by strong hydrogen bonds.

The transition from hydrophilic, *i.e.*, when the polymer is dissolved, to hydrophobic, *i.e.*, when the polymer chains collapse, above the LCST can be explained in terms of the thermodynamics of the polymer solution. At room temperature, mixing occurs due to the increased space available to the solvent molecules when polymer segments become accessible to the solvent. On heating, the free volume of the solvent increases leading to separation of the solvent molecules since covalent bonding constrains are absent. In contrast, the relatively small increase in free volume of the polymer is due to the presence of covalent bonds between polymer segments. At temperatures close to the LCST, the hydrogen bond formation between solvent molecules and polymer segments decreases the entropy of the system. When this decrease in

entropy is sufficiently large, mixing becomes thermodynamically unfavourable. At high temperatures, the free energy of mixing [ΔG_m in Equation (1.9)] becomes positive and phase separation takes place. In most cases, the replacement of polymer-water interactions with polymer-polymer and water-water interactions is exhibited by polymer precipitation.[11]

1.1.5 Polymers at Interfaces

The adsorption of homopolymers to a particular substrate is influenced by solvent type, hydrophilicity/hydrophobicity of the polymer and nature of the surface. In addition, van der Waals forces, dipolar forces or hydrogen bonds are possible between solid substrates and polymer chains. Copolymers tend to adsorb at the interface between two immiscible solvent phases (*e.g.*, emulsions) since it is more energetically favourable than complete dissolution in either phase. This is a consequence of the fact that copolymers used to stabilise emulsions are usually made up of hydrophilic and hydrophobic segments. The former tends to immerse itself in the aqueous/polar phase, while the latter preferentially dissolve in the organic/non-polar phase. In addition, the adsorbed amount of copolymers depends on its primary structure. For instance, for a block copolymer, the hydrophobic portion (usually the backbone) usually adsorbs on the surface (the 'anchor') while the hydrophilic segment extends away from the surface ('the buoy').

Segments of adsorbed polymer are classified into three types (Figure 1.4). Those constrained to the surface are known as 'trains' and these trains are connected together by 'loops' that have no contacts with the surface. 'Tails' are the segments at the end of the attached polymer and are usually extended into the bulk of the solution.

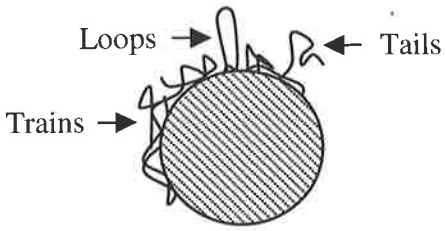

Figure 1.4: The tails, loops and trains model for polymer adsorption.

From Figure 1.4 it is clear that an adsorbing polymer does not usually produce a uniform layer, but gives rise to an inhomogeneous profile. Thus, any experimental method to estimate the thickness of the adsorbed layer provides some average where the contribution of different segments may vary. For instance, photon correlation spectroscopy (PCS) calculates the hydrodynamic thickness, δ_h, which is mainly determined by the tails of the adsorbed polymer.

The relationship between polymer structure and polymer solutions that exhibit phase separation behaviour above the LCST was pioneered by de Gennes and co-workers[12] using the concept of 'n-cluster'. They postulated that as temperature increases, the solvent quality for these interfacial polymer chains progressively worsens, leading to the formation of intramolecular clusters of hydrophobic segments, analogous to micelle formation in surfactants above the critical micelle concentration. This is a consequence of the fact that polymer at the interface can be considered to have two distinct layers; an inner dense and an outer dilute layer. The interactions between polymer segments in the outer layer are repulsive while attractive interactions dominate within the inner layer, *i.e.*, formation of n-clusters. This gives rise to the polymers collapsing at temperatures below the LCST of equivalent polymer chains in solution. The n-cluster theory has been utilised by Zhu and Napper[13] to explain the collapse (and swelling) of poly(NIPAM) chains at latex interfaces in aqueous alcohol solutions.

1.1.6 Thermothickening Behaviour

In Section 1.1.4.2 it was mentioned that above c_p^* polymer chains start to overlap and entangle with one another, resulting in viscosity enhancement. When an appreciable amount of polymer chains exhibits attractive interactions for segments from neighbouring chains, *e.g.*, hydrophobic attraction, the polymer solution forms physical gels. The minimum concentration at which physical gels are formed is also known as the gelation concentration, c_{gel}.[14] Note that c_{gel} is higher than c_p^* in polymer solutions. In the case of polymers that exhibit LCST behaviour at sufficiently high concentrations (and temperatures greater than the LCST), the increase in intermolecular interactions between hydrophobic segments (due to thermal disruption of hydrogen bonds), leads to the formation of transient network. This network consists of collapsed hydrophobic clusters inter-connected by soluble chains. This phenomenon is also known as temperature-induced gelation or thermothickening.

For thermothickening to occur, polymers must posses a temperature sensitive segment which exhibits phase transition behaviour. A hydrophilic segment which stabilises the aggregates upon collapse of the hydrophobic segments to prevent phase separation of the polymer from solution should be present. In addition, the polymer must contain a structure that will permit formation of a physical network through the bridging of the elastic chains of the hydrophilic segments between the cross-links of the temperature sensitive segments.[15]

Transient network theory has been invoked to explain the qualitative features of gelation in polymers.[16,17] The theory was originally devised by Green and Tobolsky[18] and has been more recently developed by Tanaka *et al.*[19,20] This theory envisages a model network made up of polymer chains with 'sticky' end groups which can form stable aggregates. In essence these aggregates or hydrophobic clusters are junction points. The formation of a physical network (gel)

may result from inter-chain junctions, where an effective chain is created when both ends of the chain are embedded within a junction that is connected to at least two other junctions (Figure 1.5). The formation of a large network spanning the entire system results in gelation. The junction points are dynamic and are continuously forming and disappearing.

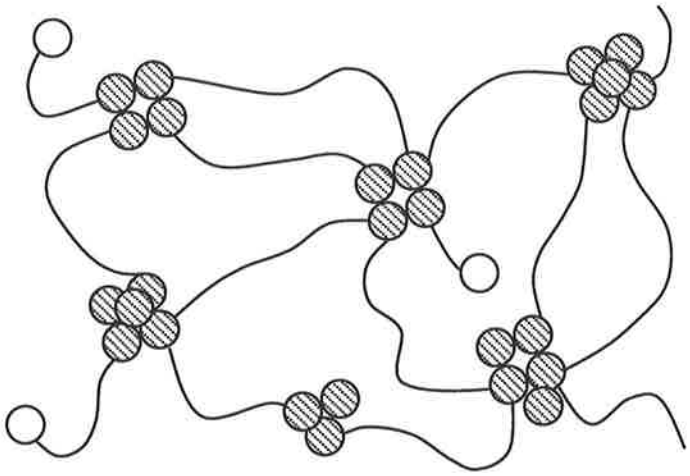

Figure 1.5: Transient network theory according to Green and Tobolsky.[18] The network is made up of polymer chains with sticky end groups (clusters of collapsed hydrophobic segments). An ineffective chain results when only one end of the chain is embedded within a junction that is connected to at least two other junctions (open circles).

The physical and chemical properties of these systems are greatly affected by the number of elastically effective chains and the average time the chain ends spend within a junction. This is shown in Equation (1.14), which describes the elastic modulus of the network, G_∞:[21]

$$G_\infty = \upsilon_{eff} kT \tag{1.14}$$

where υ_{eff} is the number of elastically effective chain in network and k is the Boltzman's constant. Note that the transient network theory has not been extended to consider thermothickening polymers. For these systems, υ_{eff} is an increasing function of temperature.

1.1.7 Responsive Polymers: A Literature Review

The solubility of many water-soluble polymers is dependent on the solution temperature. Although these polymers are soluble at room temperature, increasing or decreasing the temperature may result in phase transition. Examples include poly(acrylic acid) and poly(ethylene oxide) which phase separate upon heating and cooling, respectively.[22]

Recently, responsive polymers, *i.e.*, polymers that respond to external physical and chemical stimuli such as temperature, pH, ionic strength, solvent composition, electric field and light, have attracted attention.[16,23-29] Polymers that respond to temperature usually show temperature-dependent solubility, *i.e.*, LCST behaviour. Responsive polymers have found applications in fields such as pharmaceutics, personal care, colloid stabilisation coatings and oil recovery. The importance and potential of these polymers for commercial purposes have led to research on improving microstructural features of current responsive polymers and synthesising novel polymers to optimise the responsiveness of responsive polymers to external physical and chemical stimuli.

Virtanen and co-workers[30-32] have shown that changes in physical and chemical properties of poly(NIPAM-*g*-PEO) graft copolymers were attributed to sensitivity of the NIPAM segment to variation in temperature and polymer concentration. The functional backbone was grafted by amino-terminated PEO in water or in dioxane to yield the copolymers. According to the authors, an increase in temperature (above the LCST) caused the copolymer to form spherical

particles sterically stabilised by an outer layer of PEO. They proposed that increasing the temperature led to shrinking of the individual chains, and later, at even higher temperatures (above the LCST), the formation of aggregates. The latter was marked by increase in viscosity of the copolymer solution from viscosity measurements.

Ivanov *et al.*[3,33] also studied poly(NIPAM-*g*-PEO) copolymers and suggested that the onset of temperature-induced gelation behaviour observed for the same copolymer corresponded to the NIPAM side chains self aggregating, while the PEO backbone stabilised the NIPAM phase at the macroscopic level. They further concluded that in semi-dilute solutions, the NIPAM microdomains were connected through the highly soluble PEO chains into a physical three-dimensional network. L'Alloret *et al.*[34] in their study, investigated the temperature dependent viscosity of poly(AMPS-*g*-PEO) copolymer (AMPS is 2-acrylamido-2-methylpropane sulfonic acid) in the presence of salt. They observed a viscosity enhancement with increasing temperature and this was attributed to temperature-induced hydrophobic microdomain formation.

Polymers may undergo conformational changes or phase transitions in response to changes in aqueous solution pH. For example, poly(NIPAM-*g*-AAc) copolymers exhibits physical and chemical changes when the pH and/or temperature of the solution are varied (AAc is acrylic acid).[35-39] Chen and Hoffman[40] proposed a mechanism by which hydrogen bonding occured between the NIPAM graft chains and the AAc backbone at low pH. This lowered the cloud point (or LCST) because the polymers were more hydrophobic compared to NIPAM homopolymer. They reasoned that at high pH, hydrogen bondings were disrupted and electrostatic interaction, due to the presence of the $RCOO^-$ groups, increased the LCST. Thus, the cloud point of the polymer was higher than at lower pH.

The response to external conditions is not restricted to temperature and pH. Photochromic compounds undergo a conformational change, such as isomerisation or dimerisation, or a phase transition in response to exposure to light of an appropriate wavelength. The existence of two such states may be reversibly switched by means of an external light stimulus. The property changes of the chromophores that occur after irradiation have been utilised to induce conformational changes in polymers to which they have been bound. Recently, Porcar *et al.*[41] prepared a mixture of two polyelectrolyte surfactants. Upon irradiation of UV-visible light, the azobenzene chromophores randomly distributed along the photoresponsive polymer [poly(sodium acrylate)] changed the hydrophilic-lipophilic properties of the polymeric emulsifier.

In all cases, the conformation of the responsive polymers controls the physical and chemical properties of the solutions. When the conformation is reversibly controlled by external conditions, such as pH and temperature, the conformation change induces changes in solution properties, such as viscosity and turbidity.

1.2 Emulsions

An emulsion[42] is a heterogeneous system consisting of at least one immiscible liquid dispersed in another in the form of droplets, whose diameters exceed 0.1 μm. Microemulsions[42] are systems having droplets of diameter less than 0.1 μm. The discontinuous phase is commonly referred to as the dispersed phase, and the term continuous phase is given to the phase in which the dispersion occurs, *e.g.*, milk consists of fat droplets (the dispersed phase) dispersed in water (the continuous phase). An emulsion is usually made up of an oil and aqueous phase; if water is the continuous phase, the emulsion is termed oil-in-water (O/W) and if the oil is the continuous phase, the emulsion is termed water-in-oil (W/O). When the dispersed phase contains smaller droplets of the other liquid phase dispersed within it, multiple emulsions are formed. Many everyday examples of emulsion systems exist in foods, *e.g.*, mayonnaise, milk and margarine; cosmetics, *e.g.*, sunscreens and mosturising creams; agricultural formulations, *e.g.*, emulsifiable concentrates and in medicine, *e.g.*, drug delivery systems.[42] In drug delivery system, the release of the drug encapsulated in O/W emulsions is governed by the rate of diffusion and dissolution. This technique is also known as microencapsulation.[43]

1.2.1 Theoretical Aspects of Emulsion Formation

Since emulsions are composed of two liquid phases that are mutually insoluble (or slightly soluble), there are many ways that can be used for their preparation. However, in all cases, mechanical energy needs to be applied for the formation of droplets from the bulk liquid phases. The mechanical action deforms the interface between the two phases to such an extent that droplets form. This results in an increase in the interfacial area, ΔA. The free energy change accompanying emulsion formation, ΔG_{form}, is given by:[44]

$$\Delta G_{form} = \gamma_{12}\Delta A - T\Delta S_{config} \quad (1.15)$$

where γ_{12} is the interfacial tension between phases 1 and 2 and ΔS_{config} is the entropic contribution resulting from the increase in configurational entropy due to a large number of droplets being formed. Usually, the entropy term is negative (emulsification results in an increase in configurational entropy) and smaller in magnitude than $\gamma_{12}\Delta A$. Therefore, ΔG_{form} is positive *i.e.*, emulsion formation is thermodynamically unfavourable. It must be noted that the free energy of coalescence, ΔG_{coal}, is of equal magnitude and of opposite sign to ΔG_{form}. Hence, coalescence is thermodynamically spontaneous for emulsions.

The formation of microemulsions is thermodynamically favourable due to the very low interfacial tension accompanying it. The droplets produced are so small and the interfacial tension so low, such that the entropy term in Equation (1.15) outweighs the additional interfacial energy needed for droplet formation. Thus, ΔG_{form} is zero or negative. This is why some microemulsions are thermodynamically stable.

As mentioned above, energy needs to be supplied into the system for the formation of emulsion droplets from a bulk liquid. This deforms both the bulk interface and the droplets formed initially, which are then broken into smaller droplets. The energy needed for emulsifacation is considerably larger than $\gamma_{12}\Delta A$, since the Laplace pressure, which is the pressure difference between the concave and convex sides of a curved interface (higher in the former), opposes the deformation of droplets.[45]

1.2.2 Role of Emulsifying Agents in Emulsion Formation

The utilisation of emulsifiers in emulsion preparation not only reduces the amount of energy needed to increase ΔA during the emulsification process, by lowering the interfacial tension and hence, facilitates droplet break-up, but also make the emulsion more stable. The latter is due to adsorption of emulsifier molecules at the interface. Since a high proportion of the emulsifier molecules lie within or close to the droplet interface, the physical and chemical properties of the emulsions are governed by contributions from these emulsifier molecules in the interface region.

Surfactants are the most common type of emulsifier used in emulsification and are classified as non-ionic, anionic or cationic depending on the charge carried by the hydrophilic part of the molecule. Surfactant molecules consist of two parts with very different characteristics. One moiety is the hydrophilic or water-loving portion. The other moiety is the hydrophobic or water-hating segment and usually consists of hydrocarbon chains.

Non-ionic surfactants are characterised by the presence of a neutral polar group. An example is ethylene oxide (EO), *i.e.*, $-CH_2CH_2O-$. Ionic surfactants contain charged groups, *e.g.*, phosphates or sulphates.

Since surfactant molecules are composed of two moieties having different solubilities, they have very limited solubilities in any one solvent and tend to accumulate at the interface between two immiscible solvent phases. As the surfactant concentration increases, adsorption at the interface increases. A point is reached at which adsorption becomes even more favourable since the adsorbed molecules are able to interact laterally with one another through the interactions of their hydrophobic segments. The surfactant molecules aggregate to form micelles when dissolution through adsorption at the interface ceases. The concentration at which this

process occurs is known as the critical micelle concentration, or cmc. The physical properties of a surfactant solutions, *e.g.*, electrical conductance, surface tension, turbidity and osmotic pressure, changes abruptly at the cmc.[46]

The type of emulsion formed is influenced by the surfactant chosen, since surfactant tends to stabilise an emulsion whose continuous phase in which the surfactant is preferentially soluble. This is known as the Bancroft's rule.[47] A useful method of estimating the emulsifying properties of a surfactant, *i.e.*, the type of emulsion that will be formed, is the hydrophilic-lipophilic balance or HLB. The HLB value is a measure of the 'hydrophilicity' of a surfactant. The least hydrophilic surfactants have a low HLB number, while increasingly hydrophilic surfactants have higher HLB numbers. Table 1.2 shows the relationship between emulsion type and HLB of the surfactants.

Table 1.2: HLB ranges and applications

HLB	Application
3 - 6	W/O emulsifier
7 - 9	Wetting agents
8 - 13	O/W emulsifier
13 - 15	Detergent
15 - 18	Solubiliser

Source: Ref. 48.

The HLB value for a particular surfactant can be calculated according to the method devised by Davies:[49]

$$HLB = 7 + \Sigma \text{ (hydrophilic group numbers)} - \Sigma \text{ (hydrophobic group numbers)} \quad (1.16)$$

where the group numbers for each component are given in Table 1.3.

Table 1.3: HLB group numbers

Hydrophilic Group	HLB Number	Lipophilic Group	HLB Number
$-SO_4^-Na^+$	38.7	-CH-	
$-COO^-K^+$	21.1	$-CH_2-$	-0.475
$-COO^-Na^+$	19.1	$-CH_3-$	
-N (tertiary amine)	9.4	=CH-	
Ester (ring)	6.8	Derived group	
Ester (free)	2.4	$-(CH_2-CH_2-O)-$	0.33
-COOH	2.1	$-CH_2-CH(CH_3)-O)-$	-0.15
OH (free)	1.9		
-O-	0.5		

Source: Ref. 49.

The assumption that all EO groups make the same contribution to the hydrophilicity of the surfactant in Equation (1.16) is incorrect. Hence, the equation fails with increasing EO units. This is especially true for long chain polymeric surfactants used to prepare emulsions.[48]

Polymeric surfactants, *e.g.*, graft and block copolymer, generally display surface and interfacial properties similar to that of surfactants. This comes from the contrasting behaviour of the segments connected together in the same macromolecules, *i.e.*, they posses hydrophilic and

hydrophobic segments.[50] Emulsion stability is rendered through electrostatic and/or steric stabilisation (see below) from the adsorbed polymeric surfactants. In addition, the viscosifying nature of non-adsorbing polymers may increase emulsion stability by reducing the rate of creaming. Thus, the chemical structure of polymeric surfactants, *e.g.*, degree of grafting, length and type of the segments and molar mass, play a vital role in emulsion properties.[50,51]

1.2.3 Emulsification Methods

The common method of preparing emulsions involves the application of force to break-up the oil and water interface into fine droplets. High shear mixing involves the production of droplets when the liquid is mixed with a rotating shaft at a high speed.[45] The distribution of the droplets formed is determined by the balance between droplet break-up and coalescence. Droplet break-up is dependent on the type of flow that the rotating shaft induces on the liquid.[52] Homogenisation involves forcing the liquid through a small orifice under very high pressure.[53] This method of emulsification produces very small droplets. For example, the diameter of fat globules in homogenised milk is < 1 μm.[47] Ultrasonic emulsification involves the preparation of emulsions using ultrasonic vibrations. These acoustic waves can be generated either by piezoelectric, electromagnetic, magnetostriction or mechanical effects.[53]

Emulsions may be produced by phase inversion, whereby the dispersed and continuous phases spontaneously invert upon agitation, *e.g.*, W/O to O/W or vice versa, under conditions determined by the system properties.[54] This technique is usually employed when preparing emulsions of very viscous liquids in less viscous liquids, *e.g.*, W/O emulsions. This is because droplets cannot be broken-up by shear in a liquid having a viscosity which is four times lower than that of the liquid to be dispersed.[47] These emulsions are prepared by first having the low

viscosity liquid (usually aqueous phase) as the dispersed phase, which is then brought to inversion. Phase inversion has been found to occur as a result of changes in the temperature, chemical composition of the surfactant, properties of the dispersed and continuous phases and mixing rate.[55-60]

Recently, Weitz and co-workers[61] have produced monodisperse droplets using a fine capillary. Having added the phase to be dispersed into the capillary containing a flow of the continuous phase, droplets were produced at the tip of the capillary once the interfacial tension was exceeded. The tip diameter of the capillary, extrusion rate and velocity of the continuous phase were found to affect the droplet size of the emulsions. Bibette and co-workers[62-64] developed a method of fractionated crystallisation based on liquid-solid phase transition induced by attractive depletion flocculation to produce monodisperse droplets from polydisperse samples. In the presence of an excess of surfactant in the continuous phase, the droplets undergo depletion flocculation. This led to phase separation, since depletion attraction is sensitive to droplet size. After separating the two phases under gravity, the samples were subjected to a purification process which was then followed by fractionated crystallisation.

1.2.4 Emulsion Stability

Emulsions are thermodynamically unstable due to their large interfacial area [Equation (1.15)]. Emulsions may be rendered kinetically stable by the addition of surfactants or polymers. In the absence of an energetic barrier, emulsion droplets spontaneously coalesce in order to reduce the total interface area. An unstable emulsion may undergo several consecutive and parallel steps before the final stage of phase separation is reached (Figure 1.6).

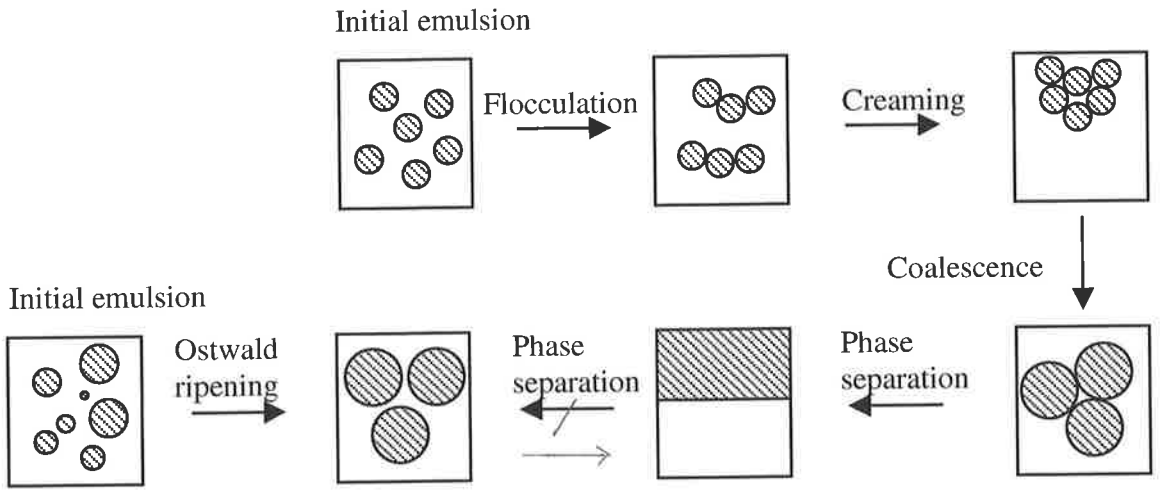

Figure 1.6: Illustration of the ways in which an emulsion may become unstable. Note that the density of the dispersed phase is lower than that of the continuous phase in this example.

The breakdown of emulsions can be described as follows. Initially, droplets may collide due to Brownian motion, diffusion or mixing. If the attraction is stronger than the repulsion between droplets, aggregation of droplets may occur; this process is also known as flocculation. Due to the density difference, $\Delta\rho$, the droplets may cream or sediment ($\Delta\rho = \rho_c - \rho_d$, where subscripts c and d denote the continuous and dispersed phase, respectively). Creaming occurs when droplets move under gravity to form a concentrated layer at the top of the sample ($\Delta\rho > 0$), while sedimentation results from the density of the dispersed phase being greater than that of the continuos phase ($\Delta\rho < 0$). Larger droplets (or aggregates of droplets) move faster than smaller ones (or isolated droplets), causing increased creaming (or sedimentation) rates because droplet (or aggregate) velocity, V, is proportional to the square of the droplet (aggregate) radius, as indicated by the Stokes equation:[65]

$$V = \frac{2\Delta\rho g a^2}{9\eta} \tag{1.17}$$

where g is the acceleration due to gravity, a is the droplet radius and η is the continuous phase viscosity. Note that Equation (1.17) is only applicable for dilute emulsions. The viscous forces and Brownian motion of the droplets oppose both creaming and sedimentation phenomena. As can be seen from Equation (1.17), a key method for improving emulsion stability would be to increase the viscosity of the continuos phase ($V \propto 1/\eta$). In this project, a new method is used for reversibly forming a gel which effectively increases η to high values and prevents creaming in a reversible manner.

Coalescence results from the rupture of the thin film separating the aggregated droplets. This rupturing process usually starts at a specified place in the film, due to thinning in that area. Film thinning depends on the hydrodynamics interactions and forces acting across the film, while the rupturing stage is dependent on the thickness and mechanical properties of the film.[42] The film is essentially made up of two flat, parallel interfaces of thickness δ_i, separated by a distance b_i (Figure 1.7).[65] At distances of $b_i > 2\delta_i$, the forces acting across the film are van der Waals and electrical double layer interactions. But as $b_i < 2\delta_i$, the droplets experience steric interactions.

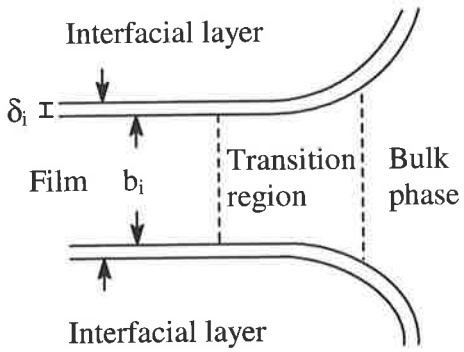

Figure 1.7: Schematic representation of the thin film and regions between two liquid droplets in a continuous phase. *Source*: Ref. 65.

Ostwald ripening is the process by which larger droplets grow at the expense of smaller ones due to the difference in solubility of the dispersed phase material in the two phases.[66] The solubility of a spherical particle, *e.g.*, oil droplets in water, increases with decreasing size, as shown by the Kelvin Equation:[67]

$$c(a) = c(\infty)\exp\left(\frac{2\gamma_{12}v_m}{aRT}\right) \tag{1.18}$$

where $c(a)$ is the solubility surrounding a droplet of radius a, $c(\infty)$ is the bulk phase solubility, v_m is the molar volume of the dispersed phase and R is the gas constant. As can be seen from Equation (1.18), $c(a)$ increases with decreasing a. Thus, the material contained in smaller droplets tends to diffuse through the continuous phase, recondensing onto larger droplets. This process leads to droplet size increase and lowering in the interfacial area of the emulsion.

1.2.5 Structure and Properties of the Interfacial Region

The interaction forces between droplets as well as the properties at the oil-water interface govern emulsion properties such as the viscosity, stability and droplet size distribution. For example, the double layer structure and distribution of polymeric surfactant chains at the interface determine the attractive and repulsive forces between droplets. Depending on the net interaction, these forces may cause emulsion droplets to flocculate or coalesce.

1.2.5.1 Electric double layer

Most droplets in aqueous medium are charged due to various reasons, such as the ionisation of surface groups and specific adsorption of ions. The surface charge influences the

distribution of nearby ions; ions of opposite charge (counter-ions) are attracted towards the surface and ions of like charge (co-ions) are repelled away from the surface.

Figure 1.8 shows the model developed by Stern[46] for the formation of an electrical double layer at the interface. Part of the counter-ion charge is located close to the droplet surface (the so-called Stern layer) and the diffuse layer, which extends to some distance from the surface. The most relevant electrical potential to the interaction is at the boundary between the Stern and diffuse layer, *i.e.*, the Stern potential, ψ_d, rather than the potential at the surface, ψ_0. This boundary (the Stern plane) is generally considered to be at a distance of about 0.3 - 0.5 nm from the droplet surface, corresponding to the diameter of a hydrated counter-ion.[46] The surface potential decreases linearly to a value of ψ_d at the Stern plane. This is usually equated with the zeta (ζ) potential which can be defined as the potential at the plane of the shear. When subjected to an electric field, the shear plane contains ions that are dragged along with the moving droplet; those in the diffuse layer remain behind. In cases where neutral polymers are adsorbed to a charged droplet surface, then $\psi_d \neq \zeta$ potential, but $|\zeta \text{ potential}| < |\psi_d|$.

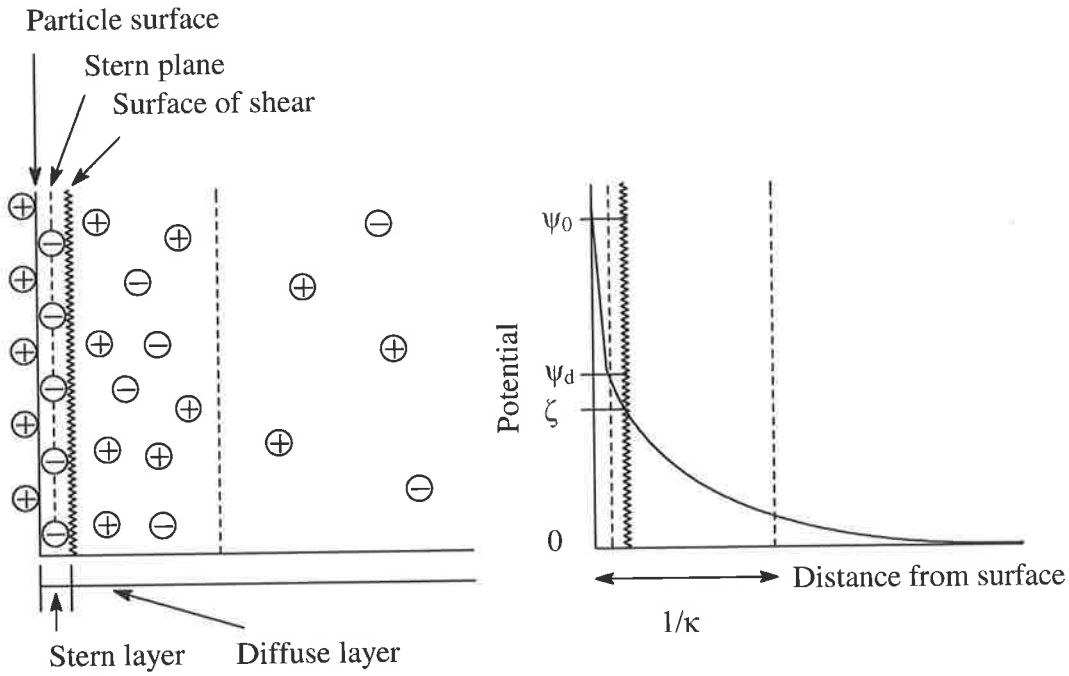

Figure 1.8: Structure of the electrical layer. The surface is positively charged despite the adsorption of some counter-ions. The Stern plane and surface of shear are distinguished in these diagrams, however, they are usually co-incident. *Source*: Ref. 46.

Electrostatic interaction (or double layer repulsion) occurs as a result of finite Stern potential. When two droplets having a double layer of the same sign approach each other to a distance where the two layers begin to overlap, this causes local increase in the concentration of counter-ions. This results in electrostatic repulsion and work must be performed if the droplets are to come together. The double layer thickness, $1/\kappa$, which gives a measure of the extent of the repulsive interaction is simply the distance at which ψ_d has fallen to a value of 37% of its initial value. It is related to the concentration of electrolyte, c_e, by:[46]

$$\left(1/\kappa\right)=\left(\frac{\varepsilon\varepsilon_o kT}{2Z^2e^2N_A c_e}\right)^{1/2} \tag{1.19}$$

where ε is the permittivity, ε_o is the permittivity of free space, Z is the charge number of the electrolyte, e is the electron charge and N_A is Avogadro's number.

1.2.5.2 DLVO theory

Deryagin, Landau, Verwey and Overbeek were the first to quantitatively describe the total interaction energy, V_{tot}, between two droplets (DLVO theory).[46] The theory involves estimation of the energy due to the overlap of electrical double layers (usually repulsion), in the case of charged droplets, and the van der Waals energy (usually attraction) as a function of droplet separation, H.

The repulsive interaction, V_R , can be expressed as:[46]

$$V_R = \frac{32\pi a k^2 T^2 \gamma^2}{e^2 Z^2} \exp(-\kappa H) \tag{1.20}$$

where

$$\gamma = \tanh\left(\frac{Ze\kappa a}{2kT}\right) \tag{1.21}$$

The attractive interactions between droplets arise mainly from van der Waals interactions between constituent molecules; the important interactions are dipole-induced dipole (Debye) and dispersion (London) interactions. Dispersion forces arise from charge fluctuations within a molecule associated with the motion of its electron. Thus, they operate even between non-polar molecules. The London dispersion interaction energy, V_A, is given by:[46]

$$V_A = \frac{A_{eff} a}{12H} \tag{1.22}$$

where A_{eff} is the effective Hamaker constant that is given by:

$$A_{eff} = \left(A_{11}^{1/2} - A_{22}^{1/2}\right)^2 \tag{1.23}$$

where A_{11} and A_{22} are the Hamaker constants for the dispersed and continuous phase, respectively. Thus, V_{tot} is given by:

$$V_{tot} = V_R + V_A \tag{1.24}$$

Figure 1.9 shows variation in V_{tot} as a function of H. Droplets relatively far from each other will experience significant van der Waals attraction, but at smaller values of H, double layer repulsion dominates and it increases rapidly with further decrease in H, giving rise to a primary maximum. At still smaller values of H, V_{tot} becomes negative again, *i.e.*, attractive interactions dominate, before becoming infinitely large (positive) at very close distances due to electron cloud overlap. This gives rise to a very deep minimum (or primary minimum) at close inter-droplet approach and at large distances, another attractive minimum (or secondary minimum) emerges which has a much lower depth than the primary minimum. The depth of the primary minimum represents the barrier to strong irreversible droplet association, *i.e.*, coagulation, whereas the depth of the secondary minimum represents the energy for flocculation, and if comparable to the thermal energy, kT, the process is reversible.

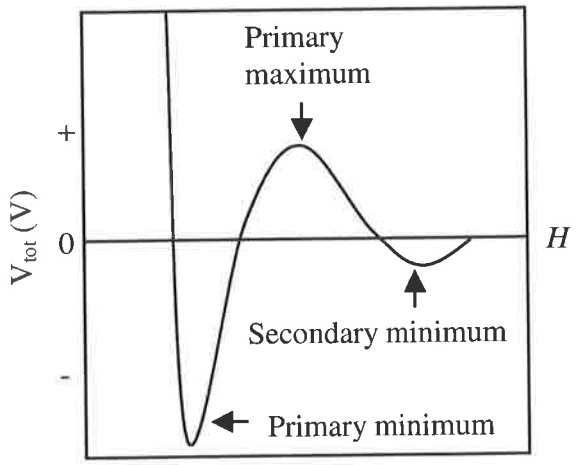

Figure 1.9: Relationship between force and distance according to the DLVO theory.

Although the DLVO theory assumes that droplets behave as hard spheres when interacting with one another, Danov *et al.*[68] showed that the interaction between deformable droplets and non-deformable droplets, *i.e.*, hard spheres, is very different. For example, the electrostatic interaction for deformable droplets can change from repulsive to attractive or vice versa during deformation (the extent of deformation depends on parameters such as droplet size, ionic strength, film thickness and γ_{12}).

1.2.5.3 Polymeric Stabilisation of Colloids

As mentioned in Section 1.2.2, polymeric surfactants may be used in place of surfactants to stabilise emulsions. But in this case, the mechanism by which droplets are stabilised is different to that observed in emulsions containing short-chain surfactants. If the droplets are coated with an adsorbed layer of polymer chains of thickness δ_a, repulsive force between the adsorbed layers provides an additional barrier to aggregation when they approach each other at $H < 2\delta_a$ (Figure 1.10). This is known as steric stabilisation and the mechanism by which it operates

is as follows.[4,46] The adsorption and desorption of polymer chains is relatively slow compared to the time it takes for droplet-droplet encounter. Thus, it is unlikely that sterically stabilised droplets will reach the primary minimum for coagulation to occur. If interpenetration with no compression takes place, the local concentration of polymer chains will increase. This occurs at distances $\delta_a < H < 2\delta_a$ and depending on the polymer-polymer and polymer-solvent interactions, the droplets may attract or repel through osmosis. The adsorbed layers are compressed and interpenetrate into one another when $H < \delta_a$, leading to decrease in the number of possible configuration that the chains can adopt. This decreases the entropy and increases the free energy. Thus, aggregation of droplets becomes an unfavourable process.

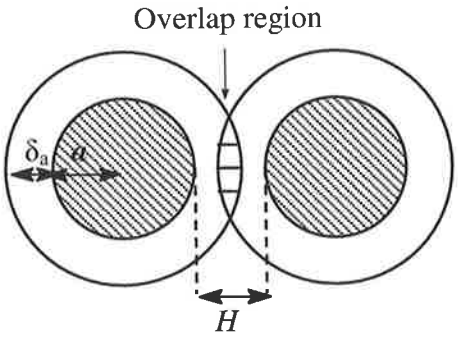

Figure 1.10: Schematic diagram of droplets with adsorbed polymeric surfactants (indicated by adsorbed layer of polymer chains, δ_a) showing the interpenetration or overlap region.

Thus, a sterically stabilising polymer must contain groups anchoring to the dispersed phase droplets and solvatable stabilising chains extending into the continuous phase (see Section 1.1.5). This is usually achieved by utilising amphiphatic polymers, *e.g.*, block and graft copolymers, that contain groups that are insoluble (anchoring) and soluble (stabilising) in the

continuous phase (see Figure 1.4). Solvent quality plays a major role in steric stabilisation. If the polymer is in a good solvent for the stabilising chains, inter-layer penetration is not favoured resulting in droplet-droplet repulsion. On the other hand, if the solvent is poor, *e.g.*, above theta solvency (Section 1.1.4.3), penetration is favoured and flocculation results.

For sterically stabilised systems, V_{tot} can be written as:[46]

$$V_{tot} = V_R + V_A + V_S \tag{1.25}$$

where V_S is the steric interaction. The potential energy diagrams are shown in Figure 1.11.

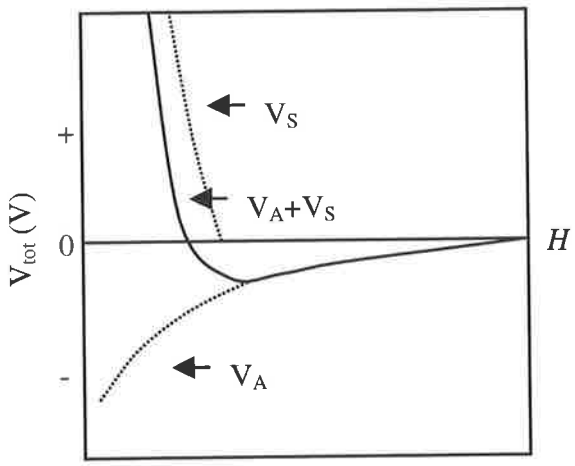

Figure 1.11: Potential energy diagrams for sterically stabilised systems (in the absence of double layer repulsion). *Source*: Ref. 46.

At large distance of separation, V_A dominates. But when the droplets (more precisely the adsorbed layer) start to overlap, a very steep repulsion occurs that prevents further approach. Note that the curve only shows one minimum, whose depth depends on δ_a, a and A_{eff}.

1.2.6 Emulsion Stabilisation Using Responsive Polymers: A Literature Review

Surfactants have proved to be efficient and cost effective emulsifiers and effective stabilisers, *i.e.*, to confer prolonged kinetic stability to emulsions. Thus, the majority of emulsions studied or produced commercially are prepared using short-chain surfactants. The unique properties of copolymers have been exploited in the preparation and stabilisation of emulsions using polymeric surfactants.[23-25,29] One of the advantages of using them for emulsion preparation is the large degree of architectural control that can be exerted in order to explore and optimise copolymer structure-emulsion property relationships. Recently, much interest has been focused on polymeric surfactants that undergo a conformational change or phase transition in response to an external stimulus, *i.e.*, responsive polymers (see Section 1.1.7). Several workers have incorporated these responsive polymers in emulsions and have shown to be sensitive to environmental conditions.

Mathur *et al.*[69] successfully used polyethylene glycol segments grafted onto polymethacrylic acid backbone [poly(PEG-*g*-PMMA)] to stabilise O/W emulsions, whereby the stabilising properties ~~was~~ reversibly switched on and off when the pH of the solution was varied. The formation of hydrogen bonded hydrophobic complexes (PMMA with PEG) ~~were~~ favoured at low pH giving rise to alternating hydrophilic (uncomplexed PMMA segments) and hydrophobic (complexed) segments that were able to stabilise O/W emulsions. The complex formation was suppressed at high pH leading to emulsion breaking.

Perrin *et al.*[50] showed that the stability of the O/W emulsions was influenced by the molar mass and hydrophobic modification, *i.e.*, degree of grafting, of low hydrophobically modified poly(acrylic acid) copolymers. The copolymers were synthesised by grafting dodecylacrylamide

groups to the poly(sodium acrylate) precursor polymer. The non-adsorbing copolymers present in the continuous phase caused an increased viscosity in the emulsions, *i.e.*, viscosifying effect. At low copolymer concentrations where this viscous effect was not present, they found that increased degree of grafting of the copolymers gave the emulsion droplets a better resistance to coalescence. In a related work[51], the authors investigated the types of emulsions formed when the chemical architecture of the copolymers was varied. Oil-in-water emulsions were favoured when the degree of grafting and/or length of the grafts were decreased. On the other hand, W/O emulsions were produced when twin-tailed rather than single-tailed copolymers were employed. They also noted that inversion of O/W to W/O emulsions occurred when the salt concentration in the emulsions was increased. In ground-breaking research, Porcar *et al.*[41] demonstrated that light can be used to invert O/W to W/O emulsions. The n-dodecane-in-water emulsions were stabilised by a combination of two polyelectrolyte surfactants. The presence of the photoresponsive amphiphilic polymer in one of them enabled adjustment of its hydrophobicity upon irradiation by near-UV light. This led to the formation of unstable emulsions.

In their study, Philip *et al.*[70] induced gelation of asphalt-in-water emulsions by addition of salt at room temperature. After adding NaOH and leaving it to stand, microscopic observation revealed that the droplets became mutually adhering and formed a three-dimensional network. The time delay for gelation to occur was found to vary between 1 - 10000 min. and was dependent on the oil volume fraction and concentration of NaOH. Once this network was formed, the gel started to contract by reducing its surface area. This led to strong volume contractions and expulsion of water from the space-filling network.

In general, the studies conducted were based on the idea that responsive polymers posses the unique attributes of undergoing a sharp conformation transition upon a small modification of

an environmental parameter (*e.g.*, pH) near a critical point. This conformation change is usually a consequence of the polymer chains being soluble (insoluble) or extended (collapsed) in solution. Prior to the external stimuli being varied, the induced conformational changes resulted in macroscopic changes in the polymer, *e.g.*, viscosity and turbidity, which in turn affected the emulsion properties, *e.g.*, viscosity, stability and emulsion type.[41]

1.3 Aims of the Research

The aims of the research are two-fold. The first is to prepare and characterise new responsive amphiphilic comb copolymers. The second aim concerns the preparation of responsive emulsions using these copolymers. It was hypothesised that the switching behaviour of the copolymers would induce temperature-response of emulsions when heated. The adsorption of the responsive copolymer at the oil-water interface would cause the emulsion to be temperature responsive since emulsion stability and properties are largely governed by its interface. To the author's knowledge, there have not been any studies that involve the preparation of temperature-responsive emulsions using synthetic responsive polymers to date.

The aims of the work are:

(i) To synthesise and characterise a range of poly(NIPAM-*co*-PEGMA) copolymers (PEGMA is polyethylene glycol methacrylate).

(ii) To study the properties of the copolymers.

(iii) To prepare O/W emulsions using these copolymers and investigate their properties.

(iv) To study the relationship between copolymer structure and emulsion properties.

(v) To establish a mechanism for temperature-dependent emulsion behaviour.

1.4 Thesis Outline

Chapter 2 describes the synthesis and characterisation of the thermally-responsive copolymers. Proton nuclear magnetic resonance and gel permeation chromatography are used to investigate the composition and molar mass of the copolymers, respectively. This allows the reactivity ratio of the monomers to be determined. Turbidity and viscosity measurements are used to study the temperature-responsive behaviour of the copolymers.

Chapter 3 reports small-angle neutron scattering studies for the copolymer solutions. Structural features and size of the copolymer chains at different temperatures obtained from these studies are discussed.

Chapter 4 describes the preparation, characterisation and properties of the emulsions containing these thermally-responsive copolymers. The effects of changing the type and volume fraction of the oil phase and concentration and structure of the copolymer on emulsion properties are studied. Results from the preliminary studies of emulsion gelation will be discussed.

Chapter 5 describes the rheological studies of the copolymers and emulsions at various temperatures using steady shear and oscillatory measurements. Here it is proposed to relate the gelation temperature and gel strength to the copolymer concentration, oil volume fraction (in the case of emulsions) and sample temperature from the rheological data.

Finally, Chapter 6 provides the proposed mechanism for temperature-induced gelation based on the results obtained. The major conclusions of this thesis are then presented.

CHAPTER 2 POLYMER SYNTHESIS, CHARACTERISATION AND PROPERTIES

2.1 Introduction and Aims

Poly(NIPAM) has been widely studied in the literature because of its interesting thermal behaviour in aqueous media. Poly(NIPAM) solutions are characterised by a LCST at 32°C. The polymer is soluble in water at room temperature, but undergoes phase separation upon warming to above 32°C (see Section 1.1.4.3).[71] NIPAM can be copolymerised with a number of other monomers to give thermally-sensitive copolymers.[3,30,31,33] This chapter examines the synthesis, characterisation and properties of poly(NIPAM-*co*-PEGMA) copolymers. Utilisation of PEGMA as the other co-monomer allows the possibility of modifying the length of the EO chain. Thus, the influence of copolymer structure on emulsification capacity and emulsion stability can be investigated. This is discussed in Chapter 4.

In addition, poly(NIPAM) and poly(PEGMA) homopolymers were synthesised and investigated. These "control" polymers allowed comparison of physical and chemical properties, as well as emulsification capacity and emulsion stability. As will be discussed in detail later, the conditions used for the preparation of the copolymers in this work were specifically designed to promote copolymerisation through an excess of PEG macromonomer at the onset of polymerisation. Compositional asymmetry (*i.e.*, a non-random sequence distribution of monomers) of the copolymer was to be necessary for the preparation of thermally-responsive emulsions.

The aims of this section of the work were:

(i) To synthesise poly(NIPAM-*co*-PEGMA), poly(NIPAM) and poly(PEGMA) polymers.

(ii) To characterise the polymers using techniques such as nuclear magnetic resonance (NMR), gel permeation chromatography (GPC) and UV-VIS spectrophotometry.

(iii) To investigate the copolymerisation kinetics of NIPAM and PEGMA.

(iv) To investigate the effect of temperature on the solution properties, *e.g.*, LCST, viscosity and diffusion coefficient.

2.2 Experimental

2.2.1 Reagents

NIPAM (Acros Organics, 99%), PEGMA (average molar mass *ca.* 360 g/mol, Aldrich), MPEGMA (average molar mass *ca.* 475 and 1100 g/mol, Aldrich) (MPEGMA is polyethylene glycol methyl ether methacrylate), AIBN (EZF Atochem), APS (Aldrich, 98%) (APS is ammonium persulphate), hydroquinone (Merck, 99%) and TEMED (Aldrich, 98%) (TEMED is N, N, N', N'-tetramethylethylenediamine) were used as received. Reagent grade solvents were used without purification and water was Millipore Milli-Q quality.

2.2.2 Polymer Syntheses

Poly(NIPAM)

Poly(NIPAM) was synthesised according to the method reported by Winnik.[71] Typically, a solution of NIPAM (5 g) in *tert*-butyl alcohol (50 ml) was added to a nitrogen purged five-necked 250 ml round-bottomed flask equipped with a burette, Teflon stirrer blade, condenser, thermometer and nitrogen inlet. Nitrogen gas was passed through the stirred monomer solution for 30 min. prior to the addition of the initiator solution to purge the reaction mixture of dissolved oxygen and carbon dioxide. The solution was then heated to 80°C under nitrogen, before AIBN (0.03 g) in *tert*-butyl alcohol (3 ml) was added. The solution was stirred for 4.5 hours at 80°C, before it was cooled to room temperature. The solvent was then evaporated, the residual material dissolved in tetrahydrofuran (THF) (30 ml) and precipitated in hexane (1 litre) to give a white powder.

Poly(PEGMA)

A nitrogen purged five-necked 250 ml round-bottomed flask equipped with a burette, Teflon stirrer blade, condenser, thermometer and nitrogen inlet was initially set up. A solution of PEGMA (5 g) in *tert*-butyl alcohol (50 ml) was heated to 80°C under nitrogen. AIBN (0.03 g) in *tert*-butyl alcohol (3 ml) was then added at once. The solution was stirred for 4.5 hours at 80°C, before it was cooled to room temperature. The solvent was then evaporated to give a cloudy viscous material. The product was dissolved in water at a concentration of 5 wt% and dialysed against water before the product was freeze-dried to give a waxy material.

Copolymers

The basic structure of all copolymers prepared is shown in Figure 2.1, although a range of copolymers from different synthesis routes and varying compositions and structures were attempted in this work (Table 2.1). Note that the purification of the synthesised copolymers involved removing any unreacted monomers from the product.

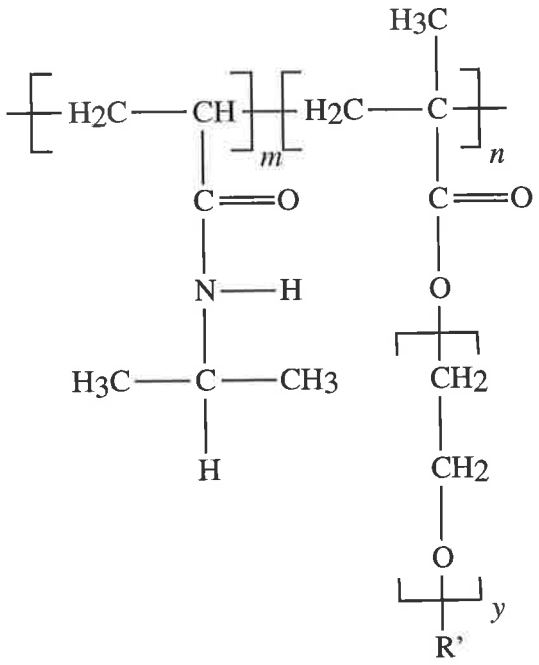

Figure 2.1: The basic structure of the copolymers prepared. Note that R' represents the terminal group of the EO chain (R' = OH and CH_3 for PEGMA and MPEGMA, respectively).

Table 2.1: Summary of conditions used for various polymer preparations

Sample	Identification	Target mol% NIPAM[a]	Nominal y[b]	Synthetic method[c]	Solvent[d]	Initiator	Monomer to initiator mole ratio
Poly(NIPAM)		100	0	*b*	*t*-OH	AIBN	240
Poly(PEGMA)		0	6	*b*	*t*-OH	AIBN	80
Poly(NIPAM-*co*-PEGMA)	P1	95	6	Nf	*t*-OH	AIBN	190
Poly(NIPAM-*co*-PEGMA)	P2	86	6	Nf	*t*-OH	AIBN	190
Poly(NIPAM-*co*-PEGMA)	P2A	86	6	df	*t*-OH	AIBN	190
Poly(NIPAM-*co*-PEGMA)	P2B	86	6	df	*t*-OH	AIBN	30
Poly(NIPAM-*co*-PEGMA)	P2C	86	6	df	*t*-OH	AIBN	1300
Poly(NIPAM-*co*-PEGMA)	P2D	86	6	df	H_2O	APS	370
Poly(NIPAM-*co*-PEGMA)	P3	67	6	Nf	*t*-OH	AIBN	190
Poly(NIPAM-*co*-MPEGMA)	MP1	86	9	Nf	*t*-OH	AIBN	190
Poly(NIPAM-*co*-MPEGMA)	MP2	86	23	Nf	*t*-OH	AIBN	190

[a] $\text{Target mol\% NIPAM} = \left(\frac{m}{m+n}\right)\times 100$

[b] Number of EO repeat units based on supplier's information. [c] *b* = batch, Nf = NIPAM-feed, df = dual-feed. [d] *t*-OH = *tert*-butyl alcohol.

The copolymers were prepared either by the NIPAM-feed or the dual-feed method. The methods differ only in the initial contents and feed compositions. A detailed description for the preparation of the copolymers (except for P2D) is given below and summarised in Table 2.2.

A nitrogen purged five-necked 250 ml round-bottomed flask equipped with a burette, Teflon stirrer blade, condenser, thermometer and nitrogen inlet was set up before the initial contents were added. It was allowed to degas for 0.5 hours before the reactor was heated to 80°C under nitrogen. The feed was added dropwise with stirring over 1 hour. The mixture was refluxed for a further 4.5 hours before it was allowed to cool and then added dropwise to 2.5 litre of diethyl ether with constant vigorous stirring. The product that precipitated was filtered and dissolved in water (concentration of 5 wt%). The solution was extensively dialysed and then freeze-dried to give a white powder.

The polymerisation route adopted for the synthesis of P2D was a variation to the method reported by Shibayama and Tanaka[72]. The initial contents were added to a nitrogen purged 250 ml round-bottomed flask equipped with a burette, Teflon stirrer blade and nitrogen inlet. It was allowed to degas for 0.5 hours at room temperature before the feed was added dropwise with stirring over 2 hours. The mixture was then left to react overnight at room temperature before the product was dialysed with water and freeze-dried.

Table 2.2: Summary of the initial contents and feed compositions utilised for various copolymer syntheses[a]

Identification	Synthetic method[b]	Initial contents (g)[c]	Feed compositions (g)[c]
P1	Nf	PEGMA (0.75) + *t*-OH (30)	NIPAM (4.25) + AIBN (0.035) + *t*-OH (10)
P2	Nf	PEGMA (1.75) + *t*-OH (30)	NIPAM (3.30) + AIBN (0.030) + *t*-OH (10)
P2A	df	*t*-OH (30)	PEGMA (1.75) + NIPAM (3.30) + AIBN (0.030) + *t*-OH (10)
P2B	df	AIBN (0.205) + *t*-OH (30)	PEGMA (1.75) + NIPAM (3.30) + AIBN (1.7×10^{-3}) + *t*-OH (10)
P2C	df	AIBN (4.0×10^{-3}) + *t*-OH (30)	PEGMA (1.75) + NIPAM (3.30) + AIBN (3.15×10^{-4}) + *t*-OH (10)
P2D[d]	df	H_2O (90) + TEMED (0.18)	PEGMA (1.75) + NIPAM (3.30) + APS (0.02) + H_2O (10)
P3	Nf	PEGMA (3.05) + *t*-OH (30)	NIPAM (1.90) + AIBN (0.025) + *t*-OH (10)
MP1	Nf	MPEGMA[e] (1.65) + *t*-OH (30)	NIPAM (3.35) + AIBN (0.030) + *t*-OH (10)
MP2	Nf	MPEGMA[f] (1.50) + *t*-OH (30)	NIPAM (3.50) + AIBN (0.030) + *t*-OH (10)

[a] Refer to text for detailed description of the methods used for the synthesis of the copolymers. [b] Nf = NIPAM-feed, df = dual-feed.

[c] *t*-OH = *tert*-butyl alcohol. [d] Polymerisation route was a variation to the method reported by Shibayama and Tanaka[72].

[e] Molar mass = 475 g/mol. [f] Molar mass = 1100 g/mol.

2.3 Physical Measurements

Characterisation of polymers is vital to allow the synthesis and molecular properties and molecular and bulk relationships to be understood.[1] Furthermore, a thoroughly characterised polymer allows prediction and understanding of its in-use performance. A number of instruments were used to characterise the synthesised polymers. A brief description of the theory and methods is given below.

2.3.1 ^{1}H Nuclear Magnetic Resonance

2.3.1.1 Background Theory

In this work, ^{1}H nuclear magnetic resonance (NMR) was employed to characterise and determine the composition of the polymers. This spectroscopic technique is based on transitions between nuclear spin states. Bohr postulated that the intrinsic angular momentum possess by nuclei was quantised. This angular momentum is termed 'spin' and every nucleus has an angular momentum/spin quantum number, I_s. Quantisation leads to a nucleus of I_s having $2I_s + 1$ possible orientations with respect to a reference axis. For example, ^{1}H has $I_s = ½$ and exhibits two possible orientations (or quantum states) with respect to a reference axis. Note that these states are degenerate in the absence of a magnetic field. When placed in a strong magnetic field the nuclear spin states of protons will be of unequal energy, since neighbouring atoms affect the magnetic environment of protons. This difference is energy, ΔE, is given by:[73]

$$\Delta E = \frac{h\gamma_m B_0}{2\pi} \qquad (2.1)$$

where h is the Planck's constant, γ_m is the magnetogyric ratio (a proportionality constant, which has a specific value for each nucleus) and B_0 is the strength of the applied magnetic field. The ratio of the number of nuclei in the low-energy spin state (which have an antiparallel alignment with B_0), N_α, and the number in the high-energy state (which aligns in the same direction as B_0), N_β, is governed by Boltzmann distribution:[73]

$$\frac{N_\beta}{N_\alpha} = \exp\left(-\frac{\Delta E}{kT}\right) \tag{2.2}$$

When a radio frequency is applied to the system, some of the nuclei will be promoted from the ground energy state to the high-energy state. The energy diagram is shown in Figure 2.2.

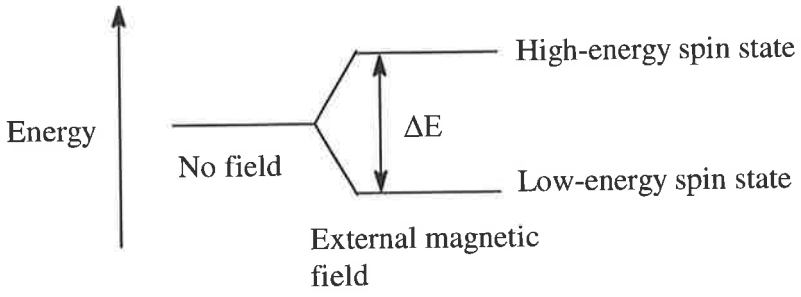

Figure 2.2: The splitting of spin states for ^1H by an applied magnetic field.

The frequency, in Hz, at which promotion occurs, *i.e.*, the resonance frequency, is given by:[73]

$$\nu_r = \frac{\gamma_m B_0}{2\pi} \tag{2.3}$$

Thus, the resonance frequency is influenced by the applied field strength and nature of the nucleus. Note that the latter is usually caused by fluctuations in electron density in the neighbourhood of each nucleus.

The change in the position of the nucleus, induced by its molecular environment, is known as chemical shift. Chemical shifts are used to compare the level of shielding of protons of a particular sample to a reference. This standard substance is usually tetramethysilane, $(CH_3)_4Si$, abbreviated as TMS. The chemical shift of a peak, in δ units, is reported in parts per million (ppm) from the TMS peak. Since protons in different environments will experience different amount of shielding, protons in different chemical environments have different chemical shifts. In general, intra and intermolecular forces, solvents and temperature affect the chemical shift.

2.3.1.2 Applications of ^{1}H NMR to Polymers

Polymer compositions may be obtained from the relative intensities of proton(s) of characteristic groups. For example, Berlinova *et al.*[33] compared the intensity of the methine protons of the isopropyl group of NIPAM to that of the oxyethylene protons of the end-functionalised PEO side chains, to determine the composition of their graft copolymers.

In the case of copolymers, ^{1}H NMR may be used to provide structural information such as distribution of monomer units along the polymer chain and the length of monomer sequences. This is because chain structures are dependent on the reactivity of the monomers and reaction conditions employed (Section 1.1.3). In other words, the monomer sequences, copolymer composition, configurational sequences and reaction mechanisms may vary throughout the course of the reaction.

2.3.2 Gel Permeation Chromatography

A polymer's properties are significantly influenced by its molar mass distribution; thus, knowledge of this distribution is vital. In this work gel permeation chromatography (GPC) was employed to measure the molar mass distribution of the polymers. This technique was developed during the mid-1960s and depends on the utilisation of a stationery phase which consists of a column packed with beads of gel having porosity between 50 - 10^6 Å. The porosity of the gel is important since GPC works by means of a size fractionation procedure. Larger polymer molecules which occupy a greater volume in solution are excluded from the smaller pore size in the gel. Hence, they spend less time inside the beads and move quickly through the column and are eluted rapidly. On the other hand, smaller polymer molecules have the possibility of diffusing into the smaller pores. This increases their retention time in the column. Thus, an effective size separation can be obtained with time.

The volume of solvent needed to elute a particular polymer from the point of injection to the detector is known as its elution volume, v_e, and is given by:[1]

$$v_e = v_0 + K_{se} v_i \tag{2.4}$$

where v_0 is the interstitial void volume, K_{se} is the fraction of the internal pore volume accessible to a given polymer molecule and v_i is the total internal pore volume. For large polymer molecules, $K_{se} = 0$ and $v_e = v_0$, whereas $K_{se} = 1$ and $v_e = v_0 + v_i$ for very small molecules.

v_e is related to the molecular size, L, as shown by:[1]

$$v_e = v_0 + v_i \exp\left[-\frac{A_s L}{2}\right] \tag{2.5}$$

where A_s is the surface area per unit pore volume. The molecular size can be represented by the hydrodynamic volume, v_h, of the polymer which is proportional to $[\eta]M$. Note that $[\eta]$ is known as the intrinsic viscosity and is a measure of the ability of a polymer to increase the viscosity for a given solvent at a given temperature.[1] Log$[\eta]M$ is related to M as given by the Mark-Houwink equation:[1]

$$\log([\eta]M) = \log K + (1 + a')\log M \tag{2.6}$$

where K and a' are constants for a given polymer/solvent/temperature system. From Equation (2.6), log($[\eta]M$) increases with increasing log$M$, provided K and a' remain constant. The calibration plot for the polymer under investigation can be obtained by measuring v_e for a series of molar mass distribution samples of the polymer, *e.g.*, polystyrene, with different M.

2.3.3 Viscosity Measurements

Dilute polymer solutions have viscosities higher than the pure solvent due to differences in size between the polymer chains and solvent molecules. In addition, the extent of viscosity is related to the dimensions of the chains. In this study, viscosity measurements of dilute polymer solutions were conducted to characterise the polymer. The concentration and temperature dependence of the polymer viscosity were investigated in an effort to provide information concerning polymer-solvent interactions.

Viscosity measurements are usually performed using capillary viscometers, which generally consist of a measuring and a reservoir bulb and a capillary tube (Figure 2.3). The liquid is sucked into the measuring bulb from the reservoir bulb attached to the bottom of the capillary

tube. The time taken for the solution to flow back between the two etched marks is then recorded.

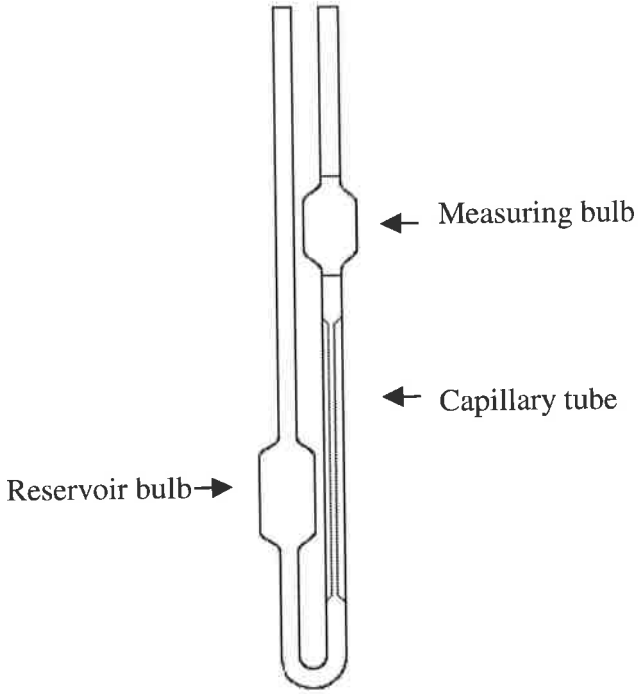

Figure 2.3: Schematic representation of an Ostwald U-tube viscometer.

Under conditions of steady laminar Newtonian flow, the pressure difference, ΔP, across the capillary tube and the viscosity of the liquid, η_l, can be related to the volume of the liquid, v_l, which flows in time, t_l, through the capillary tube having a length L_t and radius r_t, according to Poiseuille's equation:[1]

$$\frac{v_l}{t_l} = \frac{\pi r_t^4 \Delta P}{8 \eta_l L_t} \qquad (2.7)$$

ΔP decreases during measurement and is given by:

$$\Delta P = h_l \rho_l g \tag{2.8}$$

where h_l is the average height of the pressure head and ρ_l is the density of the liquid. Thus, Equation (2.7) can be rearranged to give:

$$\eta_l = \frac{\pi r_t^4 h_l \rho_l g t_l}{8 v_l L_t} \tag{2.9}$$

which can be shown as:

$$\eta_l = A \rho_l t_l \tag{2.10}$$

where A is a constant for a given viscometer and is given by:

$$\eta_l = \frac{\pi r_t^4 h_l g}{8 v_l L_t} \tag{2.11}$$

The relative viscosity, η_r, is given by:

$$\eta_r = \frac{\eta_l}{\eta_0} = \frac{\rho_l t_l}{\rho_0 t_0} \tag{2.12}$$

where ρ_l and ρ_0 are the densities, and t_l and t_0 are the flow times of a liquid, *e.g.*, polymer solution, and pure solvent, respectively. Usually ρ_l is approximated to equal ρ_0 since the

measurements involve dilute solutions (*i.e.*, $\rho_l \sim \rho_0$). Thus, η_r is simply the ratio of the flow times t_l/t_0. Table 2.3 shows a summary of the quantities required and terminology that are commonly used in viscosity measurements.

Table 2.3: Quantities and terminology employed in viscosity measurements

Common name	Symbol and definition[a]
Relative viscosity	$\eta_r = \eta_l/\eta_0$
Specific viscosity	$\eta_{sp} = \eta_r - 1$
Reduced viscosity	$\eta_{red} = \eta_{sp}/c_l$
Inherent viscosity	$\eta_{inh} = \ln(\eta_r)/c_l$
Intrinsic viscosity	$[\eta] = \lim_{c_l \to 0} (\eta_{red})$

[a] c_l is the concentration of the liquid.

2.3.4 Turbidity Measurements

As mentioned earlier, poly(NIPAM) exhibits a phase transition behaviour at temperatures greater than the LCST. In this study, turbidity measurements were used to investigate changes on this phase transition when NIPAM was incorporated into the copolymers.

Much information has been known about scattering of light by particles ever since Faraday helped explain optical properties of finely dispersed systems. Rayleigh developed the first theory in 1871 and was subsequently extended by Mie (1908), Debye (1915) and Gans (1925).[74] The basic geometry for studying light scattering is shown in Figure 2.4. The incident light (intensity, I_0) is scattered by the sample at an angle, θ_s, and the detector at a distance, L_{sd}, from the sample measures the intensity of the scattered light, I_s. The intensity of the transmitted light is I_t.

The turbidity of a material is given by:[75]

$$\frac{I_t}{I_0} = \exp(-\tau L) \tag{2.13}$$

where τ is the turbidity and L is the sample thickness. The optical density, OD, is related to the turbidity as follows:

$$\tau = \frac{2.303}{L}(\text{OD}) \tag{2.14}$$

Although OD and absorbance are numerically equivalent, the former is used in this work because the systems under investigation do not absorb light, but scatter it.

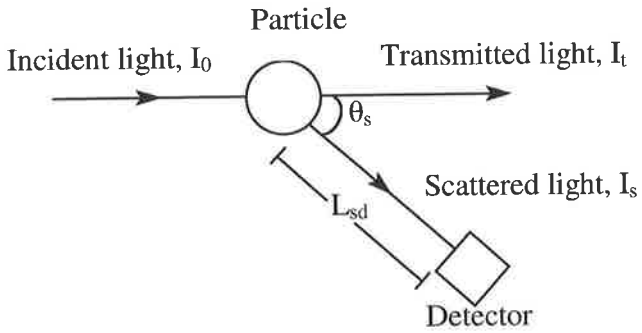

Figure 2.4: Experimental geometry for studying light scattering.

In the case of dispersions, which scatter as point sources, integrating the scattered intensity over the surface of a sphere gives the total scattered intensity:[74]

$$\tau = \frac{24\pi^3}{\lambda^4}\left(\frac{m_r^{\,2}-1}{m_r^{\,2}+1}\right)v_1^{\,2}c_1 \qquad (2.15)$$

where m_r is the relative refractive index, *i.e.*, $m_r = m_1/m_0$ (m_1 and m_0 are the refractive indices of the particle and continuous medium, respectively). As can be seen from Equation (2.15), turbidity increases with v_1 and c_1. The strong wavelength dependence of the scattering intensity can be used to account for the appearance for the blueness of the sky and the redness of the setting sun. During the day the scattered light has a blue appearance since scattering (by particles, dust and water droplets in the atmosphere) is strongest in the blue region, while the transmitted light, e.g., when sun sets, is richer in red light.

For non-absorbing particles the turbidity at a concentration c_1 is related to the wavelength by:[76]

$$\left(\frac{\tau}{c_1}\right)_{c_1\to 0} = \frac{k_1}{\lambda^n} \qquad (2.16)$$

where k_1 is a constant which is dependent on particles size and m_r. For particles having a diameter much less than the wavelength ($< \lambda/20$), $n = 4$ and the particles essentially scatter as point sources. This is also known as Rayleigh scattering. On the other hand, n decreases gradually to zero and oscillates positive and negative for larger particles.

2.3.5 Photon Correlation Spectroscopy

In this work, the size of the polymer chains as a function of temperature and concentration were obtained using a photon correlation spectroscopy (PCS) instrument. PCS uses dynamic light scattering to determine the hydrodynamic diameter, d_h, of particles.

Dispersion particles are continuously moving due to Brownian effect. Bright spots appear and disappear as a consequence of the particles moving in and out of the specific area of view. Thus, this twinkling effect is influenced by particle motion. In PCS, a photon correlator senses the nature of the twinkling, in that the instrument analyses the correlation in time between the fluctuations in the intensity of the light. When the correlation time, τ, is large, the intensity at a time t [*i.e.*, I(t)] and that at time ($t + \tau$) [*i.e.*, I($t + \tau$)] are independent of one another. On the other hand, they are closely related when the delay time is short. The correlation function, $g(\tau)$, which measures the probability of a particle travelling a given distance in a time τ, is given by:[77]

$$g(\tau) = \exp(-\tau/\tau_c) \tag{2.17}$$

where τ_c is related to the diffusion coefficient, D_0, of the particles:[77]

$$\tau_c = 1/D_0 q^2 \tag{2.18}$$

where q is the scattering vector. The diffusion coefficient is related to the particle size by the Stokes-Einstein equation:[77]

$$D_0 = \frac{kT}{3\pi\eta d_h} \tag{2.19}$$

By combining Equation (2.18) with (2.19), d_h is given by:

$$d_h = \left(\frac{kT}{3\pi\eta} \right) q^2 \tau_c \tag{2.20}$$

The diffusion coefficient can be obtained by measuring τ_c at various q values and plotting $1/\tau_c$ vs. q^2 for the determination of d_h.

2.4 Polymer Characterisation

2.4.1 Average Composition of Polymer Chains

The composition of the polymers was determined by ^{1}H NMR using a Varian spectrometer operating at 300 MHz. The samples were dissolved in $CDCl_3$ containing TMS as the reference in a dried NMR tube. The relative intensities of the peaks were determined from the relative peak areas after the base line was corrected.

Figures 2.5 to 2.7 show the spectra of NIPAM, PEGMA and MPEGMA (molar mass = 475 g/mol), respectively. The peaks in the δ 5.5 to 7 ppm region are indicative of the presence of vinyl groups in the monomers. The value of y, *i.e.*, number of EO repeat units in PEGMA or MPEGMA, was calculated according to Equation (2.21) and was found to be 7, 9 and 23 for PEGMA, MPEGMA (molar mass = 475 g/mol) and MPEGMA (molar mass = 1100 g/mol), respectively. Note that the nominal and experimental y values for the monomers were found to be similar to each other except for PEGMA, where the values differed by 1.

$$\frac{A_{3.7}}{A_{4.4}} = \frac{4y-2}{2} \tag{2.21}$$

where $A_{3.7}$ and $A_{4.4}$ are the areas of the EO protons at δ 3.7 and 4.4 ppm, respectively. The value of y is given by:

$$y = \left(\frac{A_{3.7}}{A_{4.4}} + 1 \right) \Big/ 2 \tag{2.22}$$

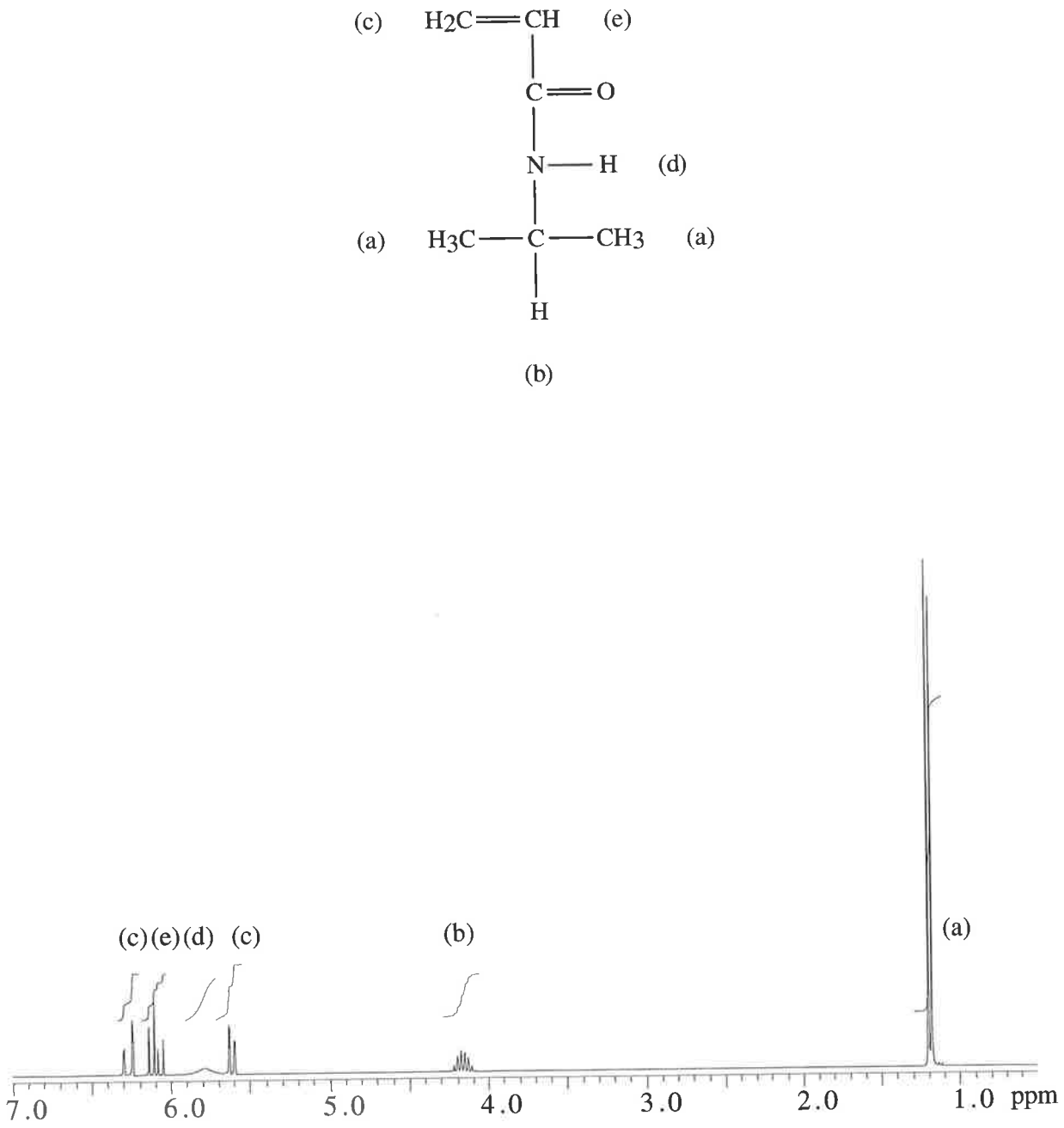

Figure 2.5: ^{1}H NMR spectrum of NIPAM in $CDCl_3$ at room temperature; (a) methyl protons of the N-isopropyl group, (b) lone proton of the N-isopropyl group, (c) methylene protons of the vinyl group, (d) proton of NH and (e) methyne proton of the vinyl group.

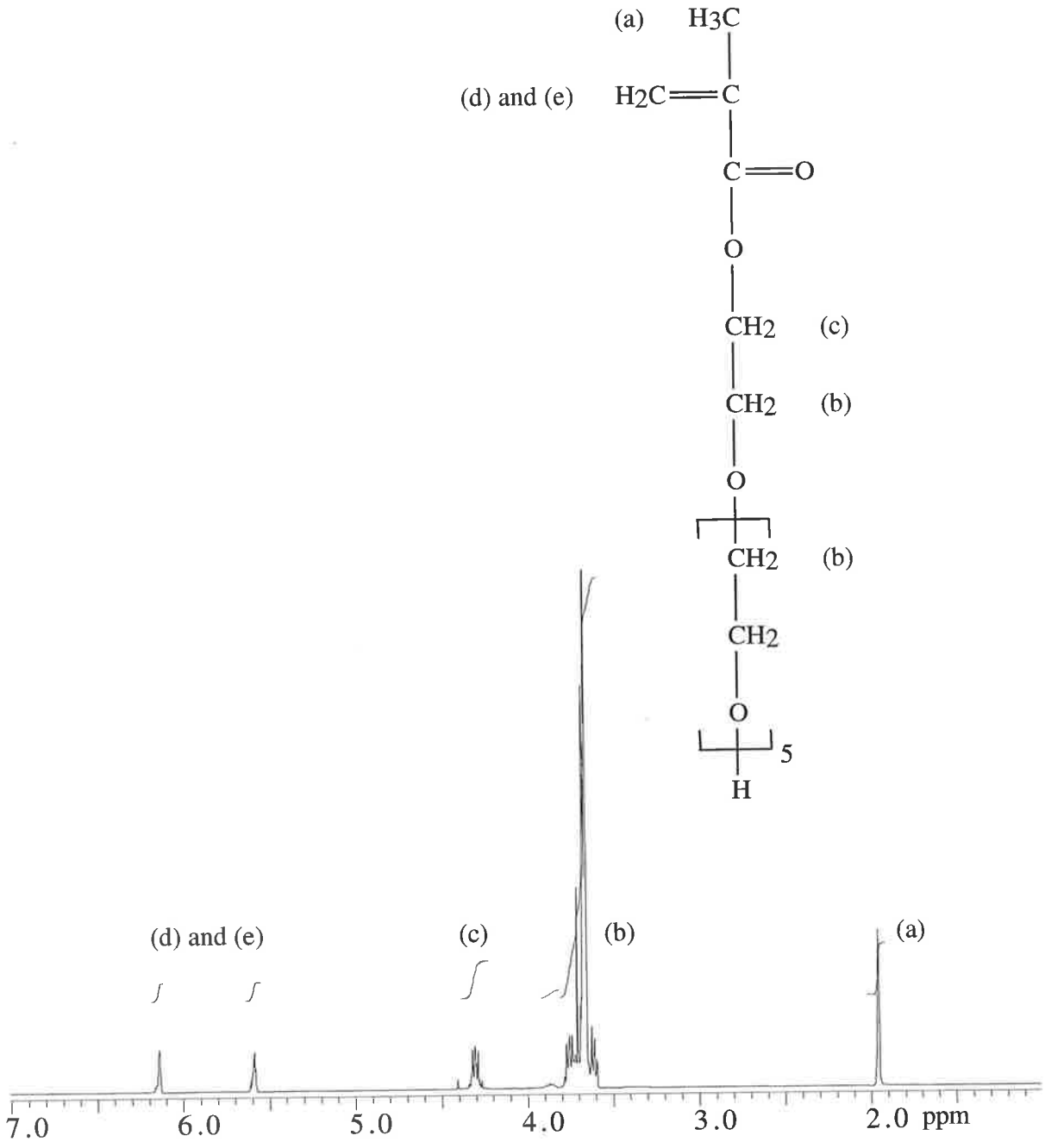

Figure 2.6: ^{1}H NMR spectrum of PEGMA in $CDCl_3$ at room temperature; (a) methyl protons, (b) EO protons, (c) methylene protons of the EO chain closest to carbonyl group, (d) and (e) methylene protons of the vinyl group.

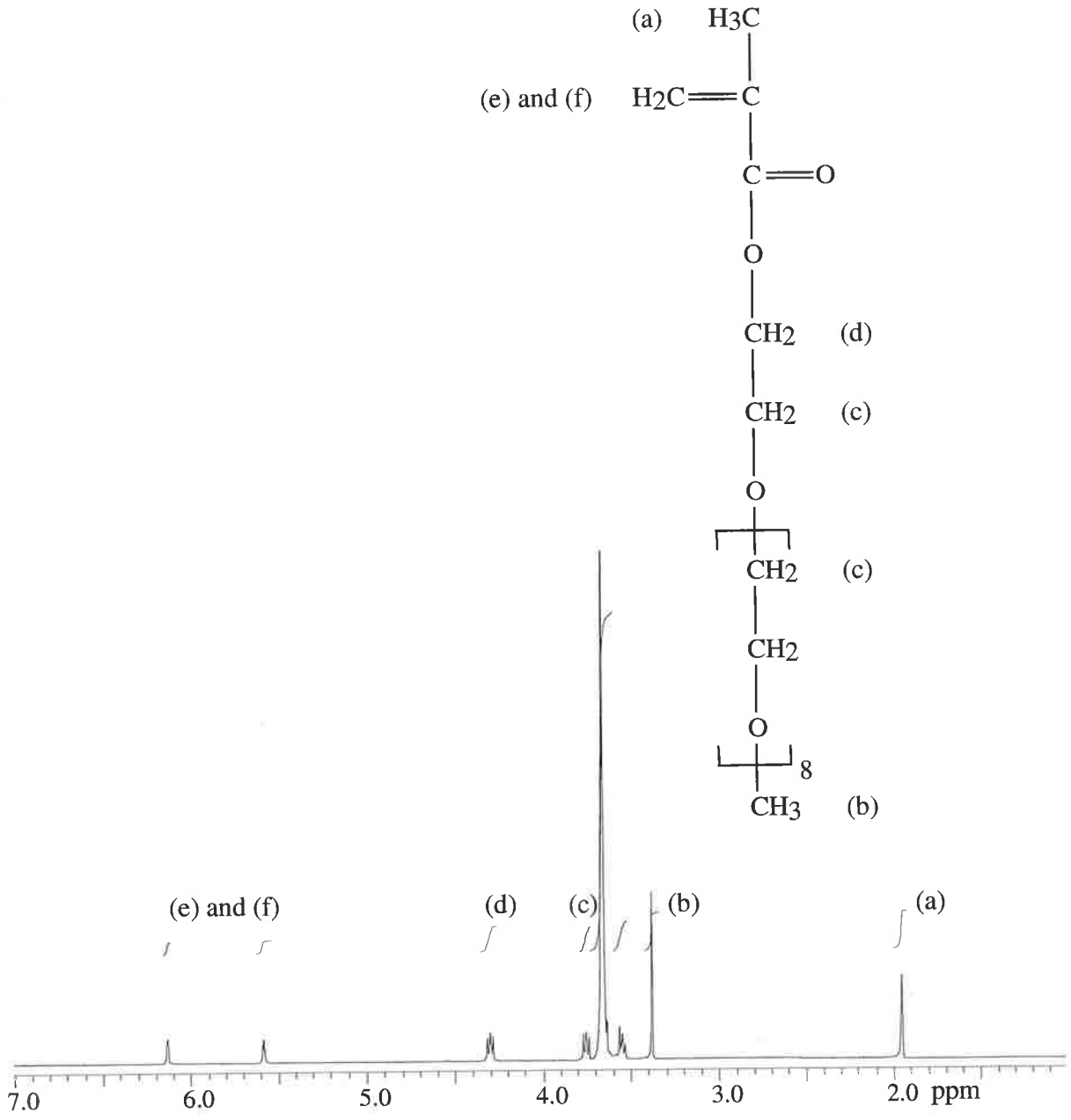

Figure 2.7: ^{1}H NMR spectrum of MPEGMA (molar mass = 475 g/mol) in $CDCl_3$ at room temperature; (a) methyl protons, (b) methoxy end group, (c) EO protons, (d) methylene protons of the EO chain closest to carbonyl group, (e) and (f) methylene protons of the vinyl group.

The spectra of poly(NIPAM) and poly(PEGMA) (Figures 2.8 and 2.9, respectively) show that the monomers have polymerised as indicated by the absence of vinyl peaks in the δ 5.5 to 6.5 ppm region (*cf.* spectra of NIPAM and PEGMA monomers in Figures 2.5 and 2.6, respectively). The spectrum for poly(NIPAM) is similar to that reported by Zeng *et al.*[78] who investigated the phase separation behaviour of poly(NIPAM) using NMR.

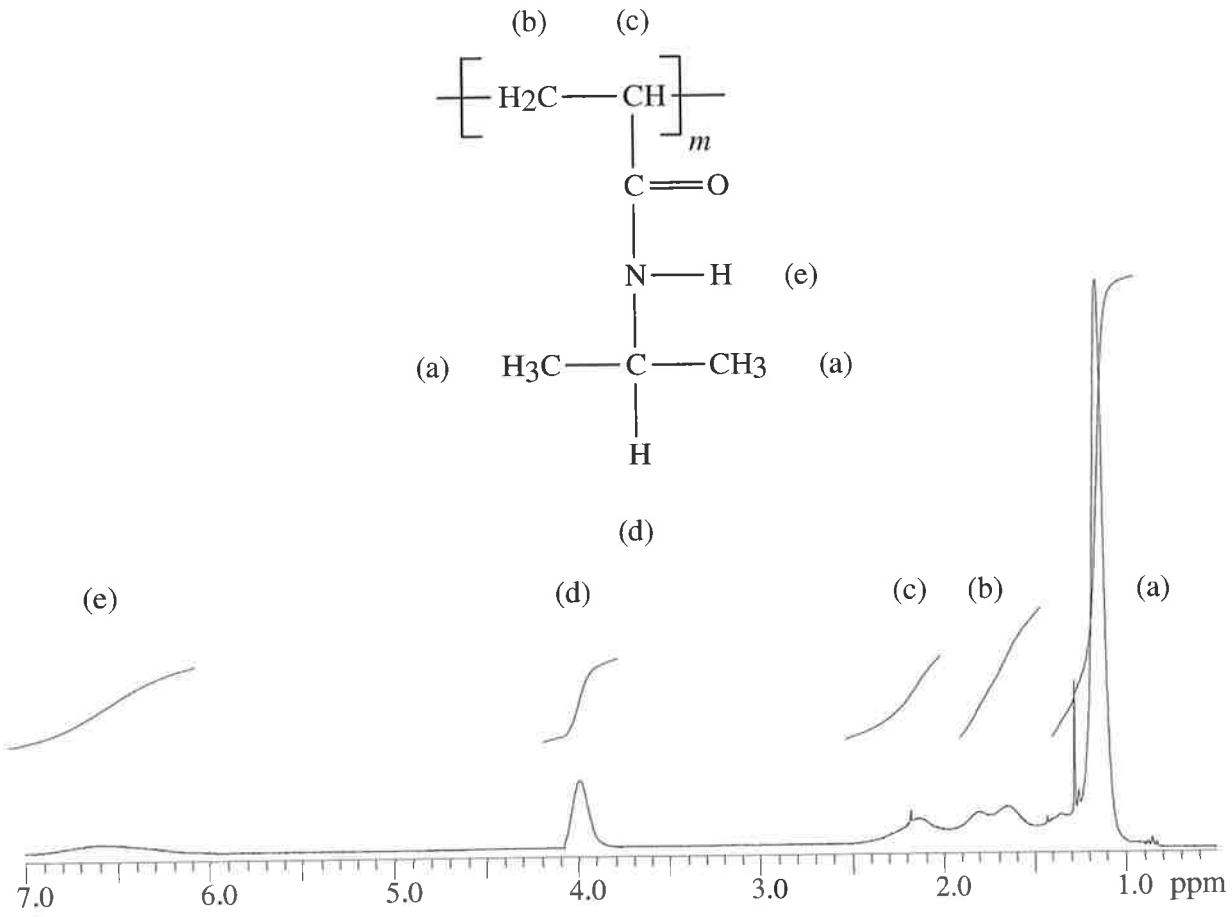

Figure 2.8: ^{1}H NMR spectrum of poly(NIPAM) in $CDCl_3$ at room temperature; (a) methyl protons of the isopropyl group, (b) methylene protons, (c) methyne protons, (d) lone proton of the N-isopropyl group and (e) proton of NH.

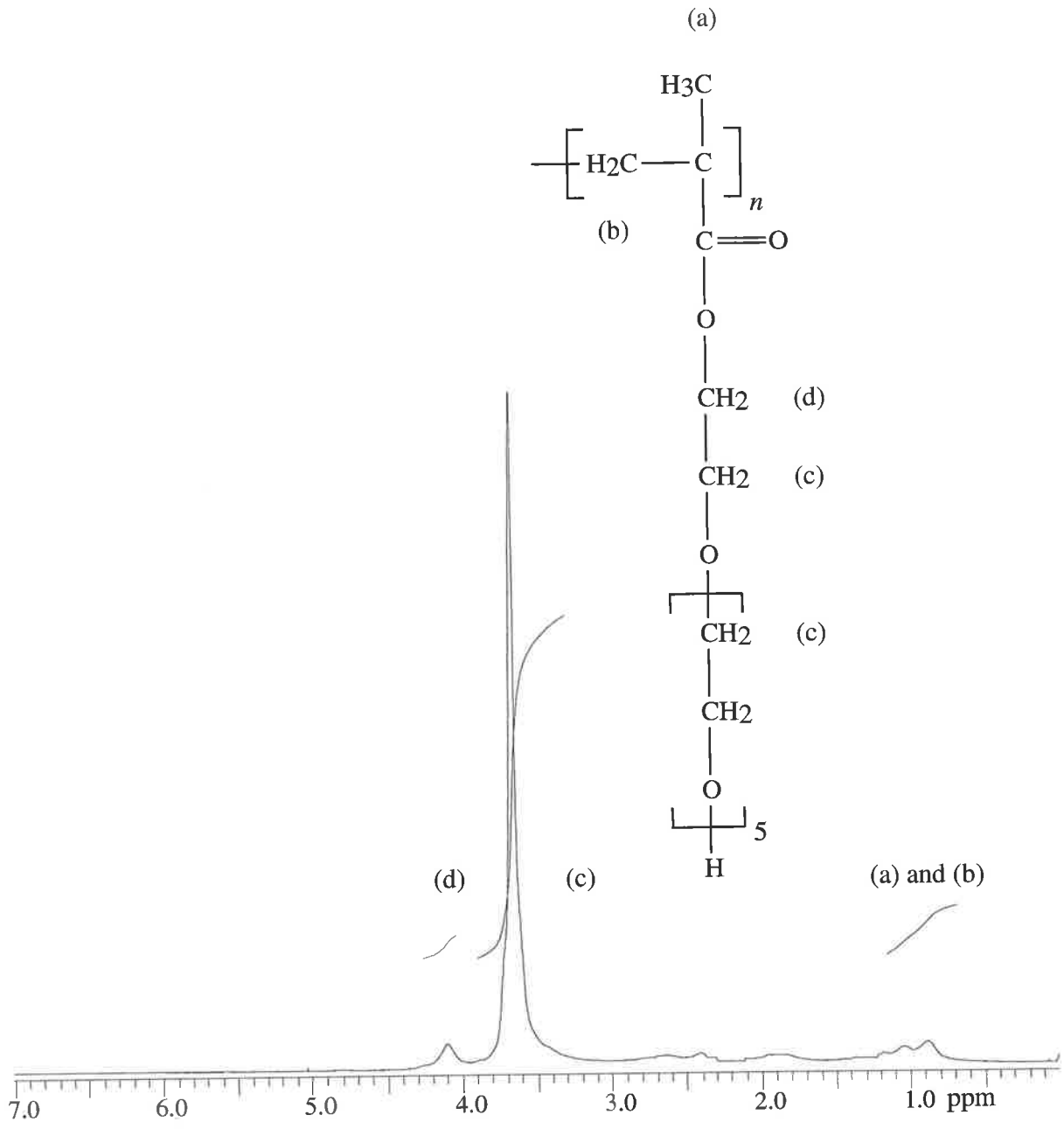

Figure 2.9: ^{1}H NMR spectrum of poly(PEGMA) in $CDCl_3$ at room temperature; (a) methyl protons, (b) methylene protons, (c) EO protons and (d) methylene protons of the EO chain closest to carbonyl group.

The representative ^{1}H spectra of the major copolymers are shown in Figures 2.10 and 2.11. The assignment of each proton shows that the ^{1}H NMR spectra are consistent with the expected copolymer structure depicted in Figure 2.1. The spectra contain several characteristic features that can be used to determine the composition of the copolymers. Typical assignments of the resonances are as follow. The peak at δ 1.2 ppm is due to the methyl protons of the N-isopropyl group. The poly(PEGMA) or poly(MPEGMA) backbone show resonances in the δ 1.5 to 2.3 ppm region.[79] The methylene and methyne protons of the poly(NIPAM) chain backbone are indicated by the relatively broad signal at δ 2.4 ppm. According to Qiu and Wu[80] the signals from the poly(NIPAM) backbone are separated by δ 0.1 ppm. The EO protons (except for the methylene protons closest to the carbonyl group) appear at δ 3.7 ppm. The peak at δ 4.0 ppm can be attributed to the methine protons of the isopropyl group and the EO protons closest to the carbonyl group. The proton of NH appears at δ 6.5 ppm.

The composition of the copolymers was determined from the relative areas (integration) of the methine protons of the isopropyl group [assignment (g) in Figure 2.10] and the EO protons closest to the carbonyl group at δ 4.0 ppm, A_B, and the EO protons at δ 3.7 ppm, A_C. This is shown mathematically in Equation (2.23).

$$\frac{A_B}{A_C} = \frac{\text{area of methine and oxyethylene protons at } \delta \text{ 4.0 ppm}}{\text{area of oxyethylene protons at } \delta \text{ 3.7 ppm}} = \frac{m+2n}{(4y-2)n} \qquad (2.23)$$

The number of NIPAM to PEGMA or MPEGMA repeat unit ratio in the copolymers (*i.e.*, *m*/*n*) can be obtained by rearranging Equation (2.23) to give:

$$\frac{m}{n} = \left[\left(\frac{A_B}{A_C}\right)(4y-2)\right] - 2 \qquad (2.24)$$

The mol% NIPAM in the copolymers was calculated using Equation (2.25).

$$\text{mol\% NIPAM in copolymer} = \frac{m}{m+n} \times 100 \qquad (2.25)$$

For example, in the case of P2 there are *ca.* seven NIPAM units per PEGMA unit, *i.e.*, $m/n = 7$. Thus, mol% NIPAM = [7/(7 + 1) x 100] = 88 %. Table 2.4 shows the data and analysis obtained from the ^{1}H NMR spectra of the copolymers.

Table 2.4: ^{1}H NMR results for the copolymers

Identification	Target mol% NIPAM[a]	Experimental y[b]	A_B/A_C[c]	m/n[d]	Mol% NIPAM in copolymer[e]
P1	95	7	1.06	21.46	96
P2	86	7	0.41	7.06	88
P2A	86	7	0.38	6.30	86
P2B	86	7	0.39	6.57	87
P2C	86	7	0.42	7.22	88
P2D	86	7	0.44	7.60	88
P3	67	7	0.18	1.97	66
MP1	86	9	0.30	9.54	91
MP2	86	23	0.23	20.34	95

[a] From Table 2.1. [b] Based on spectra of the monomers and calculated according to Equation (2.21). [c] Calculated using Equation (2.23). [d] Calculated using Equation (2.24). [e] Calculated using Equation (2.25).

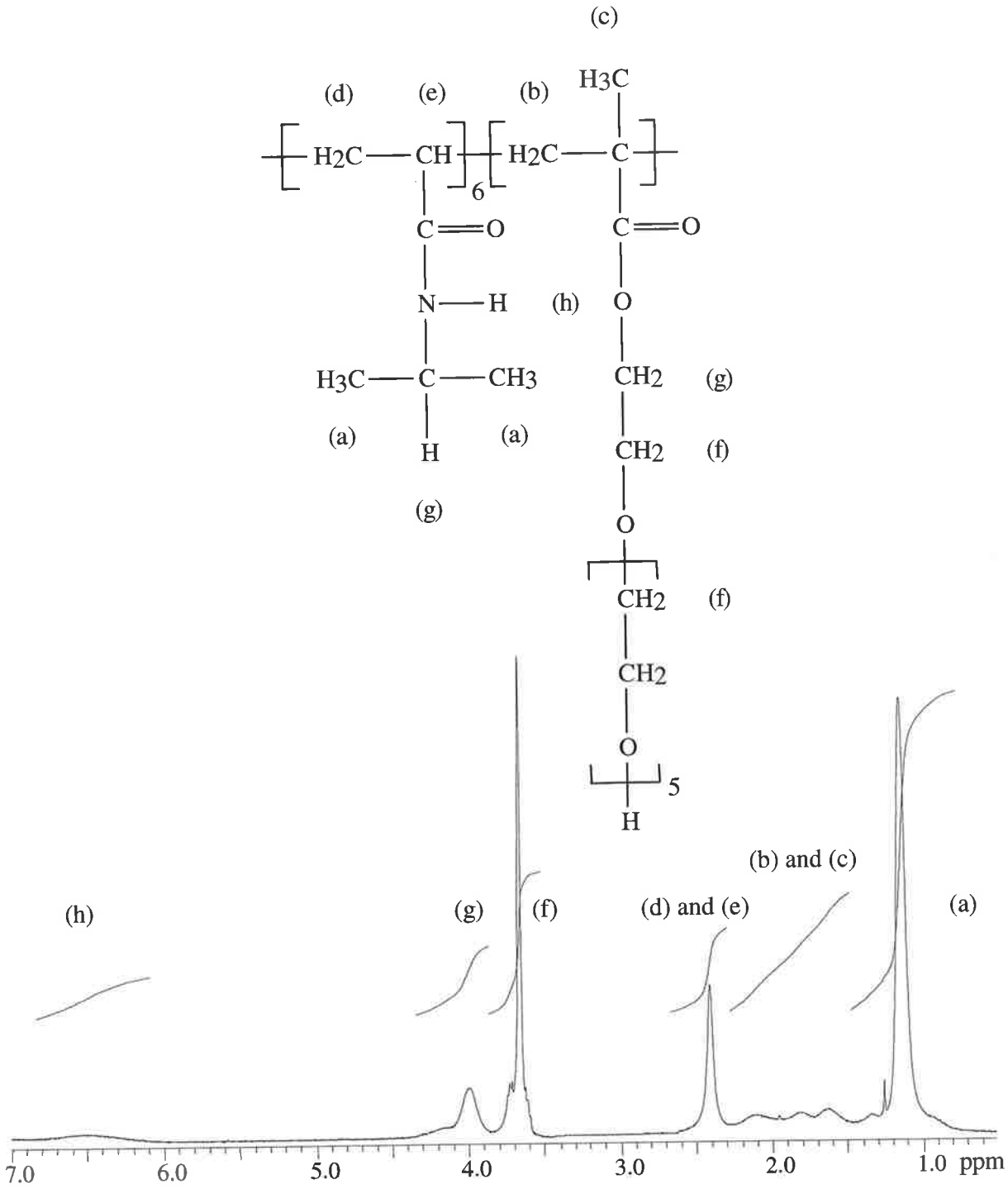

Figure 2.10: ^{1}H NMR spectrum of P2 in $CDCl_3$ at room temperature.

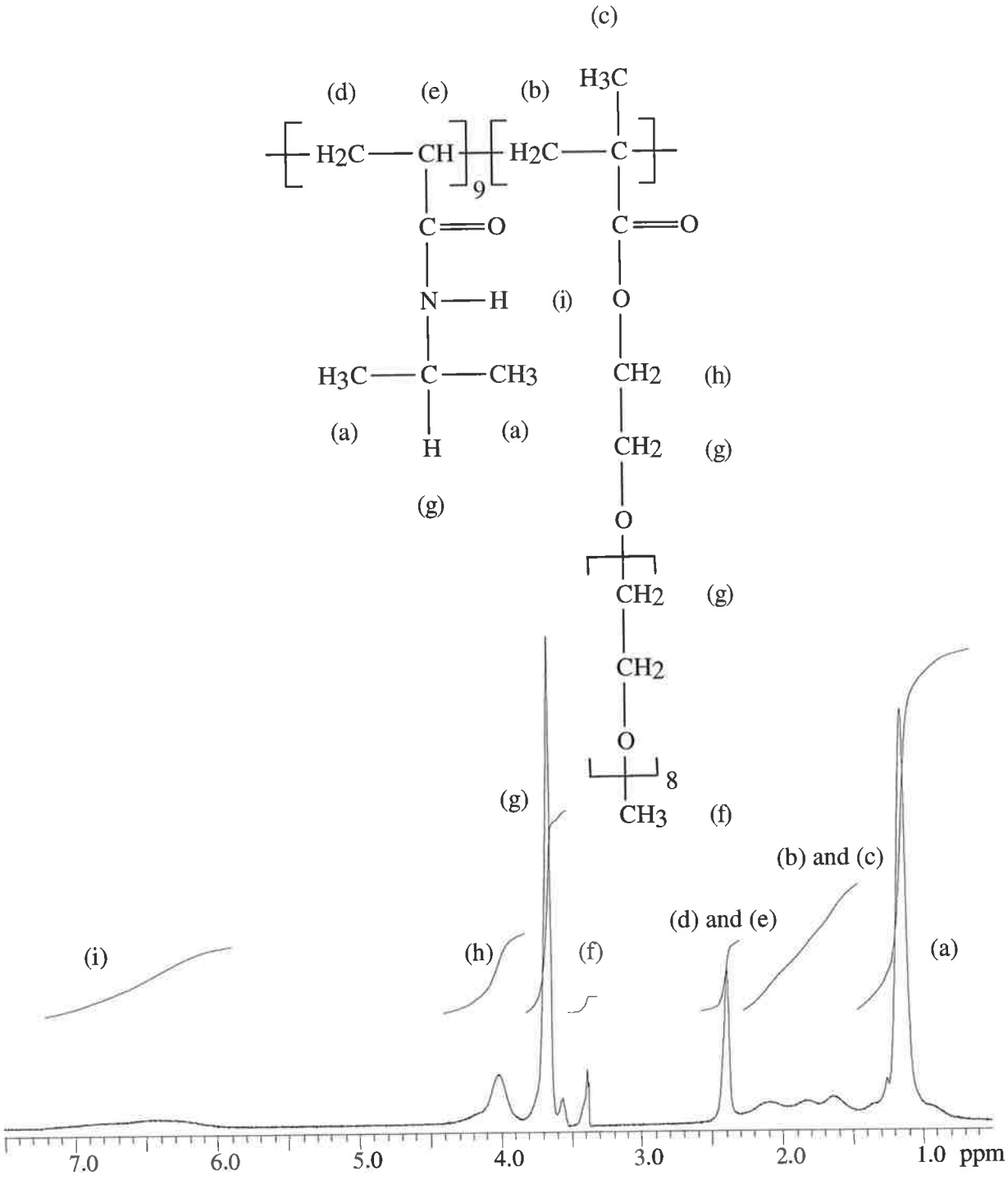

Figure 2.11: ^{1}H NMR spectrum of MP1 in $CDCl_3$ at room temperature.

Examination of the data in Table 2.4 revealed that the mol% NIPAM in the copolymers corresponds closely to the target composition regardless of the synthetic approach employed, although in general the former is slightly higher than the latter. This could be due to the more reactive nature of NIPAM monomer over PEGMA or MPEGMA monomers (later). This is illustrated more clearly in Figure 2.12, which shows the relationship between the target mol% NIPAM and the compositions of the P1, P2 and P3 copolymers.

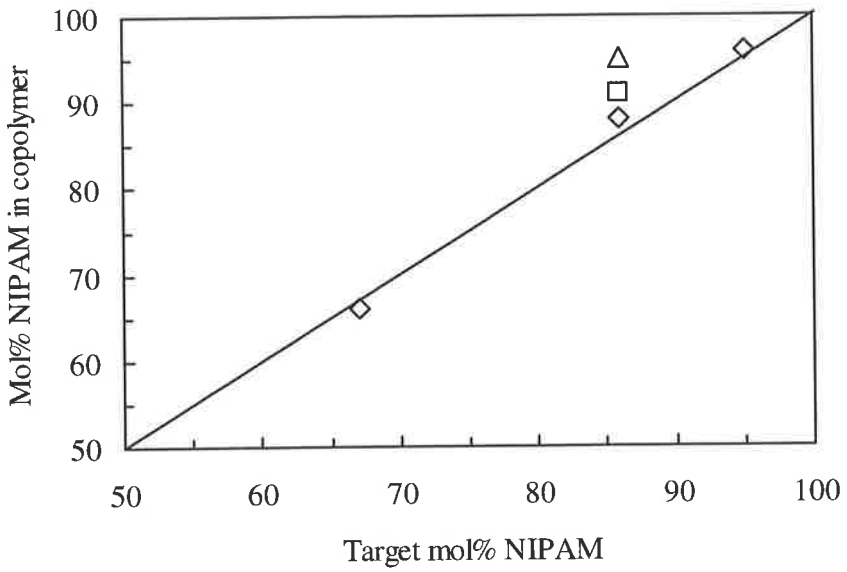

Figure 2.12: Mol% NIPAM in the poly(NIPAM-*co*-PEGMA) copolymers (◇) as a function of target mol% NIPAM. Also shown are the data for MP1 (□) and MP2 (Δ). The diagonal solid line corresponds to equality of the copolymer and monomer composition.

2.4.2 Molar Mass Studies

The weight average molar mass, M_w, and number average molar mass, M_n, of the polymers were obtained from GPC using Waters Styragel columns. THF and dimethylformamide were used as the eluent and the columns were calibrated with polystyrene and PEG/PEO equivalent standards. The breadth of the distribution or polydispersity, PD, was obtained from the ratio of M_w to M_n, while the *m* and *n* values for the copolymers were calculated based on ^1H NMR and GPC data. These results are tabulated in Table 2.5. Although obtaining good quality GPC results is challenging for poly(NIPAM) due to filtration problems prior to analysis as a result of chain entanglement,[81,82] several researches have found success employing this instrument for their poly(NIPAM) systems. Hasan and co-workers[3] determined the molecular mass and PD of their graft copolymers based on poly(ethylene oxide-*co*-glycidol) backbone and relatively short grafts of poly(NIPAM) using GPC. Schild and Tirell[9] investigated the molecular architecture dependence of the LCST using a sensitive solution microcalorimeter. They characterised the poly(NIPAM) samples synthesised from a number of methods and having varying chain length using GPC.

The characteristics and properties of the polymers are tabulated in Table 2.5. The relatively high PD of poly(PEGMA) could be due to the tendency for the PEG chains to self aggregate, giving rise to an uneven distribution of chain lengths, *i.e.*, high proportion of long and short chains. This is supported from visual inspection of the synthesised homopolymers which showed the presence of a gel. The low PD of P2A, P2B and P2C is due to the synthetic approached employed, in that the copolymers were prepared by having the monomers in the feed. This resulted in an even distribution of the monomers along the polymer chain. In contrast, the relatively high PD of P2 is a consequence of the high proportion of PEGMA and NIPAM in

the mixture during the initial and latter stages of the reaction, respectively. The very high PD for P2D could be a result of the different solvent and initiator used for its synthesis compared to that used for the other copolymers. Xue *et al.*[83] conducted copolymerisation of NIPAM with AAc and found that the extent of reaction was dependent on the choice and concentration of the solvent and initiator, as well as temperature and reaction time employed. Except for P2C, the reasonably close M_n for poly(NIPAM), P2, P2A, P2B, MP1 and MP2 could be attributed to the similarity in the monomer to initiator mole ratio for the preparation of these polymers, since the concentration of initiator used governs the length of the polymer chain formed (Section 1.1.2).

Table 2.5: Characteristics and properties of the polymer samples

Sample	Identification	Yield (%)	Mol% NIPAM in copolymer[a]	M_n[b] (g/mol)	PD	m[c]	n[c]	y[d]	LCST (°C)[e]	Gel content (%)[b]	τ/c_p at 25°C[f]
Poly(NIPAM)		94	100	41700	2.3	370	0	-	33 ± 3	4	50
Poly(PEGMA)		90	0	43000	3.0	0	120	6	-		-
Poly(NIPAM-*co*-PEGMA)	P1	50	96					6	35 ± 5		55
Poly(NIPAM-*co*-PEGMA)	P2	50	88	44600	2.9	270	40	6	35 ± 5	-	130
Poly(NIPAM-*co*-PEGMA)	P2A	46	86	34500	2.2	200	30	6	39 ± 6	1	70
Poly(NIPAM-*co*-PEGMA)	P2B	38	87	14900	1.4	90	15	6	40 ± 3	1	5
Poly(NIPAM-*co*-PEGMA)	P2C	30	88	45900	2.6	280	40	6		15	
Poly(NIPAM-*co*-PEGMA)	P2D	20	88	132100	11.6	800	100	6	36 ± 4	1	160
Poly(NIPAM-*co*-PEGMA)	P3	75	66					6	48 ± 5		1650
Poly(NIPAM-*co*-MPEGMA)	MP1	78	91	46000	2.2	280	30	9	38 ± 3		190
Poly(NIPAM-*co*-MPEGMA)	MP2	60	95	50000	2.3	300	15	23	36 ± 1		330

[a] From Table 2.4. [b] Determined by GPC. [c] Based on *m/n* and M_n from ^{1}H NMR (Table 2.4) and GPC data, respectively. [d] Based on supplier's information. [e] Obtained from turbidity measurements. [f] c_p = Concentration of polymer (g/ml).

2.4.3 Critical Overlap Concentration Studies

The values for the copolymer concentration are related to [η] by the following equation:[1]

$$\eta_{sp} = k_0[\eta]c_p + k_1[\eta]^2 c_p^{\,2} + k_2[\eta]^3 c_p^{\,3} + \ldots\ldots \quad (2.26)$$

where k_0, k_1, k_2, *etc.* are constants. Equation (2.26) can be truncated and rearranged to give the Huggins equation:[1]

$$\eta_{red} = [\eta] + k_H[\eta]^2 c_p \quad (2.27)$$

where k_H is the Huggins constant. An alternative to the Huggins equation is the expression given by Kraemer:[1]

$$\eta_{inh} = [\eta] + k_K[\eta]^2 c_p \quad (2.28)$$

where k_K is the Kraemer constant. Thus, [η] can be determined from the dual extrapolation of the data obtained at a series of polymer concentrations according to the Huggins and Kraemer equations, *i.e.*, the average intercept gives [η]. The intrinsic viscosity is related to c_p^* by:[7]

$$c_p^* = \frac{1.08}{[\eta]} \quad (2.29)$$

The change in viscosity as a function of concentration for P2 was measured using an Ostwald viscometer (Figure 2.3) in order to obtain c_p^* for the copolymer. Samples were left to

equilibrate in the temperature controlled water bath for 0.5 hours prior to measurement. The average value was taken from the three runs performed for each measurement. As can be seen from Figure 2.13, the average y-intercept gives [η] = 120 ml/g. Using Equation (2.29) the critical overlap concentration at 25°C for P2 was found to be *ca.* 0.01 g/ml. Thus, below this concentration, the polymer chains can be viewed as having infinite dilution radii. Above 0.01g/ml the chains begin to overlap and entangle with one another. In other words, c_p^* = 0.01g/ml demarcates the boundary between dilute and semi-dilute regions for P2 (Section 1.1.4.2).

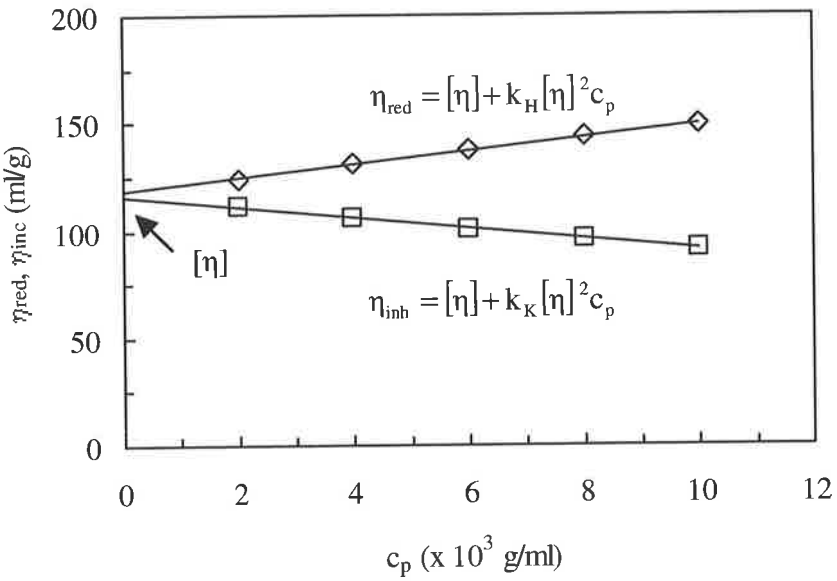

Figure 2.13: Determination of intrinsic viscosity, [η], for P2 at 25°C using a dual Huggins-Kraemer plot. The correlation coefficient, R^2, values for both plots were greater than 0.994. Using [η] = 120 ml/g and Equation (2.29), c_p^* at 25°C for P2 is *ca.* 0.01 g/ml.

2.4.4 Lower Critical Solution Temperature Measurements

The phase transition as a function of temperature for the polymers was monitored by the OD at 600 nm using a 1 cm sample cell referenced against milli-Q water. A Cary 2200 UV-visible spectrophotometer was used for the measurements. Samples (0.5 wt%) were heated at a rate of 0.5°C min.$^{-1}$ in a thermally controlled cell holder. Figure 2.14 shows the variation of τ vs. T for poly(NIPAM) and P2. Turbidity curves for P1 and P3 are shown for comparison.

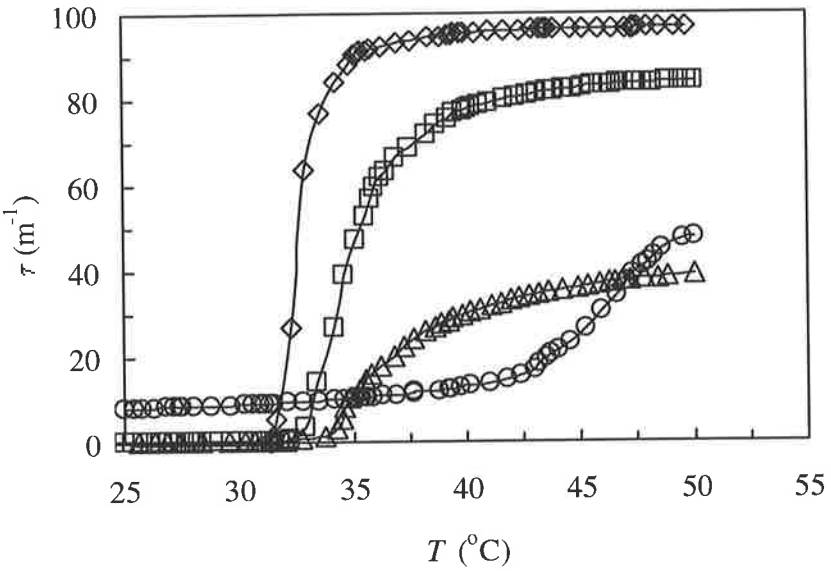

Figure 2.14: Variation of the turbidity (measured at λ = 600 nm) with temperature for the polymer solutions (0.5 wt%); (◇) poly(NIPAM), (□) P1, (Δ) P2 and (○) P3.

The increase in turbidity with temperature for all the samples is consistent with that reported in the literature for polymers having similar structures.[9,26] This behaviour is attributed to the collapse of the NIPAM segments as a result of hydrophobic interactions as temperature

increases. The increased turbidity upon collapse of the polymer chains can be explained by examining Equation (2.15). If it is assumed that $m_r \geq 1$ for all cases, at room temperature where the polymer chains are well solvated in solution and $m_r \sim 1$, then $\tau = 0$ since the term inside the brackets, *i.e.*, $[(m_r^2 - 1)/(m_r^2 + 1)], \sim 0$. On the other hand, as temperature increases, $m_r \rightarrow m_{max}$ (note that $m_{max} = m_{polymer}/m_{water}$), which increases the turbidity of the sample. Note that the slight increase in turbidity at low temperatures for P3 compared to the rest of the samples can be attributed to the former having a high proportion of PEGMA, which might have given rise to a high gel content. The LCST for the polymers were taken as the point of inflection on the curves in Figure 2.14, *i.e.*, the point at which $d\tau/dT$ is at a maximum. The data are tabulated in Table 2.5 and shown graphically in Figure 2.15. The arrows in Figure 2.15 show the LCST for the polymers.

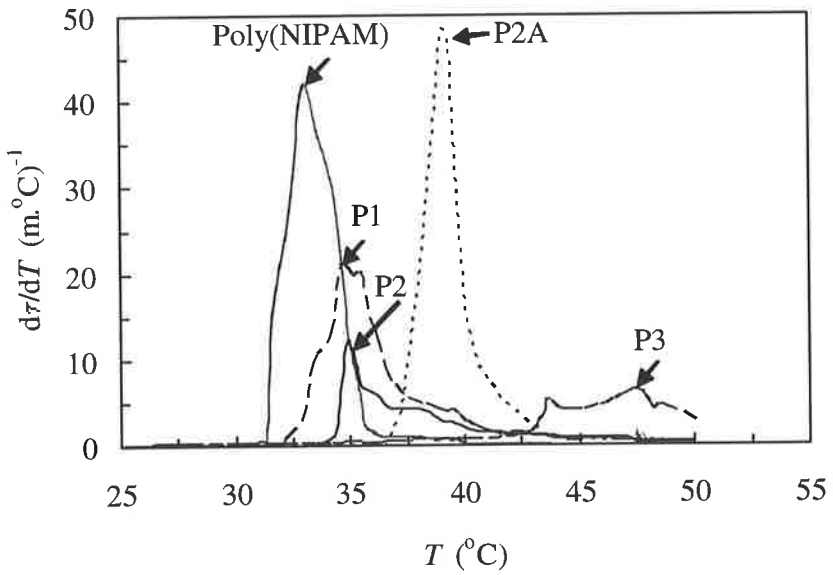

Figure 2.15: First derivative, $d\tau/dT$, vs. temperature for the polymers in Figure 2.14. The LCST is taken at the point where $d\tau/dT$ is at a maximum (indicated by the arrow).

The LCST of the copolymers is shifted to higher temperatures compared to the value for poly(NIPAM), indicating that the PEGMA units are dispersed along the copolymer chains. According to several workers,[26,30,40,84] increase in the hydrophilicity of the repeat unit by structural modification, in this case by incorporating PEGMA units into the polymers, increases the LCST of poly(acrylamide)s. The competition between hydrophobic interactions in NIPAM and the solubilising effect of the EO units can be observed indirectly by comparing the LCST of a particular series of polymers having different mol% NIPAM. This is shown schematically in Figure 2.16. Decreasing the mol% of NIPAM (or increasing mol% PEGMA) increases the LCST of the copolymer due to the larger number of PEGMA units present that is able to retard the collapse of the NIPAM segments more extensively as temperature increases. Note that the effect is most pronounced when mol% NIPAM < 70%.

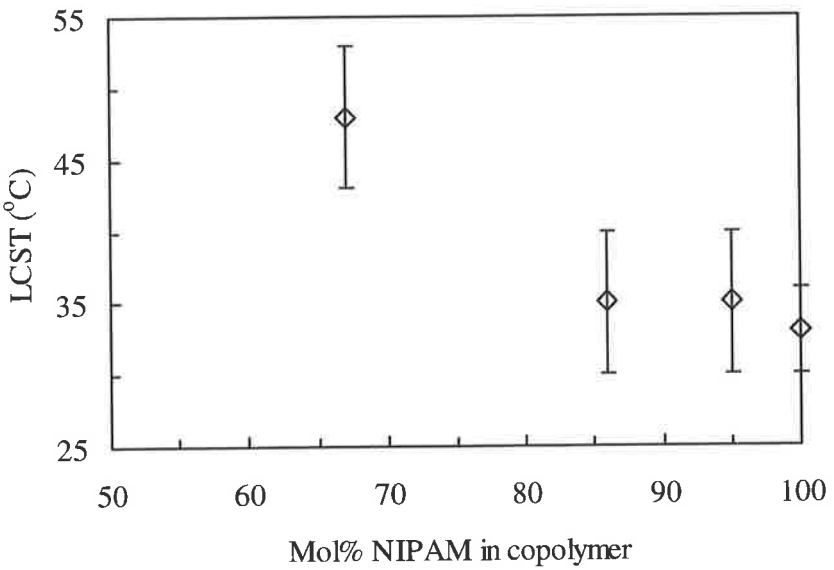

Figure 2.16: Plot of LCST vs. mol% NIPAM for the polymers in Figure 2.14. 100% = poly(NIPAM), 95% = P1, 86% = P2 and 67% = P3.

The reasonable symmetry and relative narrowness of the plot in Figure 2.15 suggests a single LCST for poly(NIPAM), while for the copolymers the presence of a broad shoulder of the first derivative plots extending to higher temperatures indicates a range of LCSTs. Thus, the copolymers are compositionally asymmetric and collapse of the chains continues above the LCST for poly(NIPAM). This is congruent with the manner in which these copolymers were prepared, *i.e.*, NIPAM-feed method (Table 2.1). In contrast, copolymers prepared from the dual-feed method, *e.g.*, P2A and P2B, which yielded symmetrical copolymers (indicated by the low PD), showed a single LCST as indicated by the symmetry of the first derivative plots.

The first derivative, $d\tau/dT$, vs. temperature plots for the poly(NIPAM-*co*-MPEGMA) copolymers are shown in Figure 2.17. As in the case with P2, the high shoulder of the first derivative plot extending to high temperatures indicates a range of LCSTs for MP1. This points to the copolymer being compositionally asymmetric. On the other hand, MP2 showed a more symmetric composition. This is expected since the copolymer is comprised of large proportion of poly(NIPAM) chains separated by a smaller number of MPEGMA units [from Table 2.4 *m/n* is *ca.* 20 (*cf.* $m/n = 10$ for MP1)].

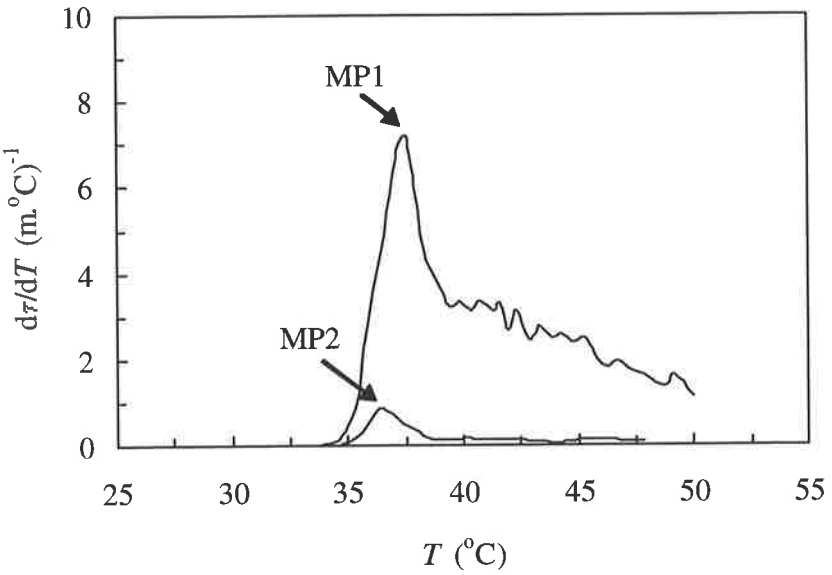

Figure 2.17: First derivative, dτ/d*T*, vs. temperature for MP1 and MP2. The LCST is taken at the point where dτ/dT is at a maximum (indicated by the arrow).

2.5 Polymer Chain Composition

2.5.1 Reactivity Ratio Determination

Knowledge of the monomer reactivity ratios is necessary in order to predict copolymer compositions [see Equation (1.5)]. If it is assumed that the drift in copolymer composition is negligible at low monomer conversions (*ca.* 5%) and the instantaneous composition is approximately equal to the composition in the accumulated copolymer, then the composition of copolymers formed at low conversions can be employed for the determination of the reactivity ratio of the monomers.

In this work, the monomer reactivity ratio of NIPAM (r_{NIPAM}) and PEGMA (r_{PEGMA}) were determined from the compositions of the poly(NIPAM-*co*-PEGMA) copolymers formed at low conversions (*ca.* 5%) in a series of copolymerisations performed using solutions of known initial comonomer compositions.

The synthetic approach adopted for the preparation of the copolymers was different to the methods described in Section 2.2.2, since a batch method was used in the former. A representative synthesis for the copolymers is as follows. For the target copolymer having a mole fraction of NIPAM, f_{NIPAM}, of 0.86, NIPAM (0.65 g) and PEGMA (0.35 g) monomers (in this case the mole fraction of NIPAM in the feed, f_{NIPAM}, is 0.86) in *tert*-butyl alcohol (10 ml) were added to a nitrogen purged 250 ml round-bottomed flask equipped with a burette, Teflon stirrer blade, condenser, thermometer and nitrogen inlet. The stirred solution was allowed to degas for 0.5 hours before the mixture was heated to 80°C under nitrogen. AIBN (0.006 g) was then added to the mixture. Hydroquinone (0.08 wt%) was added to the reaction mixture to terminate the reaction after 3 min. of reflux (preliminary experiments showed that a yield of around 5% was obtained when the reaction was stopped during this time, regardless of the initial comonomer

composition). The mixture was allowed to cool and then added dropwise to 0.4 litre of diethyl ether with constant vigorous stirring. The white solid that precipitated was redissolved in minimal amounts of *tert*-butyl alcohol before adding the product dropwise to 0.4 litre of diethyl ether with constant vigorous stirring. The precipitated product was then left to dry overnight. Although the copolymers were not dialysed, ^{1}H NMR spectra showed absence of NIPAM and PEGMA monomers in the products, *i.e.*, absence of vinyl peaks in the δ 5.5 to 6.5 ppm region. From the ^{1}H NMR spectra the composition of the copolymers were calculated using Equations (2.23) and (2.24). The results are tabulated in Table 2.6.

Table 2.6: Compositions of poly(NIPAM-*co*-PEGMA) copolymers used to determine the reactivity ratio of NIPAM and PEGMA monomers

f_{NIPAM}	Yield (%)	A_B/A_C[a]	m/n[b]	F_{NIPAM}[c]
0.86	5	0.40	6.7	0.87
0.75	4	0.24	3.2	0.76
0.65	4	0.19	2.2	0.69
0.50	5	0.15	1.2	0.55
0.45	4	0.14	1.0	0.51
0.35	4	0.13	0.7	0.42
0.25	4	0.12	0.6	0.36

[a] Calculated according to Equation (2.23). [b] Calculated according to Equation (2.24).[c] $F_{NIPAM} = m/(m + n)$.

The reactivity ratio of the monomers was determined from the data shown in Table 2.6 (*i.e.*, variation of F_{NIPAM} with f_{NIPAM} at low conversions) using the rearranged form of the Lewis-Mayo equation [Equations (1.7)]. Note that the subscripts A and B in Equation (1.7) correspond to NIPAM and PEGMA, respectively. The data points were fitted to a straight line, from which the slope gave r_{NIPAM} and the intercept r_{PEGMA}. The plot shown in Figure 2.18 gives $r_{NIPAM} = 1.05$ and $r_{PEGMA} = 0.63$.

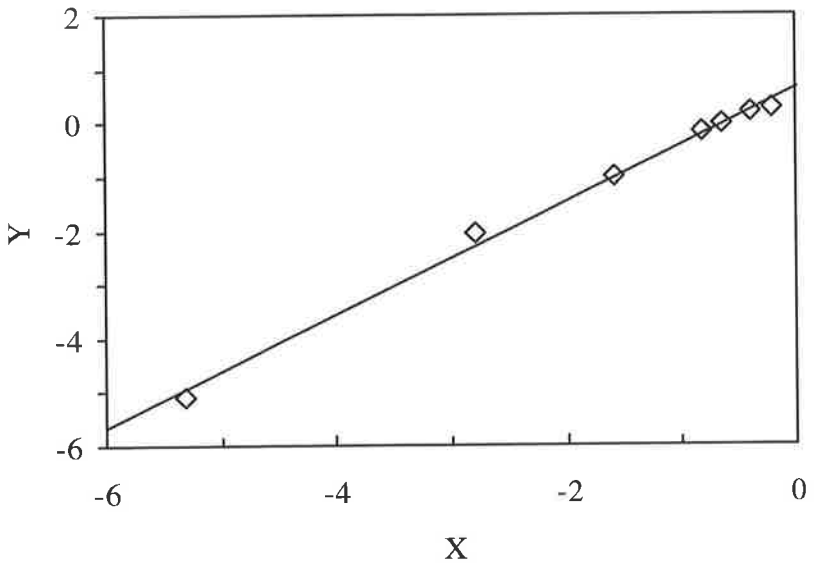

Figure 2.18: Monomer reactivity ratio determined from the rearranged form of the Lewis-Mayo equation [Equation (1.7)] for the copolymerisation of NIPAM with PEGMA. The slope gives r_{NIPAM} and the intercept r_{PEGMA}, *i.e.*, $Y = r_{PEGMA} + Xr_{NIPAM}$. The fit gave R^2 value of *ca.* 0.995.

This method for determining the monomer reactivity ratios was compared to the procedures developed by Kelen-Tudos[85] which is based on the Lewis-Mayo model [Equation (1.5)] and can be expressed by:[85]

$$\eta' = r_A \xi - \frac{r_B}{\alpha}(1-\xi) \tag{2.30}$$

where the subscript A corresponds to the NIPAM monomer while the subscript B is for PEGMA. Note that η' and ξ are mathematical functions of mole compositions of the monomers in the feed and copolymer, respectively. These parameters are defined as:

$$\eta' = \frac{G}{\alpha + H'} \qquad \text{and} \qquad \xi = \frac{H'}{\alpha + H'} \tag{2.31}$$

where

$$G = \frac{f_A(F-1)}{F_A} \quad , \quad H' = \frac{f_A^{\,2}}{F_A} \quad , \quad \alpha = \sqrt{H'_{min} \times H'_{max}} \tag{2.32}$$

From Equation (2.30), a plot of η' vs. ξ yields r_A as the value of η' (at $\xi = 1$). The value for $-r_B/\alpha$ is obtained from the extrapolated intercept at $\xi = 0$ (Figure 2.19). From the plot $r_{NIPAM} = 0.98$ and $r_{PEGMA} = 0.54$.

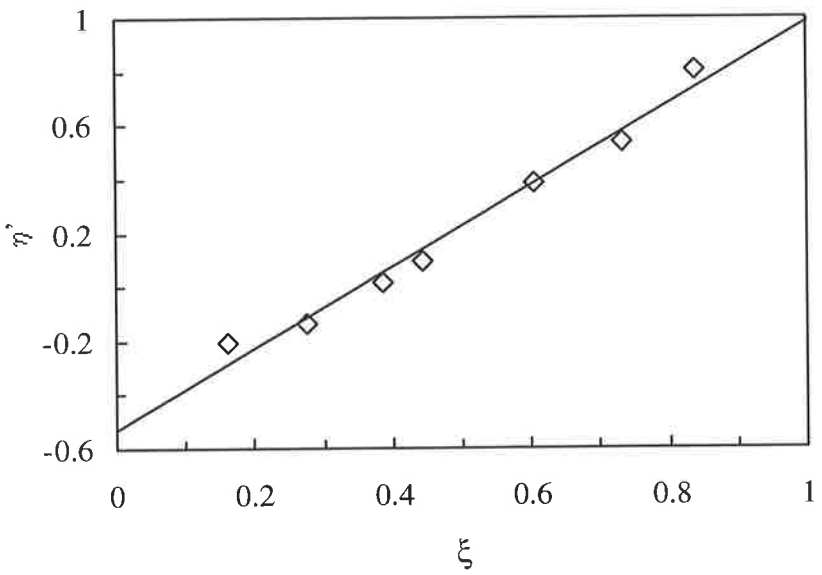

Figure 2.19: Determination of the reactivity ratios by the Kelen-Tudos method [Equation (2.30)] for the copolymerisation of NIPAM with PEGMA.

The monomer reactivity ratio values obtained from these methods are tabulated in Table 2.7. As can be seen, the values are similar for each of the methods employed. This can be attributed to the procedures which are based on the terminal model, *i.e.*, polymer chain growth is dependent only on the nature of the terminal monomer unit (Section 1.1.3). Thus, the reactivity ratio for the monomers was obtained from the Lewis-Mayo method (see Figure 2.18).

Table 2.7: Monomer reactivity ratios of NIPAM with PEGMA

Method	R^2	r_{NIPAM}	r_{PEGMA}
Lewis-Mayo	0.995	1.05	0.63
Kelen-Tudos	0.982	0.98	0.54

The relatively high value for r_{NIPAM} indicates a more pronounced tendency for this monomer to react with itself, *i.e.*, homopolymerise, while the lower value for PEGMA shows a tendency of it to copolymerisation. This can be attributed to the fact that the reactivity of a particular monomer is influenced by the ability of its substituent group(s) to stabilise the corresponding polymeric radical thorough resonance, polar or steric effects. The greater the stability of the radical, the more readily the radical is formed. Thus, the reactivity of a particular monomer is greatest when the polymeric radical is most stable (and unreactive) and vice versa. Looking at the monomer structures (Figures 2.5 and 2.6), it can be seen that the radical produced in NIPAM will be more stable than that for PEGMA since the former has an amide group which is electron withdrawing. In other words, the substituent groups of NIPAM are more effective in aiding delocalisation of the radical compared to PEGMA. This makes NIPAM a more reactive monomer than PEGMA.[86] The monomer reactivity ratios (Table 2.7) suggest that the distribution of the two monomers in the copolymers will tend toward a blocky character with high content of the NIPAM monomer in the early stages of copolymerisation.

Having determined the reactivity ratio values on the basis of the terminal model [Equation (1.5)], the mole fractions of the monomers in the poly(NIPAM-*co*-PEGMA) copolymer for a range of initial comonomer compositions were calculated. The results shown in Figure 2.20 indicate that for the present system, $F_{NIPAM} > f_{NIPAM}$ throughout the entire composition range.

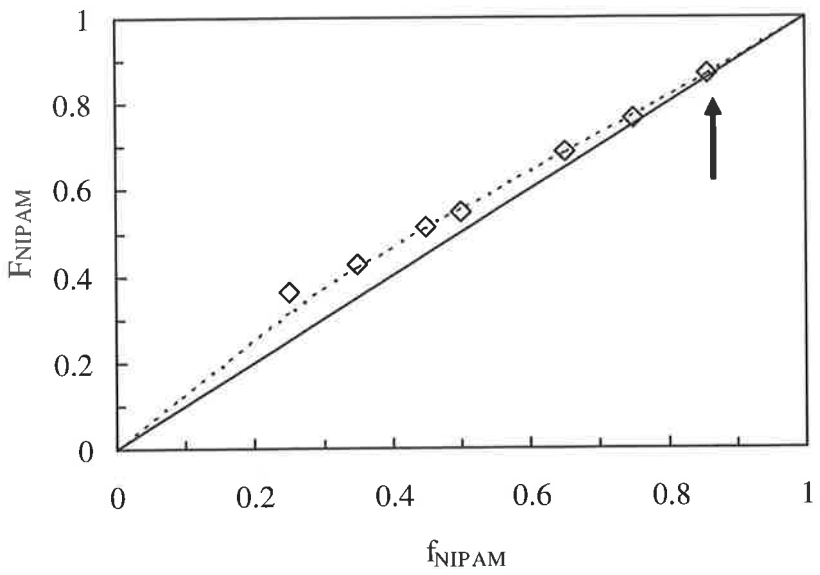

Figure 2.20: Mole fractions of NIPAM in copolymer, F_{NIPAM}, and in feed, f_{NIPAM}, for poly(NIPAM-*co*-PEGMA) copolymers. (◇) Experimentally determined data (Table 2.6). The broken line corresponds to the compositions calculated for r_{NIPAM} = 1.05 and r_{PEGMA} = 0.63 (Table 2.6) using the Lewis-Mayo equation [Equation (1.5)]. The solid line corresponds to equality of the copolymer and monomer compositions, *i.e.*, $F_{NIPAM} = f_{NIPAM}$. The arrow indicates the feed composition in the comonomer mixture used for the synthesis of P2.

2.5.2 Copolymerisation Composition Simulation

The experimentally determined reactivity ratios can be used to simulate the entire copolymerisation as a function of feed ratio as well as of the conversion in terms of the monomer consumption, sequence distribution and sequence length. Thus, the copolymerisation simulation based on the reactivity ratios values can be important as it can provide fundamental information regarding depletion of one monomer during the course of polymerisation, homogeneity of copolymers produced (*e.g.*, random vs. blocky) and compositional drift.[87]

The instantaneous composition of the copolymer is related to the fractional conversion, θ, by the Skeist equation:[88]

$$\ln(1-\theta) = \int_{f_{Ai}}^{f_{Aj}} \frac{df_A}{F_A - f_A} \tag{2.33}$$

where the subscript A refers to the NIPAM monomer. Thus, the conversion of the feed composition from a value of f_{Ai} to a value of f_{Aj} is used to calculate θ. Integrating Equation (2.33) gives:[89]

$$\theta = 1 - \left(\frac{f_{Aj}}{f_{Ai}}\right)^{\alpha}\left(\frac{1-f_{Aj}}{1-f_{Ai}}\right)^{\beta}\left(\frac{f_{Ai}-\delta}{f_{Aj}-\delta}\right)^{\gamma} \tag{2.34}$$

where

$$\alpha = \frac{r_B}{(1-r_B)} \quad , \quad \beta = \frac{r_A}{(1-r_A)} \quad , \quad \gamma = \frac{(1-r_A r_B)}{[(1-r_A)(1-r_B)]} \quad \text{and} \quad \delta = \frac{(1-r_B)}{(2-r_A-r_B)} \tag{2.35}$$

where the subscript B refers to the PEGMA monomer.

Figure 2.21 shows the seven different feed compositions considered for the polymerisation of NIPAM with PEGMA using Equation (2.34) and reactivity ratio values of 1.05 and 0.63 for NIPAM and PEGMA, respectively (Table 2.7). At low conversions ($\theta < 0.1$), the values for F_{NIPAM} are greater than their respective feed compositions investigated due to the reactive nature of NIPAM. F_{NIPAM} continues to maintain relatively constant until $\theta \sim 0.9$, *i.e.*, when most of the NIPAM monomer in the feed has been consumed. In all cases, a drift of the

copolymer composition with θ is observed due to the reactivity ratio of the monomers being different (Table 2.7).

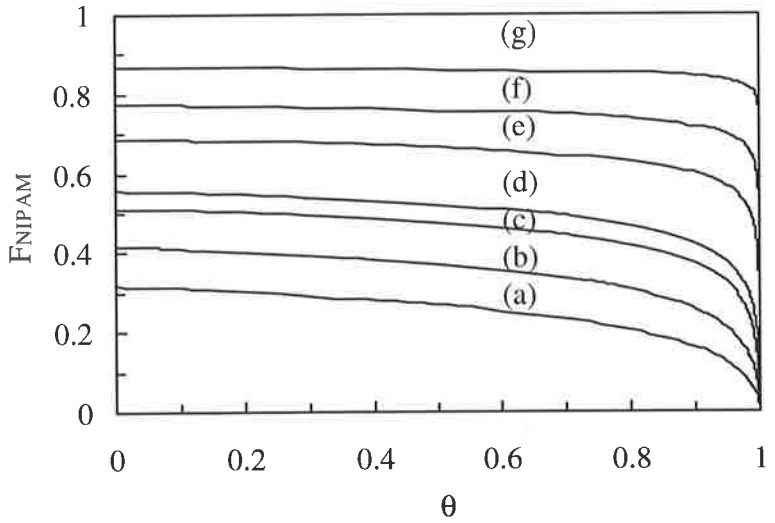

Figure 2.21: The variation in instantaneous mole fraction of NIPAM in the copolymer, F_{NIPAM}, with fractional conversion, θ, using Equation (2.34). The reactivity ratios used were r_{NIPAM} = 1.05 and r_{PEGMA} = 0.63 (Table 2.7). The curves represent fraction of NIPAM in the feed, f_{NIPAM}, and are as follows. (a) 0.25, (b) 0.35, (c) 0.45, (d) 0.50, (e) 0.65, (f) 0.75 and (g) 0.86. Note that curve (g) represents the comonomer mixture used to prepare P2.

The simulation of the variation of F_{NIPAM} with conversion for the comonomer mixture used for the synthesis of P2 is depicted in curve (g). At low conversions ($\theta < 0.1$), the copolymer contains a high proportion of NIPAM segments ($F_{NIPAM} > 0.86$). However, as the copolymerisation reaction progresses the concentration of NIPAM monomer diminishes. The simulation predicts that the copolymer will only have a high proportion of PEGMA segments at $\theta > 0.9$. Thus, the copolymer formed contains a high proportion of NIPAM during the initial

stages of the reaction, whilst the copolymer becomes progressively PEGMA-rich as the polymerisation continues. It should be noted that the simulation is based on the assumption that the copolymer is prepared by the batch method. However, P2 was synthesised using the NIPAM-feed method. Initially there was an excess of the PEGMA monomer in the reaction mixture and during later stages of the reaction there was an abundance of NIPAM monomer. Due to the method in which the copolymer is prepared and differences in the monomer reactivity ratios, the initial copolymer is PEGMA-rich, whilst the final copolymer is NIPAM-rich. Thus, the conditions used in this work were chosen to promote compositional asymmetry (blockiness) in the copolymer. This was necessary since conditions designed to promote symmetric copolymers yielded copolymers that would not stabilise O/W emulsions at room temperature and/or promote emulsion gelation (Chapter 4).

2.6 Physical Measurements of the Polymers

In order to obtain an improved understanding of the properties of the polymers, a comprehensive study of the behaviour of the copolymers and homopolymers in solution was undertaken. As will be shown later in Chapter 4, a range of copolymer compositions and/or having different synthesis routes (Table 2.1) were evaluated prior to deciding upon the optimum copolymer composition and the synthesis method for this work. A key criterion for deciding the suitability of a given copolymer for further study was its ability to stabilise emulsions at room temperature, whilst exhibiting temperature-induced gelation behaviour. P2 was found to meet these conditions; hence, the data discussed in the remainder of this part of the work concerns this copolymer.

2.6.1 Temperature-dependent Viscosity Studies

The viscosity data of the copolymer solution measured using an Ostwald viscometer are presented in Figure 2.22. As expected, the viscosity steadily decreases with increasing temperature. But close to the LCST of the copolymer (*ca.* 35°C), this decrease in viscosity is only slightly apparent. This can be attributed to the temperature-induced collapse of the NIPAM segments. This effect appears to be dominated by intra-chain interactions. Extensive inter-chain aggregation would result in gel formation and an increase in the viscosity. The viscosity approaches the viscosity of water at elevated temperatures, indicating that the copolymer chains are in their fully collapsed, compact state (*i.e.*, aggregates) and flow freely with water. The relationship between volume fraction, ϕ, of chains and the viscosity of the polymer solution, η_p, can be explained using the following equation:[46]

$$\eta_p = \eta(1 + k_s \phi_{eff}) \tag{2.36}$$

where k_s is a constant equal to 2.5 for non-interacting hard spheres and ϕ_{eff} is the effective volume fraction. As the coils collapse, ϕ_{eff} decreases, leading to a decrease in η_p.

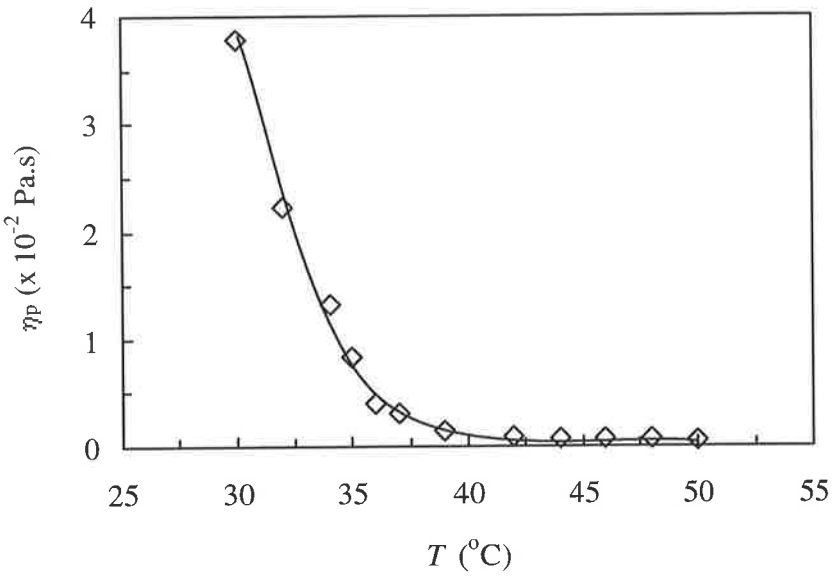

Figure 2.22: Plot of the viscosity of the copolymer solution (c_p = 0.025 g/ml) vs. temperature measured using an Ostwald viscometer.

2.6.2 Photon Correlation Spectroscopy Studies

The temperature dependence of D_0 of P2 dispersed in H_2O was measured using a PCS NOVA 901 instrument (Group Scientific) and a scattering angle of 90°, in order to provide information about the solution species. Samples were left to equilibrate at a given temperature for 0.5 hours prior to measurement. The average value was taken from the five runs performed for

each measurement. The d_h values provided by the software were used to calculate D_0 using Equation (2.19) and values for η and T.

The plot of D_0 as a function of copolymer concentration at 40°C is shown in Figure 2.23. It was assumed that the copolymer chains have collapsed to form aggregates at that temperature since the LCST of P2 is *ca.* 35°C (see Figure 2.15). As the copolymer concentration increases, the effect of inter-chain interactions becomes more significant since it is proportional to the average inter-chain distance, d_p. The collision frequency will increase with increasing copolymer concentration. This is evident in Figure 2.23 where D_0 decreases with increasing c_p.

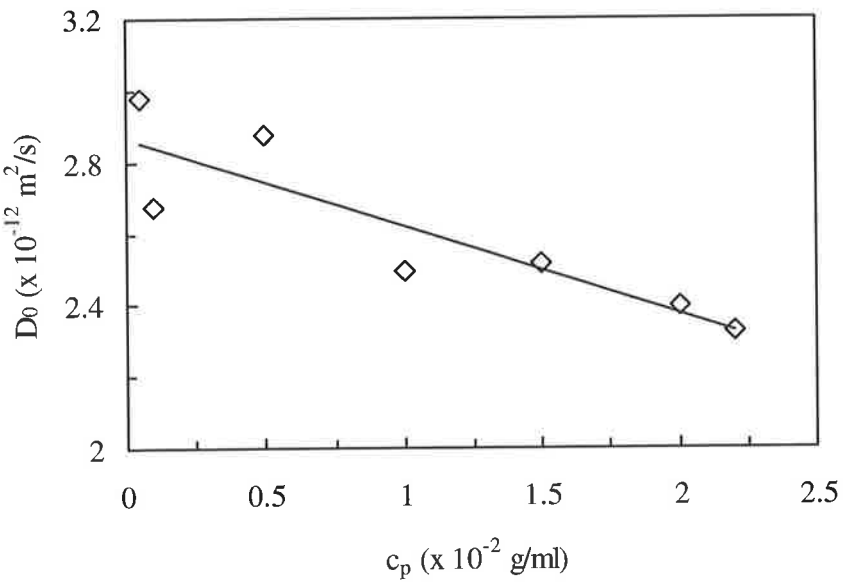

Figure 2.23: Plot of D_0 as a function of c_p at 40°C for P2 determined from PCS measurements.

The data for the temperature dependence of D_0 at c_p = 0.005 g/ml are tabulated in Table 2.8. To compensate for the decrease in the viscosity of water with increasing temperature, the D_0 values were normalised on the viscosity of water and temperature. This is shown in Figure 2.24.

Table 2.8: Data Obtained from PCS measurements for aqueous solutions of P2

c_p (x 10^{-2} g/ml)	T (°C)	η (x 10^{-4} Pa.s)[a]	n_p[b]	d_h (x 10^{-7} m)	D_0 (x 10^{-12} m^2/s)[c]
0.50	30	8.0	120	16.0	0.35
0.50	32	7.6	120	14.0	0.40
0.50	34	7.2	115	11.0	0.55
0.50	36	6.9	675	4.3	1.50
0.50	38	6.6	970	3.0	2.30
0.50	40	6.3	1140	2.5	2.90
0.50	50	5.3	860	2.0	4.60

[a] *Source*: Ref. 90. [b] n_p = Count rate, *i.e.*, number of photons/second detected by the PCS instrument. [c] Calculated using Equation (2.19).

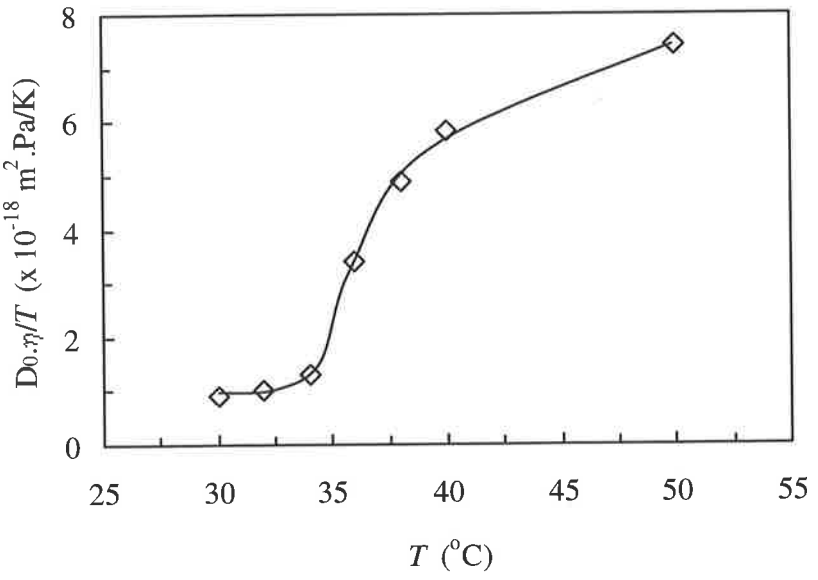

Figure 2.24: Diffusion coefficient normalised on the viscosity of water and temperature, $D_0.\eta/T$, as a function of temperature for P2 measured at c_p = 0.005 g/ml. Note that $D_0.\eta/T = k/(3\pi d_h)$.

Generally across the temperature range examined, the $D_0.\eta/T$ values increased with temperature. Below the LCST, $D_0.\eta/T$ did not change significantly with increase in temperature. At the LCST at *ca.* 35°C, the values increased dramatically. According to Larsson *et al.*[91] the observed D_0 at these temperatures might be attributed to mobile chains segments attached to already collapsed copolymer chains. The large increase in $D_0.\eta/T$ across a temperature range (*ca.* 35 - 40°C) may indicate a relatively high compositional polydispersity of P2.

2.7 Conclusions

Poly(NIPAM-*co*-PEGMA) copolymers have been successfully synthesised using free-radical polymerisation. The copolymers were shown to have different chemical properties, *e.g.*, LCST and polydispersity, depending on the reaction conditions used. The composition of the copolymers was determined by ^{1}H NMR. GPC data indicated that the copolymers were polydisperse, *i.e.*, PD > 1, and were attributed to the method of copolymerisation employed. The critical overlap concentration at 25°C for P2 was found to be *ca.* 0.01 g/ml. Turbidity data showed that the LCST of the copolymers, taken as the point of inflection on the turbidity curves, was shifted to higher temperatures compared to the value for poly(NIPAM). Increasing the proportion of PEGMA resulted in an increase in the LCST of the copolymer, since these segments were able to retard the collapse of the chains more extensively as temperature was increased. From the first derivative plots, poly(NIPAM) was found to have a single LCST. On the other hand, the presence of a broad shoulder of the plots extending to higher temperatures indicated a range of LCSTs for copolymers prepared from the NIPAM-feed method, *e.g.*, P1 and P2. In contrast, copolymers prepared from the dual-feed method, *e.g.*, P2A and P2B, showed a more uniform LCST as shown by the symmetry of the first derivative plots.

The monomer reactivity ratios were calculated from the initial monomer feed composition and the copolymer composition, by means of the Lewis-Mayo method. They were found to be 1.05 and 0.63 for NIPAM and PEGMA, respectively. From the simulation of the copolymerisation of NIPAM and PEGMA for P2 using the Skeist equation, a drift of the copolymer composition with monomer conversion was observed due to the reactivity ratio of the monomers being different and the synthetic method employed. More specifically, the NIPAM-feed method was found to produce copolymers which contained a high proportion of PEGMA

during the initial stages of the copolymerisation reaction, whilst the copolymer chains became progressively NIPAM-rich as the polymerisation continued. The conditions used in this work were designed to synthesise copolymers having asymmetric compositions (*i.e.*, blocky). This was necessary since conditions designed to promote symmetric compositions yielded copolymers that would not stabilise and/or promote emulsion gelation.

The criterion for deciding the suitability of a given copolymer for further study was its ability to stabilise emulsions at room temperature, whilst exhibiting temperature-induced gelation behaviour. P2 was found to meet these conditions. Thus, the physical properties of P2 were investigated most extensively in this work. The viscosity of the copolymer solutions, measured using an Ostwald viscometer, steadily decreased with increasing temperature. But close to the LCST (*ca.* 35°C), this decrease in viscosity was only slightly apparent. This was attributed to the temperature-induced collapse of the NIPAM segments. This effect appeared to be dominated by intra-chain interactions, as inter-chain interactions would have resulted in gel formation and an increase in viscosity. The diffusion coefficient, measured using a PCS instrument, was found to be dependent on copolymer concentration and temperature. Although, there was no significant increase in D_0 below the LCST, it increased dramatically above this temperature. This is a consequence of the fact that the free chains in solution were collapsing to form aggregates above the LCST.

CHAPTER 3 SMALL-ANGLE NEUTRON SCATTERING STUDIES

3.1 Introduction and Aims

Small-angle neutron scattering (SANS) is a diffraction technique which involves the wave-particle duality and the nuclear properties of neutrons, allowing information about the size and shape of molecules to be determined.[92] Although much work on polymers involving SANS has been performed,[72,93-95] this technique has not been previously utilised to study solutions of poly(NIPAM) copolymers. Mao *et al.*[96] used SANS to investigate the temperature-induced conformational changes of PEO-PPO-PEO block copolymer micelles in aqueous solution. The amphiphilic copolymers were found to comprise of Gaussian coils and rods. The temperature dependent behaviour was enhanced in the presence of electrolyte. Using SANS, Hourdet *et al.*[27] investigated the aggregation behaviour of aqueous solutions of poly(PAANa-*g*-PEO) copolymers [PAANa is poly(sodium acrylate)] with temperature as the trigger. They explained that at low temperatures the PEO grafts behaved as isolated chains. When a critical temperature of *ca.* 29°C was exceeded, they reasoned that the PEO chains started to self-aggregate. This was indicated by the scattering function increasing dramatically upon heating. They ascribed the presence of a scattering maximum, which remained at a fixed scattering vector across the temperature range examined, to the distance between the microdomains being independent of the temperature.

Gladman and co-workers[97] studied the structure of adsorbed polymer layers on titanium dioxide/toluene dispersions by SANS. By employing contrast variation, the authors were able to determine the interfacial scattering without significant contributions from the particles. This enabled the authors to obtain information on adsorbed polymer layers. The preferential

adsorption of low molecular mass polymer chains was supported by the SANS data. Washington *et al.*[98,99] investigated the behaviour of the PEO-PPO-PEO block copolymer at the surface of emulsions using SANS. From the polymer volume fraction profiles constructed using the SANS data, they concluded that the PPO blocks of the copolymer were mostly adsorbed at the oil-water interface and the PEO blocks were extended into the continuous phase. This is reasonable given that PPO is more hydrophobic than PEO.[100] The authors also concluded that the copolymers physically adsorbed from solution as single chains to form densely-packed adsorbed layers. These adsorbed layers were dependent on temperature and electrolyte concentration. Staples *et al.*[101] measured the adsorption of mixed non-ionic/anionic surfactants of $C_{12}E_6$ and SDS at the hexadecane/water interface using SANS. They revealed that with increasing concentration of the surfactants, the non-ionic surfactant partitioned into the oil phase and some of the hexadecane solubilised into the mixed micelles. The authors were able to estimate the monomer concentration of the surfactants in both the oil and water phases from the SANS data. Hatto *et al.*[102] studied the temperature responsive behaviour of poly(NIPAM) adsorbed to silica particles. The SANS data indicated that as the polymer chains collapsed with increasing temperature, the layer thickness decreased at the silica surface.

This part of the work investigates the behaviour poly(NIPAM-*co*-PEGMA) copolymers in aqueous solutions across a temperature range using SANS. The aims of the work were to:

(i) Identify the scattering exponents.

(ii) Obtain physical insights through fitting the data with appropriate models.

(iii) Use the data to propose a model for the temperature-induced structural changes for poly(NIPAM-*co*-PEGMA) copolymer solutions.

3.2 Theory

3.2.1 The Neutron

Neutrons have no charge and possess a mass virtually equal to that of a proton. This results in neutrons interacting with the nuclei rather than the electrons when they are scattered from materials. The wavelength, λ, of a neutron is dependent upon its velocity, υ, as shown by the de Broglie's equation:[103]

$$\lambda = \frac{h}{m\upsilon} \tag{3.1}$$

where h is the Planck's constant *and* m is the mass. The refractive index of neutrons, n_N, is slightly less than unity, allowing neutrons to be externally reflected. This provides the basis for neutron reflection.

3.2.2 The Scattering Vector

The neutron scattering experiment consists of bringing a beam of radiation to a sample and measuring the intensity of the scattered neutrons as a function of scattering vector, q. The scattering vector is the resultant between the incident, $\mathbf{k_0}$, and scattered, $\mathbf{k_s}$, wave vectors as shown by:[92]

$$q = |q| = |\mathbf{k}_s - \mathbf{k}_0| = \frac{4\pi n_N}{\lambda} \sin\left(\theta_s/2\right) \tag{3.2}$$

where θ_s is the scattering angle and n_N can be equated to unity. When θ_s is small, Equation (3.2) may be approximated as:[92]

$$q \approx \frac{4\pi}{\lambda}\left(\frac{R_{det}}{L_{sd}}\right) \tag{3.3}$$

where R_{det} is the radial distance on the detector and L_{sd} is the sample-detector distance. Figure 3.1 shows the relationship between q and the wave vectors.

Figure 3.1: Relationship between the incident, $\mathbf{k_0}$, and scattered, $\mathbf{k_s}$, wave vectors and momentum transfer for elastic scattering. *Source*: Ref. 103.

In a SANS experiment the modulus of q measures length scales in reciprocal space and is the independent variable. Substituting Equation (3.2) into Bragg Law of diffraction gives:

$$\lambda = 2d_1 \sin\left(\theta_s/2\right) \tag{3.4}$$

gives:

$$d_1 = \frac{2\pi}{q} \tag{3.5}$$

where d_1 is the molecular-level length scale. Thus, large-scale structures are observed at small values of q while small-scale structures are observed at large q values.

3.2.3 The Differential Scattering Cross-section

The dependent variable in a SANS experiment is the differential scattering cross-section, $I(q)$, or more commonly known as the intensity of scattering and is represented by:

$$I(q) = \phi_p v_p^2 (\Delta\rho)^2 P(q) S(q) + B_{inc} \tag{3.6}$$

where ϕ_p is the volume fraction of the scattering centre, v_p is the volume of one particle, $(\Delta\rho)^2$ is the contrast, $P(q)$ is the form factor, $S(q)$ is the structure factor and B_{inc} is the incoherent background. The differential scattering cross-section contains all the information on the size, shape and interactions between the scattering centres in the sample.

3.2.4 The Neutron Scattering Length Density

The neutron scattering length density, ρ, is calculated from the expression:

$$\rho = \Sigma_i b_i \frac{DN_A}{M} \tag{3.7}$$

where b_i is the neutron scattering length of nucleus, i, and D is the bulk density of the scattering body. The neutron scattering length density varies irregularly between nuclei and is dependent on the isotope used. This is important since the difference in sign and magnitude between the scattering lengths of hydrogen and deuterium (-3.741 x 10^{-5} Å and 6.671 x 10^{-5} Å, respectively[92]) allows manipulation of ρ simply by replacing hydrogen in a molecule with deuterium.

The contrast term is the square of the difference in neutron scattering length density between the solute, ρ_n, and the surrounding medium, ρ_0, *i.e.*, $(\Delta\rho)^2 = (\rho_n - \rho_0)^2$. When $(\Delta\rho)^2 = 0$ the scattering centers are contrast matched, allowing simplification of the scattering patterns.

3.2.5 The Form Factor

The form factor, $P(q)$, is a dimensionless function that describes how interference effects between neutrons scattered by different parts of the *same* scattering centre affect the overall scattering. Consequently, $P(q)$ is influenced by the size and shape of the particle. Since the samples studied contained scattering contributions from rods, Gaussian chains and spheres, the form factor for these structures will be discussed.

The form factor for rods is given by:[103]

$$P_r(q) = \frac{1}{2}\int_0^{\pi/2} F^2(q)\sin\gamma d\gamma \tag{3.8}$$

where γ is the angle between the q vector and the rod axis. $F(q)$ is given by:

$$F(q) = \frac{\sin\left(\frac{1}{2}qL_r\cos\gamma\right)2J_1(qR_r\sin\gamma)}{\left(\frac{1}{2}qL_r\cos\gamma\right)(qR_r\sin\gamma)} \tag{3.9}$$

where J_1 is a first order Bessel function of the first kind. The length and radius of the rods are given by L_r and R_r, respectively. It follows for a sample of rods for which B_{inc} has been subtracted:

$$I_r(q) = \phi_r v_r (\Delta\rho_r)^2 P_r(q) \tag{3.10}$$

where the volume of the rod, $v_r = \pi R_r^2 L_r$ and $S(q) = 1$.

The form factor for Gaussian chains is given by:[103]

$$P_c(q) = \frac{2}{x^2}\left(x - 1 + e^{-x}\right) \tag{3.11}$$

where $x = q^2 R_g^2$. In this case, the polymer has a Gaussian distribution of segment density about the center-of-mass of the polymer chains, in both theta and good solvent conditions. It follows that for a sample of Gaussian chains where B_{inc} has been subtracted and $S(q) = 1$:

$$I_c(q) = \phi_c v_c (\Delta\rho_c)^2 P_c(q) \tag{3.12}$$

where the volume of the coil, v_c, is given by:

$$v_c = N_{agg}\left(\frac{M_c}{D_c N_A}\right) \tag{3.13}$$

where N_{agg}, M_c and D_c are the aggregation number, molecular mass of the individual chains and the bulk density of the polymer, respectively. As q approaches zero, Equation (3.12) can be reduced to the following:

$$I_c(0) = \lim_{q \to 0} I_c(q) = \phi_c v_c (\Delta\rho_c)^2 \tag{3.14}$$

The form factor for Porod scattering from spheres of radius, R_p, is given by:[103]

$$P_p(q) = \frac{9}{2q^4 R_p^4} \tag{3.15}$$

provided $qR_p >> 1$. The scattering from a sharp interface for large particles on any shape is given by:[103]

$$I(q) = \frac{2\pi S_T (\Delta\rho_p)^2}{q^4} \tag{3.16}$$

where the total surface area per unit volume is given by $S_T = 4\pi R_p^2 N_p$ and N_p is the number density of particles. For spheres:

$$S_T = \frac{3\phi_p}{R_p} \tag{3.17}$$

The scattering for large particles (*cf.* $1/q$) with a diffuse interface is modulated by an $\exp(-\sigma^2 q^2)$ term,[104] which generates gradients steeper than q^{-4} for $\sigma > 0$:

$$I_p(q) = \frac{2\pi S_T (\Delta\rho_p)^2 \exp(-\sigma^2 q^2)}{q^4} \tag{3.18}$$

3.2.6 The Structure Factor

The structure factor, $S(q)$, is a dimensionless function which describes interference effects between neutrons scattered by *different* scattering centers. ~~It can give interparticle distances and forces~~. This function is influenced by the degree of order in the sample and the interactions between scattering centres. Note that $S(q) = 1$ for dilute dispersions at any q values in the range studied here.

3.2.7 The Incoherent Background

The incoherent background, B_{inc}, arises when the phase of neutrons is randomised during a scattering event, *i.e.*, no correlation between the position in the sample of the nucleus and its scattering length. Since not all of the nuclei of the same atom type will have the same neutron scattering length (this could be due to different spin states), there will be coherent and incoherent scattering. Incoherent scattering, which forms a background, must be removed if structures are to be elucidated from SANS analysis. Note that B_{inc} is independent of q.

3.2.8 Neutron Instrumentation for Performing SANS

Neutrons are produced either by nuclear fission in a reactor or in pulses by spallation from a metal target bombarded by protons arriving at close to the speed of light from a particle accelerator. In the former, nuclear chain reaction (usually fission of uranium-235) produces a continuous flux of neutrons. The most powerful spallation neutron source in the world is the ISIS facility at the Rutherford Appleton Laboratory, Didcot, United Kingdom,[103] which is where the SANS experiments described in this work were conducted.

The spallation process at ISIS can be summarised as follows. The H^- ions produced from the ion source are accelerated in a pre-injected column. Inside the linear accelerator (LINAC) the H^- ions are accelerated up to energy of 70 MeV from 665 keV. The electrons are removed from the H^- ions by a thin aluminium foil to give rise to a beam of protons. Generally, an 800 MeV, 200 μA proton beam is delivered in 50 Hz pulses to the tantalum target which is cooled by heavy water.[104] The neutrons produced when the high-energy proton beam interacts with the tantalum are then guided to the LOQ instrument.

A schematic representation of the LOQ instrument is shown in Figure 3.2. The neutrons are moderated by passing through liquid hydrogen to allow reduction in its kinetic energy and velocity. Neutron guide transports the moderated neutrons with minimum loss of flux and the supermirror removes neutrons < 2 Å. The chopper only permits sharp burst of polychromatic neutrons to be passed through, while the frame mirror removes neutrons with wavelength > 12 Å. The incident beam is collimated to an appropriate size and shape by the apertures prior to encountering the sample. The incident beam may be transmitted, adsorbed or scattered upon contact with the sample. A two-dimensional detector then records the scattered intensity at an angle, θ_s.

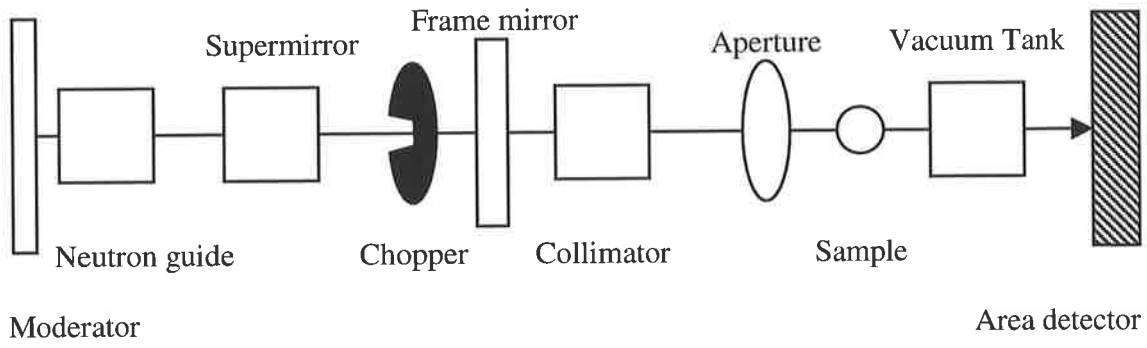

Figure 3.2: SANS instrument set up at LOQ. *Source*: Ref. 92.

3.2.9 Data Reduction

The process of recovering I(q) from what the detector records is known as data reduction and is usually performed using instrument specific software. The scattered neutrons which arrive at the area detector produce a series of diffraction rings. Within a ring, a radial integration over some range of solid angle is performed. The data are then placed on a per neutron basis. This is

done by using the transmitted and integrated counts recorded by the monitor detector and the area detector efficiency ratio. Similarly processed background rata is subtracted ring by ring and the location of each ring is then converted to q using Equation (3.3).

The absolute values of the scattered intensities from a sample can be calculated from the scattering and transmission of a standard sample, *e.g.*, D_2O, as the background. Note that the latter is usually a sample of 'known' differential cross-section. The corrected signal, I_{corr}, may be obtained by dividing the signal from the standard sample, allowing many instrument variables to be omitted:

$$I_{corr} = \frac{\left(I_s / M_s\right)\left(1 - T_w\right)}{\left(4L\pi T_s\right)\left(I_w / M_w\right)} \tag{3.19}$$

where I_s is the sample intensity, M_s is the sample monitor count, T_w and T_s are the transmission signals from water and the sample, respectively, L is the sample thickness and I_w and M_w are the intensity and monitor count, respectively of the standard sample.

Once the data have been reduced, the molecular information can then be extracted by methods of data analysis. Note that different regions of the scattering curve may provide information about different features of the system under investigation.

3.3 Experimental Details

The polymers were synthesised according to the methods given in Section 2.2.2. D_2O was used for dilution of the polymers. Note that the copolymer of choice for this part of the study was copolymer P2. As will be shown in Chapter 4, P2 demonstrated the ability to stabilise emulsions at room temperature, whilst exhibiting temperature-induced gelation behaviour. The SANS experiments were performed using LOQ (running at 50 Hz) at the ISIS facility (Rutherford Appleton Laboratories, Didcot, UK). The polymer solutions (3.5 wt%) were measured in the 2 mm thick Helma quartz cuvettes. The effective q-range of the instrument was 0.009 - 1.6 $Å^{-1}$. The data from the detector was fed into a DEC VAX workstation, where the scattered intensity data was corrected for the sample transmission and background scattering, using the instrument specific data reduction program COLETTE.[105]

3.3.1 Data Reduction Details

The incoherent background level for the samples was determined as follows using an Excel spreadsheet. The scattering exponent, n, for the high q contribution, *e.g.*, q^{-n}, was determined from the plot of $d\ln I(q)/d\ln q$ vs. q. Except for P2 at 50°C where $n = 4$, the value of n for all the samples was 2 for the $I(q)$ data for q values greater than a minimum value, q_2. A plot of $I(q)$ vs. q^{-2} was then constructed for $q > q_2$. Using the gradient from the plot and $I(q) = A_2q^{-2} + B_{inc}$ allowed A_2 to be determined. Subtracting each value for A_2q^{-2} from $I(q)$ (for a given $q > q_2$) gave a value for B_{inc}. The values for B_{inc} (for $q > q_2$) were then averaged to give an average value for B_{inc}. The coherent scattering from the poly(NIPAM) particles was then determined by subtracting B_{inc} from the scattering data. The value B_{inc} for P2 at 50°C was determined from the gradient[94] of a plot of $I(q)q^4$ vs. q^4.

3.4 Identification of the Scattering Exponents

The scattering profiles for aqueous solutions of poly(NIPAM), poly(PEGMA) and P2 at 25°C are shown in Figures 3.3 and 3.4. The data for P2 were similar to that for poly(PEGMA), especially at low and medium q ranges. This indicates that the copolymer is structurally similar to the poly(PEGMA) copolymer at 25°C.

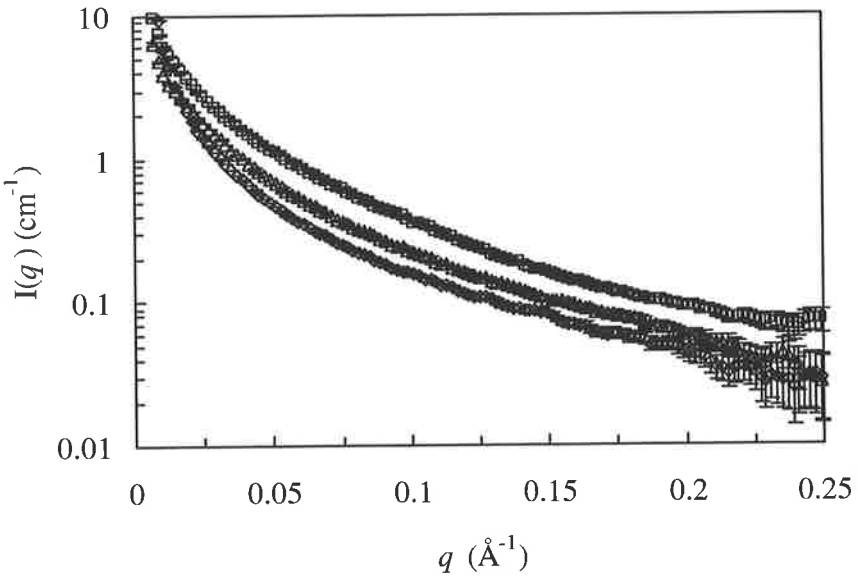

Figure 3.3: SANS data from the 3.5 wt% polymer samples in D_2O at 25°C; (◇) poly(NIPAM), (□) poly(PEGMA) and (Δ) P2. The error bars for the data are also shown.

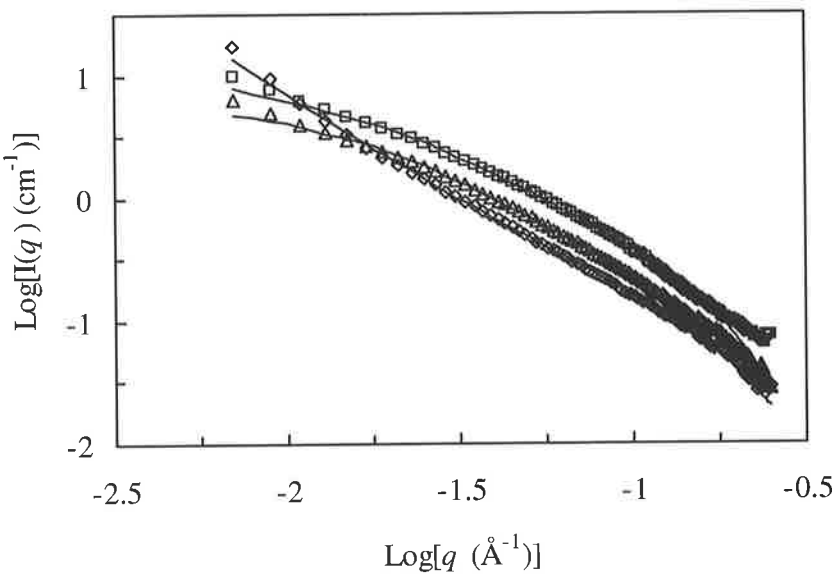

Figure 3.4: Experimentally determined scattering profiles for poly(NIPAM) (◇), poly(PEGMA) (□) and P2 (Δ) in D_2O. The concentration of the polymers was 3.5 wt%. The continuous lines are the theoretical fits corresponding to Equation (3.25) for poly(NIPAM) and Equation (3.24) for both poly(PEGMA) and P2.

The scattering profiles for the 3.5 wt% P2 sample as a function of temperature are shown in Figure 3.5. The data indicate that the scattering intensity at low q increases with temperature. At 50°C, a pronounced increase in the scattering intensity is observed at low q values. This indicates that a change in microstructure of the sample has occurred above this temperature. At 50°C, a large increase in the magnitude of the gradient at low q was observed.

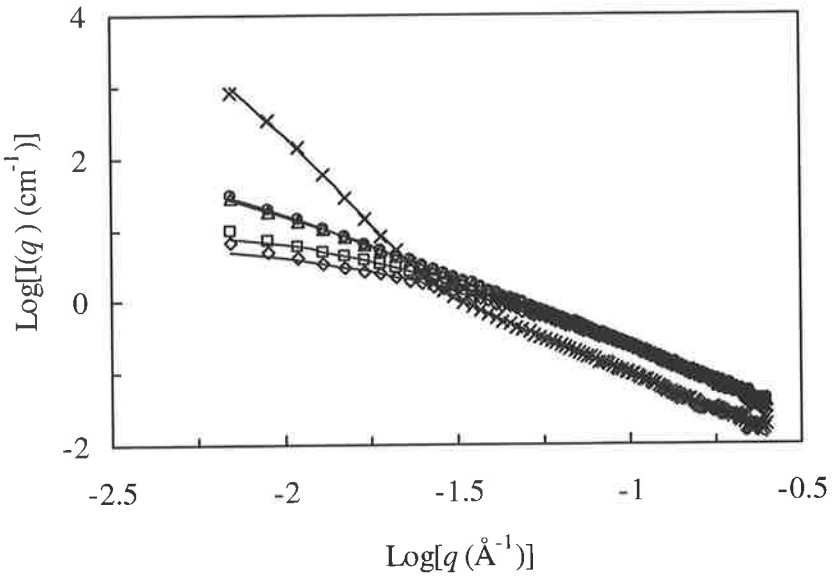

Figure 3.5: Experimentally determined scattering profiles for the 3.5 wt% P2 copolymer in D_2O at various temperatures; (◇) 25, (□) 32, (Δ) 36, (○) 40 and (x) 50°C. The continuous lines are the theoretical fits corresponding to Equation (3.24) at 25 and 32°C, Equation (3.12) at 36 and 40°C and Equation (3.25) at 50°C.

The analysis of the data was extended by investigating changes in the scattering exponent as a function of temperature for the 3.5 wt% P2 sample. Figure 3.6 shows the instantaneous gradients for the data shown in Figure 3.5 in the region $0.07 \leq q \leq 0.1$ Å^{-1}. Note that $I(q) = A_n q^{-n}$ where A_n is a constant. This method allows variation in n as a function of the scattering vector to be determined. The data show the presence of n = -1 and -2, respectively at low and medium q at T = 25°C. At 50°C, Porod scattering can be observed at low q as indicated by $n \sim -4$. The scattering functions can be summarised as follows for the 3.5 wt% P2 sample:

$$T \leq 32^{\circ}C \qquad I(q) = A_1 q^{-1} + A_2 q^{-2} \tag{3.20}$$

$T = 36$ and 40°C $\quad I(q) = A_2 q^{-2}$ (3.21)

$T = 50$°C $\quad I(q) = A_2 q^{-2} + A_4 q^{-4}$ (3.22)

where A_1, A_2 and A_4 are constants for a given temperature.

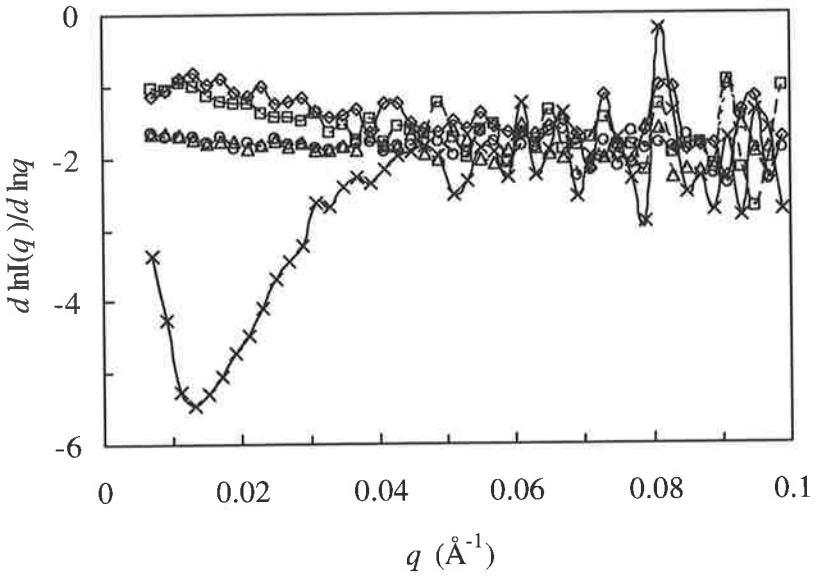

Figure 3.6: Plot of $d\ln I(q)/d\ln q$ as a function of q for the 3.5 wt% P2 solution measured at 25 (◇), 32 (□), 36 (Δ), 40 (○) and 50°C (x).

To further investigate the contribution from each scattering exponent over a given q range, a plot of $I(q)q^2$ vs. q was constructed (Figure 3.7). The presence of q^{-1} and q^{-2} scattering will be seen from a linear relationship and zero gradient, respectively. At $T = 25$ to 40°C linearity is present at low q, while zero gradients can be seen at higher q values across the temperature range examined (*i.e.*, contributions from both q^{-1} and q^{-2} scattering). The increase in R_g of

Gaussian coils with temperature results in q^{-2} scattering to move to lower q values. Thus, the zero gradient region extends to lower q values with increasing R_g. This can be observed by comparing the plot at 40°C which has a more extended zero gradient region at low q values to that at 25°C. At 50°C, there is a significant increase in n at low q values. This is attributed to Porod scattering.

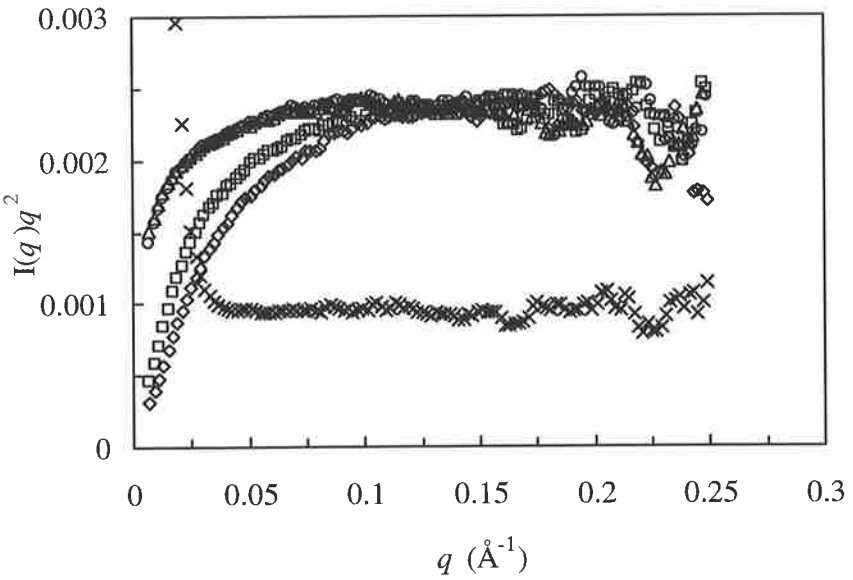

Figure 3.7: Plot of $I(q)q^2$ as a function of q for the 3.5 wt% P2 solution measured at 25 (◇), 32 (□), 36 (Δ), 40 (○) and 50°C (x).

According to Equation (3.22), the scattering intensity is proportional to the scattering contribution from Gaussian coils, *i.e.*, $I(q) \sim q^{-2}$. In order to determine this, both sides of the equation is multiplied by q^4 to give:

$$I(q)q^4 = A_2q^2 + A_4 \tag{3.23}$$

Thus, a linear fit over the q range from a $I(q)q^4$ vs. q^2 plot will suggests q^{-2} contribution within that q region. Note that a non-zero intercept with $A_4 > 0$ is consistent with Porod contribution at low q. Figure 3.8 shows the Kratky plot of $I(q)q^4$ vs. q^2 for the 3.5 wt% P2 in D_2O at 50°C. The linearity over the entire q range indicates scattering from the sample.

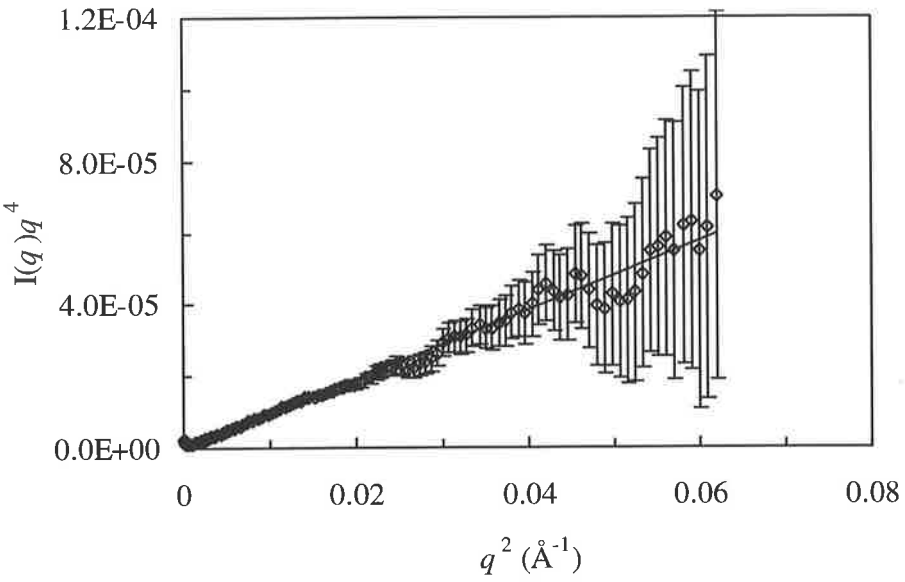

Figure 3.8: Kratky plot of $I(q)q^4$ vs. q^2 for the 3.5 wt% P2 in D_2O at 50°C. The error bars shown were based on the error bars of $I(q)$.

3.5 Analysis of the Structure Factor

It is assumed in this work that $S(q) = 1$. As indicated in Section 3.2.6, the structure factor describes how $I(q)$ is influenced by interference effects between neutrons scattered by *different* scattering centers. A sample containing a variety of species, *e.g.*, rods and coils, will have its $I(q)$ dependent on a range of $P(q)$ and $S(q)$ for the different structures; thus, complicating the analysis of the SANS data. The critical overlap concentration measured for P2 at 25°C was *ca.* 1 wt% (Section 2.4.3). Equation (2.33) was used to calculate c_p^*. This equation is usually employed for linear polymers.[106] In the case of poly(NIPAM-*co*-PEGMA) copolymers, the real value for c_p^* will be higher than the calculated value [*i.e.*, using Equation (2.33)] since the segment concentration will be much higher for branched copolymers compared to a linear polymer.[106]

For the majority of the data, $S(q) = 1$ for the following reasons.[107] The repulsive interactions which may cause $S(q)$ not equal to unity are unlikely due to the copolymer chains being uncharged. As will be discussed in Section 4.4.2.2, the ζ potential is low (insignificant) in the case of emulsions containing poly(NIPAM-*co*-PEGMA) copolymers. Seelenmeyer *et al.*[108] showed that SANS is sensitive to the volume fraction of scattering material dispersed in the solvent. Since neutrons scatter most effectively from segments close to polymer coil centres, the effective size of the coils that scatter neutrons is less than its hydrodynamic coil size. Thus, the 'effective' concentration of coils present is decreased. At 50°C, the separation between the coil aggregates is sufficiently large that a structure term is unlikely. The scattering exponent at low q for the copolymer at 25°C is -1 from the data shown in Figures 3.6 and 3.7. This is consistent with rods and has been observed elsewhere for related systems.[96] Contributions from $S(q) \neq 1$ probably occur at the smallest q values (*e.g.*, < 0.01 Å^{-1}) for the data at 25 and 32°C. However, these data are a minor part of the entire data considered here.

3.6 Model Fitting of the SANS data

The scattering contributions for P2 are given by Equations (3.20) to (3.22). The presence of long thin rods[103] and Gaussian chains[96] are indicated by q^{-1} and q^{-2} scatterings, respectively. The presence of q^{-4} scattering is due to Porod scattering from a sharp interface of large particles.[109]

The scattering data for the polymers were fitted to the following combinations of Equations (3.10), (3.12) and (3.18):

$$I(q) = I_c(q) + I_r(q) \tag{3.24}$$

was utilised for poly(PEGMA) at 25°C and P2 at T: $25 \leq T \leq 32$°C, while,

$$I(q) = I_c(q) + I_p(q) \tag{3.25}$$

was used for poly(NIPAM) at 25°C and P2 at 50°C. Equation (3.12) was used to fit the data for P2 at 36 and 40°C. The fitted scattering profiles are shown in Figures 3.4 and 3.5 and the fitted parameters appear in Table 3.1.

The fits for the polymers (Figure 3.4) are reasonable over the entire q range except at $\log q$ = -2.15 (q = 0.007 Å^{-1}) for the polymers and at $\log q \geq$ -1.10 for poly(NIPAM). The former may be attributed to $S(q)$ not equal to unity at this concentration. However this effect is believed to be not significant at higher q values. The poor fit for poly(NIPAM) at high q values is considered not significant since it was the most weakly scattering of all the systems studied. The high q data are most susceptible to error.

Table 3.1: Fitting parameters for Gaussian coils plus rods model[a]

Polymer	T (°C)	$I(0)_{c,T}$ (cm^{-1})	R_g (Å)	$\psi_{r,T}$[b] (cm^{-4})	R_r (Å)	$2\pi S_T(\Delta\rho_p)^2$ (cm^{-5})	σ (Å)	$N_{agg,T}$[c]	$\phi_{c,T}$	$\phi_{r,T}$
Poly(NIPAM)[e]	25	2.86	65.8	-	-	4.80×10^{24}	31.7	-	-	-
Poly(PEGMA)	25	3.09	77.6	-	14.4	-	-	1.0	0.010	0.025
P2	25	2.78	75.8	1.70×10^{19}	10.3	-	-	1.0	0.024	0.011
P2	32	6.35	99.6	1.18×10^{19}	11.5	-	-	2.1	0.027	0.008
P2[d]	36	31.6	169	-	-	-	-	8.0	0.035	0
P2[d]	40	33.3	172	-	-	-	-	8.4	0.035	0
P2[e]	50	30.8	257	-	-	2.80×10^{26}	59.6	27[f]	0.010[f]	0

[a] Data obtained using $\phi_p = 0.035$. Columns 3 - 8 show fitting parameters obtained from the FISH program.[110] Columns 9 - 11 are variables calculated using the fitting parameters. [b] $\psi_{r,T} = \phi_{r,T}(\Delta\rho_r)^2$. [c] Calculated using Equation 3.26. [d] Gaussian coil model. [e] Coil plus spherical particle model. [f] It was assumed that all of the NIPAM segments had collapsed at this temperature.

The fits are in good agreement with the scattering profiles for P2 as a function of temperature (Figure 3.5). The tabulated data (Table 3.1) allow a number of the parameters to be studied in detail. These are discussed below.

3.6.1 Data Analysis for the Polymers at 25°C

The values of R_g for the polymers at 25°C are in the range 66 - 78 Å, which are consistent with Gaussian chains of polymers with a molar mass of *ca.* 10^4 - 10^5 g/mol (Table 2.5). The fits for poly(PEGMA) included contributions from rods having R_r of *ca.* 14 Å. The fact that rods are evident from the scattering data of P2 at 25°C and absent in poly(NIPAM) at the same temperature suggests that the structural feature is characteristic of PEGMA-rich polymer segments. As temperature increases, there is a higher scattering contribution from the coils compared to the rods, *i.e.*, $q^{-2} > q^{-1}$.

The value for N_{agg} for P2 at 25°C was calculated using Equation (3.14). The value for $\Delta\rho_c$ can be calculated using $\Delta\rho_c = \rho_n - \rho_0$. The value for ρ_n (P2) of 0.8 x 10^{10} cm^{-2} was calculated using the copolymer composition, density and literature values for the scattering lengths of the atoms present[92] using Equation (3.7). The value for ρ_0 (D_2O) of 6.4 x 10^{10} cm^{-2} was taken from the literature.[92] Thus, the magnitude of $\Delta\rho_c$ is 5.6 x 10^{10} cm^{-2}. Assuming $\phi_c = 0.035$, then N_{agg} = 0.33 and 0.67 when calculated using M_n and M_w, respectively. These values are consistent with isolated chains with N_{agg} of *ca.* 1.

In order to obtain an experimental value for $\Delta\rho_c$ at 25°C, expressions that relate ϕ_c at a given temperature, $\phi_{c,T}$, and $\phi_{r,T}$ were needed. The following assumptions were made: (a) only rods and coils were present for P2, *i.e.*, $\phi_c + \phi_r = 0.035$ and (b) species present in the rods and coils have similar compositions, *i.e.*, $\Delta\rho_r = \Delta\rho_c = \Delta\rho$. From Equation (3.14):

$$\phi_{c,T} = \frac{I_{c,T}(0)}{N_{agg,T}(\Delta\rho_C)^2}\left(\frac{d_c N_A}{M_c}\right) \tag{3.26}$$

$$\phi_{c,T} + \phi_{r,T} = 0.035 \tag{3.27}$$

For simplification the FISH fitting program[110] which gives values for $\phi_{r,T}\Delta\rho_r^2$ were equated to $\psi_{r,T}$:

$$\psi_{r,T} = \phi_{r,T}(\Delta\rho_r)^2 \tag{3.28}$$

Using the assumption that $N_{agg} = 1$ at 25°C and Equations (3.26) to (3.28):

$$\Delta\rho_n = \left[\frac{I_{c,25}(0)}{0.035}\left(\frac{d_c N_A}{M_c}\right) + \left(\frac{\psi_{r,25}}{0.035}\right)\right]^{1/2} \tag{3.29}$$

Using values of M_c = 44600 g/mol, d_c = 1.0 g/cm^3, $I_{c,25}(0)$ = 2.78 cm^{-1} and $\psi_{r,T}$ = 1.7 x 10^{19} cm^{-4}, $\Delta\rho$ was found to be *ca.* 3.9 x 10^{10} cm^{-2}. This value is lower than the value of 5.6 x 10^{10} cm^{-2} calculated above. This could be due to a non-uniform density or blockiness within the polymer chains. In addition, exchange of the OH groups of PEGMA to OD would contribute to a decrease in $\Delta\rho$.

The volume fraction of rods in poly(PEGMA) was calculated using the data given in Table 3.1 and the assumptions outlined above. Inserting Equation (3.28) into Equation (3.26):

$$\phi_{r,T} = \frac{\phi_{c,T}\psi_{r,T}}{I_{c,T}(0)}\left(\frac{M_c N_{agg,T}}{d_c N_A}\right) \tag{3.30}$$

Assuming that N_{agg} = 1.0 and M_n = 40000 g/mol for poly(PEGMA) at 25°C, ϕ_r = 0.025 and ϕ_c = 0.010. Thus, about 30% of the scattering observed originates from rods. These could be chains with long persistence length or cylindrical aggregates.

3.6.2 Data Analysis for Poly(NIPAM-*co*-PEGMA) Copolymers at Various Temperatures

The proportions of coils and rods in P2 across the temperature range examined were estimated in order to determine the values for N_{agg}. The polymer chains responsible for the Gaussian coil scattering were expected to have a solvent-polymer interaction that was largely temperature-independent. This leads to $\Delta\rho$ being constant. The values for $\phi_{r,T}$ and $\phi_{c,T}$ were calculated using Equations (3.27) and (3.28) and the values of $\psi_{r,T}$ from fitting the data at 25 and 32°C (Table 3.1). Note that at 36 and 40°C only coils were present. It was assumed that only the PEGMA segments of P2 remained as coils at 50°C. Thus, $\phi_{c,T}$ = 0.01 from the vol% of PEGMA in P2 (34%), *i.e.*, 0.035 x 0.34 ~ 0.01.

The values for N_{agg}, calculated using Equation (3.26), and the values for $\phi_{c,T}$ appear in Table 3.1. The values for $N_{agg,T}$ calculated from the Gaussian segment of the scattering together with the R_g values are plotted as a function of temperature in Figure 3.9. The data support the view that the increase in R_g between 30 and 50°C is because of aggregation of coils. Further aggregation can be seen at T > LCST (*ca.* 35°C). In their work on arborescent polystyrene graft copolymers in *d*-cyclohexane solutions, Choi *et al.*[111] noted an increase in R_g as solvent conditions progressively worsen across a temperature range. The increase in R_g was attributed to increasing molar mass of the copolymers through successive grafting. The N_{agg} values at 36 and 40°C which appear smaller than those reported for PEO-PPO-PEO copolymer by Mao *et al.*[96],

may be due to structural differences between comb and block copolymers. The hydrophilic segments of the former generally offer a greater steric barrier to aggregation.

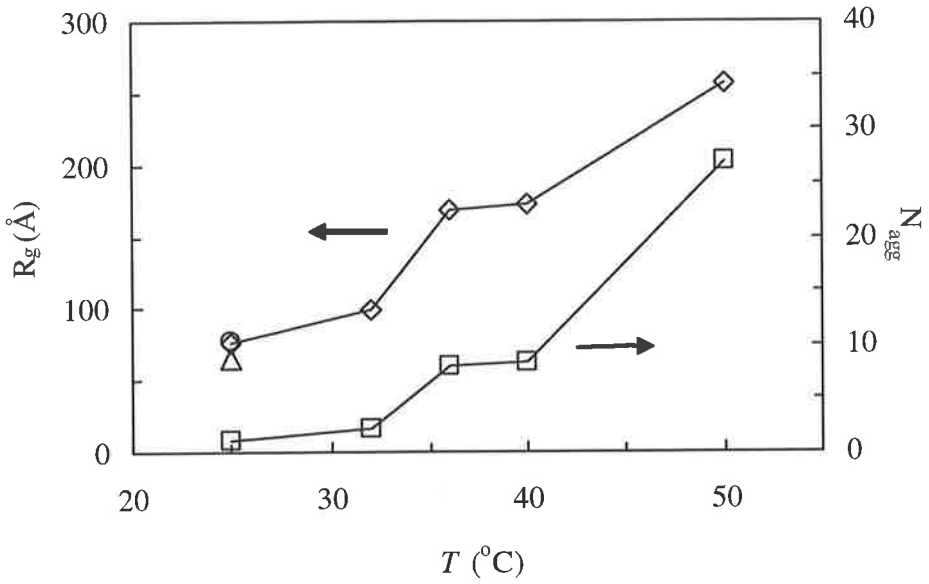

Figure 3.9: The effect of temperature on the radius of gyration (◇) and aggregation numbers (□) for P2. Also shown are R_g values for poly(NIPAM) (Δ) and poly(PEGMA) (○).

The scattering data at 50°C (Figure 3.5) indicate the presence of a particulate phase. The observed Porod scattering is due to the collapse of the NIPAM segments. It is expected that the particle phase is NIPAM-rich with a diffuse shell containing mostly PEGMA segments. The average size of the particles was estimated using Equation (3.17). The value for $2\pi S_T(\Delta\rho_p)^2$ is tabulated in Table 3.1 with the assumption that the particles were NIPAM-rich (since these segments collapse at $T >$ LCST):

$$R_p = \frac{6\pi\phi_p(\Delta\rho_p)^2}{\Theta_p} \tag{3.31}$$

where $\Theta_p = 2\pi S_T(\Delta\rho_p)^2$. Assuming that $\phi_p = 0.025$ (from $\phi_{p,50} + \phi_{c,50} = 0.035$ and $\phi_{c,50} = 0.01$) and that ρ_n is equal to the NIPAM value reported by Cosgrove *et al.*[112] of 0.6 x 10^{10} cm^{-2}, then $\Delta\rho_p$ = 5.8 x 10^{10} cm^{-2}. Thus, the size of the particles at 50°C is *ca.* 120 nm.

3.6.3 Conceptual Model for Temperature-induced Aggregation

The information and analysis from the SANS data enables one to propose a model for the temperature-induced aggregation of the poly(NIPAM-*co*-PEGMA) copolymer chains in water (3.5 wt%) between 30 and 50°C. At 25°C, the chains exists as individual coils and having a R_g of *ca.* 8 nm. As temperature increases the aggregation number increases due to a greater extent of hydrophobic interactions. At T > LCST, aggregation of the coils leads to formation of copolymer micelles with an aggregate size of *ca.* 17 nm. Aggregation is induced by attractive interactions between the NIPAM-rich segments. At 50°C the NIPAM-rich particle phase having a diffuse shell emerges. Gaussian coils that are rich in PEGMA connect the particles through the diffuse shell. Particle precipitation causes further aggregation of the coils and R_g increases to 26 nm.

As will be discussed in Section 4.5.3, the proposed mechanism for gelation will rely upon the formation of hydrophobic junctions which act as physical cross-links. The strength and number density of these junctions determine the gel strength. Although the number of cross-links probably decreases with increasing temperature, the number of effective cross-links per junction will increase with the emergence of the particulate phase, since neighbouring junctions of NIPAM-rich segments will aggregate further with increasing temperatures to form particles, which are connected through the PEGMA-rich coils. This particulate phase will increase the

elastic modulus of the polymer network due to the increased density and strength of the cross-links. As will be investigated in Chapter 5, these structural changes would be consistent with the rheological data for the copolymers and emulsions, in that there should be an increase in the elastic modulus with increasing temperature for concentrated poly(NIPAM-*co*-PEGMA) copolymer solutions (Figure 5.14) and emulsions containing poly(NIPAM-*co*-PEGMA) copolymers (Figure 5.31).

3.7 Conclusions

Analysis of the SANS data revealed that the copolymer chains of poly(NIPAM-*co*-PEGMA) (3.5 wt%) contained three structural features at temperatures between 25 and 50°C, namely, rods, coils and particles. At room temperature, there were evidence of coils and rods. As temperature increased only coils were present and the chains aggregated to form micelles. This temperature-induced aggregation was accompanied by an increase in the radius of gyration. At 50°C particles rich in NIPAM segments were formed.

The data also indicated the existence of different types of transient cross-linking junctions within the copolymer aggregates during temperature-induced gelation at temperatures greater than the LCST. Although the number of junctions decreased with increasing temperature, larger ones appeared in the form of particulate phase. As will be discussed in Chapter 5, this would be responsible for the increase in the elastic modulus for the copolymer solutions with increasing temperature.

CHAPTER 4 EMULSION PREPARATION, CHARACTERISATION AND PROPERTIES

4.1 Introduction and Aims

The majority of emulsions studied or produced commercially are prepared using short-chain surfactants. Thus, the properties of these systems are reasonably well understood.[42,65,113] In most cases, the stability of the emulsions was investigated since emulsion behaviour is largely governed by droplet interactions and interfacial properties. The latter ~~is~~ are largely influenced by adsorbed surfactants or polymeric surfactant molecules (Section 1.2.2). Binks *et al.*[114] studied the stability of O/W emulsions containing *bis*(2-ethylhexylsulfosuccinate) (an anionic surfactant) with respect to creaming and coalescence as a function of salt concentration. They found that Ostwald ripening caused the rate of creaming to be accelerated at low salt concentrations, while at high concentrations flocculation of droplets led to enhanced coalescence. Chanamai and McClements[115] prepared monodisperse O/W emulsion droplets for creaming studies. By measuring the back-scattered light intensity from the emulsions as a function of height, the authors showed that the creaming velocity increased with droplet flocculation because of the increase in effective droplet size. On the other hand, increase in the concentration of oil droplets decreased the creaming velocity. This was attributed to hydrodynamic effects and particle-particle interactions. Dickinson and Ritzoulis[116] studied the properties of emulsions containing sodium dodecyl sulphate (SDS) and sodium caseinate. Although the addition of SDS and sodium caseinate increased the overall emulsion stability, they concluded that an excess of SDS led to faster creaming. This effect was reduced when sodium caseinate was present. They also found that adding salt to the SDS-containing emulsions led to a higher degree of creaming. However,

the presence of caseinate reduced this effect since the SDS molecules were bound to the protein molecules.

Microelectrophoretic measurements are usually conducted to enable the ζ potential to be calculated. Changes in the ζ potential with variation in solution conditions, *e.g.*, temperature and pH, may provide vital information regarding interfacial properties, which determines the life of the emulsion. In their study of the stability of *n*-octance and isooctane-in-water emulsions, Avranas *et al.*[117] showed that the ζ potential increased with added SDS concentrations before reaching a plateau at a concentration close to the cmc of the anionic surfactant. Adding cetyldimethylbenzylammonium chloride (CDBACl), a cationic surfactant, resulted in the reversal of the charge of the droplets. They showed that the droplets were stabilised by these ionic surfactants through electrostatic repulsive forces and that a critical surfactant concentration was needed to achieve maximum stability. Stachurski and Michalek[118] suggested that the initial negative charge of their emulsion droplets in the pH range investigated was attributed to the preferential adsorption of OH^- ions over H^+ ions. The length of the hydrocarbon chain of the emulsion droplets was found to affect the course of changes of the ζ potential when the pH was varied.

The presence of non-adsorbing polymer in emulsions may result in a depletion attraction between the droplets. This may cause a phase separation into a droplet-rich phase and a polymer-rich phase largely devoid of emulsion droplets. At high enough droplet concentration, however, this phase separation is kinetically trapped to a gel-like state where clusters of droplets are weakly connected. In this case, the term emulsion gel is used, since the liquid emulsion is not able to flow unless a large enough shear is applied to the system, *i.e.*, gel-like consistency. Recently, Perrin and co-workers[119] synthesised hydrophobically modified poly(sodium acrylate)

(HMPAANa) and poly(sodium acrylate) (PAANa) for the preparation of emulsion gels. In the presence of hexamethylene diamine, these linear polymers cross-linked to induce gelation when incorporated into emulsions. They concluded that the emulsion droplets were suspended in a viscoelastic matrix regardless of the dispersed phase concentration. Bibette *et al.*[120] prepared emulsion gels using the fractionated crystallisation method [80-82] described in Section 1.2.3. The emulsions were composed of silicone oil droplets in water stabilised by SDS. In the presence of salt, the emulsions were fluid and homogeneous at 25°C. Adhesion between droplets became apparent below this temperature, resulting in gelation. They showed that gelation occurred at volume fraction of oil, ϕ_o, at less than *ca.* 0.01 and the phase transition behaviour was reversed upon increased in temperature, *i.e.*, emulsion remained a fluid at high temperatures. The emulsion gels described by Kunieda *et al.*[121] consisted of a high dispersed phase volume fraction and low surfactant concentration. According to the authors, emulsion gels may be prepared by using the multiple emulsion method or the spontaneous formation method. In the former, all the weighed components (surfactant, water and oil phases) are shaken or stirred and emulsification is facilitated by the addition of small glass beads. In the latter, emulsification is achieved by changing the temperature of the mixture, in the absence of mechanical stirring. They stated that by choosing the appropriate variables and temperature, optically transparent emulsion gels could be obtained.

Recently, there has been wide interest in the utilisation of polymeric surfactants as emulsion stabilisers due to its architectural flexibility.[23,41,51,69,70] This chapter reports a new type of O/W emulsion whose physical and chemical properties are temperature dependent. This interesting phenomenon is attributed to the incorporation of poly(NIPAM-*co*-PEGMA) copolymers as stabilisers in the preparation of O/W emulsions.

The aims of this section of the work can be summarised as follows:

(i) To prepare O/W emulsions using the polymers synthesised in Section 2.2.2.

(ii) To investigate the physical and chemical properties of the emulsions at room temperature.

(iii) To study the effects of temperature on the properties of the emulsions.

(iv) To identify a mechanism for temperature-induced emulsion gelation.

4.2 Experimental

4.2.1 Materials

1-bromohexadecane, toluene, benzene, *n*-decane (all from BDH Chemicals), poly(dimethylsiloxane) (PDMS) (Wacker Chemie GmbH), perfluoroperhydrophenanthrene and perfluorodecalin (both from Flurochem) were employed as the oil phase. All the chemicals were used as received. The water used was milli-Q quality. The polymers were prepared according to the procedures described in Section 2.2.2. C_9E_6 was kindly donated by Flexichem Pty. Ltd (*C* and *E* represent the number of carbons of the hydrophobic segment and EO units of the hydrophilic segment, respectively of the non-ionic surfactant).

4.2.2 Emulsion Preparation

Since the properties of an emulsion can depend on the method of preparation, it was important to adopt a standard method. A representative preparation for the emulsions is as follows. Sufficient time (one day) was allowed for the polymers to dissolve in water to ensure complete dissolution. To obtain $\phi_o = 0.3$, the 3.5 wt% polymer solution (3.5 ml) was placed in a 10 ml beaker before the addition of the oil phase (1.5 ml). The mixture was homogenised using a Silverson SL2T laboratory mixer (Figure 4.1) for 5 min. at 8000 rpm at room temperature. After emulsification the emulsion was cooled to room temperature and stored for further analysis. Note that the temperature of the samples remained below 30°C during mixing. This suggests that the polymer chains were not collapsed and were able to participate in the emulsification process. It is important to note that it was not possible to prepare emulsions containing poly(NIPAM-*co*-PEGMA) copolymers when using this method when the temperature was greater than the LCST.

(a)

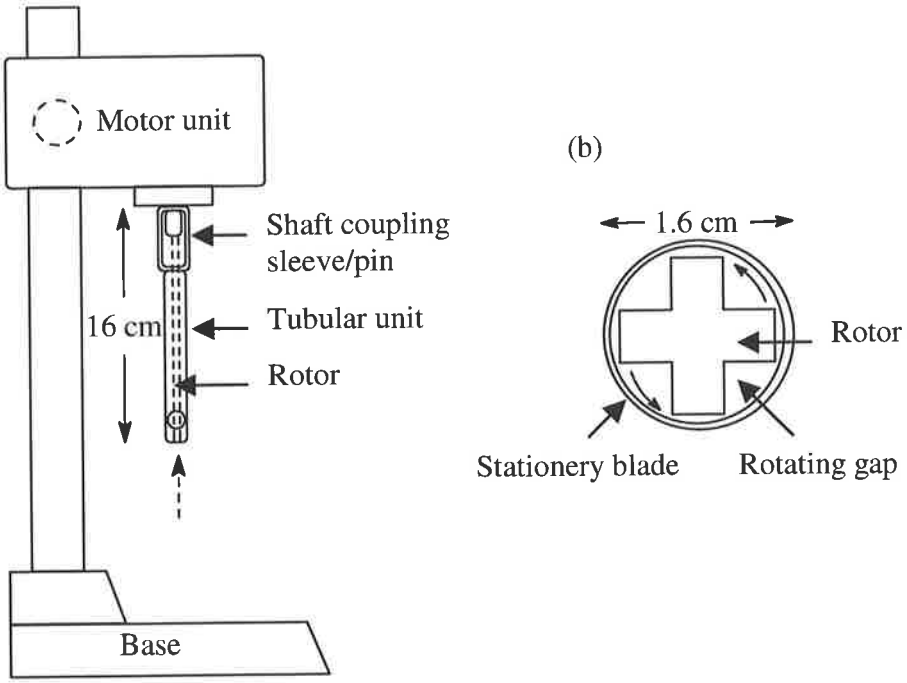

Figure 4.1: (a) Schematic representation of the Silverson SL2T laboratory mixer used to prepare the emulsions. The broken arrow indicates the tubular unit [shown in (b)].

4.3 Physical Measurements

4.3.1 Emulsion Type

To assess the types of emulsion formed, samples were diluted in water or oil at room temperature (the oil used was the same as that employed for the emulsion preparation). The emulsion was concluded to be of O/W type when it could only be diluted with water. If the emulsion could only be diluted with the organic phase then it was inferred to be of W/O type.

4.3.2 Optical Microscopy

In this work, droplet size distribution of the emulsions was assessed by averaging the values of droplet diameter, d_i, measured from images taken with an optical microscope (Olympus Model CH-30). In order to maintain the polymer concentration in the continuous phase, polymer solutions with the same continuous phase concentration were used for preparation of the diluted emulsions. Images obtained from the COHU video camera were digitised using a frame grabber card and analysed using Scion Image software. The image analysis was performed using NIH software and involved counting an average of *ca.* 2000 droplets having $d_i > 2$ μm.

The droplet size distribution for the emulsions was assessed by averaging the values of d_i. The relative percentage frequency distribution function can be calculated from:[4]

$$dn_i = F(d_i)d\ln d_i \tag{4.1}$$

where dn_i is the number of droplets in the range d_i to $d_i + dd_i$ and $F(d_i)$ is the distribution function. The number of droplets, n_i, is related to the droplet volume fraction, ϕ_i, by:

$$\phi_i = \frac{n_i}{N_i} \tag{4.2}$$

where N_i is the total number of droplets. Since most of the emulsion work conducted concerned large droplets and optical microscopy is more sensitive towards large droplets, the volume average diameter, d_v, was calculated from the droplet size distribution and is given by:[4]

$$d_v = \left(\frac{\Sigma n_i d_i^3}{\Sigma n_i} \right)^{1/3} \tag{4.3}$$

4.3.3 Electrophoretic Mobility

Electrophoretic mobility of the emulsions was measured using a Rank Brothers Microelectrophoresis Instrument Mk II. The microelectrophoresis cell was immersed in a water bath controlled at 25 ± 0.1°C. Prior to measurement emulsions were diluted to ϕ_o = 0.05 with a 10^{-4} M NaCl solution and the pH adjusted using 0.1 M solutions of either NaOH or HCl. Note that PDMS was used as the oil phase for the emulsion. Measurements were made at the stationary plane to ~~reduce conductive currents~~ negate electro-osmotic flow which may interfere with droplet movement. Note that the Smoluchowski equation[46] was used for the calculation of the ζ potential.

4.3.4 Gelation Studies Using the Tube Inversion Method

Preliminary gelation studies of the emulsions were performed by visual observations. Samples were allowed to equilibrate for 30 min. in a temperature controlled water bath before the tubes were inverted. The criterion for gelation was that the gels were not able to flow under gravity for 5 min., whilst emulsions flowed when the tubes containing the samples were inverted. Typical dimensions are as follow: diameter and height of tube = 1.5 and 6.0 cm, respectively and height of emulsion in tube = 3.0 cm.

4.4 Emulsion Properties at Room Temperature

4.4.1 Emulsion Characterisation

4.4.1.1 Emulsion Type Determination

Dilution tests confirmed that all the emulsions formed were of O/W type, *i.e.*, the organic phase is the dispersed phase.

4.4.1.2 Optical Microscopy Studies

The optical micrograph for the 1-bromohexadecane-in-water emulsion containing P2 is shown in Figure 4.2. The initial sample which contained $\phi_o = 0.3$ was diluted to $\phi_o = 0.1$ using a 3.5 wt% P2 solution for optical microscopy studies. It is evident that the droplets are rather polydisperse and weakly flocculated, *i.e.*, small aggregates are present. The relatively large droplet size of *ca.* 9.8 μm is reasonable for emulsions stabilised with polymeric surfactants (*cf.* emulsions containing short-chain surfactants[113]). In their work, Cardenas-Valera and Bailey[122] found that the toluene-*n*-heptane-in-water emulsions stabilised with poly(methyl methacrylate-*g*-PEO) graft copolymers had an average droplet size of *ca.* 13 μm, while the *n*-dodecane-in-water emulsions containing modified poly(acrylic acid) sodium salts investigated by Perrin and Lafuma[50] had an average droplet diameter of 10 and 4 μm at polymer concentrations of 1 and 4%, respectively.

The reason for emulsions containing polymeric surfactants having a larger average droplet size compared to emulsions with short-chain surfactants is due to the fact that the latter are able to pack more efficiently at the oil-water interface compared to polymeric surfactants. Better packing of the chains facilitates the emulsification process and imparts a lower surface tension and a greater stability to the emulsion against droplet flocculation and coalescence. In

addition, the adsorption of polymer chains may display complex phenomena. Small changes in polymer structure or in solvent properties may lead to drastic changes in adsorption.

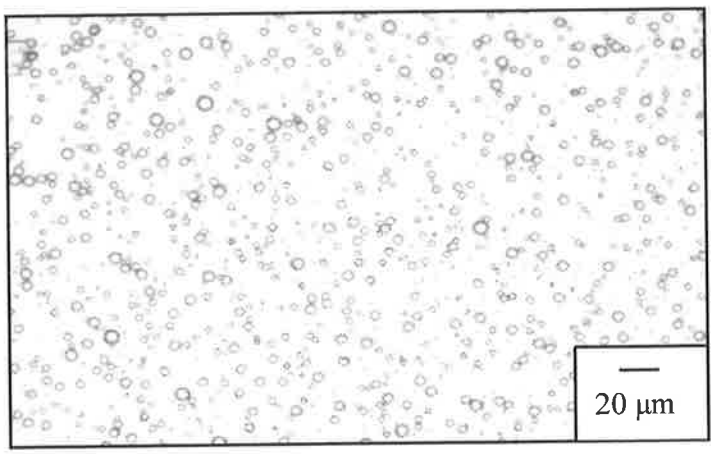

Figure 4.2: Optical micrograph of 1-bromohexadecane-in-water emulsion containing P2 (3.5 wt% with respect to the aqueous phase) immediately after preparation (diluted to $\phi_o = 0.1$).

Figure 4.3 shows the droplet size distribution for the 1-bromohexadecane-in-water emulsion containing P2. Note that logarithmic distributions as opposed to linear distributions were employed in this study to accommodate the spread of the values. Using Equation (4.3) and the data in Figure 4.3, d_v for the 1-bromohexadecane-in-water emulsion containing P2 was found to be *ca.* 9.8 μm.

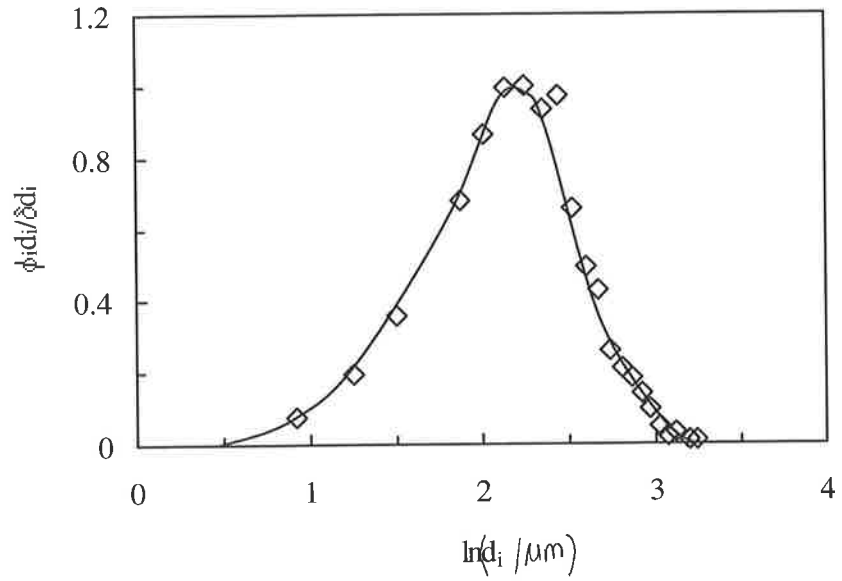

Figure 4.3: The relative frequency distribution function plotted against $\ln d_i$ for the emulsion shown in Figure 4.2 using Equation (4.1). Note that δd_i is the interval of the size range.

4.4.1.3 Effect of Oil Type

The effect of the oil type on droplet size was investigated by examining photomicrographs of various emulsions. Figure 4.4 shows the photomicrograph of the perfluorodecalin and perfluoroperhydrophenanthrene (13% of the total oil volume)-in-water emulsion containing P2 (3.5 wt% with respect to the aqueous phase). Note that perfluoroperhydrophenanthrene is a fluorocarbon oil which is completely miscible with perfluorodecalin and decreases the rate of Ostwald ripening of the oil droplets.[123] Ostwald ripening is not expected to be significant for these emulsions due to their large droplet size (the use of these fluorinated solvents was used for SANS studies in which preliminary data for the O/W emulsions were collected. The SANS data for the emulsions is not included in this thesis). As can be seen, the droplets are rather polydisperse compared to the emulsion droplets shown in

Figure 4.2. This is could be due to the fact that the high density of perfluorodecalin of *ca.* 2 g/ml (*cf.* $\rho_{1\text{-bromohexadecane}}$ ~ 1 g/ml), may have resulted in a high rate of sedimentation, leading to a higher possibility for droplet coalescence to occur due to the close proximity of the droplets in the sediment layer.

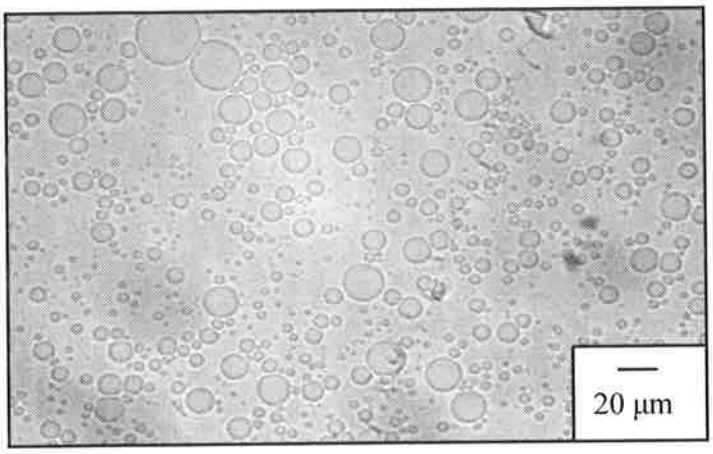

Figure 4.4: Optical micrograph of a perfluorodecalin/perfluoroperhydrophenanthrene-in-water emulsion containing P2 (3.5 wt% with respect to the aqueous phase) immediately after preparation (diluted to $\phi_o = 0.1$). Using Equation (4.3) and the distribution of the droplets (not shown), $d_v = 8.5$ μm. The mixed oil phase contained 13 vol% perfluoroperhydrophenanthrene.

Since creaming/sedimentation rates are dependent on the density of the dispersed phase [Equation (1.18)], it was decided that 1-bromohexadecane, having a density closest to the continuous phase, would be used as the oil phase in the emulsions for the remainder of this part of the work (unless otherwise stated).

4.4.1.4 Effect of Oil Volume Fraction

Emulsions containing a range of ϕ_o values were prepared and investigated for changes in droplet size. Figure 4.5 shows photomicrographs of the emulsions containing $\phi_o = 0.1$ (a) and 0.5 (b) (concentration of P2 was *ca.* 3.5 wt% with respect to the aqueous phase for both of the emulsions). For clarity the sample containing $\phi_o = 0.5$ was diluted to $\phi_o = 0.1$ prior to observation under the microscope. No apparent difference in droplet distribution was obtained when ϕ_o was varied [*cf.* d_v = 9.8 μm for emulsion containing ϕ_o = 0.3 (Figure 4.2)]. This suggests that the droplet size is independent of ϕ_o at the copolymer concentration employed. It is possible that a significant proportion of the copolymer does not adsorb on the droplet surface during emulsification, thus allowing a high volume fraction of oil to be emulsified. The ratio of copolymer to the oil volume fraction could have minimal influence on the emulsification process, leading to optimum packing of copolymer chains at the droplet surface in all the samples. From this investigation it was decided that the emulsions to be prepared in this work contained $\phi_o = 0.3$.

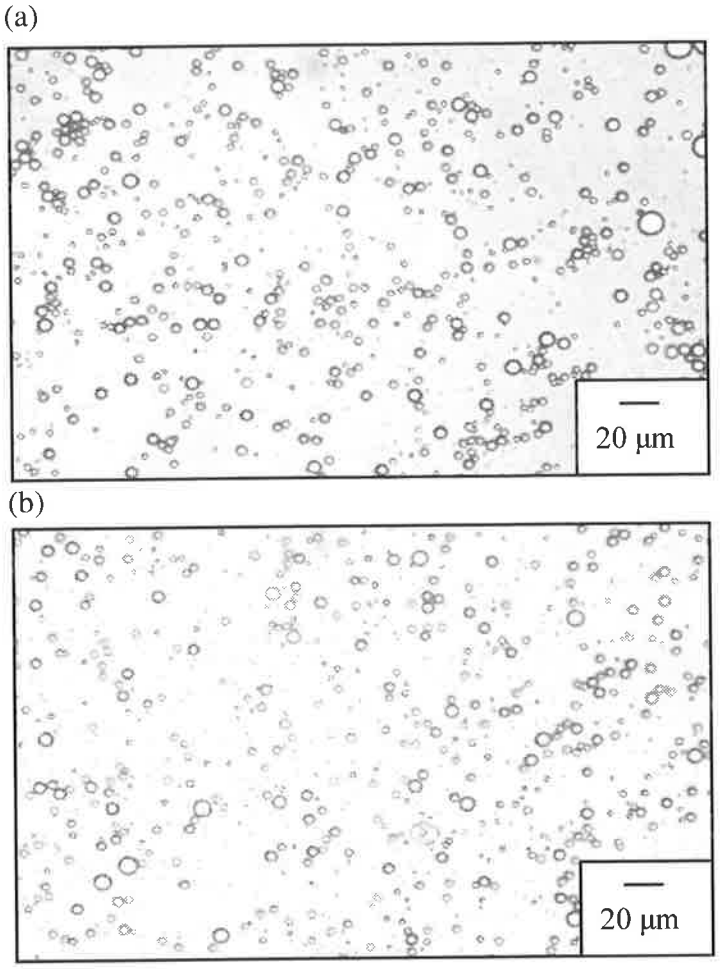

Figure 4.5: Optical micrograph of 1-bromohexadecane-in-water emulsions (concentration of P2 was *ca.* 3.5 wt% with respect to the aqueous phase for the emulsions); (a) $\phi_o = 0.1$ and (b) $\phi_o = 0.5$. Note that the sample containing $\phi_o = 0.5$ was diluted to $\phi_o = 0.1$ prior to observation under the microscope. Using Equation (4.3) and the distribution of the droplets (not shown), $d_v = 11.1$ and 12.1 μm for (a) and (b), respectively.

4.4.1.5 Effect of Copolymer Concentration

The effect of varying the copolymer concentration in the emulsions was investigated by studying the changes in the size distribution of the droplets. Figure 4.6 shows the photomicrographs of the emulsions (ϕ_o = 0.3) containing a range of copolymer concentrations with respect to the aqueous phase. Increasing the concentration of the copolymer resulted in smaller droplets produced since more of the copolymer chains are able to pack at the interface. The substantial decrease in interfacial tension facilitates the emulsification process, *i.e.*, break-up of large droplets into smaller ones proceeds with relative ease. The emulsion containing the highest copolymer concentration [Figure 4.6(c)] should be the most stable since the droplets will contain the highest number of adsorbed chains, allowing steric interaction to operate extensively compared to droplets with a lower fraction of adsorbed chains on its surface. In addition, a higher concentration of copolymer will result in an increase in the number of chains present in solution. This may induce a thickening effect, in which the increased viscosity of the continuous phase (due to copolymer present) restricts the movement of the droplets, *e.g.*, emulsion creaming [Equation (1.18)].

Interestingly, double emulsion droplets of the type water-in-oil-in-water (W/O/W) can be seen for the most dilute sample [Figure 4.6(a)]. Presumably, in order to compensate for the relatively low concentration of copolymer present, water droplets are trapped within the oil droplets. This may increase the effective concentration of copolymer in solution, allowing the formation of O/W emulsion to proceed with ease. From this investigation it was decided that the emulsions to be prepared in this work contained a copolymer concentration of *ca.* 3.5 wt% with respect to the aqueous phase.

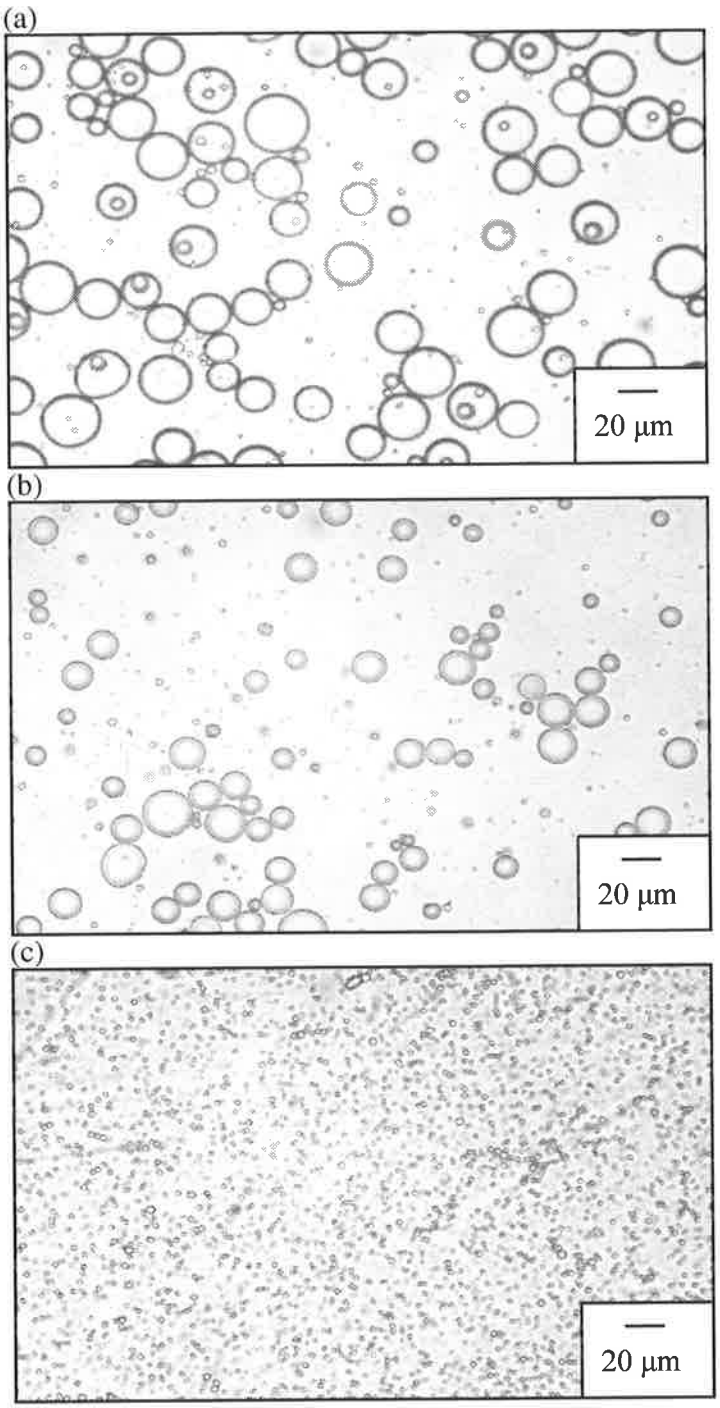

Figure 4.6: Optical micrograph of 1-bromohexadecane-in-water emulsions (ϕ_o = 0.3) containing 0.1 (a), 1 (b) and 10 (c) wt% copolymer with respect to the aqueous phase. Samples were diluted to ϕ_o = 0.1 prior to observation under the microscope. Using Equation (4.3) and the distribution of the droplets (not shown), d_v = 20.4, 10.7 and 8.0 μm for (a), (b) and (c), respectively.

4.4.1.6 Effect of Copolymer Structure

The effect of altering the copolymer structure on emulsion droplet size was investigated by observing the changes in the droplet size distribution and d_v for emulsions stabilised by MP1 and MP2 [Figures 4.7(a) and (b), respectively]. The structure of the copolymers is illustrated in Figure 2.1. The HLB of the end group of the EO units may have played a role in governing emulsion droplet size. Qualitatively, MP2 which contained an OH group at the end of the EO chain gave smaller droplets, compared to the larger droplets produced in the presence of MP1 (which had a methoxy end group). The HLB group number for OH is 1.9 (Table 1.4), while the methoxy end group is -0.475. The difference in HLB may have influenced the emulsification process, affecting the size of the droplets produced.

The relationship between copolymer structure and emulsion properties can be seen more clearly when comparing the emulsions containing P2 and MP2. The two copolymers differ most notably in the number of EO units (6 and 23, respectively). A noticeable difference can be seen from the droplet size of the emulsions (10 and 16 μm, respectively). It is possible that the long EO chain may have caused the hydrophilic part of MP2 to wrap around the hydrophobic unit, effectively forming a unimolecular micelle.[124] The HLB ranges and application shown in Table 1.3 indicate that for a range of *ca.* 15 - 18, the emulsifier is often used as a solubiliser. As a consequence, the concentration of copolymer available to facilitate the emulsification process is reduced (because of less interfacial adsorption) and the extent of steric interaction between droplets is diminished. This would lead to a lower surface excess concentration of copolymer and larger droplets being produced. The effect of reducing adsorbed polymer layer thickness on steric interaction between droplets will be discussed in more detail later. The relative absence of

the solubilisation effect in P2 (due to the relatively short EO chain length) presumably results in a higher surface excess and concentration and allows the copolymer to produce smaller droplets.

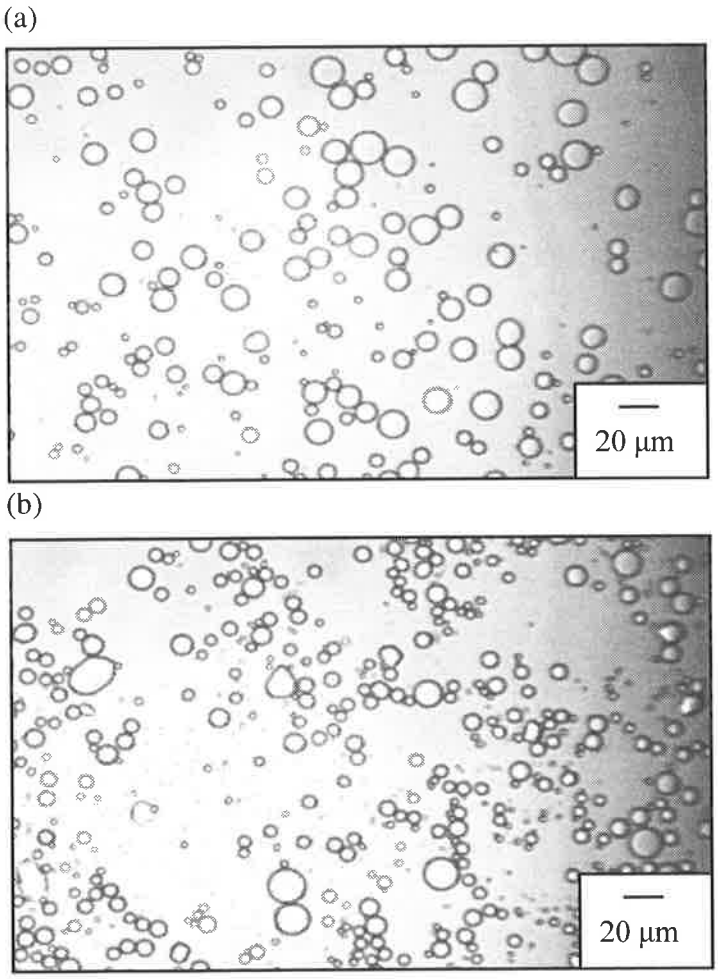

Figure 4.7: Optical micrograph of 1-bromohexadecane-in-water emulsion containing MP1 (a) and MP2 (b) immediately after preparation (diluted to ϕ_o = 0.1). Note that the concentration of copolymer was 3.5 wt% with respect to the aqueous phase for both of the emulsions. Using Equation (4.3) and the distribution of the droplets (not shown), d_v = 17.4 and 15.6 μm for (a) and (b), respectively.

4.4.1.7 Effect of Polymer Composition

The various poly(NIPAM-*co*-PEGMA) copolymers synthesised in Section 2.2.2 were screened prior to deciding upon the optimum copolymer composition for emulsion preparation. The key criterion for assessing the suitability of the copolymers was its ability to stabilise the O/W emulsions at room temperature, whilst conferring thermally-induced gelation. The emulsions were inspected visually to determine if the polymers present had successfully promoted emulsion formation. The results tabulated in Table 4.1 were obtained according to the visual observation that emulsions were able to flow under gravity while gel samples were not, *i.e.*, using the tube inversion method (Section 4.3.4).

Both poly(NIPAM) and poly(PEGMA) did not stabilise emulsions of oil and water. This can be attributed to the fact that poly(PEGMA) is mostly hydrophilic and lacks strong hydrophobic anchoring points for the oil droplets. On the other hand, there are insufficient poly(NIPAM) chains that extent towards the aqueous phase, although it adsorbs strongly on the droplet surface (since it is mostly hydrophobic). Neutron scattering studies conducted by Pelton *et al.*[125] have revealed that poly(NIPAM) adsorbs readily at the air and water interface to give a thin layer with a low content of water at temperatures below the LCST. This suggest that during emulsification the poly(NIPAM) chains are poorly solvated and do not impart steric stabilisation effectively to the droplets, leading to enhanced coalescence.

Table 4.1: Emulsifying and gelation capabilities for the polymers synthesised in Section 2.2.2

Polymer in emulsion[a]	Emulsion at room temperature	Gelation at at 50°C[b]	Observation
Poly(NIPAM)	No	-	-
Poly(PEGMA)	No	-	-
P1	Yes	Yes	Oil layer present after 1 day of preparation
P2	Yes	Yes	No oil layer present after gelation experiment
P3	Yes	No	-

[a] The emulsions contained $\phi_o = 0.3$ and 3.5 wt% polymer with respect to the aqueous phase. [b] Based on visual observations that emulsions were able to flow under gravity while gel samples were not, *i.e.*, tube inversion method (Section 4.3.4).

A sterically stabilising polymer must contain chains anchoring to the dispersed phase droplets and highly hydrated and stabilising chains that extend into the continuous phase. In addition, these segments of vastly contrasting behaviour need to be well separated to allow adsorption and steric stabilisation. The realisation of this concept involves copolymers containing segments that are anchoring (NIPAM units) and stabilising (EO units) in the continuous phase. Support for this can be seen from the emulsification of the oil and water mixture when the copolymers are present. It is noted that there is no direct proof available from this study for this structural model.

Although both P1 and P3 (mol% NIPAM in copolymer = 91 and 67%, respectively) were able to stabilise the O/W emulsions, the emulsion containing P3 did not exhibit gelation behaviour at 50°C. This may be attributed to the fact that there were insufficient NIPAM units, *i.e.*, temperature sensitive segments, in the copolymer to allow a significant inter-layer aggregation to occur which is needed for the formation of polymer chain network, *i.e.*, gelation to occur, at 50°C. As will be discussed in more detail below, polymer chains adsorbed on the surface of the oil droplets play a crucial role in emulsion gelation. The emulsion containing P1 showed evidence of slight phase separation after 1 day. This could be a result of the copolymer not having sufficient stabilising moieties, *i.e.*, the EO units, for steric stabilisation to operate extensively to keep the droplets from flocculating and/coalescing (section 1.2.5.3). From this study, it was decided that the emulsions to be prepared for the rest of the work consist of copolymers having a composition of 86 mol% NIPAM (*e.g.*, P2), since these emulsion exhibited gelation behaviour and absence of phase separation on heating.

4.4.1.8 Effect of Synthesis Conditions

The relationship between copolymer synthesis methods (more specifically comparison between NIPAM-feed and dual-feed methods from the P2 series) and emulsion properties can be seen from the data shown in Table 4.2. Except for P2D, the copolymers prepared from the dual-feed method (which produced compositionally symmetric copolymers) did not yield emulsions which showed gelation behaviour at 50°C. In contrast, the emulsion containing compositionally asymmetric copolymer, *i.e.*, P2 prepared from the NIPAM-feed method, exhibited gelation behaviour and absence of phase separation on heating, *i.e.*, no oil present.

It is possible that the compositionally symmetric copolymers did not achieve sufficient coverage on the droplet surface during emulsification. This leads to a fewer number of copolymer chains available for the formation of chain network at elevated temperatures. The hydrophobicity of these copolymers is lower compared to P2, which is 'blocky' in nature. P2 can be viewed as a 'blocky copolymer' with a high NIPAM content at one end and PEGMA the other (Section 2.5.2). Presumably the NIPAM-end readily absorbs on the emulsion droplet surface, while the PEGMA-end extends into the continuous phase, to give stable emulsions. At elevated temperatures, this relatively high concentration of adsorbed chains collapse to form network of polymer chains, which induces gelation in emulsions.

Table 4.2: Emulsifying and gelation capabilities for the copolymers synthesised in Section 2.2.2

Polymer in emulsion[a]	Synthetic method of copolymer[b]	Emulsion at room temperature	Gelation at at 50°C[c]	Observation
P2	Nf	Yes	Yes	No oil layer present after gelation experiment
P2A	df	Yes	No	Oil layer present during gelation experiment
P2B	df	Yes	No	Oil layer present during gelation experiment
P2C	df	Yes[d]	No	-
P2D	df	Yes	Yes	Oil layer present during gelation experiment
MP1	Nf	Yes	No	-
MP2	Nf	Yes	No	-

[a] The emulsions contained ϕ_o = 0.3 and 3.5 wt% polymer with respect to the aqueous phase. [b] Nf = NIPAM-feed, df = dual-feed.

[c] Based on visual observations that emulsions were able to flow under gravity while gel samples were not, *i.e.*, tube inversion method. [d] Only part of the oil and mixture remained emulsified after shear.

The presence of oil layers in the emulsions containing the symmetric copolymers further supports the view that the surface of the oil droplets in these emulsions are not sufficiently covered by the copolymers. At 50°C, the oil droplets experience significant Brownian motion. Droplets containing bare surfaces will be prone to flocculation and coalescence, since steric interaction is absent. Enhanced coalescence leads to phase separation (Figure 1.6). In the case of the blocky copolymer, the oil droplets which are sufficiently covered by the copolymer allows steric interaction to operate extensively, to give stable emulsions at room and gels at elevated temperatures. It is for these reasons, *i.e.*, ability to impart stability to emulsions at room temperature, whilst conferring gelation at elevated temperatures that P2, prepared using the NIPAM-feed method, was chosen as the copolymer of choice for the preparation and stabilisation of emulsions for the remainder of this work.

The fact that emulsions stabilised by MP1 and MP2 did not exhibit gelation properties at 50°C is interesting. As indicated in Section 1.1.6, transient network theory predicts that for gelation to occur there need to be a network of polymer chains containing 'sticky' end groups which can form aggregates (Figure 1.5). In other words, the formation of gels requires extensive inter-chain polymer aggregation. It is possible that the long EO chains of MP1 and MP2 (9 and 23 EO groups, respectively for MP1 and MP2, *cf.* 6 EO groups for PEGMA) may have resided in the periphery of the adsorbed chains, preventing further aggregation of the MP1 and MP2 copolymer chains at temperatures above the LCST and hence, the formation of copolymer chain network. Presumably, the shorter EO chain length of PEGMA did not have sufficient steric stabilisation to prevent extensive aggregation at elevated temperatures. In a related work, the poly(methyl methacrylate-*g*-polystyrene) copolymers investigated by Kikuchi and Nose[124] were found to exist as rod-like unimolecular micelles at high branch density (*cf.* MP1 and MP2). They

concluded that those micelles, which were connected to each other, comprised of a polystyrene core and poly(methyl methacrylate) chains which extended into the continuous phase. At low branch density (*cf.* P2), they found that intermolecular association took place, instead of unimolecular micelle formation.

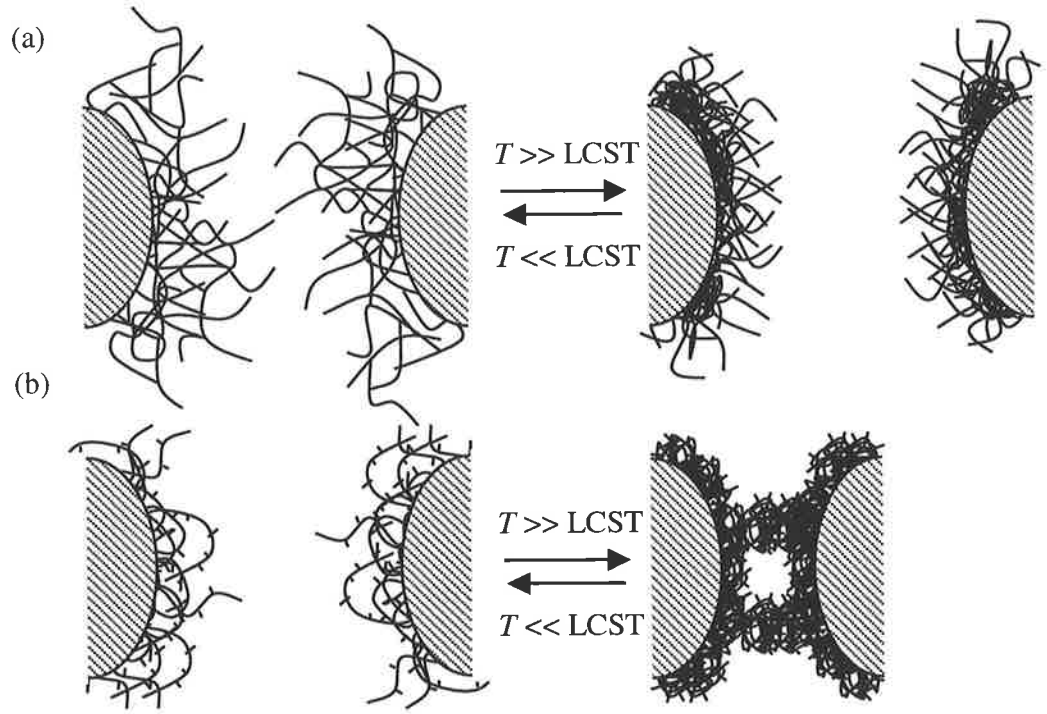

Figure 4.8: Proposed representation of adsorbed MP2 (a) and P2 (b) copolymers on emulsion droplet surface at temperatures below and above the LCST. The relatively long EO chains of MP2 reside in the periphery of the adsorbed chains preventing further aggregation upon collapse of the copolymer, *i.e.*, steric interaction. In contrast, the short EO chain length of P2 may not be sufficient to prevent extensive aggregation (via bridging flocculation), leading to the formation of large aggregates and droplet flocculation at elevated temperatures. This gives rise to gelation when the copolymer is adsorbed onto emulsions.

4.4.2 Physical Measurements

4.4.2.1 Emulsion Creaming Studies

The freshly prepared 1-bromohexadecane-in-water emulsion containing P2 was stored at room temperature in a stoppered calibrated cylindrical glass tube. Stability was investigated by both (i) measurements of the height of the separated water phase/serum in the tube with time and (ii) evaluation of changes in the average droplet size of the stored samples.

Figure 4.9 shows the fraction of the serum layer at the bottom that formed due to creaming, ϕ_s, with time (ϕ_s = height of serum phase/height of initial emulsion). For comparison, emulsion stabilised by C_9E_6, a type of short-chain surfactant, is shown. As can be seen, the emulsion containing the copolymer started to cream after half an hour (indicated by the serum layer at the bottom). The volume of serum phase increased dramatically during the first twenty hours of the experiment and remained fairly constant after that. The droplets were weakly flocculated as gentle inversion by hand redispersed the emulsion, *i.e.*, breaking of the weak flocs. Although flocculation is quite significant, the extent of coalescence was minimal, as indicated by the relatively similar droplet size distribution at the end of the experiment (Figure 4.10) and absence of oil layer at the top of the emulsion, *i.e.*, no phase separation.

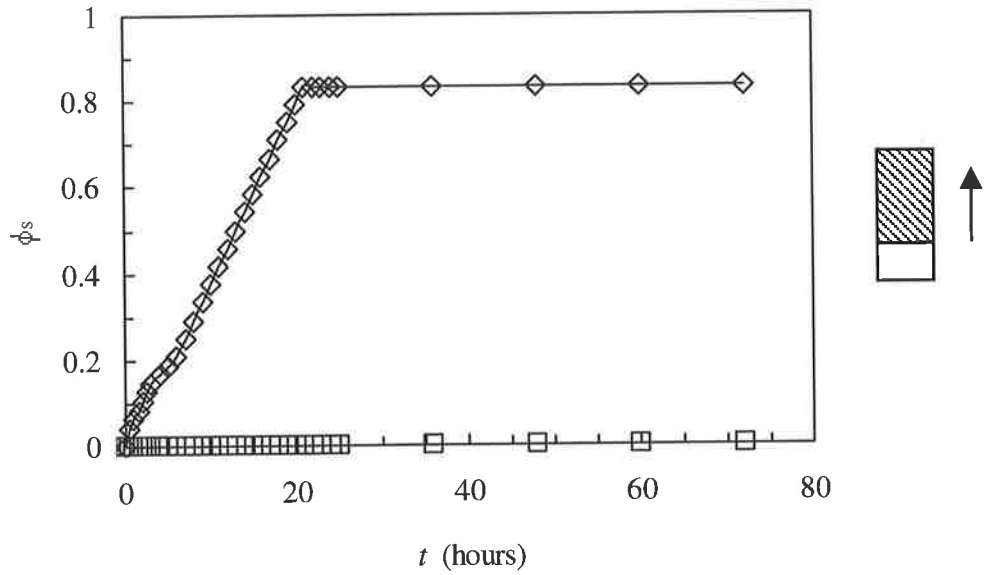

Figure 4.9: Volume fraction of serum layer for the emulsions containing P2 (◇) and C_9E_6 (□) as a function of time measured at room temperature. Note that ϕ_o = 0.1 and concentration of each stabiliser was *ca.* 3.5 wt% with respect to the aqueous phase for both of the emulsions.

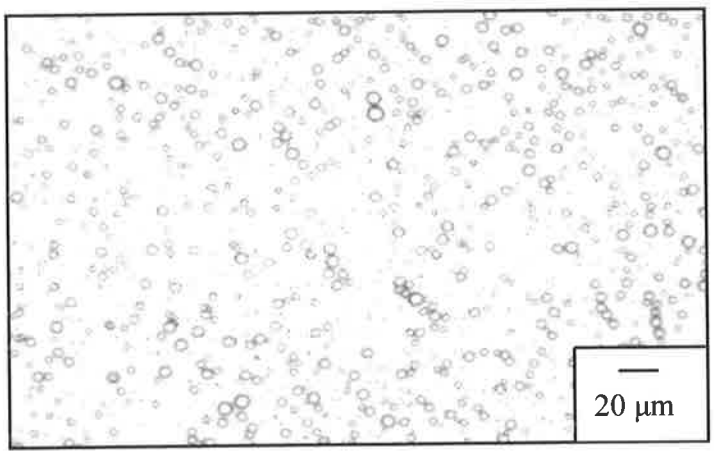

Figure 4.10: Optical micrograph of emulsion containing P2 after three days. ϕ_o = 0.1 and concentration of the copolymer was *ca.* 3.5 wt% with respect to the aqueous phase. The creamed emulsion was gently inverted to redisperse the droplets prior to observation. d_v = 11 μm.

The critical distance for which steric stabilisation operates, H_c, for droplets coated with an adsorbed layer of polymer chains may be calculated using the DLVO theory. For emulsions having a negligible ζ potential, *i.e.*, $V_R \sim 0$, then $V_{tot} = V_A$ [see Equation (1.24)]. Using Equation (1.22), the critical attractive energy for flocculation to occur, V_A^c, is given by:

$$V_A^{\ c} = -\frac{A_{eff}\, a}{12H_c} \tag{4.4}$$

Assuming that
The value of V_A^c must become greater in magnitude than the thermal energy, *kT*, for droplets to flocculate, then Thus, V_A^c can be expressed as:

$$V_A^{\ c} = \frac{A_{eff}\, a}{12H_c} \geq \frac{3}{2}kT \tag{4.5}$$

During flocculation (in the absence of droplet deformation), $H_c = 2\delta_m$, where δ_m is the minimum layer thickness required to keep the droplets from flocculating. Hence, Equation (4.5) can be rearranged to give:

$$\delta_m \geq a\left(\frac{A_{eff}}{36kT}\right) \tag{4.6}$$

Using Equation (4.6) and values of $A_{eff} = 2.8 \times 10^{-21}$ J and $a = 4.9 \times 10^3$ nm, δ_m for the emulsion containing P2 was found to be *ca.* 92 nm at 25°C. Note that $A_{11} = 6 \times 10^{-20}$ J and $A_{22} = 3.7 \times 10^{-20}$ J was used for the calculation of A_{eff}.[46,113] Assuming that the adsorbed copolymer is fully extended, the maximum chain length, δ_{max}, is *ca.* 100 nm (the C-C bond length[126] is 1.54 Å). The value for δ_m is comparable to that of δ_{max} indicating that the adsorbed copolymer chains

are close to fully extended in solution. This is because weak flocculation is apparent from Figure 4.10. The value of δ_a for poly(vinyl alcohol-*co*-vinyl acetate) copolymers having a M_n of *ca.* 5 x 10^4 g/mol adsorbed on polystyrene latex particles in water have been found to be[8] *ca.* 75 nm. Given that M_n for P2 is *ca.* 44600 g/mol (Table 2.5), the calculated δ_m seems slightly high for monolayer copolymer adsorption. It can be inferred that a monolayer of polymer brush at the interface could not provide a sufficient layer thickness for stable dispersion of droplets having a radius of 4.9 μm. The data are indicative of a weakly flocculated system. However, multiple layers of adsorbed chains at the interface cannot be ruled out.

In the presence of the commercial surfactant, C_9E_6, stable emulsion was produced. No serum layer was observed within the time scale of the experiment, *i.e.*, no aqueous layer at the bottom. This was due to the small monodisperse droplets in the emulsion which slowed the process of flocculation and coalescence [Figures 4.11(a) and (b)]. According to the Stokes equation [Equation (1.17)], droplet velocity is proportional to the square of the droplet radius. The relative rate of creaming can be obtained by comparing the ratio of a^2 for the emulsions containing P2 and C_9E_6. The creaming rate for the emulsion containing the copolymer was found to be 16 times higher than that for the emulsion with C_9E_6. Thus, larger droplets will cream/sediment faster than smaller ones. It should be noted from the data shown in Figure 4.9 that the emulsion containing C_9E_6 showed no evidence of a serum layer, *i.e.*, creaming rate = 0, throughout the duration of the experiment. Since the emulsion containing P2 (3.5 wt% with respect to the aqueous phase and ϕ_o = 0.3) was found to have the best stability at room temperature (*i.e.*, significant creaming did not occur over the duration of the experiment compared to the ϕ_o = 0.1 sample), whilst exhibiting temperature-induced gelation behaviour (Table 4.1), the data discussed in the remainder of this part of the work concerns this emulsion.

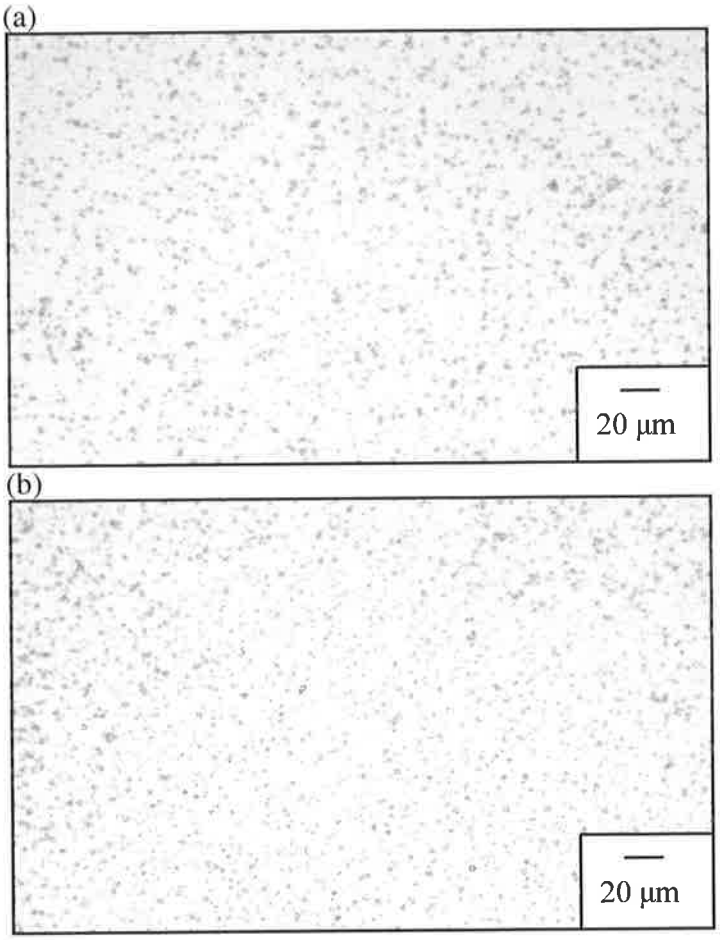

Figure 4.11: Photomicrographs of emulsion containing C_9E_6 after preparation (a) and after three days (b). Note that $\phi_o = 0.1$ and the concentration of the surfactant was *ca.* 3.5 wt% with respect to the aqueous phase. The volume average diameter for (a) and (b) is approximately *ca.* 2.5 μm.

4.4.2.2 Electrophoretic Mobility Studies

No measurable ζ potential was detected for the emulsion containing P2. This indicates that steric and not electrostatic stabilisation is the primary mechanism that contributes to stability of the emulsion at room temperature. This also suggests that the LCST of the poly(NIPAM) chains in the copolymer will not be influenced by the surface charge of the droplets, as has been reported in the literature of highly charged surfaces affecting the LCST of poly(NIPAM).[127]

4.5 Emulsion Characterisation at Elevated Temperature

4.5.1 Emulsion Characterisation

4.5.1.1 Visual Observation of Temperature-induced Gelation

As mentioned in Section 1.2.5, the properties of emulsions are strongly dependent on the interaction between the emulsion droplets as well as properties at the oil-water interface. The data in Tables 4.1 and 4.2 show that all the emulsions, except the ones containing the homopolymers and P2C, gel at 50°C. This phenomenon is due to the thermally-sensitive copolymers present in the system, since the emulsion stabilised with C_9E_6 showed no signs of gelation across the experimental temperature range (Figure 4.12). It was found that emulsion gelation could be reversed by agitation at 50°C, or cooling to room temperature in the absence of agitation, *i.e.*, the fluid-to-gel transition is reversible.

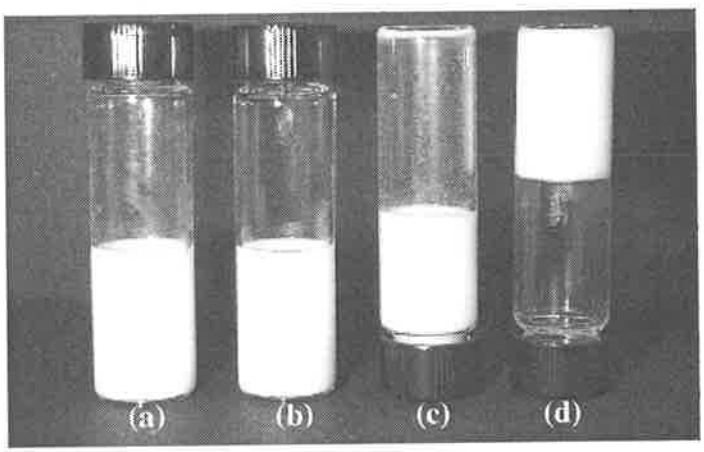

Figure 4.12: Emulsions prepared using C_9E_6 at room temperature (a) and at 50°C (c) and P2 at room temperature (b) and at 50°C (d). Note that ϕ_o = 0.3 and the concentration of each stabiliser was *ca.* 3.5 wt% with respect to the aqueous phase.

4.5.1.2 Effect of Oil Volume Fraction

The effect of changing ϕ_o on the gelation temperature, T_{gel}, was investigated by means of the tube inversion method (Section 4.3.4). Emulsions containing P2 with varying ϕ_o were prepared according to the method described in Section 4.2.2. Figure 4.13 shows the phase diagram for the effect of varying ϕ_o on the fluid-to-gel transition. Gelation behaviour was only observed for $\phi_o \geq 0.1$. Note that the parent copolymer solutions (3.5 wt%) did not gel at these concentrations. At very low ϕ_o there were not enough oil droplets in the emulsion for gelation to be observed at elevated temperatures, since the dispersion consisted mostly of copolymer chains and a low proportion of droplets. In these systems the copolymer concentration in the aqueous phase was much lower than the gelation concentration for pure solution (~ 10 wt%). At high ϕ_o, the gel was comprised of a large proportion of oil droplets that was trapped within networks of copolymer chains. This gave rise to a more solid-like sample, *i.e.*, a stronger gel formed.

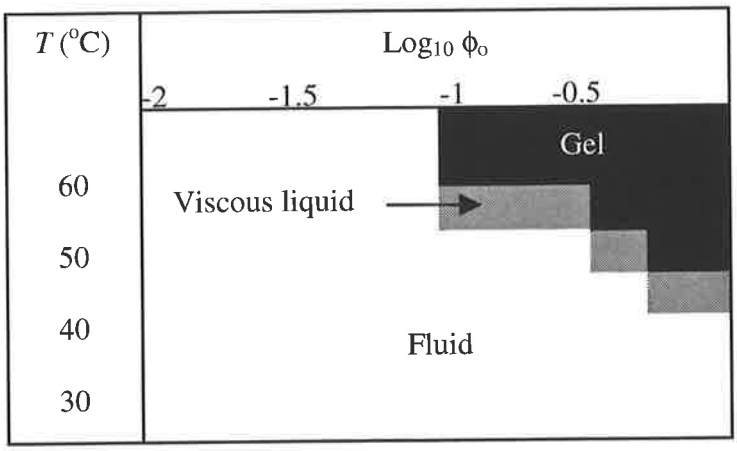

Figure 4.13: Phase diagram illustrating the effect of ϕ_o on the fluid-to-gel transition. Note that the term viscous liquid was used to describe the appearance of the sample that was neither a fluid nor solid-like.

Increasing ϕ_o resulted in a lower T_{gel} since more oil droplets were able to participate in the gelation process at a given copolymer concentration. There should come a point where the high volume fraction of oil present in the emulsion is sufficient to allow gelation to occur at a temperature equivalent to the LCST of the copolymer. At this stage the droplets can be considered 'jammed' to give continuous three-dimensional contact throughout the emulsion, thus, making flow impossible. The phase volume at which this occurs is also known as the critical volume fraction, ϕ_o^*. The temperature which corresponds to the fluid-to-gel transition (*i.e.*, upper boundary of the viscous liquid or lower boundary of the gel phase) for the various concentrations is averaged and extrapolated to the LCST of P2 (*ca.* 35°C) for the determination of ϕ_o^*. The plot in Figure 4.14 shows that $\phi_o^* \sim 0.75$. This value is comparable to the maximum packing fraction, ϕ_{max}, of *ca.* 0.74 for hexagonal close packed arrangement of monodisperse droplets.[128] The slightly higher value for the system investigated is due to the polydisperse nature of the oil droplets, which allows smaller droplets to fit into the gaps between the bigger ones. It should be noted that in the present context ϕ_{max} corresponds to adhesive droplets. At room temperature, it is expected that the non-adhesive droplets would still be able to flow. The jamming volume fraction at room temperature could be expected to be higher than 0.75. However, this was not investigated in this work.

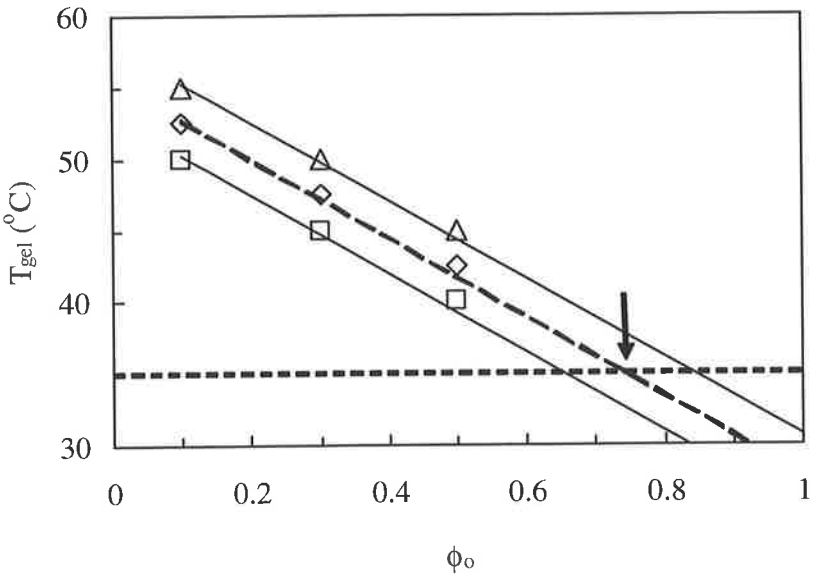

Figure 4.14: Extrapolation of T_{gel} (data from Figure 4.13) to the LCST of P2 (broken line). The arrow, which indicates ϕ_o^* and corresponds to a value of *ca.* 0.75, has been determined from the extrapolation of the average values (◇) of the upper boundary of the viscous liquid (□) and lower boundary of the gel phase (Δ), *i.e.*, fluid-to-gel transition.

4.5.1.3 Effect of Copolymer Concentration

The effect of changing c_p on T_{gel} was investigated by means of the tube inversion method. Emulsions with varying c_p (with respect to the volume of the aqueous phase) were prepared according to the method described in Section 4.2.2. Figure 4.15 shows the phase diagram for the effect of varying the concentration of P2 in the emulsion on the fluid-to-gel transition, *i.e.*, gelation. At low concentrations, the emulsions did not exhibit gelation behaviour. The solid-like sample domain, *i.e.*, gel phase, increased with increasing copolymer concentration. As shown in the Section 4.5.1.2, gelation was observed for emulsion containing ϕ_o = 0.3. Yet when the concentration of the copolymer was altered (while keeping ϕ_o constant), gelation was observed

only for the more concentrated samples. This shows the importance of the copolymer in inducing emulsion gelation. Furthermore, it was observed that c_{gel} for the emulsion coincided with c_p^* (although some of the copolymer may have adsorbed on the droplet surface, reducing its concentration in solution). Thus, it can be inferred that above c_p^* of *ca.* 1 wt%, the chains begin to overlap and entangle with one another to form a copolymer network spanning the entire emulsion to induce gelation. As the concentration of copolymer increases, more chains are present at a given temperature. The increase in the number of collapsed chains above the LCST (hence, a more extensive chain network) means that the temperature required for emulsion gelation to occur is lowered. It should be noted that the gelation concentration for the *copolymer solution* is *ca.* 10 wt% (Chapter 5), while in the presence of oil droplets ($\phi_o = 0.3$) $c_{gel} = 1$ wt%. The importance of the dispersed phase in governing gelation will be discussed in more detail in Section 4.5.3.

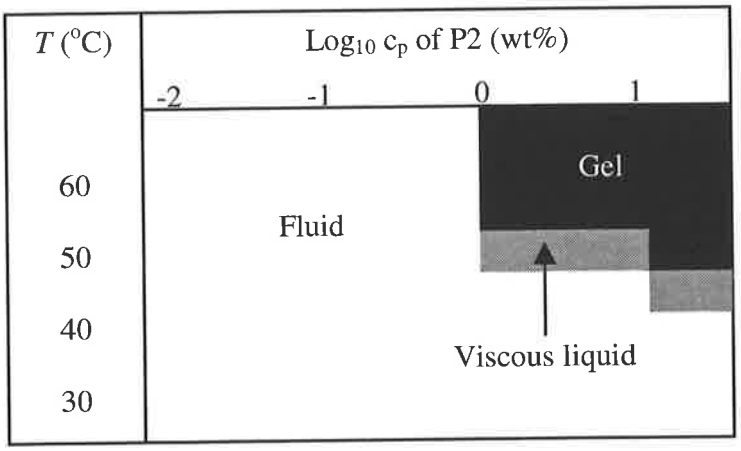

Figure 4.15: Phase diagram illustrating the effect of varying the concentration of P2 in the emulsion ($\phi_o = 0.3$) on the fluid-to-gel transition.

4.5.2 Physical Measurements

4.5.2.1 Capillary Viscometry Measurements

The temperature-induced gelation behaviour observed at elevated temperatures in the emulsion containing P2 (3.5 wt% with respect to the aqueous phase and ϕ_o = 0.3) was further investigated by studying the variation of viscosity with temperature using an Ostwald viscometer. The results shown in Figure 4.16 were compared with that obtained for the emulsion containing C_9E_6. The viscosity for the emulsion containing the copolymer decreases with increasing temperature and reaches a minimum at *ca.* 45°C. A dramatic increase in viscosity occurs above 48°C. Visual inspection of the sample revealed the viscosity increased to such an extent that the emulsion had gelled above this temperature [see Figure 4.12(d)]. Cooling the gelled emulsion resulted in the viscosity decreasing and the sample to being able to flow again. The viscosity increases again below the gel point at *ca.* 45°C (as expected for normal polymer solutions). As expected, the emulsion containing C_9E_6 showed no sign of gelation over the whole experimental range except a slight decrease in viscosity as temperature was increased. It should be noted that the rheological behaviour observed for the emulsion prepared using the copolymers is opposite to what is observed for concentrated poly(NIPAM) microgel dispersions, which form colloidal gels at room temperature and flow when the temperature decreases below the LCST.[129]

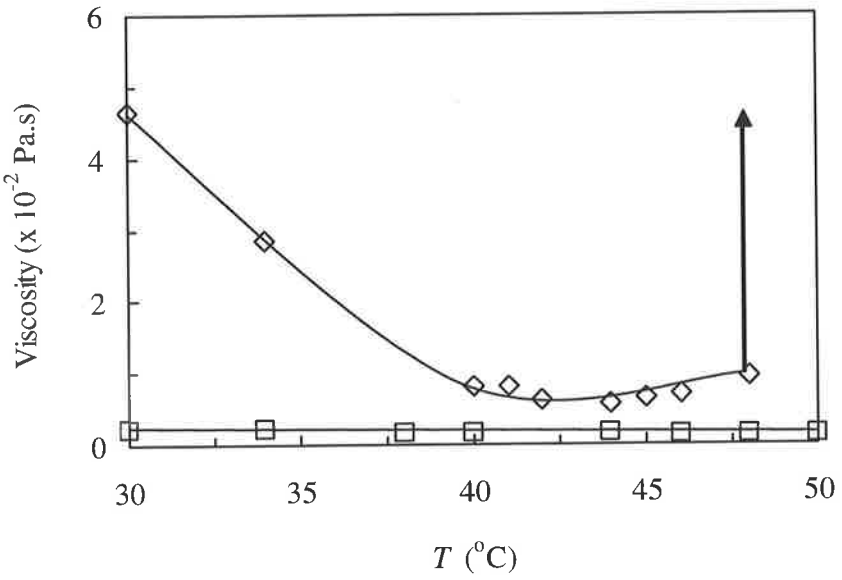

Figure 4.16: Effect of temperature on the viscosity of the samples measured using an Ostwald viscometer; (◇) and (□) represents the emulsion containing P2 and C_9E_6, respectively. For both of the emulsions Note that ϕ_o = 0.3 and the concentration of each stabiliser was *ca.* 3.5 wt% with respect to the aqueous phase.

Figure 4.17 shows the viscosity plot when the gelled emulsion was allowed to cool. For comparison the heating curve for the emulsion containing P2 in Figure 4.16 is illustrated. The higher viscosity observed for the cooling curve compared to the heating curve could be attributed to the fact that since gelation is a time-dependent phenomenon, the time scale of the experiment could be shorter than the time required for the gel to break-up as temperature decreases (*i.e.*, entanglements of nearby copolymer layers of sterically stabilised dispersions prevent redispersion when the solvency changes from good to poor and then back to good[11]). This leads to a higher proportion of flocculated droplets at room temperature. This increases the effective

volume fraction of the droplets and hence, the viscosity. The temperature-dependent rheology of the copolymer solutions and emulsions are investigated in Chapter 5.

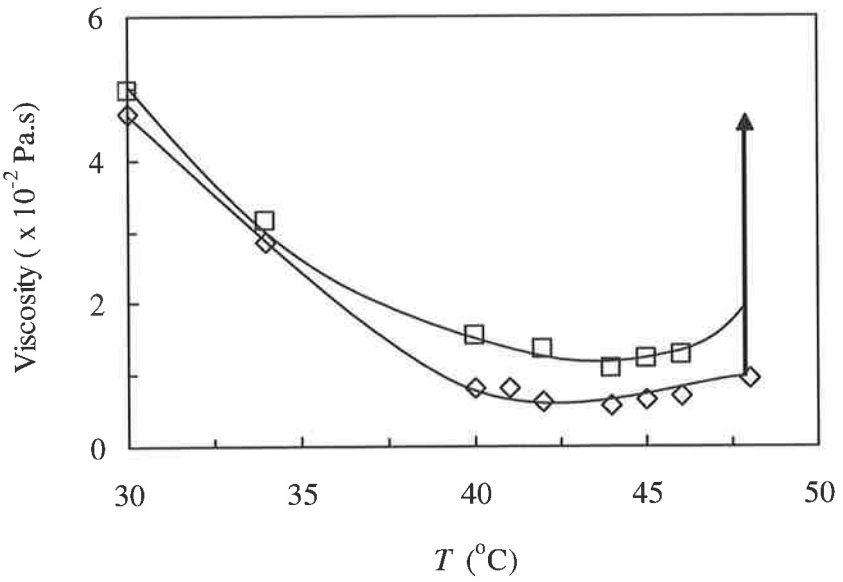

Figure 4.17: Viscosity plots for the emulsion containing P2 when heated (◇) and cooled (□). Note that ϕ_o = 0.3 and the concentration of P2 was *ca.* 3.5 wt% with respect to the aqueous phase.

4.5.2.2 Reversibility of Temperature-induced Gelation

The emulsion did not break as a result of gelation reversal, although there was evidence of an increase in the average droplet size of *ca.* 4 μm. Optical microscopy (Figure 4.18) revealed residual flocs were present in the emulsion after one temperature-induced gelation cycle, *i.e.*, heating from room temperature to 50°C and holding at that temperature for *ca.* 30 min. before cooling to room temperature. The increased number of flocs present upon gelation supports the

data presented in Figure 4.17 of the higher viscosity of the cooling curve compared to the heating curve.

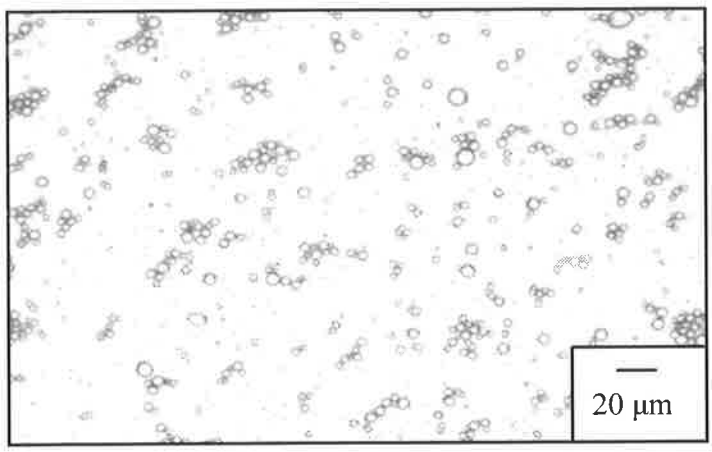

Figure 4.18: Optical microscopy of the emulsion containing P2 (3.5 wt% with respect to the aqueous phase) after one heating/cooling cycle (diluted to $\phi_o = 0.1$). Most notable is the presence of flocs. The average droplet size is *ca.* 14.0 μm.

The increased number of flocs upon gelation suggests that the extent of stabilisation in the emulsion diminishes as temperature increases [Figure 4.19(a)]. The collapse of the copolymer chains above the coil-to-globule transition temperature (*e.g.*, at *ca.* 35°C for P2) reduces δ_a. This lowers the extent of steric interaction which keeps the droplets from flocculating [Figure 4.19(b)]. At elevated temperatures, the collapse of the chains may provide a rigid interface encapsulating the droplets which opposes coalescence [Figure 4.19(c)]. This coalescence resistance behaviour at high temperatures is absent in emulsions containing short-chain surfactants, where the chains remain relatively mobile at the interface and may be

displaced upon strong droplet interactions, *e.g.*, droplet deformation due to strong flocculation, to give rise to droplet coalescence.[55]

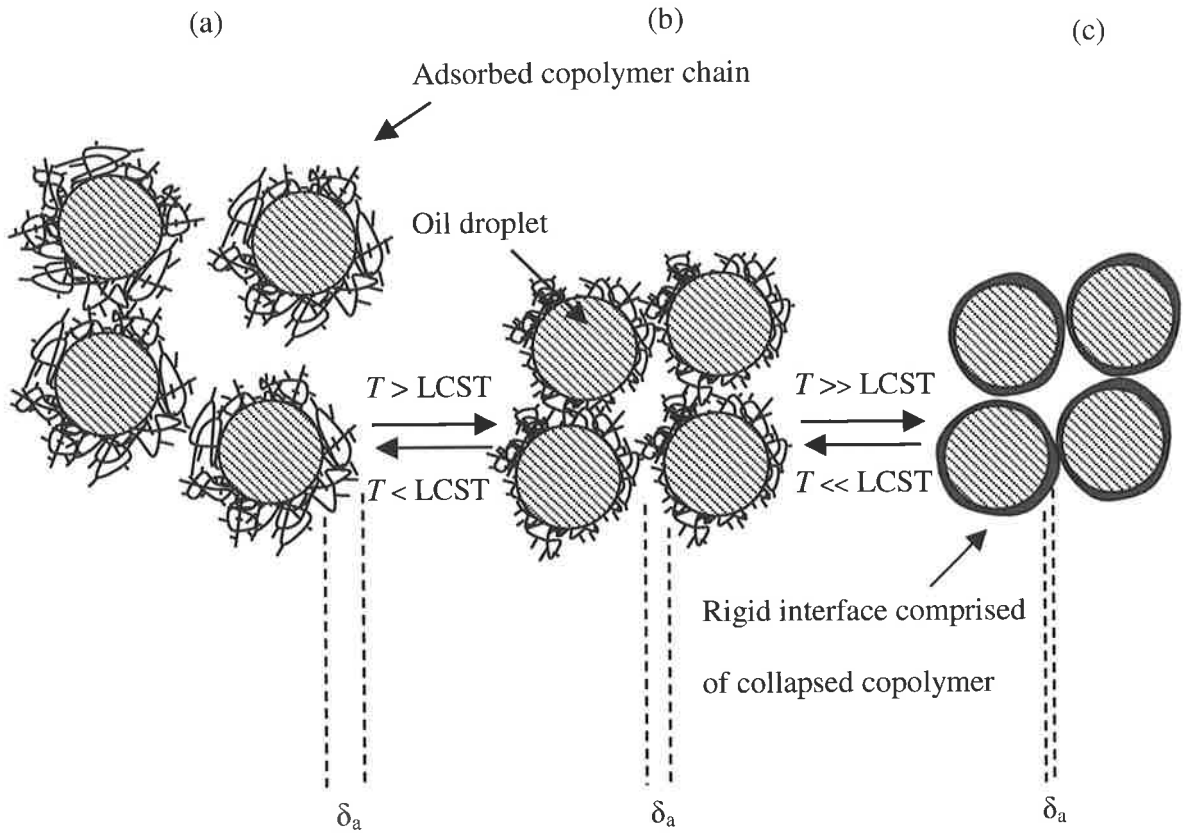

Figure 4.19: Depiction of the reduction in the layer thickness, δ_a, at $T <$ LCST (a), $T >$ LCST (b) and $T >>$ LCST (c).

As the gelled emulsion is cooled the collapsed chains begin to expand, *i.e.*, extent into the continuous phase, since the solvent quality becomes better. When the temperature is less than the LCST of the copolymer, steric interaction between droplets becomes significant and the strongly flocculated droplets begin to redisperse in solution. In addition, the positive osmotic pressure in

the interlayer region between droplets swells and disperses the droplets. At low enough temperatures, the droplets are no longer flocculated and are able to move pass each other to give a fluid emulsion. Note that this good degree of reversibility for the copolymer stabilised emulsions is distinctly different to the behaviour of emulsions stabilised by short-chain EO surfactants, *e.g.*, C_9E_6, when heated to above the phase inversion temperature.[55] For the latter, emulsion breaking results from heating to the phase inversion temperature in absence of shear.

Apart from the photomicrographs and viscosity data, the stability of the thermally-responsive emulsions can be explained using total interaction energy curves. At temperatures below the LCST, there probably exists a shallow minimum. The steric interaction operates at interparticle distances $< 2\delta_a$ [Figure 4.20(a)]. The shallow minimum may result in flocculation of the droplets if it is comparable to $3/2kT$. This flocculation is weak since the process can be reversed by applying a modest amount of shear, *e.g.*, gentle shaking of the emulsion. As temperature increases the depth of the minimum deepens (and magnitude of V_A increases) because the chains collapse. The collapse of the adsorbed chains increases the likelihood for flocculation to occur. At elevated temperatures, the minimum disappears and the droplets experience significant attractive interaction, *i.e.*, strong flocculation, resulting in emulsion gelation [Figure 4.20(b)]. The inter-chain interactions across the interface are attractive. Note that this interaction is more akin to coagulation, except that it is mostly reversible. The disappearance of the minimum can be attributed to the significant collapse of the adsorbed copolymer chains, which forms a rigid interface around the droplets that opposes coalescence, *i.e.*, the substantial decrease in the copolymer layer thickness results in negligible steric repulsion between the droplets.

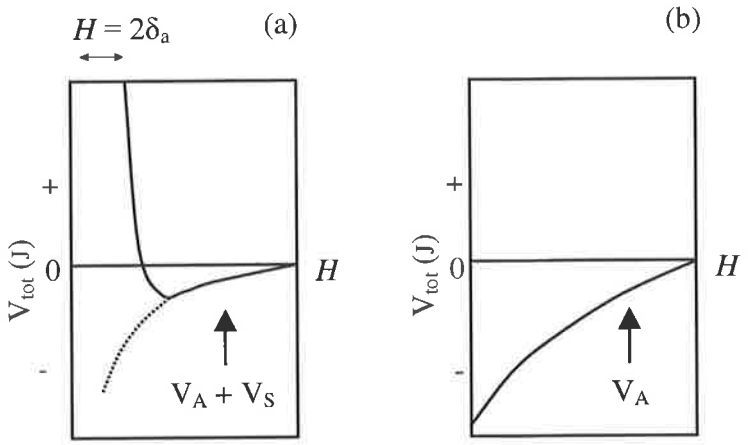

Figure 4.20: Total interaction energy curves for the emulsions containing poly(NIPAM-*co*-PEGMA) copolymers at 25 (a) and 50°C (b). As temperature increases above the LCST of the copolymer (35°C in the case for P2), the steric interaction energy which exists between droplets progressively diminishes. At elevated temperatures, the disappearance of the minimum and dominance of the attractive interaction energy result in strong droplet flocculation, which results in gelation. Note that decreasing the temperature to less than the LCST of the copolymer can reverse this process.

4.5.3 Proposed Mechanism

The data presented so far allow a preliminary mechanism for temperature-induced emulsion gelation to be proposed. As temperature increases above the LCST, the copolymer chains begin to collapse; at the same time these chains may aggregate. Aggregation occurs not only with the chains in solution but those adsorbed on the oil droplet surface as well. Consequently, copolymer chains comprised of aggregated chains are formed. Gelation results when a critical concentration of oil droplets is exceeded which allows formation of the network, or a high enough copolymer concentration is present which spans the entire system. As

temperature increases even further, a strong gel results due to the enhanced interaction between the collapsed chains, *i.e.*, strong network.

The viscosity data for the copolymer solution at $c_p > c_p^*$ (Figure 2.22) show a decrease in viscosity with increasing temperature and rules out contribution from temperature-induced continuous phase thickening (*e.g.*, associated with the copolymer chains in solution) to emulsion gelation.

The oil droplets present must act as anchoring points for the formation of copolymer chain network, leading to emulsion gelation at elevated temperatures. This is evident from the phase diagram shown in Figure 4.15 where c_{gel} (*ca.* 1 wt%) for the emulsion coincided with c_p^* (although some of the copolymer may have adsorbed on the droplet surface, reducing its concentration in solution) when a volume fraction of oil of *ca.* 0.3 was present. As ϕ_o increases, the temperature required for gelation to occur decreases since the larger number of oil droplets present allows a more extensive anchorage of the copolymer chains to the droplets. Alternatively, T_{gel} can be reduced by increasing the concentration of the copolymer in solution, since the higher number of interfacial chains present allows for the formation of a more extensive copolymer network at a given temperature.

The mechanism for emulsion gelation envisaged is similar to bridging flocculation observed in colloidal systems containing high molecular mass polymers. Bridging flocculation occurs when the added polymer concentration is lower than required for full saturation and the chains simultaneously adsorb on more than one droplet. The droplets are usually loosely aggregated and may be viewed as being connected within a network of polymer chains.[4] In this work, the surfaces of the emulsion droplets are believed to be extensively covered by adsorbed copolymer. The repulsive interaction between adsorbed copolymer chains allows the emulsion to

be sterically stabilised. At temperatures greater than the LCST of the copolymer, bridging flocculation occurs due to the attractive nature of inter-chain interactions. The copolymer chains at one droplet surface may attach to other chains which are adsorbed on a second droplet. Note that bridging flocculation is not reversible,[130] while thermally-induced emulsion gelation can be reversed.

4.6 Conclusions

Poly(NIPAM-*co*-PEGMA) copolymers have been shown to stabilise O/W emulsions at room temperature. The optimum composition of the copolymer was found to be 86 mol% NIPAM. The optimum copolymer was synthesised using the NIPAM-feed method. The large droplet size, *ca.* 10 μm, was comparable to related data reported elsewhere for emulsions stabilised with polymeric surfactants. The emulsion containing 3.5 wt% P2 (with respect to the aqueous phase) showed no noticeable change in droplet size when the oil volume fraction was varied. The ratio of copolymer to the oil volume fraction could have minimal influence on the emulsification process, leading to optimum packing of copolymer chains at the droplet surface. Increasing the copolymer concentration (while maintaining ϕ_o) gave smaller droplets, while large droplets were produced in the presence of low copolymer concentration. The HLB of the end group of the EO side chains and the length of the EO units were found to have a profound effect on the emulsion droplet size. The long EO chains of the copolymer may have wrapped around the hydrophobic unit, effectively forming a unimolecular micelle. This is believed to have reduced the surface excess concentration of copolymer and gave rise to large droplets. The homopolymers did not stabilise emulsions of oil and water due to the absence of either a stabilising (hydrophilic) or anchoring (hydrophobic) chains. The absence of gelation behaviour for the emulsion containing copolymer with a low proportion of NIPAM (P3) was attributed to insufficient NIPAM units required for inter-layer aggregation to occur, which was needed for the formation of copolymer chain network. The lack of a significant number of stabilising units, *i.e.*, EO segments, for steric stabilisation to operate may have caused the phase separation behaviour to be observed for the emulsion containing copolymer with a high mol% NIPAM (P1).

Compositionally symmetric copolymers, prepared from the dual-feed method, may not have achieved sufficient surface coverage, leading to insufficient chains required for the formation of copolymer network. The hydrophobicity of these copolymers was lower than the 'blocky'/asymmetric copolymers, prepared from the NIPAM-feed method. For the latter, the NIPAM-end readily absorbed on the emulsion droplet surface, while the PEGMA-end extended into the continuous phase, giving rise to stable emulsions at room temperature. At elevated temperatures, this relatively high concentration of adsorbed chains collapsed to form network of copolymer chains, which induced gelation in emulsions.

Stability studies showed that emulsions containing the copolymer appeared less stable compared to emulsions with short-chain surfactants, *e.g.*, C_9E_6, due to smaller droplets being produced for the latter. Steric stabilisation was the primary mechanism of stability for the emulsions containing the copolymers, since a very low ζ potential was calculated from electrophoretic measurements. The phase diagrams showed that for temperature-induced emulsion gelation to be observed, $\phi_o \geq 0.1$ and $c_p \geq 1$ wt%. Increasing the oil volume fraction and/copolymer concentration decreased the gelation temperature. The increased concentration of oil droplets allowed a more extensive bridging of the chains between the droplets, while a higher copolymer concentration allowed for the formation of a greater number of bridging points (junctions) at a given temperature above the LCST. The fluid-to-gel transition was found to be reversible. However, a modest increase in both viscosity and droplet size (average droplet size of *ca.* 14.0 μm) was detected after one heating/cooling cycle.

The gelation mechanism postulated is similar to bridging flocculation observed in colloidal systems containing high molar mass polymers. At temperatures above the LCST, the collapse of the copolymer results in inter-chain aggregation. The steric interaction which keeps

the droplets from flocculating becomes insignificant as temperature increases, due to the reduction in the adsorbed layer thickness. Gelation results when a critical temperature is exceeded. The gel ~~is comprised~~ comprises of oil droplets which are trapped within interfacial networks of collapsed copolymer chains. The gelation behaviour of thermally-responsive emulsions may be tailored to suit various applications (Chapter 6), by altering the structure and composition of the copolymers and emulsion preparation methods, *e.g.*, copolymer concentration and oil volume fraction. To the best of the author's knowledge, the work presented here was the first to use responsive copolymers to produce reversible gelation of O/W emulsions.

CHAPTER 5 RHEOLOGICAL STUDIES

5.1 Introduction and Aims

The term 'rheology' was coined by Professor Bingham of Lafayette College in Indiana and refers to the study of the deformation and flow of matter.[128] The investigation of the rheological properties of materials is essential since most of the materials we come across in our every day life ~~concerns with~~ is related to its rheological behaviour. The process of thixotropy can be seen from the ability for paint to flow only when being brushed on ~~to the surface~~ and bonds to the surface with time it after ~~brushing is due to the time-dependent~~ process known as thixotropy. In this case, when the paint is sheared at a constant rate, *i.e.*, by brushing the paint on to the wall, the apparent viscosity decreases with time until a balance is reached between structural breakdown and structure reformation. When the paint is allowed to stand/left on the wall, it regains its original structure and the viscosity increases.

Much work on polymer rheology has been done on the rheological properties of polymeric solutions. Khan and co-workers[131] investigated the solution rheology of a hydrophobically modified alkali soluble copolymer consisting of a polyelectrolyte backbone containing EO side chains capped with alkylaryl groups. They concluded that the presence of the hydrophobic groups on the chains led to the copolymer exhibiting shear thickening followed by shear thinning behaviour when a critical shear stress was applied. They reasoned that above a critical concentration, the transition from intramolecular to intermolecular association of the chains is favoured thermodynamically. Kwon *et al.*[132] investigated the gelation behaviour of aqueous solutions of PEO-PGLA-PEO triblock copolymer (PGLA is DL-lactic acid-*co*-glycolic acid) by using rheological measurements. They showed that the gelation behaviour exhibited by the polymer was dependent only on the temperature and not on copolymer concentration. The

authors attributed the former to the solution-to-gel transition induced by the attraction among the PGLA segments upon heating. In a related work, several researchers investigated the temperature sensitive behaviour of aqueous solutions of methylcellulose.[133,134] From the rheological data obtained, these authors showed that the gelation behaviour was dependent on the molar mass, degree of grafting, concentration and presence of additives. The gelation was attributed to the hydrophobic interactions between the chains.

Hourdet *et al.*[16,34] investigated the solution behaviour of copolymers containing AMPS and PEO as LCST grafts (AMPS is 2-acrylamido-2-methylpropane sulfonic acid) using rheological measurements. They noted that thermothickening occurred when the systems were in the semi-dilute region for intermolecular association to occur and when the temperature reached the critical temperature of the grafts to induce interactions between grafts. In addition, the thermothickening behaviour was found to be shear rate dependent, with the copolymer solutions showing no significant change in viscosity across the shear range at low temperatures. However, at high temperatures the increased sample viscosity decreased significantly at high shear rates.

The rheological behavior of dispersions has been studied extensively due to their importance in a wide range of industrial applications, *e.g.*, paint formulations, food concentrates and printing inks. Rheological measurements may provide information about structure, states of flocculation and strengths of inter-droplet interactions.[7] The rheological studies of latexes containing hydrophobically modified urethane-ethoxylate (HEUR) associative thickeners by Huldén[135,136] revealed that the thickening efficiency of HEUR is strongly affected by the latex particle size and the type and concentration of surfactant present. The proposed association mechanism for latex and HEUR was supported by the data obtained from rheological measurements. It was postulated that the latex particles were incorporated into a three-

dimensional thickening network. This network consisted of cross-link points that were either micelle-like aggregates of the hydrophobic segments of the HEUR chains, or latex particles with thickeners adsorbed at the surface with one terminal hydrophobic group and the other in solution. Quintana *et al.*[137] showed that blends of polystyrene-*b*-poly(ethylene/butylenes)-*b*-polystyrene and polystyrene-*b*-poly(ethylene/butylenes) copolymers in *n*-octane were able to gel across a range of temperatures when the composition and concentration of the copolymers were varied. Rheological measurements were performed to support the data obtained from the preliminary gelation experiments. They found that upon melting of the gel, the elastic modulus, G', decreased dramatically. The point at which G' = G" was considered as the melting temperature, *i.e.*, transition from a solid like sample to a viscoelastic liquid-like state (G" is the viscous modulus).

Luckham and Ukeje[138] found that the rheological properties of emulsions are dependent on its polydispsersity. The viscosity, G' and G" of the polydisperse latex dispersions containing PEO-PPO-PEO triblock copolymer (PPO is polypropylene oxide) was reduced by 2- to 20-fold in comparison to monodisperse systems.

Although viscosity measurements on the copolymers and emulsions have been performed using capillary viscometer (Sections 2.6.1 and 4.5.2.1, respectively), complimentary studies were necessary since capillary viscometry provides relative data rather than absolute data. In addition, viscometers are more suited for the measurement of simple viscosity over a specific range, *e.g.*, polymer solutions. Rheometers can provide reliable absolute viscosity data, as well as measuring viscoelasticity, since the shear rate can be varied and controlled accurately. By systematically varying the shear products in oscillatory measurements, the rheology of complex fluids, *e.g.*, emulsions and clay dispersions, can be studied.

The aims of this section of the work can be summarised as follows:

(i) To investigate the temperature-dependence rheological properties of poly(NIPAM-*co*-PEGMA) copolymers solutions using steady shear and oscillatory measurements.

(ii) To study the temperature-dependence rheological behaviour of the emulsions containing poly(NIPAM-*co*-PEGMA) copolymer using steady shear and oscillatory measurements.

(iii) To determine the effect of changing copolymer concentration or oil volume fraction in the emulsions on the gelation temperature and gel strength.

(iv) To investigate the reversibility of temperature-induced gelation using rheological measurements.

(v) To determine if the mechanism for temperature-induced emulsion gelation presented in Section 4.5.3 is consistent with the rheological data.

5.2 Theory

5.2.1 Rate of Strain of a Fluid

The stress, σ, is defined as the force, F, divided by the area, A, over which it is applied (Figure 5.1). When a shear stress is applied, flow usually occurs, *e.g.*, when sliding a piece of paper over a gummed surface. Deformation results from the application of a stress to a material. The relative deformation per unit length is also known as strain, γ, and is given by:[7]

$$\gamma = \frac{x}{z} \tag{5.1}$$

where x is the displacement produced and z is the distance between two surfaces.

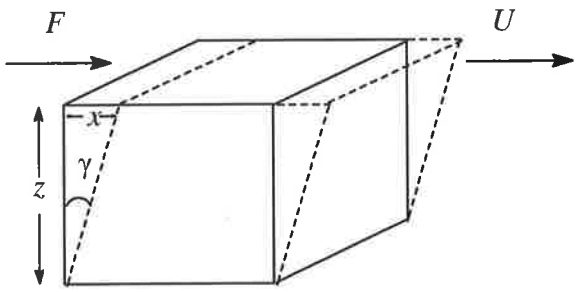

Figure 5.1: Schematic representation of two parallel plates with the intervening space, z, being filled with sheared liquid. Upon the application of a stress, σ, the upper plane moves with relative velocity, U. The strain, γ, on the plates is proportional to the displacement produced.

The rate of strain is defined as:[7]

$$\frac{d\gamma}{dt} = \frac{U}{z} \tag{5.2}$$

where U is the relative velocity.

5.2.2 Linear Behaviour

In the case of a Newtonian liquid, the flow persists as long as the stress is applied as given by:[7]

$$\sigma = \eta_s \left(\frac{d\gamma}{dt} \right) \tag{5.3}$$

where η_s is the shear viscosity. For Hookean solid, the applied shear stress results in an instantaneous deformation as shown by:[7]

$$\sigma = G\gamma \tag{5.4}$$

where G is the shear modulus.

Since this study is concerned with polymeric solutions and emulsions, a more thorough description of Newtonian behaviour is required. ~~A material is described as being~~ Newtonian ~~when only the shear stress~~ generates ~~the stress in simple shear flow~~. The shear viscosity is both independent of the shear rate and constant with respect to the shearing time. As soon as shearing stops, the stress in the liquid falls to zero.[128]

5.2.3 Non-linear Response

There comes a point where increasing the stress or strain leads to systems behaving as non-linear materials, in that the Newtonian or Hookean models fail to describe the behaviour.[7] This may be due to the flow field altering the microstructure resulting in many-body interactions, *e*.g., at sufficiently high concentrations, materials may resist deformation.

Pseudoplastic materials display a limiting high shear rate viscosity and the stress increases with the shear rate. Although the viscosity is inversely proportional to the shear rate, at low enough rates, the viscosity increase is reduced and reaches a constant.

Power law fluids[7] are different from plastic or pseudoplastic behaviour, in that shear thinning or thickening behaviour is dependent in the sign of the power law index, n_{pl}:

$$\sigma = A_c\left(\frac{d\gamma}{dt}\right)^{n_{pl}} \tag{5.5}$$

$$\eta_s = A_c\left(\frac{d\gamma}{dt}\right)^{n_{pl}-1} \tag{5.6}$$

where A_c is the consistency parameter and gives a measure of the polymer structure in solution, *e.g.*, coils or aggregates. Note that if n_{pl} is less than unity shear thinning is observed.

5.2.4 Linear Viscoelasticity

The rest condition represents a minimum energy state in structured liquids. As soon as these liquids experience deviation from the rest state, *e.g.*, when deformation sets in, thermodynamic forces try to restore the rest state. The elastic force manifests itself at small deformations as various elastic moduli, such as G', and at very large deformations, *i.e.*, steady-

state, by a normal-stress difference. Apart from these forces, viscous forces due to dissipation are present, so that together these produce viscoelastic effects, *i.e.*, solid-like and liquid-like properties.[139] Note that in the linear viscoelastic region, the response (*e.g.*, strain) at any given time is directly proportional to the value of the initiating parameter (*e.g.*, stress).

The viscoelasticity of a material may be investigated using oscillation measurements. A small oscillatory strain having a radial frequency, ω_r, and maximum strain, γ_0, is applied. In response to the applied strain, a stress develops. It should be noted that $\omega_r = 2\pi f$, where f is the applied frequency in hertz (Hz). The wave-forms from the applied strain and the resulting stress exhibited by linear viscoelastic materials are shown in Figure 5.2.

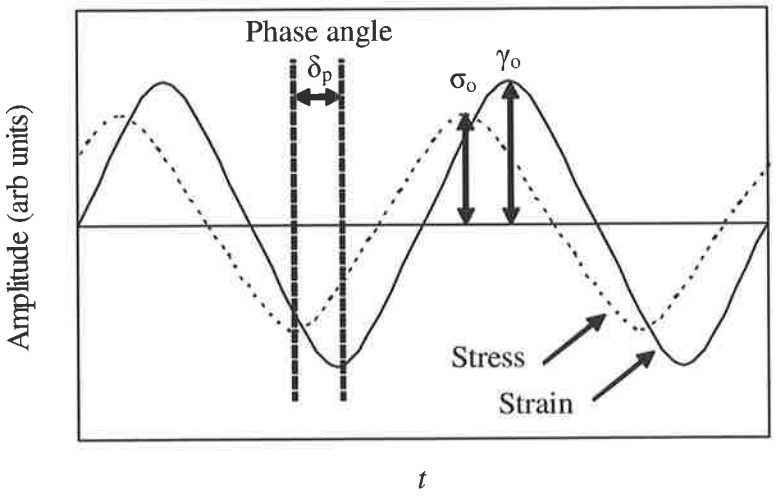

Figure 5.2: Oscillating strain and stress response for a viscoelastic material. Note that γ_o and σ_o are the maximum strain and stress, respectively. *Source*: Ref. 7.

The complex modulus, G*, is then measured:[7]

$$G^* = \frac{\sigma_0}{\gamma_0} \tag{5.7}$$

where σ_0 is the maximum stress. The elastic modulus, G', and viscous modulus, G", are determined from G* using:[7]

$$G' = G^* \cos\delta_p \tag{5.8}$$

and

$$G'' = G^* \sin\delta_p \tag{5.9}$$

where δ_p is the phase difference in radians between the peak value of the stress and the peak value of the strain (see Figure 5.2). Both G* and δ_p are constant in time and contain information about the response of the sample for any given frequency, *i.e.*, these parameters are characteristic of the material. For a perfectly elastic material, σ is in phase with γ, *i.e.*, $\delta_p = 0$, G' = G* and G" = 0. On the other hand, for a perfectly viscous sample, σ is 90° out of phase with γ, *i.e.*, $\delta_p = 90°$, G" = G* and G' = 0. The crossover point of G' and G", *i.e.*, G' = G", has been proposed as a measure of the onset of gelation.[140] However, this method is usually dependent on the frequency used in the measurement[141] and Winter and Chambon[142,143] have shown that this definition should only be applied to step-growth polymerisations of balanced stoichiometry. The elastic and viscous moduli are related by the loss tangent, $\tan\delta_p$, as given by:[140]

$$\frac{G''}{G'} = \tan\delta_p \tag{5.10}$$

5.2.5 Rheological Measurements

There are many instruments available for measuring rheology. The common rotational rheometers are either controlled-stress (employed in this work) or controlled-strain. These are shown schematically in Figure 5.3. In the former, the drag cup motor induces a known torque in the drive shaft which 'floats' on an air bearing, allowing almost frictionless application of the drive torque to the shaft. The attached geometry causes this torque to manifest as a specific stress, and the response of the material is directly measured by the rotation (displacement) of the shaft itself. The displacement is converted to a strain or strain rates using the geometry dimensions, and the viscosity is then derived. In the latter, a strain is forced and the stress is computed from the deformation of a calibrated spring system.[7]

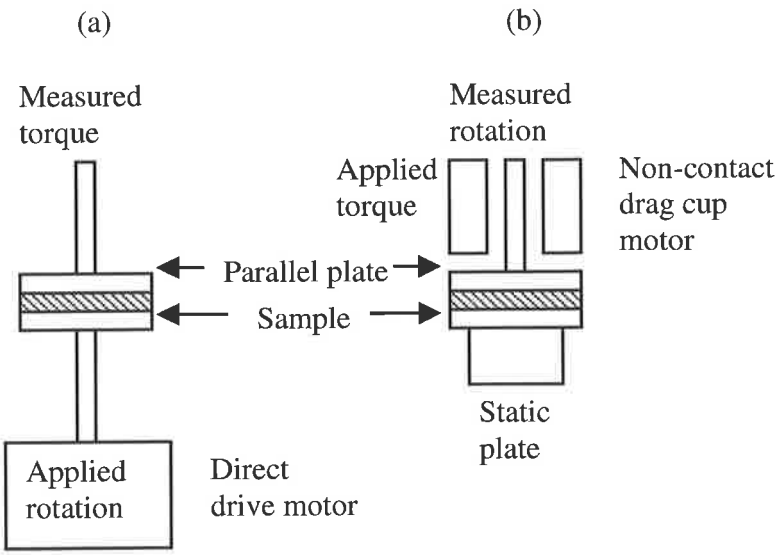

Figure 5.3: Schematic representation of controlled-strain (a) and controlled-stress (b) rheometers.

For both devices, the major geometry types are as follows: parallel plate (shown in Figure 5.3), cone and plate and concentric cylinders (Couette). These geometries are shown in Figure 5.4. Both parallel plate and cone and plate geometries require small sample volumes. The latter has the advantage of allowing the shear rate to be constant across the face of the geometry. In techniques where the strains are small, *e.g.*, oscillatory measurements, variation in the shear field from the centre to the edge of the parallel plates can be exploited, since focusing on the edge provides the maximum sensitivity from the geometry. The concentric cyclinder (Couette) geometry is relatively user-friendly as far as filling is concerned, when compared to the previous geometries. However, a large amount of sample to fill it is required. Both parallel plate and concentric cylinder geometries were used in this work.

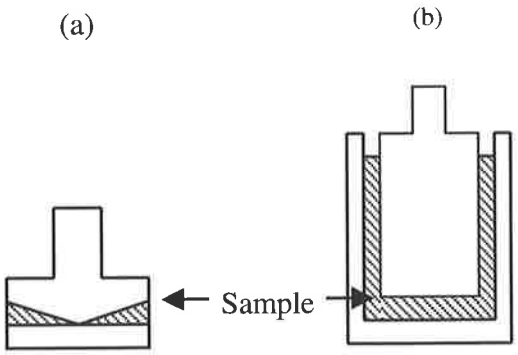

Figure 5.4: Vertical cross sections of measuring geometries utilised to allow the measurement of viscometeric flow; (a) cone and plate and (b) concentric cyclinder (Couette). The parallel plate geometry is shown in Figure 5.3.

The three major categories of rheological measurements are flow (controlled-stress or strain), oscillation testing (controlled-stress or strain) and step change tests (creep for controlled-

stress, stress relaxation for controlled-strain). In this work, controlled-stress and oscillation tests were used.

Flow tests are usually destructive of the sample's structure and typically provide viscosity data. An example of this is steady shear measurement, where known shear rates are applied to the sample at a constant temperature. The resulting stress is measured as a function of shear rate from which the viscosity is calculated. Although steady shear viscosity measurements are relatively wide spread, they do not give the extent of physical insight into the elastic behaviour of the material that can be obtained from the oscillatory measurements. Oscillatory measurements do not necessarily destroy the material's structure but can be set-up to deform the sample, such that it returns to the initial state after the test. This is done by running the parallel plates back and forth in a sinusoidal manner. The frequency is fixed and the rheological parameters, *i.e.*, storage modulus, G', and loss modulus, G", are measured as a function of stress.

As indicated in Section 5.2.4, in the linear viscoelastic region the response (*e.g.*, strain) at any given time is directly proportional to the value of the initiating parameter (*e.g.*, stress). In other words, the microstructure responds over a period of time without changing when deformation takes place.[139] Thus, for a given material this region needs to be determined if the results obtained are to have any quantitative meaning in an absolute sense. The linear viscoelastic region can be obtained by fixing the frequency in oscillatory measurements and measuring the rheological parameters, *e.g.*, stress sweep. This enables the region where G*, G' and G" are independent of the maximum amplitude or stress of the oscillation at any given frequency to be obtained. Having established the linear viscoelastic region, oscillatory measurements are conducted as a function of frequency at a fixed amplitude.

5.3 Experimental

5.3.1 Materials and Sample Preparation

Copolymer P2 was synthesised according to the methods given in Section 2.2.2. For this section of the work, P2 was chosen as the copolymer of choice as it demonstrated the ability to stabilise emulsions at room temperature, whilst exhibiting temperature-induced gelation behaviour (Table 4.2). The preparation of the emulsions containing this copolymer is described in Section 4.2.2. In the case of the samples used in Section 5.6.3, a stock emulsion (3.5 wt% P2 and ϕ_o = 0.3) was prepared according to the methods described in Section 4.2.2. The emulsion was left to stand for one day before separation of the sediment layer from the serum phase. Copolymer solutions of varying concentrations were then added to the sediment layer. The samples were gently inverted by hand to redisperse the droplets. Note that the concentration of copolymer indicated in this part of the work is with respect to the aqueous phase of the emulsion.

5.3.2 Rheological Measurements

Steady shear and oscillatory shear measurements were carried out using a controlled-stress rheometer (Rheometrics SR-5000). A concentric cylinder measurement cell was used for the copolymer solutions. The diameter of the rotating inner cylinder and static outer cylinders was 30 and 32 mm, respectively. Parallel plate geometry was employed for the rheological measurements of the emulsions, except for the samples used in Section 5.6.2, where the concentric cylinder geometry was utilised. The diameter and gap between the plates were 40 mm and 2 mm, respectively. The temperature of the samples during rheological analysis was controlled to ± 0.1°C, through a combination of Peltier element and an oil bath. Note that *f* of *ca.* 1 Hz was used for all oscillatory measurements unless otherwise stated.

5.4 Studies of Poly(NIPAM-*co*-PEGMA) Copolymer Solutions

5.4.1 Steady Shear Measurements

The flow behaviour of semi-dilute and concentrated aqueous solutions of P2 as a function of temperature was investigated. Figures 5.5 to 5.8 show the variation of the shear viscosity, at three different shear rates, with temperature for a range of copolymer concentrations. At 5 wt% (Figure 5.5), the viscosity decreases with increasing temperature. This is expected since the collapse of the chains above the LCST results in the decrease in the effective volume fraction of polymer chains, ϕ_{eff}, leading to the decrease in the sample viscosity [see Equation (2.36)]. Increasing the shear rate breaks any aggregates present allowing the copolymer chains to flow freely with water. It is possible that deformation of the copolymer coils, as a result of increased shear rates, might lead to a decrease in the viscosity. Although the copolymer concentration was above c_p^* (*ca.* 1 wt%), no increase in viscosity was observed across the temperature range. This suggests that at 5 wt% the collapse of the chains is dominated by intra-chain interactions.

In contrast to the behaviour of the semi-dilute sample, the 10 wt% copolymer solution (Figure 5.6) showed evidence of temperature-induced thickening behaviour between 35 and 40°C. This is attributed to temperature-induced network formation[16] at temperatures above the LCST and is consistent with the copolymer chains overlapping throughout the solution, *i.e.*, dominance of inter-chain aggregations. The presence of temperature-induced thickening behaviour for the more concentrated samples, *i.e.*, 15 and 20 wt% (Figures 5.7 and 5.8), suggests that c_{gel} for P2 is *ca.* 10 wt%. Visual inspection showed that the copolymer had gelled at 50°C, in that the sample did not flow under gravity when inverted (see Section 4.3.4 for gelation studies using the tube inversion method). This type of behaviour has been reported elsewhere[16] for related copolymer solutions. The fact that $c_{gel} >> c_p^*$ (*ca.* 1 wt%) indicates that for gelation to

occur in polymer solutions, a significant number of inter-chain junctions needs to be formed. In addition, these aggregates, which act as junction points, will have to form networks of chains spanning across the entire system. These results are consistent with theoretical studies on temperature-induced gelation of associating polymers[14] where calculations showed that $c_{gel} > c_p^*$.

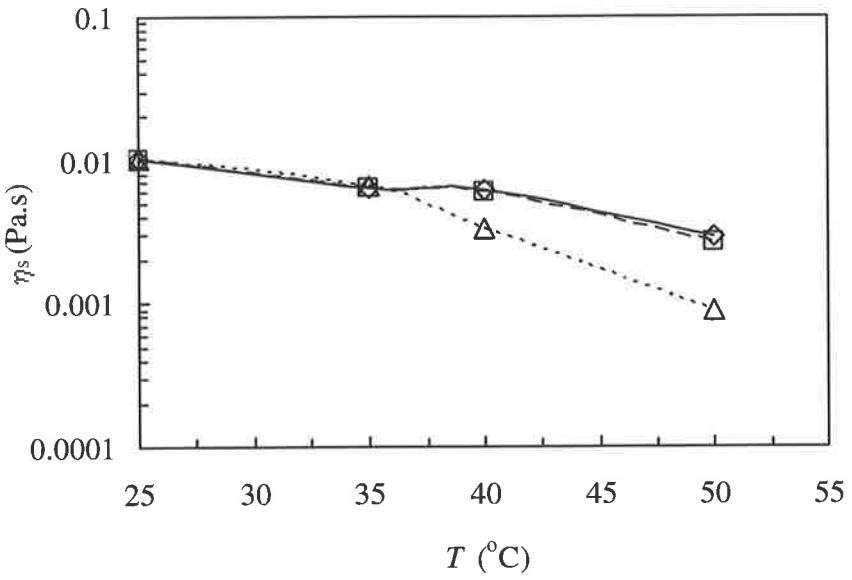

Figure 5.5: The effect of temperature on the shear viscosity of the 5 wt% P2 copolymer solution. The three shear rates used were 1 (◇), 10 (□) and 100 s^{-1} (Δ).

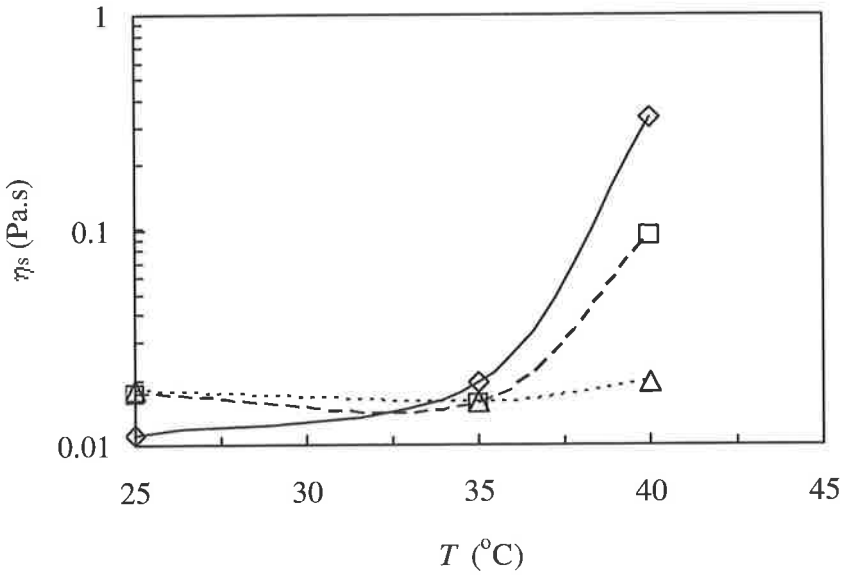

Figure 5.6: The effect of temperature on the shear viscosity of the 10 wt% P2 copolymer solution. The three shear rates used were 1 (◇), 10 (□) and 100 s^{-1} (Δ).

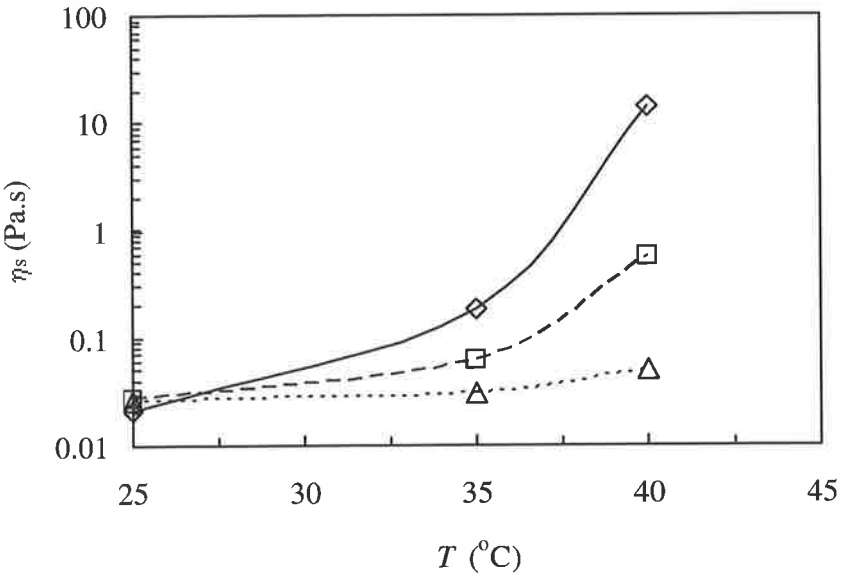

Figure 5.7: The effect of temperature on the shear viscosity of the 15 wt% P2 copolymer solution. The three shear rates used were 1 (◇), 10 (□) and 100 s^{-1} (Δ).

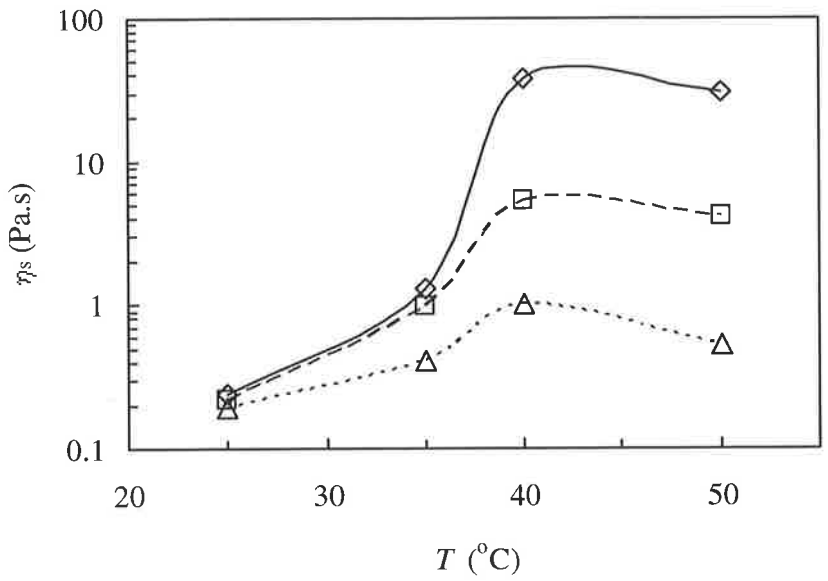

Figure 5.8: The effect of temperature on the shear viscosity, η_s, of the 20 wt% P2 copolymer solution. The three shear rates used were 1 (◇), 10 (□) and 100 s^{-1} (Δ).

The effect of shear stress on the viscosity of the 5, 10, 15 and 20 wt% copolymer solutions is shown in Figures 5.9, 5.10, 5.11 and 5.12, respectively. Note that the 5 wt% sample exhibited $\eta_s < 0.005$ Pa.s at temperatures greater than 35°C with poor signal-to-noise ratios and those data are not presented here. At the lowest concentration (Figure 5.9), the copolymer solution exhibits Newtonian behaviour since the shear viscosity is independent of the stress. This behaviour was evident for all the samples across the stress range at 25°C. However, as temperature increases, the shear viscosity increases dramatically. The Newtonian behaviour at low stresses, which is also known as the lower Newtonian region or zero-shear viscosity, is altered to a shear thinning profile at high stress values. In some cases (*e.g.*, 10 wt % sample at 40°C), in the limit of high stresses, the viscosity is again constant. This is also known as the upper Newtonian region. These trends support the view that a temperature-induced association

effect is operative above the LCST (*ca.* 35°C). An increase in the temperature increases the number and longevity for active chains [see Equation (1.14)]. The effect becomes more pronounced at increasing copolymer concentration because of a greater proportion of effective chains that are available for the formation of chain network. Note that an effective chain has both of its ends embedded within a junction which is connected to at least two other junctions (Figure 1.5). Thus, increasing the copolymer concentration and/temperature increases the gel strength. Note that the rheological profile observed for the samples exhibiting temperature-induced association is characteristic for non-Newtonian liquids which show shear-dependent viscosity. The zero shear viscosity region at low stresses followed by shear thinning behaviour have been observed for hydrophobically modified alkali-soluble associative polymers investigated by Khan *et al.*[131] Those workers attributed the shear thinning behaviour to the depletion of chain entanglement and hydrophobic association between chains when a sufficiently high shear is present.

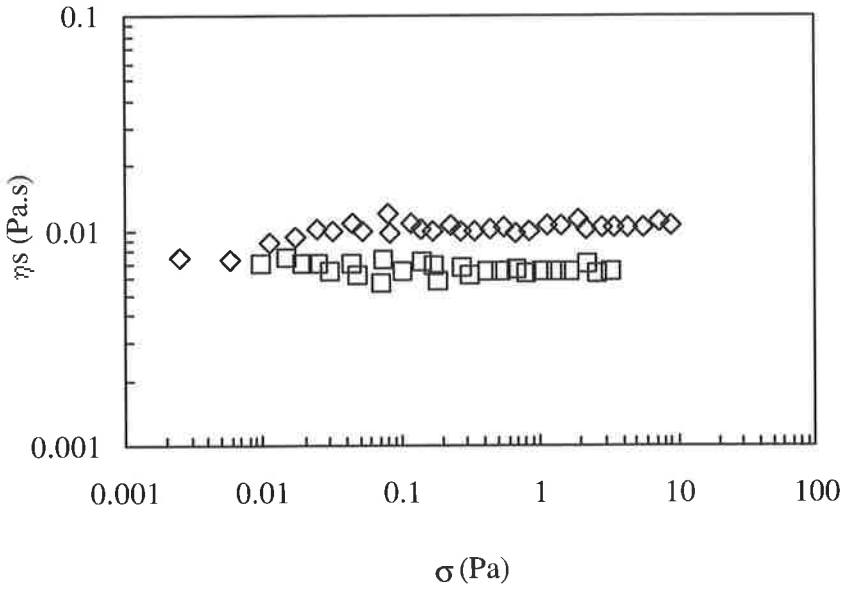

Figure 5.9: Shear viscosity as a function of shear stress for the 5 wt% P2 copolymer solution. The temperatures investigated were 25 (◇) and 35°C (□).

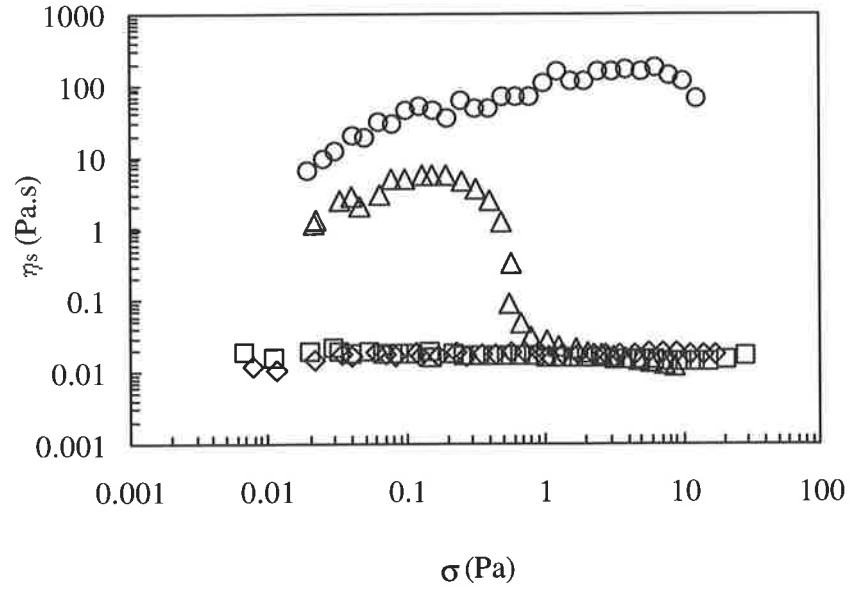

Figure 5.10: Shear viscosity as a function of shear stress for the 10 wt% P2 copolymer solution. The temperatures investigated were 25 (◇), 35 (□), 40 (Δ) and 50°C (○).

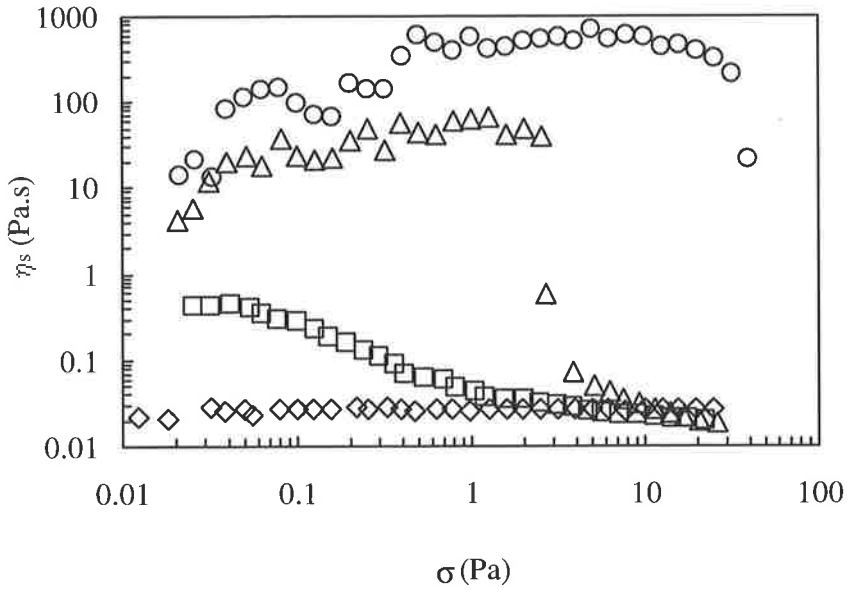

Figure 5.11: Shear viscosity as a function of shear stress for the 15 wt% P2 copolymer solution. The temperatures investigated were 25 (◇), 35 (□), 40 (Δ) and 50°C (○).

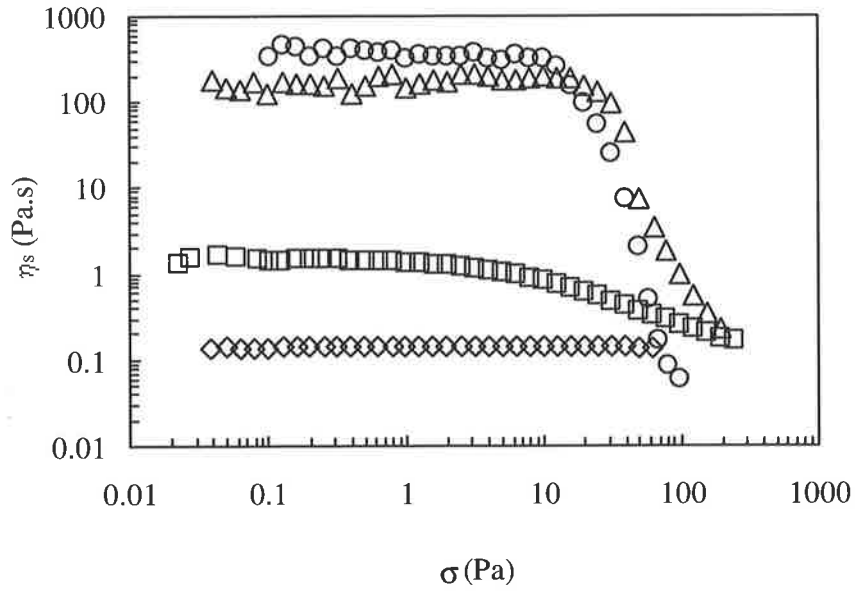

Figure 5.12: Shear viscosity as a function of shear stress for the 20 wt% P2 copolymer solution. The temperatures investigated were 25 (◇), 35 (□), 40 (Δ) and 50°C (○).

The shear thinning profile observed for the copolymers was described in terms of the power law model [Equation (5.6)]. A graph of $\ln(\eta_s)$ vs. $\ln(d\gamma/dt)$ was plotted from which $[d\ln\eta_s/d\ln(d\gamma/dt)] + 1 = n_{pl}$ and the y-intercept gave $\ln(A_c)$. A representative plot from which the parameters were obtained and the fits for the linear regions are shown in Figures 5.13 and 5.14. It is clear that the sample viscosity, which is influenced by the temperature-induced association behaviour of the copolymer chains, is shear rate dependent. At $\ln(d\gamma/dt) > 6\ s^{-1}$, the viscosity of the sample is less than that at $T \leq 35^{\circ}C$. Similar shear thinning behaviour has been observed with temperature-associative polymers of various chemical structures.[14]

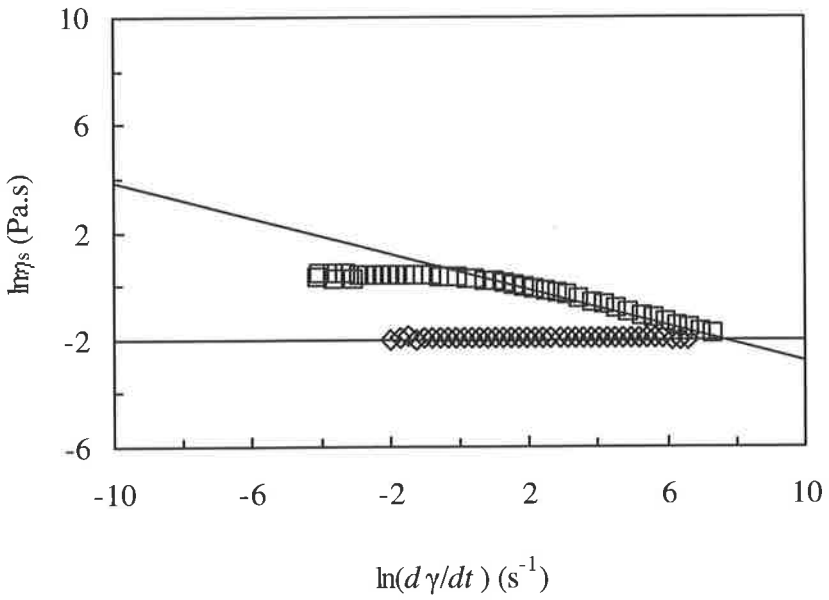

Figure 5.13: Plot of $\ln\eta_s$ as a function of $\ln(d\gamma/dt)$ for the 20 wt% P2 copolymer solution. The temperatures investigated were 25 (◇) and 35°C (□).

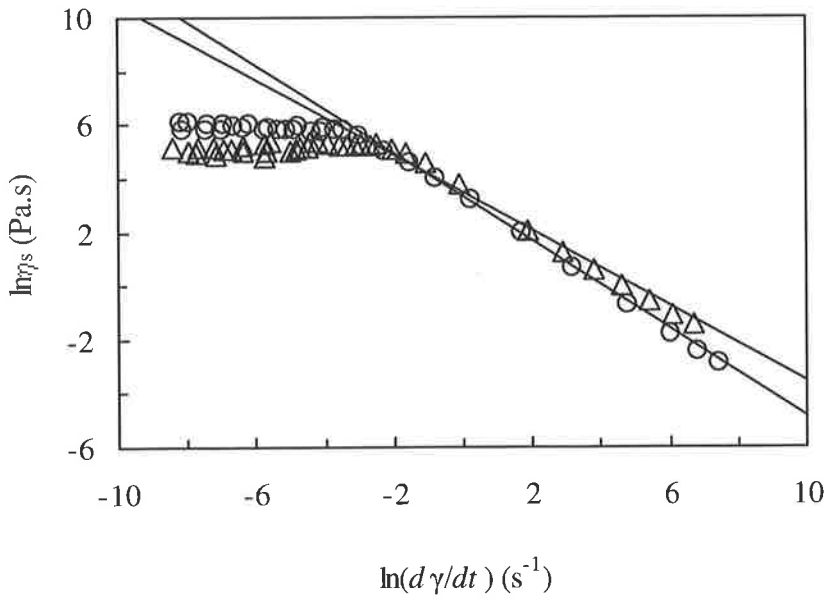

Figure 5.14: Plot of $\ln\eta_s$ as a function of $\ln(d\gamma/dt)$ for the 20 wt% P2 copolymer solution. The temperatures investigated were 40 (Δ) and 50°C (○).

The zero-shear viscosity at low to medium shear rates at temperatures below the LCST indicates an absence of a yield stress. However, this is present as soon as temperature-induced association occurs. The networks are transient since the cross-links, formed by aggregation of the chains above the LCST, are most likely continuously breaking up and reforming.[135]

Figures 5.15 and 5.16 show the data obtained from the plots for the copolymers. As temperature increases, the extent of shear thinning behaviour ($n_{pl} < 1$) for the copolymers increases. This can be seen more clearly by comparing the slope of the plot at 50°C (Figure 5.14) with that at 25°C (Figure 5.13). The former having a steeper slope, yielded a lower n_{pl} value compared to the latter.

As the shear rate increases, the chain aggregates/networks are broken up and move with the flow of the liquid. This is manifested by the shear thinning behaviour in the samples.[144]

Increasing the temperature and/copolymer concentration, which effectively increases the number of chains available for aggregation and copolymer network formation, leads to a more pronounced shear thinning behaviour.

The physical meaning of A_c changes with the power law index. When a material exhibits Newtonian behaviour, n_{pl} =1 and A_c is equal to its viscosity. The value of n_{pl} = 0 is indicative of highly viscous colloidal solids, *e.g.*, gels, and A_c relates to the yield stress required to the break the structure.[145,146] As can be seen from Figure 5.16, a pronounced increase in A_c with temperature is observed for all the samples. Note that a concomitant decrease in n_{pl} is observed with temperature (Figure 5.15). This indicates the presence of a highly structured system in the samples, *i.e.*, copolymer chain network. The higher A_c values with increasing copolymer concentration suggest a greater extent of copolymer network at T > LCST.

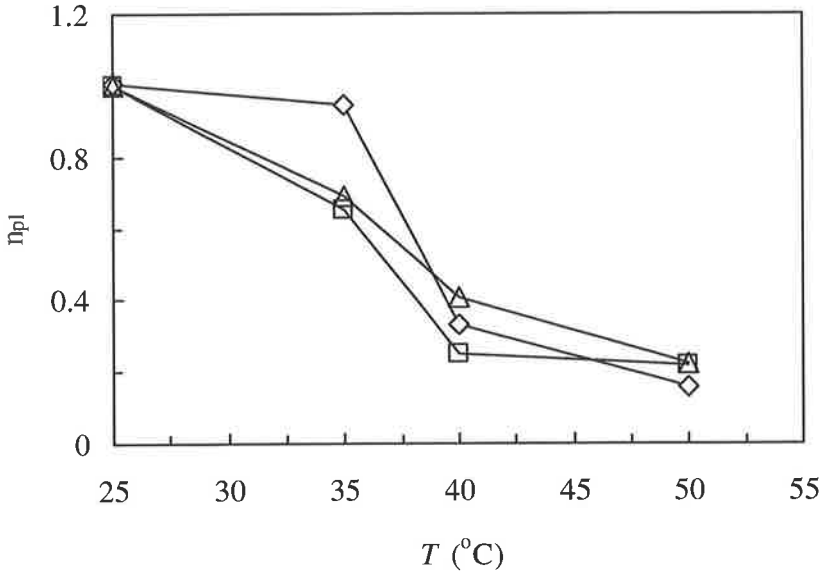

Figure 5.15: Plot of n_{pl} vs. T for the 10 (◇), 15 (□) and 20 wt% (Δ) P2 solutions. The parameter was obtained from fitting data shown in Figures 5.13 and 5.14 to Equation (5.6).

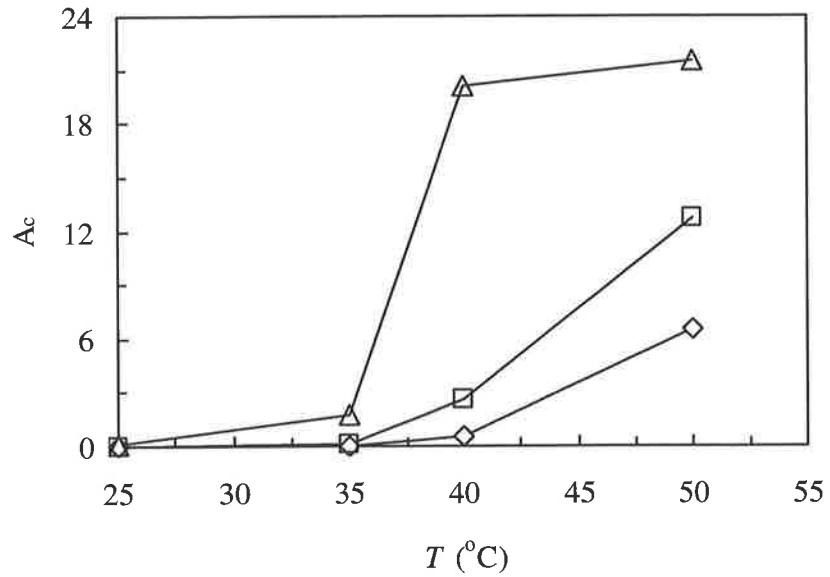

Figure 5.16: Plot of A_c vs. T for the 10 (◇), 15 (□) and 20 wt% (Δ) P2 solutions. The parameter was obtained from fitting data shown in Figures 5.13 and 5.14 to Equation (5.6).

5.4.2 Oscillatory Shear Measurements

The dynamic rheological properties of the P2 solutions were also determined as a function of temperature. Figures 5.17 to 5.19 show the variation in G' across the stress range at different temperatures for copolymer solutions containing 10 - 20 wt% P2. Both the elastic modulus values and the range where G' is independent of stress generally increase at temperatures higher than the LCST. These data support the view that an increase in temperature produces a viscoelastic network, provided the concentration of copolymer is at least 10 wt%. The dependence of T_{gel} on the copolymer concentration can be seen by observing the large increase in the initial G' with temperature. The plot of G' vs. T at σ = 0.1 Pa for the various copolymer concentrations are shown in Figure 5.20. Both the 10 and 15 wt% samples showed significant increase in G' at $T \geq 40^{\circ}C$ while that for the 20 wt% sample was at 35°C. Thus, even though these samples exhibited temperature-induced association behaviour, the temperature at which this occurs is strongly dependent on the copolymer concentration. The effect of copolymer concentration on T_{gel} will be discussed in more detail in Section 5.6.3.

Interestingly, the elastic behaviour of the gel at 40°C is nearly independent of the copolymer concentration. This is evident from the G' values at that temperature for the plots shown in Figure 5.20. If G' is approximated to be the elastic modulus of the chain network, then G' should be proportional to υ_{eff} [see Equation (1.14)]. It is then predicted that increasing the copolymer concentration should increase υ_{eff} and G'. However, it is possible that the number of intramolecular and intermolecular crosslinks are not too dissimilar as the copolymer concentration changes. This results in a negligible change in G'. The data also suggest that at 40°C, the minimum number of chain aggregates required for the formation of transient networks, N_{agg}, is reached.

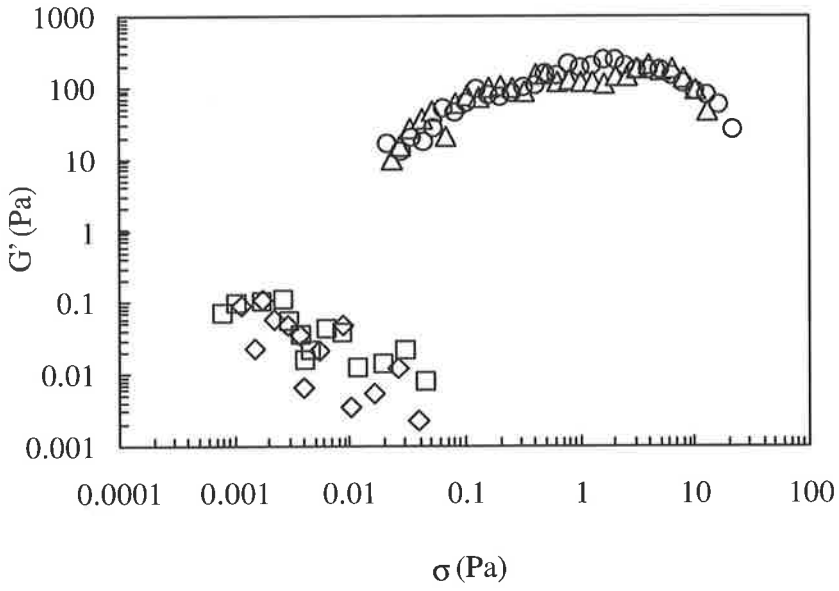

Figure 5.17: Plot of G' as a function of σ for the 10 wt% P2 copolymer solution (f = 1 Hz). The temperatures investigated were 25 (◇), 35 (□), 40 (Δ) and 50°C (○).

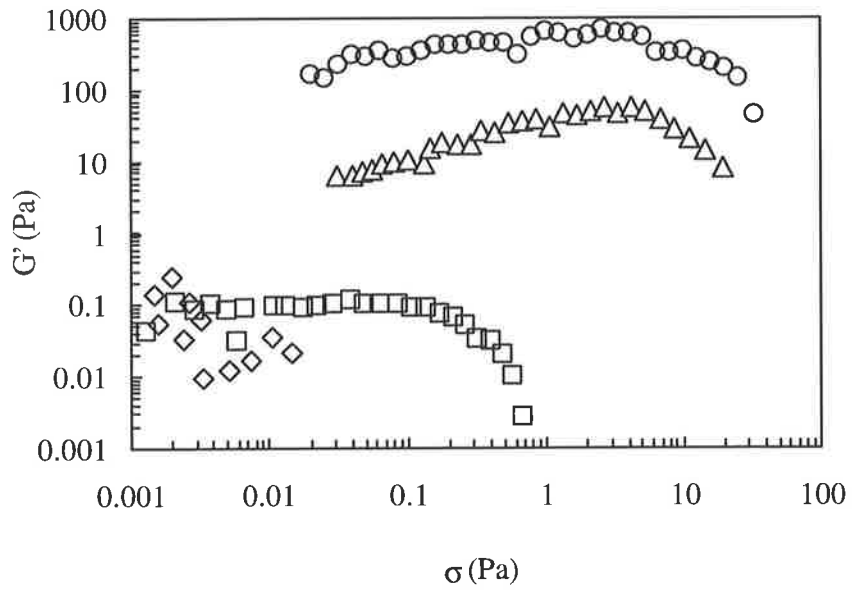

Figure 5.18: Plot of G' as a function of σ for the 15 wt% P2 copolymer solution (f = 1 Hz). The temperatures investigated were 25 (◇), 35 (□), 40 (Δ) and 50°C (○).

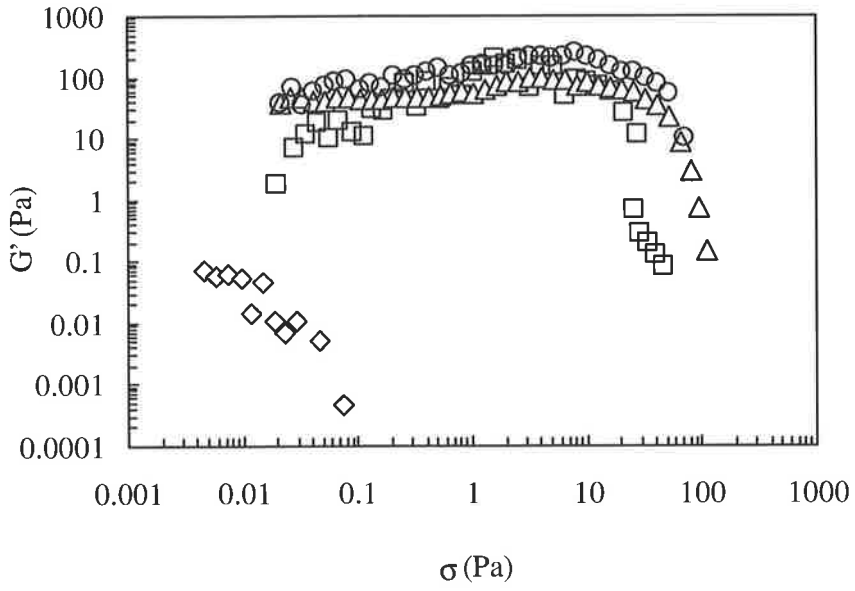

Figure 5.19: Plot of G' as a function of σ for the 20 wt% P2 copolymer solution (f = 1 Hz). The temperatures investigated were 25 (◇), 35 (□), 40 (Δ) and 50°C (○).

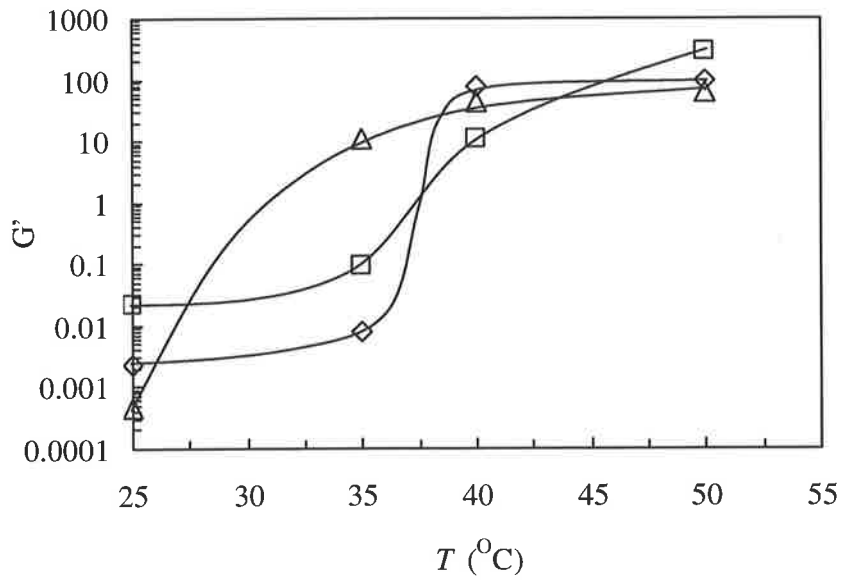

Figure 5.20: Plot of G' vs. T at σ = 0.1 Pa for the 10 (◇), 15 (□) and 20 wt% (Δ) P2 copolymer solutions. The data were obtained from the plots shown in Figures 5.17 to 5.19.

Figures 5.21 to 5.23 show the variation in $\tan\delta_p$ as a function of shear stress for the copolymer solutions containing 10 - 20 wt% P2 across a range of temperatures. The plots indicate that at room temperature, the samples behave as viscous liquids, *i.e.*, G' << G" and hence, $\tan\delta_p > 1$. As temperature increases, δ_p approaches 45°, *i.e.*, G' = G", and the samples behave as viscoelastic materials. Once $\delta_p < 45°$, then G' > G", and they behave as predominantly elastic solids. This supports the view that gelation occurs at elevated temperatures. This is attributed to temperature-induced association of the copolymer chains above the LCST. At high stress values, the physical networks are disrupted (or the gel is broken up) resulting in the loss of elasticity in the samples. This is indicated by an increase in $\tan\delta_p$ (*e.g.*, when σ = 100 Pa for the 20 wt% solution at 40°C shown in Figure 5.23). It should be noted that the elastic behaviour of a material can only be accurately determined if $\tan\delta_p < 1$ over an extended range of frequencies.[128] However, this was not investigated for this part of the work.

The effect of increasing the copolymer concentration on T_{gel} can be observed from the temperature at which G' is greater than G" and is independent of stress. The plot of T_{gel} vs. copolymer concentration shown in Figure 5.24 indicates that T_{gel} = 40°C for the 10 and 15 wt% samples and 35°C for the 20 wt% copolymer solution.

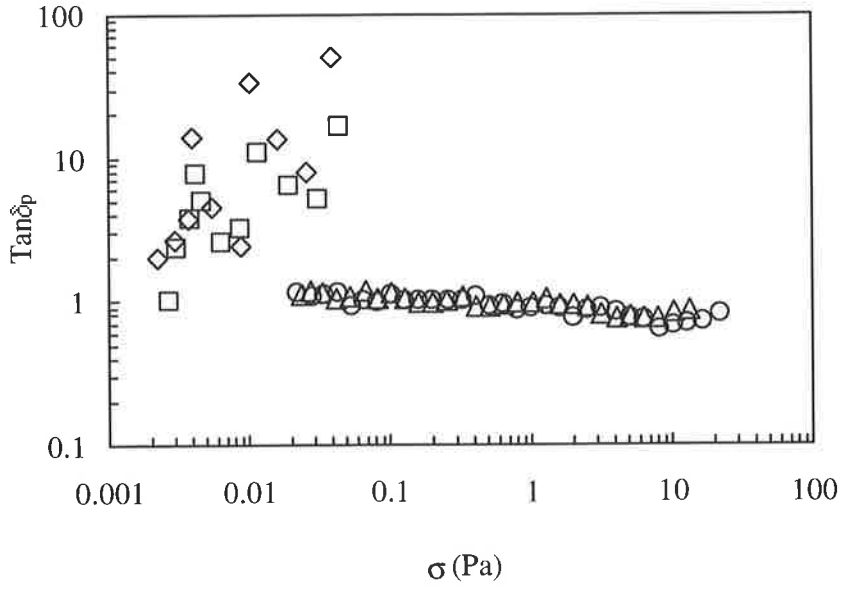

Figure 5.21: Plot of $\tan\delta_p$ as a function of σ plotted for the 10 wt% P2 copolymer solution (f = 1 Hz). The temperatures investigated were 25 (◇), 35 (□), 40 (Δ) and 50°C (○).

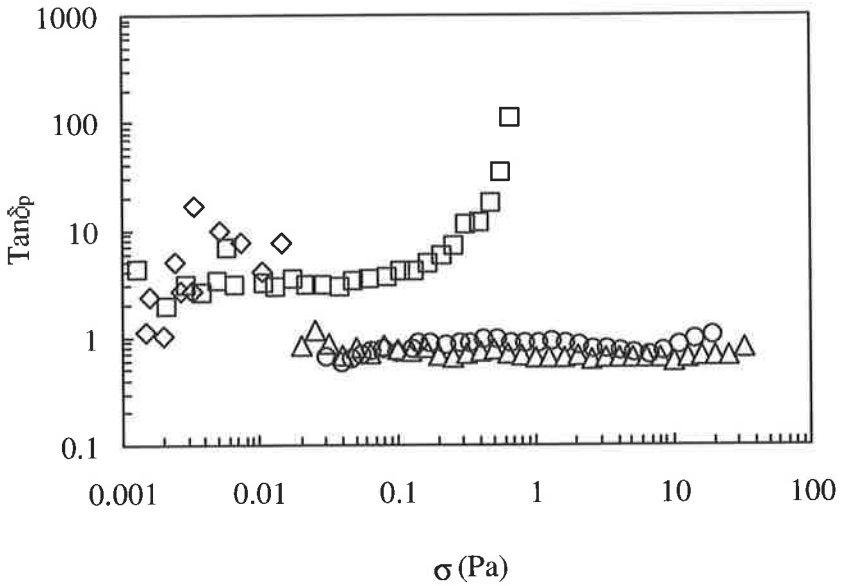

Figure 5.22: Plot of $\tan\delta_p$ as a function of σ plotted for the 15 wt% P2 copolymer solution (f = 1 Hz). The temperatures investigated were 25 (◇), 35 (□), 40 (Δ) and 50°C (○).

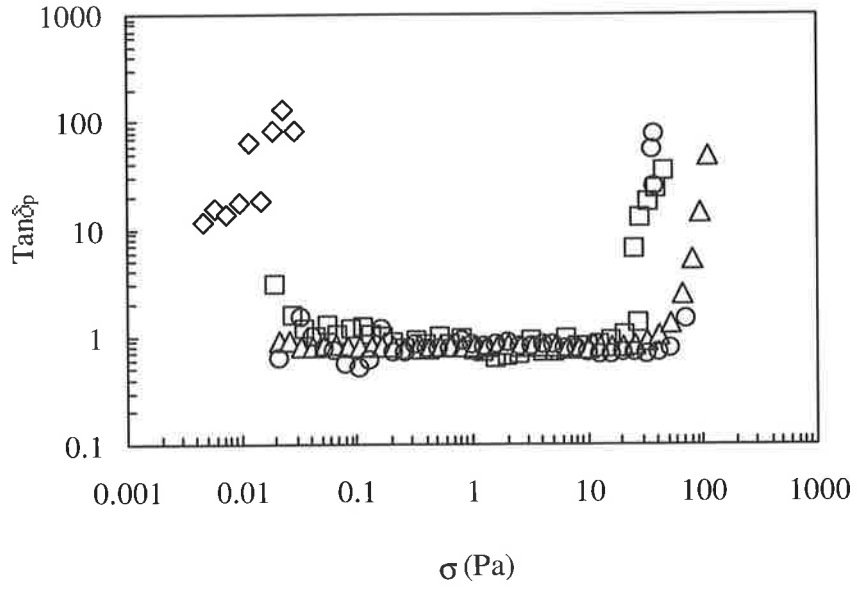

Figure 5.23: Plot of $\tan\delta_p$ as a function of σ plotted for the 20 wt% P2 copolymer solution (f = 1 Hz). The temperatures investigated were 25 (◇), 35 (□), 40 (Δ) and 50°C (○).

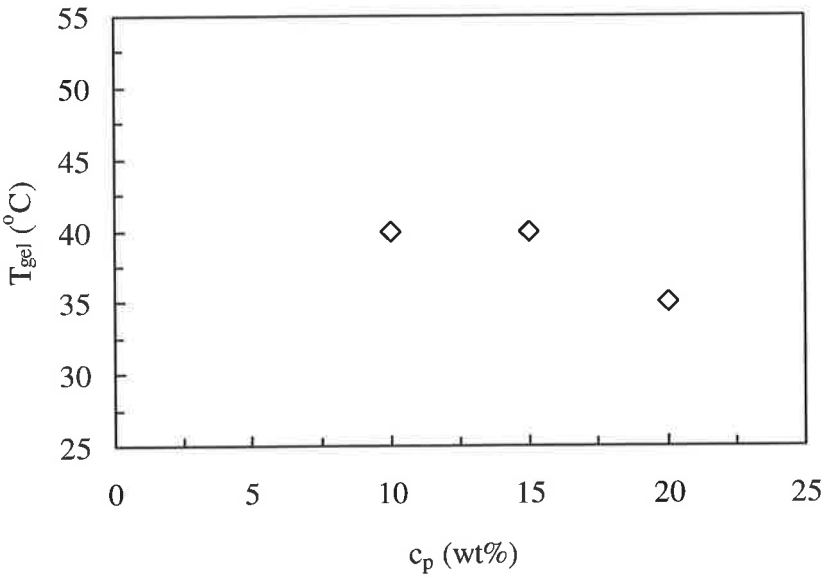

Figure 5.24: Plot of T_{gel} as a function of c_p determined from oscillatory measurements (f = 1 Hz). The data were obtained from the plots shown in Figures 5.21 to 5.23.

5.6 Studies of Emulsions

5.6.1 Initial Investigation at Fixed Oil Volume Fraction

5.6.1.1 Steady Shear Measurements

Figure 5.25 shows the variation of the viscosity with temperature for a 1-bromohexadecane-in-water emulsion (ϕ_o = 0.3) containing P2, determined at shear rates of 1, 10 and 100 s^{-1}. The trends for the viscosity data at higher shear rates (100 s^{-1}) are in agreement with data measured for related emulsions using capillary viscometry (Figure 4.17), in that there is a decrease in sample viscosity at temperatures just above the LCST of P2. However, as temperature increases further, there is pronounced thickening of the emulsion. Visual inspection of the emulsion showed gelation had occurred at high temperatures.

Interestingly, the variation of the shear viscosity with temperature for the lowest shear rate (1 s^{-1}) shows similar behaviour to the equivalent data shown in Figure 5.8 for the concentrated P2 solution up to 40°C. Above this temperature, the viscosity of the copolymer solution decreased, while the emulsion continued to exhibit thermothickening behaviour. This indicates that the oil droplets must have the same qualitative effect on the rheological properties as a substantial increase in the copolymer concentration. At T > LCST, chains adsorbed on the oil droplets may aggregate with those in solution or chains adsorbed on a second droplet, giving rise to copolymer network. This increases ϕ_{eff} of the oil phase and hence, the viscosity of the emulsion [see Equation (2.36)]. It should be noted that the addition of the oil phase results in a thermally-induced gelation which would have otherwise been absent at that temperature.

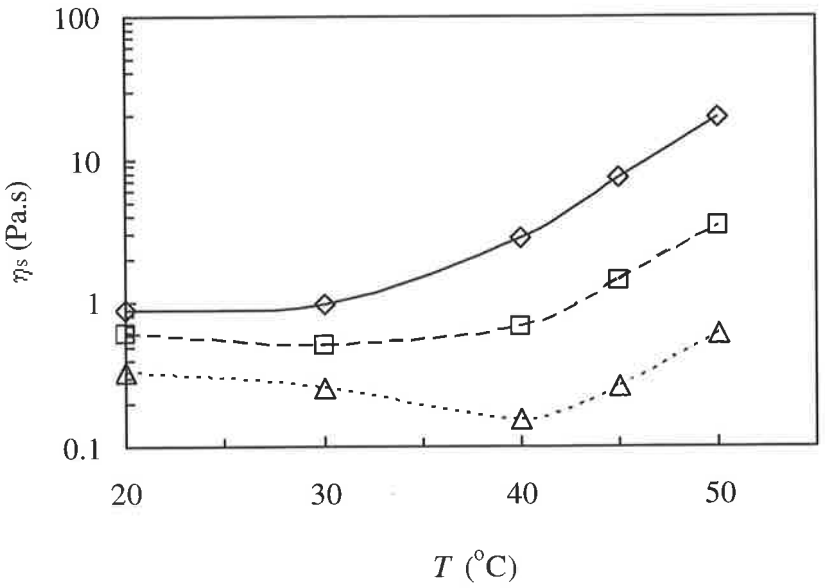

Figure 5.25: The effect of temperature on the shear viscosity of a 1-bromohexadecane-in-water emulsion (ϕ_o = 0.3) prepared using P2 (3.5 wt%). The three shear rates used were 1 (◇), 10 (□) and 100 s^{-1} (Δ).

Figure 5.26 shows the effect of shear stress and temperature on the viscosity of the emulsion. The emulsion exhibits weak shear thinning behaviour at 20°C. This may be ascribed to droplet deformation and the disruption of weak flocs (Figure 4.2). Note that the former is a well-known phenomenon for emulsions under shear.[144] Upon increase in temperature, a significant increase is observed in the viscosity at low stress, as well as the stress required for the onset of thinning. The latter can be considered as the apparent yield stress. Increasing the temperature increases the effective volume fraction of oil present, since the adsorbed copolymer may aggregate with chains in solution or those adsorbed on a second droplet. The "increased" oil volume fraction in the emulsion restricts the flow of the droplets when sheared. At high

temperatures, the droplets are trapped within the copolymer network, making droplet movement difficult. This can be seen from the high yield stress of the sample at 50°C.

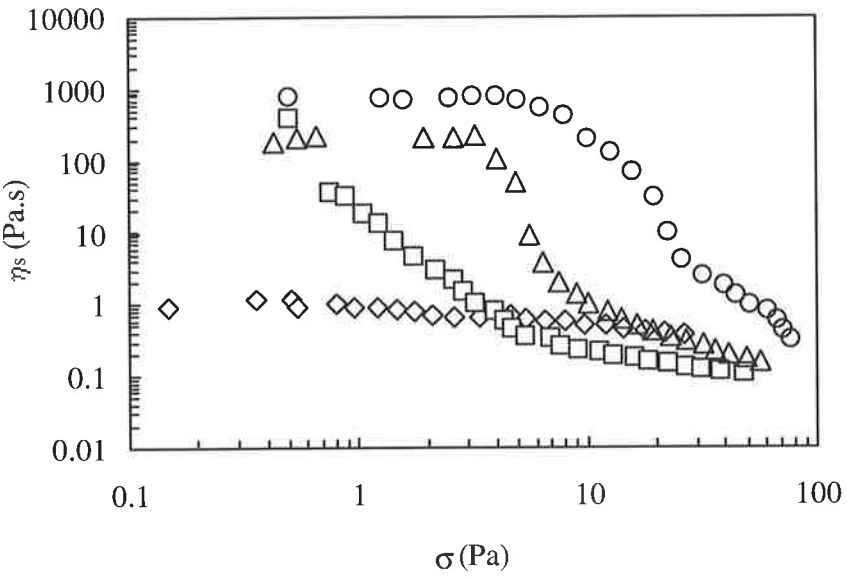

Figure 5.26: The effect of shear stress on the viscosity of the viscosity of 1-bromohexadecane-in-water emulsion (ϕ_o = 0.3) prepared using P2 (3.5 wt%). The measurement temperatures were 20 (◇), 40 (□), 45 (Δ) and 50°C (○).

The shear thinning profile observed for the emulsion was described in terms of the power law model [Equation (5.6)]. The parameters obtained (n_{pl} and A_c) were determined from the linear region of $\ln\eta_s$ vs. $\ln(d\gamma/dt)$ (Figures 5.27 and 5.28). As in the case with the copolymer solutions (Figure 5.13), the shear thinning behaviour of the emulsion is shear rate dependent. However, this behaviour is apparent at the lowest temperature (20°C) for the emulsion, while that for the copolymer was observed only at temperatures above the LCST of *ca.* 35°C. The dispersed

phase droplets and copolymer chains (adsorbed and in solution) restrict movement of the fluid when shear is applied to the emulsion. This yield stress becomes more apparent when gelation occurs as the droplets are "locked up" within the networks of copolymer chains, limiting its movement (Figure 4.19). When the yield stress is exceeded, *e.g.*, by increasing the shear rate, the droplets and copolymer chains move with the flow of the liquid. This is manifested by the presence of shear thinning behaviour as the shear rate increases.

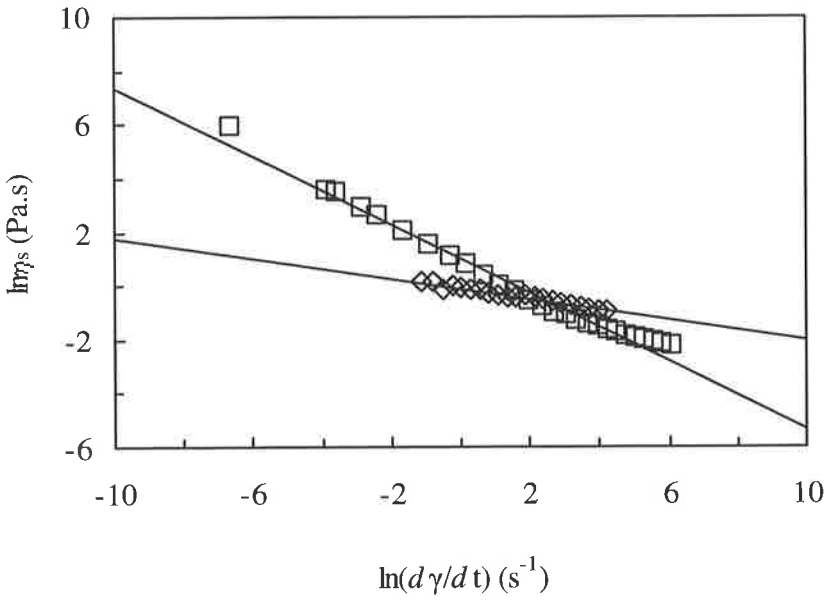

Figure 5.27: Plot of lnη_s as a function of ln($d\gamma/dt$) for 1-bromohexadecane-in-water emulsion (ϕ_o = 0.3) prepared using P2 (3.5 wt%). The measurement temperatures were 20 (◇) and 40°C (□).

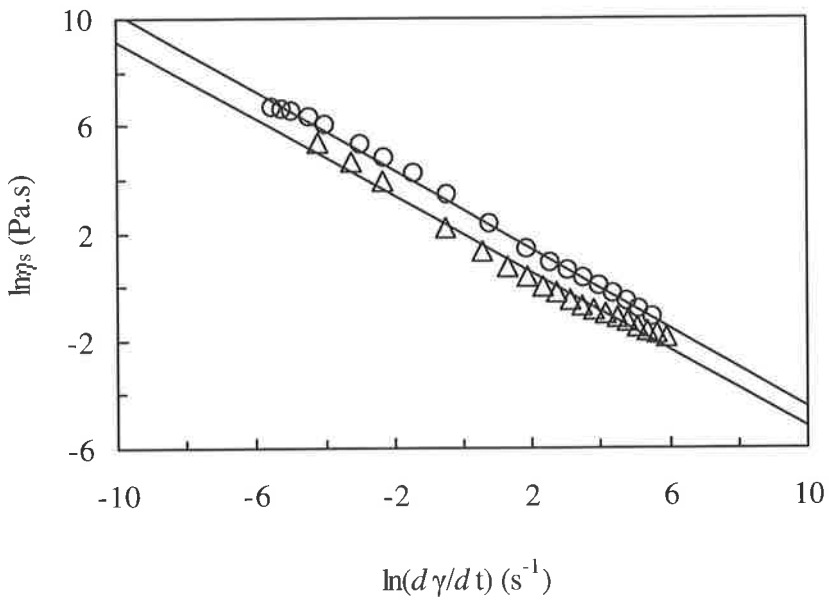

Figure 5.28: Plot of ln(η_s) as a function of ln($d\gamma/dt$) for 1-bromohexadecane-in-water emulsion (ϕ_o = 0.3) prepared using P2 (3.5 wt%). The measurement temperatures were 45 (Δ) and 50°C (○).

The n_{pl} and A_c fitting parameters derived from the plots in Figures 5.27 and 5.28 are plotted in Figures 5.29 and 5.30, respectively. Also shown are the data for the 10 wt% P2 solution for comparison. As with the copolymer solutions, the n_{pl} values for the emulsion are less than unity and are consistent with shear thinning behaviour. This can be attributed to the break-up of the chain aggregates and flocs (in the case of the emulsion). The increase in A_c with temperature indicates the formation of a more structured system in the emulsion, *i.e.*, emergence of network. The higher A_c values for the emulsion compared to the copolymer solution is indicative of the oil droplets present which participates in the temperature-induced association process; thus, participating in structuring of the emulsion.

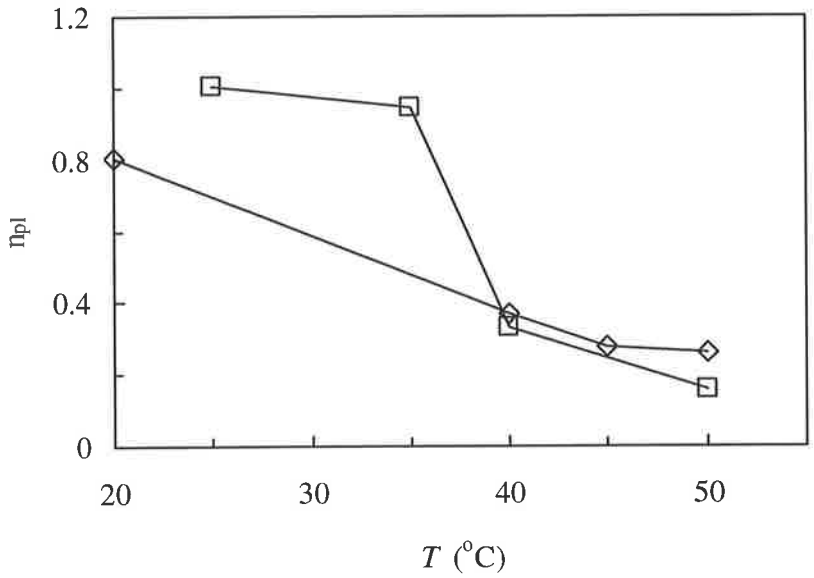

Figure 5.29: Plot of n_{pl} vs. T obtained from fitting the power law model to the $\ln\eta_s$ vs. $\ln(d\gamma/dt)$ data (Figures 5.27 and 5.28) for the emulsion (◇) and 10 wt% P2 solution (□).

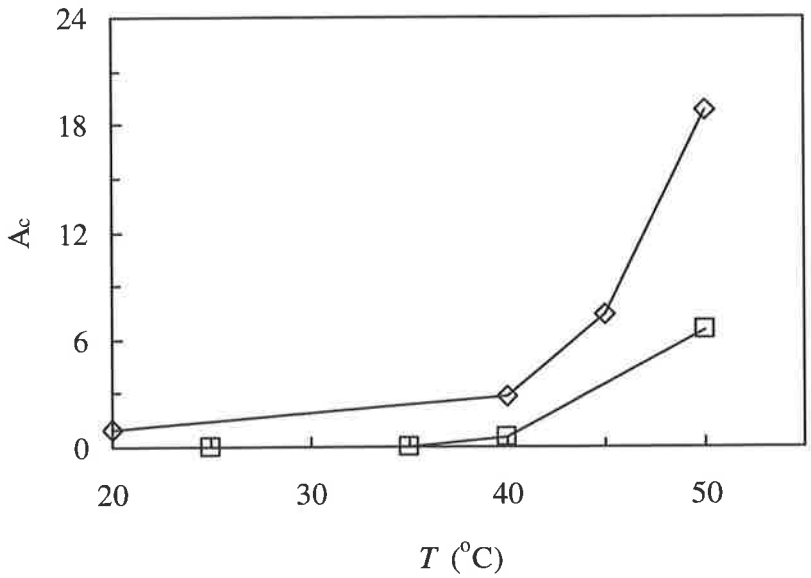

Figure 5.30: Plot of A_c vs. T obtained from fitting the power law model to the $\ln\eta_s$ vs. $\ln(d\gamma/dt)$ data (Figures 5.27 and 5.28) for the emulsion (◇) and 10 wt% P2 solution (□).

5.6.1.2 Oscillatory Shear Measurements

The dynamic rheological properties of the emulsion were also determined as a function of temperature. Figure 5.31 shows the variation of the elastic modulus with shear stress. The observed increase in G' with temperature is indicative of an increased elastic behaviour of the emulsion[128] and is consistent with network formation. The decrease in G' at high stress values is due to shear-induced break-up of the network.

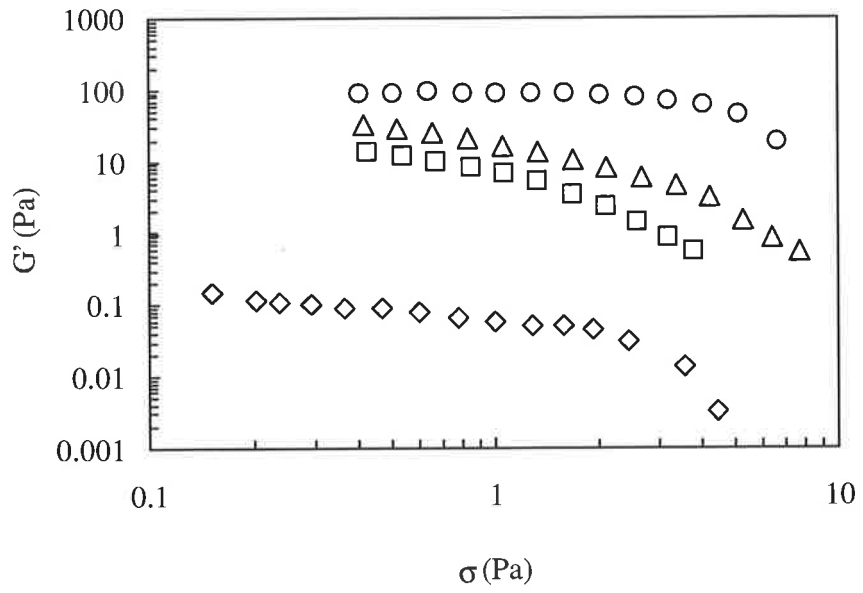

Figure 5.31: The elastic modulus, G', as a function of shear stress, σ, for a 1-bromohexadexcane-in-water emulsion (ϕ_o = 0.3) prepared using P2 (3.5 wt%). The temperatures investigated were 20 (◇), 40 (□), 45 (Δ) and 50°C (○).

Figure 5.32 shows the variation of $\tan\delta_p$ with shear stress. The values for $\tan\delta_p$ decrease with increasing temperature, which further supports the transformation from a viscous fluid to an

elastic, gel-like structure. For a perfectly elastic material, the elastic modulus approaches unity. In order for this to happen, the emulsion droplets will have to be in contact with one another to form a network of oil droplets. However, steric interaction imposed by the adsorbed copolymer prevents this from happening. It should be noted that $\tan\delta_p$ values for the emulsion are less than that for the equivalent copolymer solution. This reflects differences in microstructure and gel properties. The presence of oil droplets affects the rheological properties of the samples. In the case of the emulsion, copolymer chains and oil droplets participate in network formation. However, networks formed in the copolymer solution are comprised of copolymer chains only.

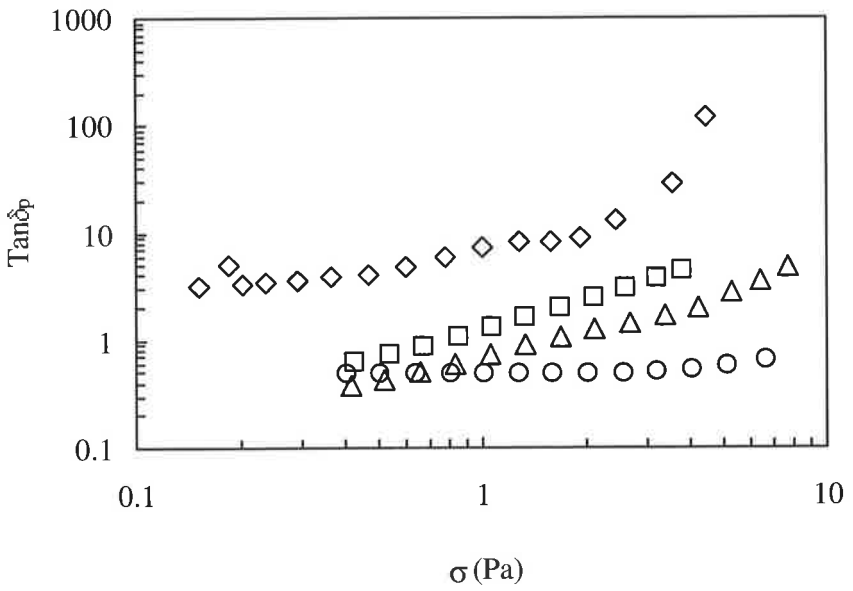

Figure 5.32: Variation of the loss tangent as a function of shear stress for a 1-bromohexadexcane-in-water emulsion (ϕ_o = 0.3) prepared using P2 (3.5 wt%). The temperatures investigated were 20 (◇), 40 (□), 45 (Δ) and 50°C (○).

5.6.2 Effect of Oil Volume Fraction

5.6.2.1 Steady Shear Measurements

The effect of changing the oil volume fraction of the emulsion on the rheological properties was investigated by conducting steady shear measurements. The effect of shear stress on the viscosity of the 1-bromohexadecane-in-water emulsions (3.5 wt% P2) across a stress range at different temperatures is shown in Figures 5.33 to 5.36. The sample containing $\phi_o = 0.5$ starts to shear thin at 35°C, while this behaviour is apparent only at 50°C for $\phi_o = 0.3$. Thermothickening seems to occur for these samples as indicated by the large increase in the viscosity at low shear rates at elevated temperatures. Increasing ϕ_o increases the viscosity at low shear rates. In addition, as ϕ_o increases, a higher stress is required before shear thinning behaviour is observed at elevated temperatures (*e.g.*, Figure 5.36). This is due to the increased proportion of droplets that are able to participate in network formation. The aggregation of adsorbed chains with those in solution and chains on a second droplet increases ϕ_{eff} of the droplets. Thus, flow of the droplets upon shear is restricted and becomes more apparent as temperature increases. The latter is evident by the onset of shear thinning at higher stress values.

The copolymer solution, *i.e.*, $\phi_o = 0$, showed shear thinning behaviour across the temperature range examined. Since the concentration of copolymer (3.5 wt%) is higher than c_p^* of *ca.* 1 wt% (Section 2.4.3), the chains entangle and overlap with one another. As the shear rate increases, these aggregates are broken up, resulting in the copolymer chains to move with the flow of the liquid. This is evident by the shear thinning behaviour. The apparent viscosity increase, *i.e.*, shear thickening, at high stress values for the sample could be due to artifacts present or poor signal to noise ratio as result of close similarity of the sample viscosity to water as temperature increases.

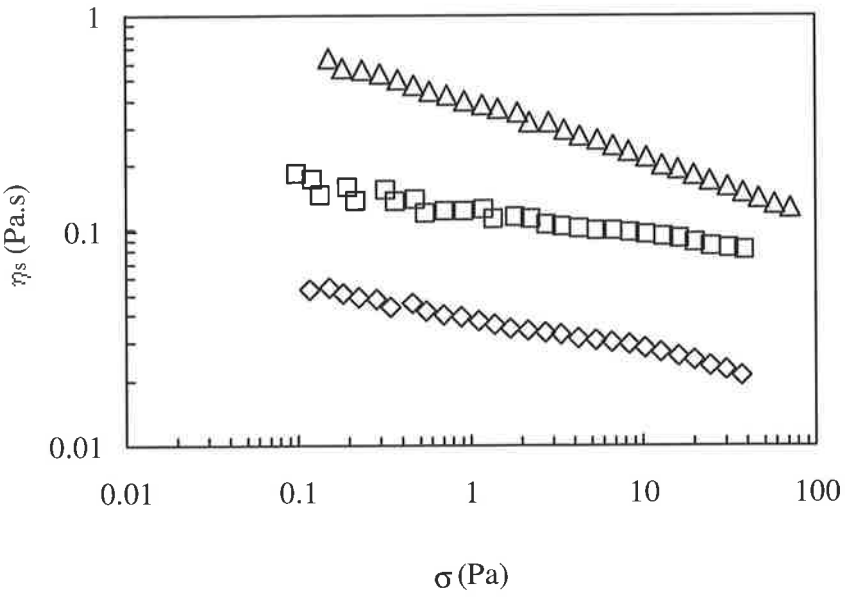

Figure 5.33: Shear viscosity as a function of shear stress at 25°C for the samples (3.5 wt% P2) containing various ϕ_o; (◇) 0, (□) 0.3, (Δ) 0.5.

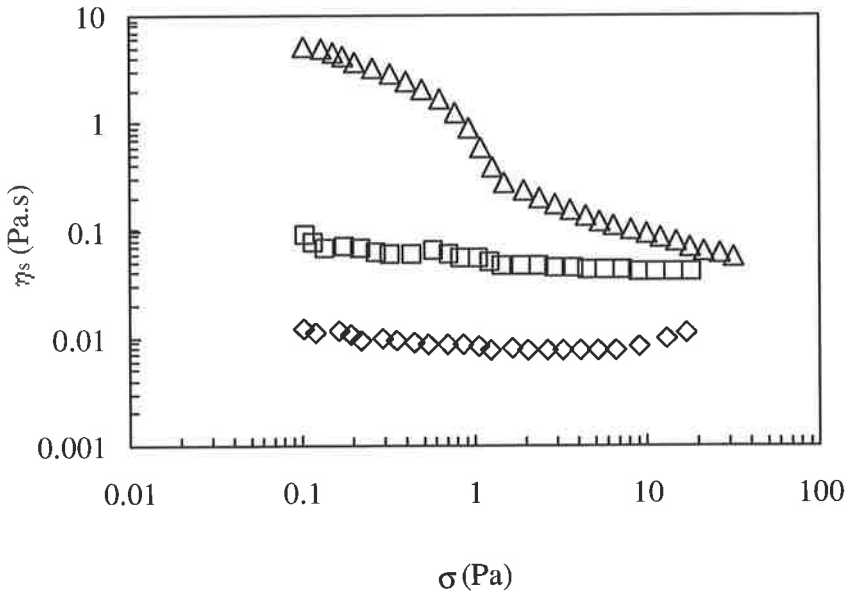

Figure 5.34: Shear viscosity as a function of shear stress at 35°C for the samples (3.5 wt% P2) containing various ϕ_o; (◇) 0, (□) 0.3, (Δ) 0.5.

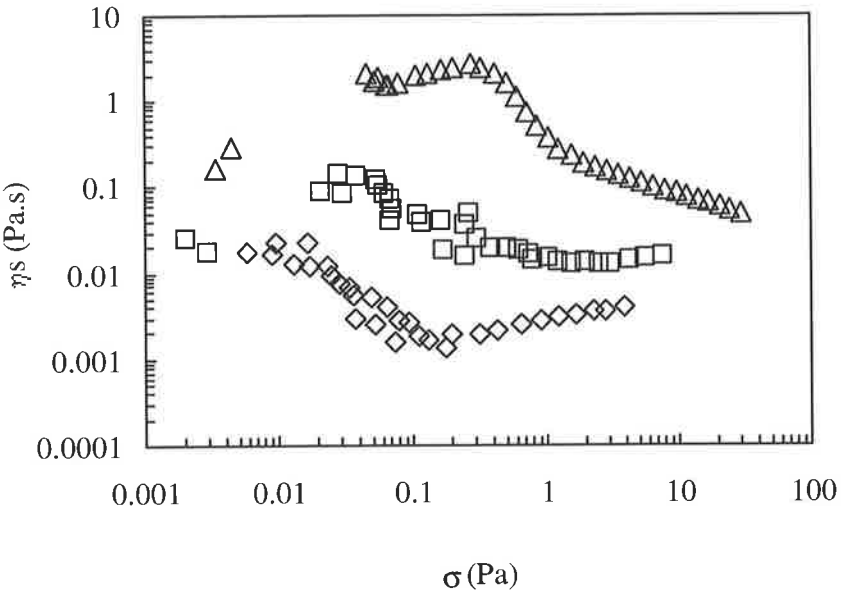

Figure 5.35: Shear viscosity as a function of shear stress at 45°C for the samples (3.5 wt% P2) containing various ϕ_o; (◇) 0, (□) 0.3, (Δ) 0.5.

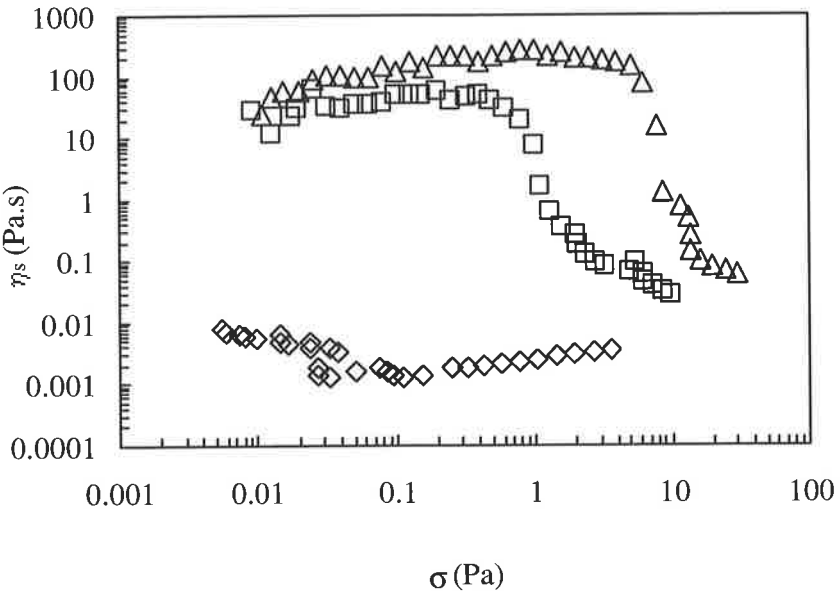

Figure 5.36: Shear viscosity as a function of shear stress at 50°C for the samples (3.5 wt% P2) containing various ϕ_o; (◇) 0, (□) 0.3, (Δ) 0.5.

The steady state rheological data for the samples were described in terms of the power law model [Equation (5.6)]. The power law index and consistency parameter were determined from the linear region of $\ln(\eta_s)$ as a function of $\ln(d\gamma/dt)$ plots (not shown). The data are plotted in Figures 5.37 and 5.38. Note that the data for the $\phi_o = 0$ sample were not fitted to the power law model as it showed shear thinning behaviour across the stress range examined.

As temperature increases, the shear thinning behaviour ($n_{pl} < 1$) becomes more significant due to the formation of copolymer chain networks trapping the droplets and resisting flow. The dramatic increase in A_c above the gelation temperature at *ca.* 50°C confirms the formation of a highly structured emulsion, *i.e.*, gel. Increasing the concentration of oil droplets results in a higher yield stress in the emulsion as indicated by the higher A_c values for $\phi_o = 0.5$ compared to $\phi_o = 0.3$ for a given temperature.[145,146] In other words, a higher stress is required for the droplets to flow for the more concentrated samples, since more of the oil droplets are available, which can participate in network formation at $T >$ LCST.

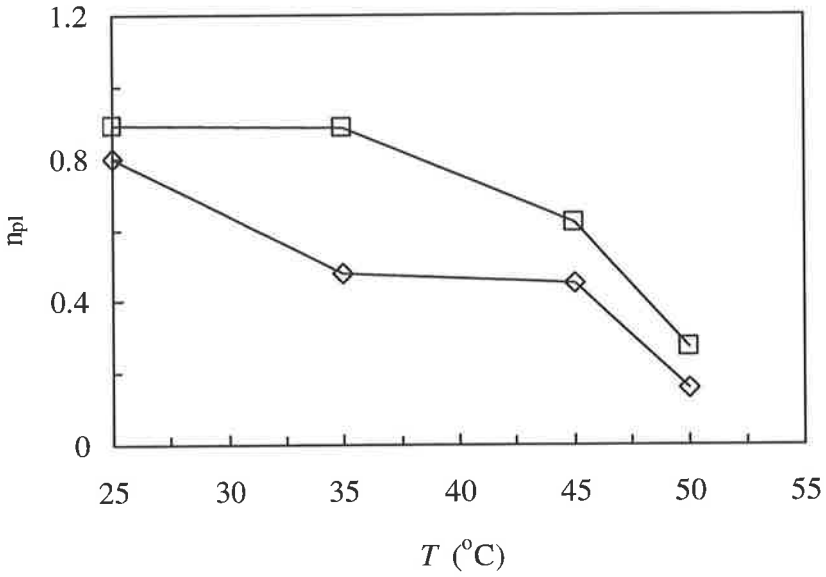

Figure 5.37: Plot of n_{pl} as function of T obtained from fitting the power law model to the $\ln\eta_s$ vs. $\ln(d\gamma/dt)$ data (not shown) for the emulsions containing $\phi_o = 0.3$ (◇) and 0.5 (□).

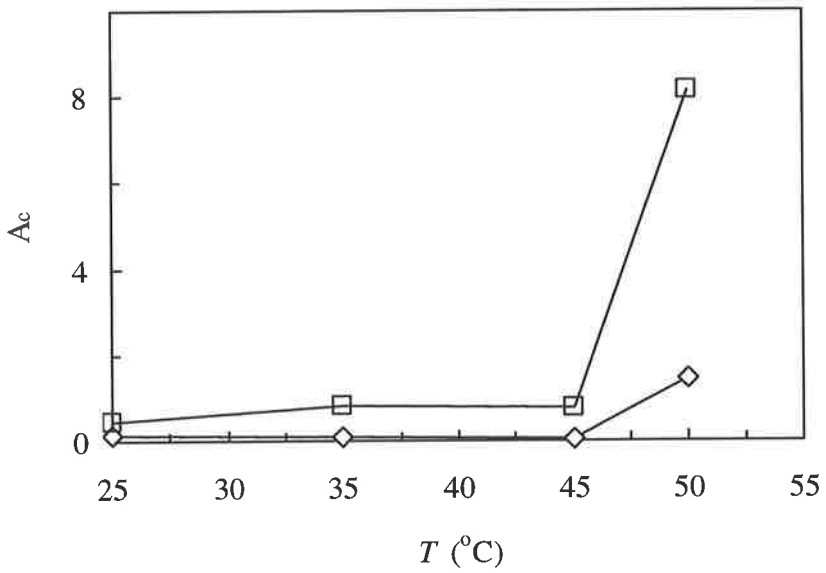

Figure 5.38: Plot of A_c as function of T obtained from fitting the power law model to the $\ln\eta_s$ vs. $\ln(d\gamma/dt)$ data (not shown) for the emulsions containing $\phi_o = 0.3$ (◇) and 0.5 (□).

5.6.2.2 Oscillatory Shear Measurements

The viscoelastic behaviour of the samples was investigated using oscillatory measurements. In initial experiments, the applied frequency was fixed (f = 1 Hz), whilst G' and G" were measured as a function of stress. This allowed the location of the linear viscoelastic region, *i.e.*, where G' and G" are independent of the applied stress at any given frequency, to be determined. Having established the linear region, measurements were made as a function of frequency at a fixed amplitude. The data are shown in Figures 5.39 to 5.46.

The slightly higher G" values compared to G' for the samples at 25°C indicates that the systems behave essentially as viscous fluids. This could be due to the influence of hydrodynamic forces, since attractive interdroplet interactions are negligible as the adsorbed copolymer chains are not collapsed and do not aggregate at this temperature. As the temperature ~~increase~~ gradually pass the LCST of the copolymer, the elastic modulus progressively increases faster than the viscous modulus, *i.e.*, G' > G". This becomes more pronounced for the more concentrated sample. For example, the G' value at f = 1 Hz for the ϕ_o = 0.5 sample is approximately 360 times higher than that for ϕ_o = 0 at the same applied frequency at 50°C (Figure 5.45). This is a consequence of the increased attractive droplet interactions due to the aggregation of the adsorbed copolymer chains with those adsorbed on a second droplet and chains in solution. At 50°C, the oil droplets which are encapsulated within the network of copolymer chains span the entire system, increasing the elastic behaviour of the emulsion. In contrast, the lower elastic behaviour of the ϕ_o = 0 sample can be attributed to the absence of networks.

The observed increase in G' with f at 25 and 35°C is characteristic of dispersions exhibiting liquid-like rheology.[147] Dispersions show some viscoelastic behaviour; thus, G' can be measured at low values of applied frequency.[139] The relatively high and independent values of

G' across the frequency range at high temperatures for the most concentrated sample suggest the presence of a highly structured system. In their work on aqueous polystyrene latex dispersions, Luckham and Ukeje[138] noted that for their more concentrated samples (ϕ = 0.5 and 0.6), G' increased and remained high at all frequencies. They attributed these phenomena to significant compression and interpenetration of the adsorbed PEO-PPO-PEO copolymer. Note that for a perfectly elastic system, G' is not expected to vary with *f*.

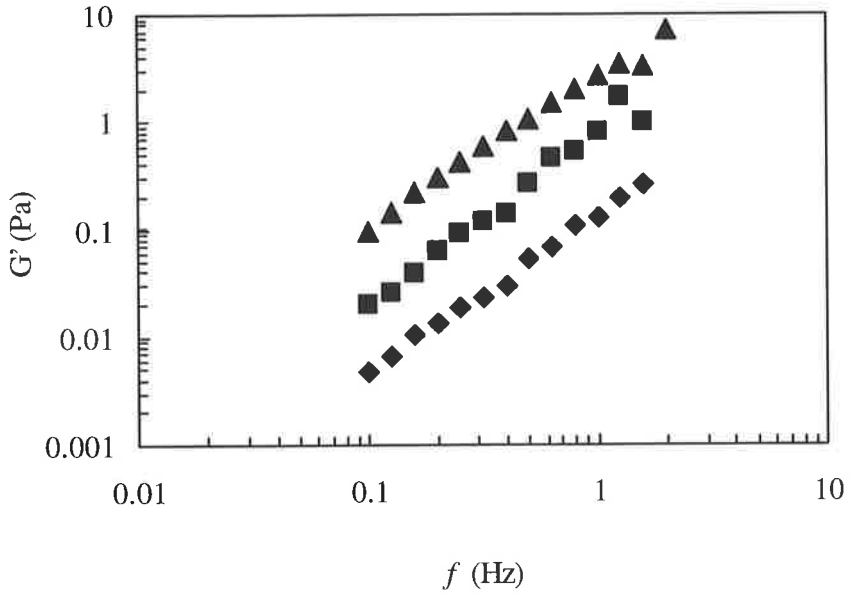

Figure 5.39: The elastic modulus as a function of frequency at 25°C for the samples containing various ϕ_o; (◆) 0, (■) 0.3 and (▲) 0.5.

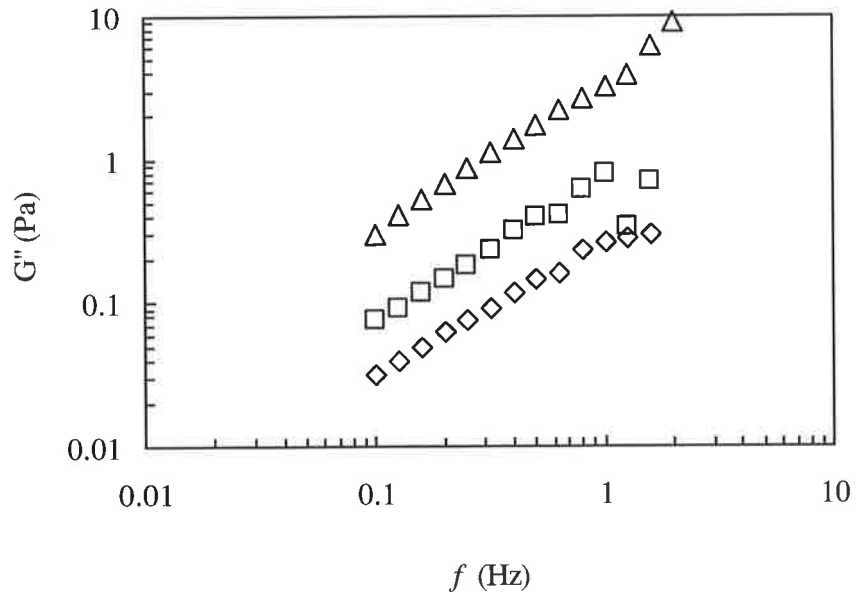

Figure 5.40: The viscous modulus as a function of frequency at 25°C for the samples containing various ϕ_o; (◇) 0, (□) 0.3 and (Δ) 0.5.

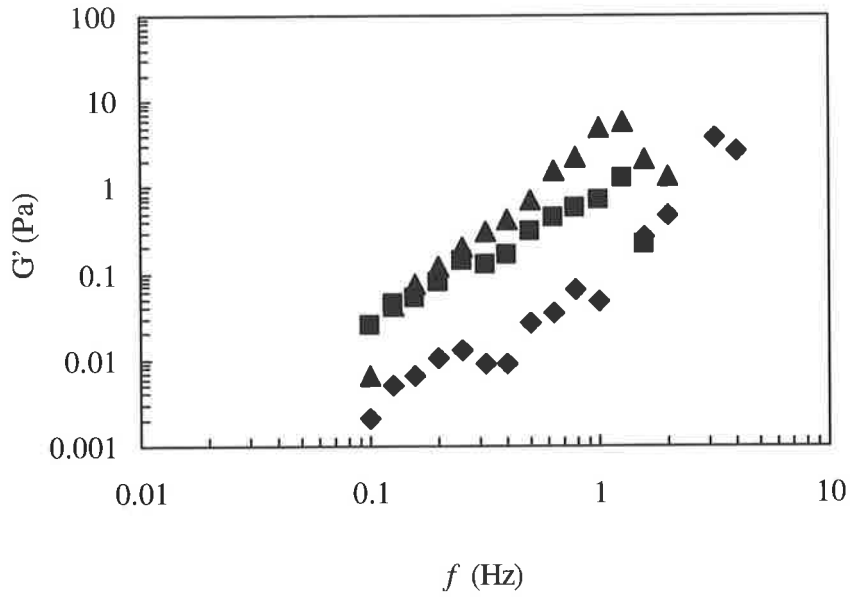

Figure 5.41: The elastic modulus as a function of frequency at 35°C for the samples containing various ϕ_o; (◆) 0, (■) 0.3 and (▲) 0.5.

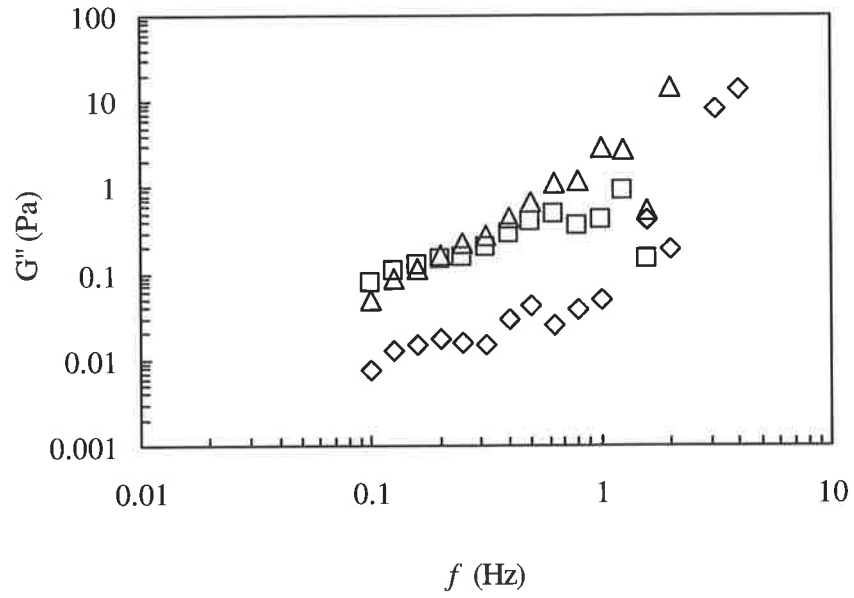

Figure 5.42: The viscous modulus as a function of frequency at 35°C for the samples containing various ϕ_o; (◇) 0, (□) 0.3 and (Δ) 0.5.

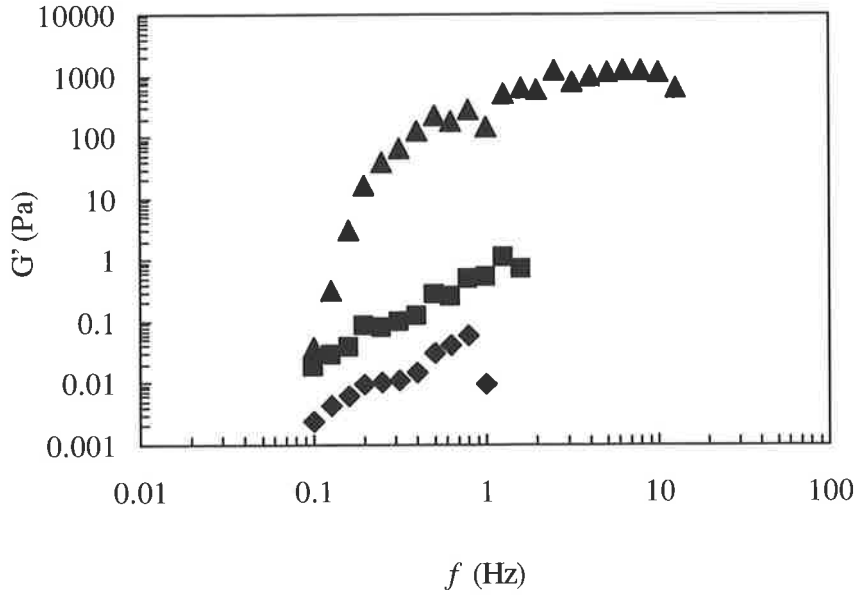

Figure 5.43: The elastic modulus as a function of frequency at 45°C for the samples containing various ϕ_o; (◆) 0, (■) 0.3 and (▲) 0.5.

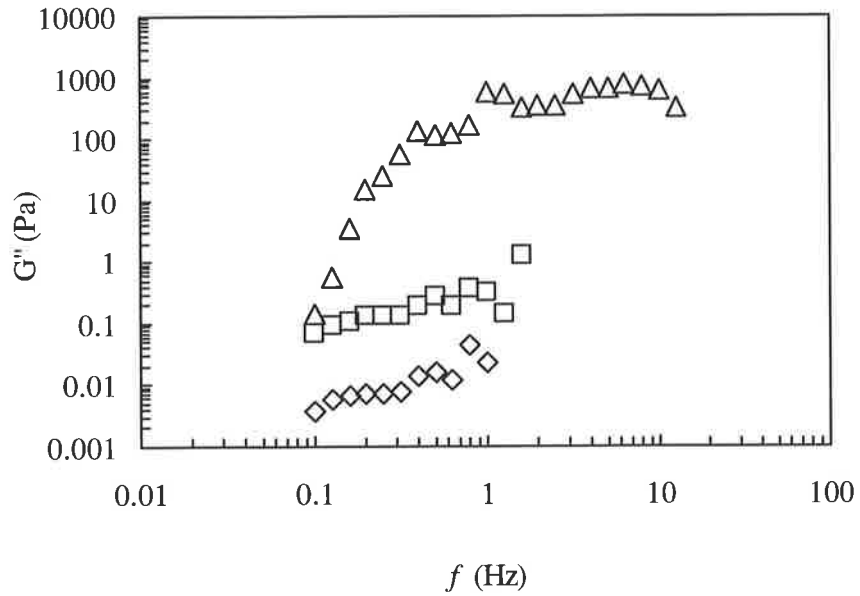

Figure 5.44: The viscous modulus as a function of frequency at 45°C for the samples containing various ϕ_o; (◇) 0, (□) 0.3 and (Δ) 0.5.

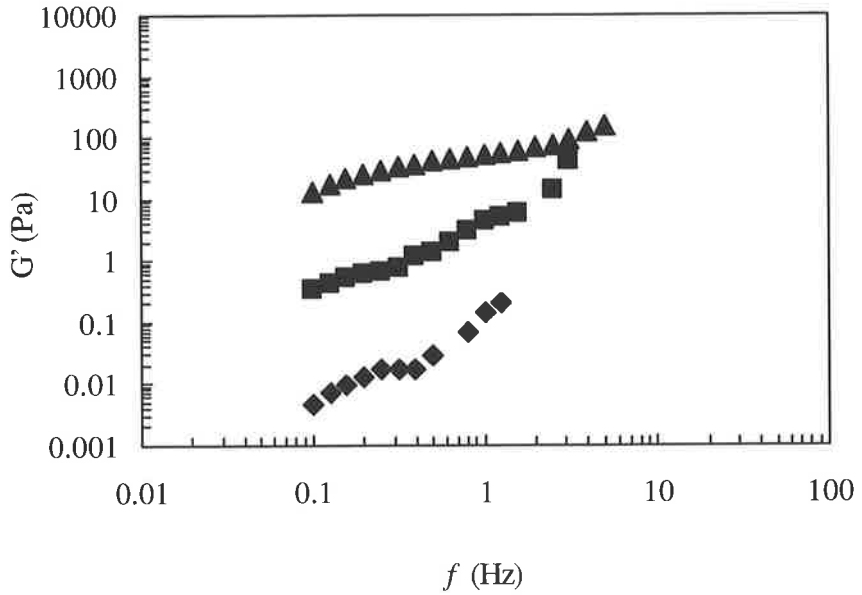

Figure 5.45: The elastic modulus as a function of frequency at 50°C for the samples containing various ϕ_o; (◆) 0, (■) 0.3 and (▲) 0.5.

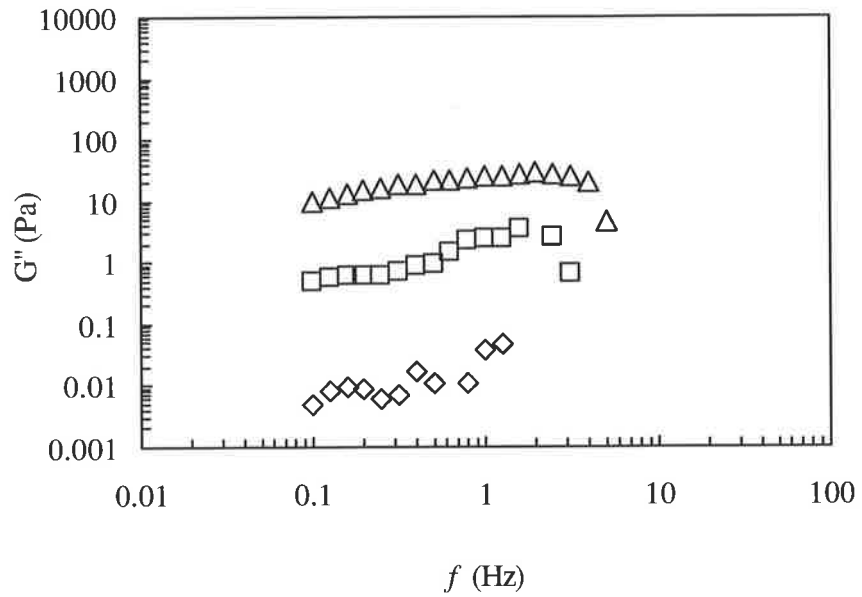

Figure 5.46: The viscous modulus as a function of frequency at 50°C for the samples containing various ϕ_o; (◇) 0, (□) 0.3 and (Δ) 0.5.

To obtain an accurate gelation temperature for each sample, $\tan\delta_p$ is plotted as a function of temperature for the various frequencies (Figures 5.47 to 5.49). Winter's group[142,143] defined the gel point as the point where $\tan\delta_p$ is independent of frequency. In other words, at the gel point with the frequency independence, G' must be parallel to G'. This method is preferred over the approach proposed by Tung and Dynes[148]. They considered the gel point to be defined as the point at which G' = G", which is valid only for stoichiometrically balanced network-forming systems.[140] As n_{pl} was found to vary with temperature and composition of the system (Figures 5.15 and 5.29), it was decided that the Winter-Chambon[142,143] gel point criterion be adopted in the present work. Note that this criterion for determining the gel point was not used for the previous oscillatory studies, *e.g.*, Sections 5.4.2 and 5.6.1.2, since measurements were not conducted as a function of frequency at a fixed amplitude. In this case, the point where the applied stress results in $\tan\delta_p \leq 1$ was taken to be the gel point.

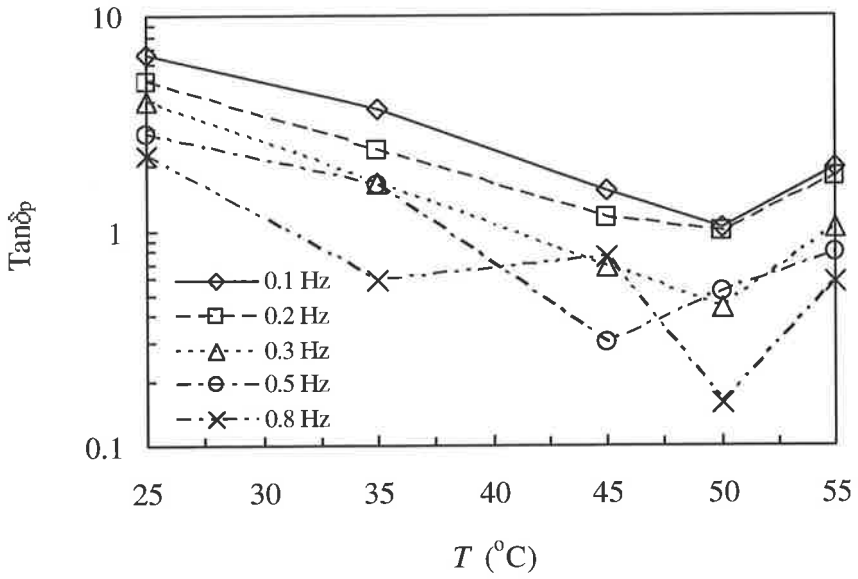

Figure 5.47: Loss tangent vs. temperature for the various frequencies for the $\phi_o = 0$ sample.

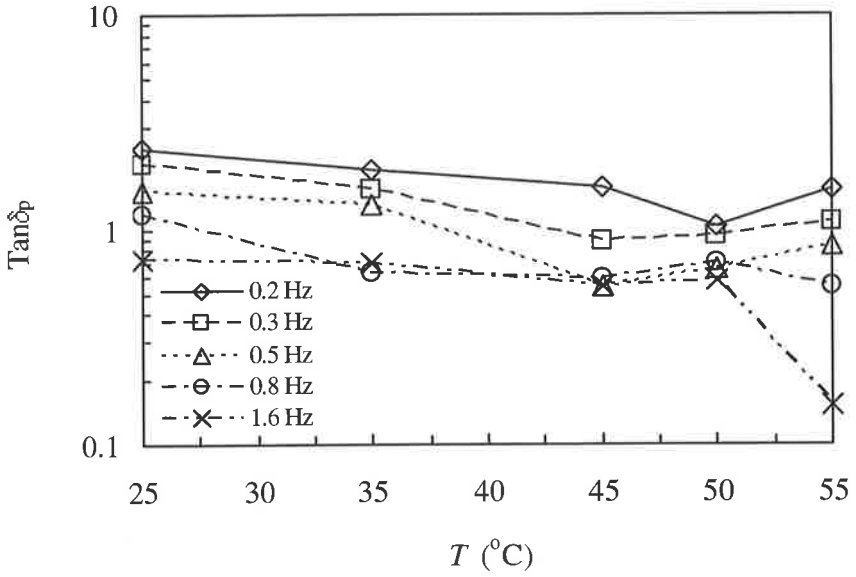

Figure 5.48: Loss tangent vs. temperature for the various frequencies for the $\phi_o = 0.3$ sample.

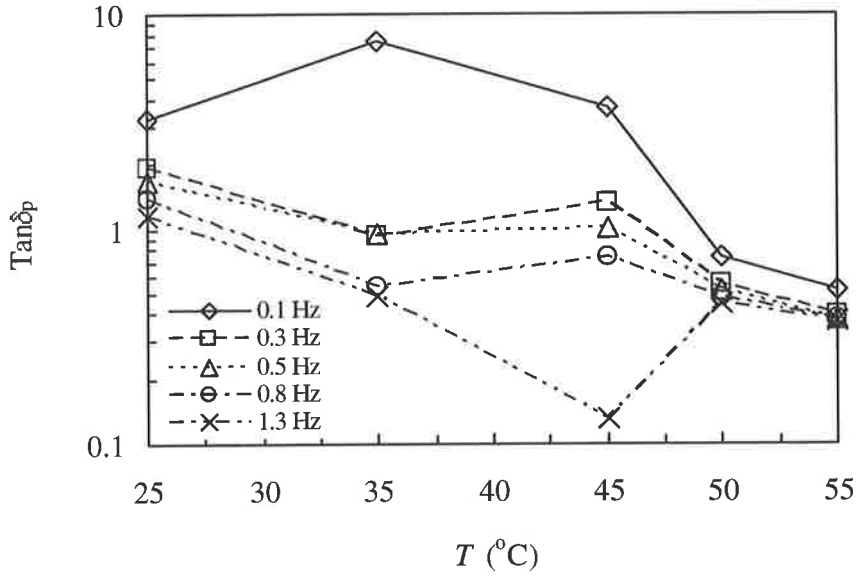

Figure 5.49: Loss tangent vs. temperature for the various frequencies for the $\phi_o = 0.5$ sample.

For the $\phi_o = 0$ sample, the frequency dependence of $\tan\delta_p$ at all temperatures indicates the absence of gelation. This is expected since the copolymer concentration of *ca.* 3.5 wt % is less than c_{gel} of *ca.* 10 wt% (Figure 5.6). It was found that the $\tan\delta_p$ values for the $\phi_o = 0.3$ sample were similar at 50°C, regardless of the applied frequency. This implies gelation at 50°C for this emulsion. Similar trends were also observed for the $\phi_o = 0.5$ sample. The rheological results for the $\phi_o = 0.3$ sample are consistent with the phase diagram shown in Figure 4.13. However, T_{gel} from the oscillatory data for the $\phi_o = 0.5$ sample is 5°C higher than the value of 45°C, indicated from the preliminary viscometry studies (data shown in Figure 4.13). The variation in T_{gel} may be due to the methods and criteria used for assessing the gelation behaviour of the samples. The tube inversion method (Section 4.3.4) is shear rate dependent and sensitive to the yield stress of the gel.[149] In addition, this approach employs a very low frequency range. Note that the high oil volume fraction may have given to the appearance of increased viscosity when the emulsion is heated to elevated temperatures. The Winter-Chambon criterion is a more thorough approach, where a strong/complete gel is required for $\tan\delta_p$ to be independent of frequency, when oscillatory measurements are performed.

5.6.3 Effect of Copolymer Concentration

5.6.3.1 Steady Shear Measurements

The effect of changing the copolymer concentration (with respect to the aqueous phase) on the rheological properties was investigated by conducting steady shear measurements. For this part of the study, perfluorodecalin and perfluoroperhydrophenanthrene (13% of the total oil volume) were used as the oil phase. The preparation of these emulsions is described in Section 5.3.1. Briefly, the sediment layer of the stock emulsion was separated in order to prepare emulsions with varying copolymer concentrations. Note that it was experimentally difficult to separate emulsions containing 1-bromehaxadecane due to its density being close to that of water.

The effect of shear stress on the viscosity of the emulsions at different temperatures is shown in Figures 5.50 to 5.52. The shear thinning behaviour observed for the emulsions containing 3.5 and 10 wt% copolymer becomes more pronounced as temperature increases. The increased ϕ_{eff} due to the adsorbed copolymer chains aggregating with chains in solution and those adsorbed on a second droplet restricts the flow of the sample when shear is applied. In addition, at concentrations where $c_p > c_p^*$ of *ca.* 1 wt%, increased degree of chain entanglement is to be expected with increasing concentration and temperature. Thermothickening seems to occur at 50°C for these samples, as indicated by the large increase in the initial viscosity.

The near constant viscosity across the stress range for the 0.1 wt% sample at all temperatures indicates the absence of temperature-induced aggregation of the droplets. The apparent viscosity increase, *i.e.*, shear thickening, at high stress values could be due to poor signal to noise ratio as a result of close similarity of the sample viscosity to water. It should be noted that stable emulsions at room temperature without aggregation of droplets as temperature increases can be obtained when using low concentrations of copolymer ($c_p \geq 0.1$ wt%).

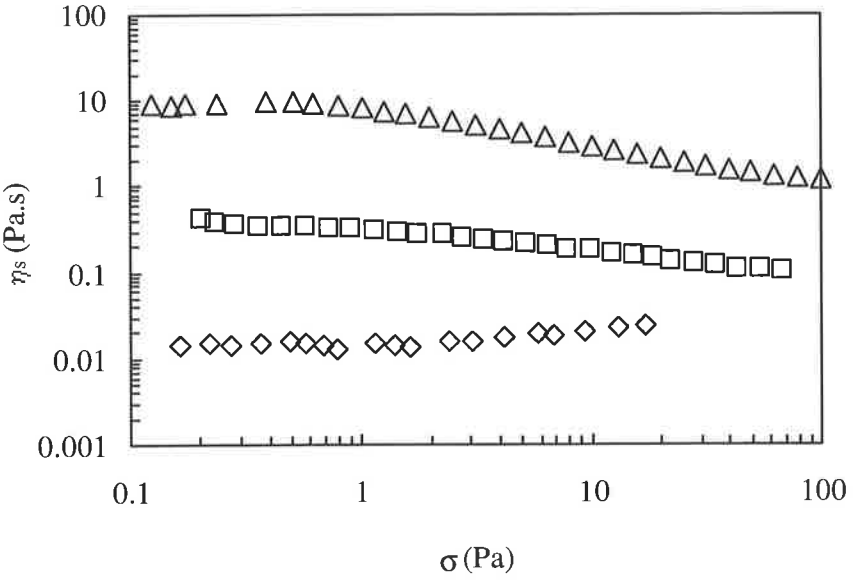

Figure 5.50: Viscosity as a function of stress at 25°C for the emulsions (ϕ_o = 0.3) containing 0.1 (◇), 3.5 (□), and 10 wt% (Δ) P2.

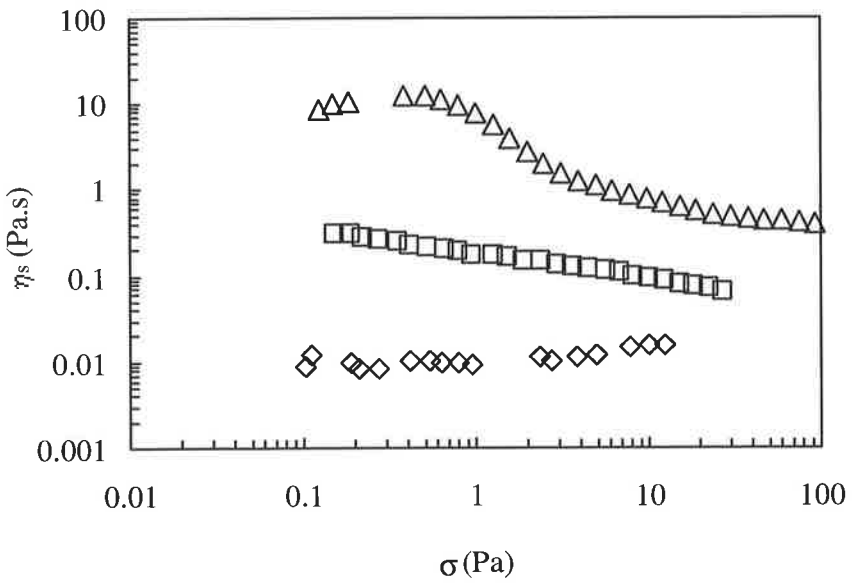

Figure 5.51: Viscosity as a function of stress at 35°C for the emulsions (ϕ_o = 0.3) containing 0.1 (◇), 3.5 (□), and 10 wt% (Δ) P2.

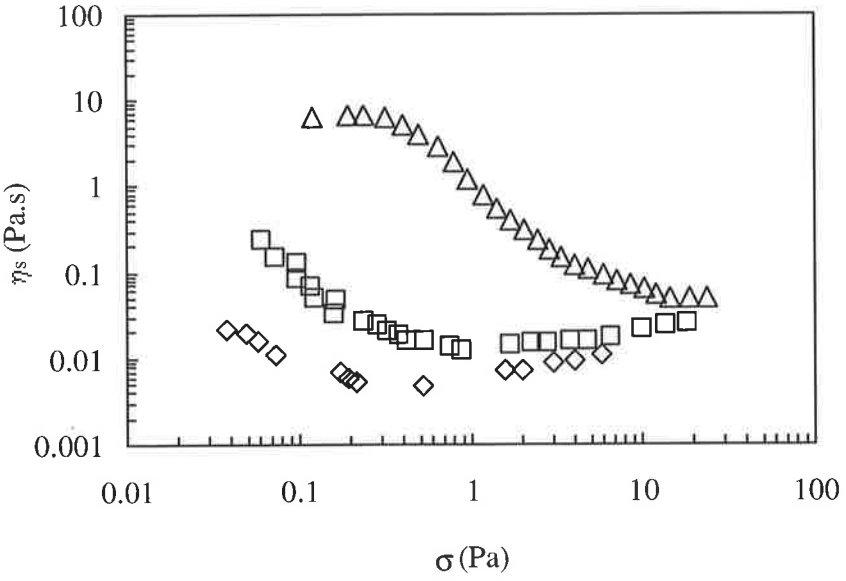

Figure 5.52: Viscosity as a function of stress at 45°C for the emulsions (ϕ_o = 0.3) containing 0.1 (◇), 3.5 (□), and 10 wt% (Δ) P2.

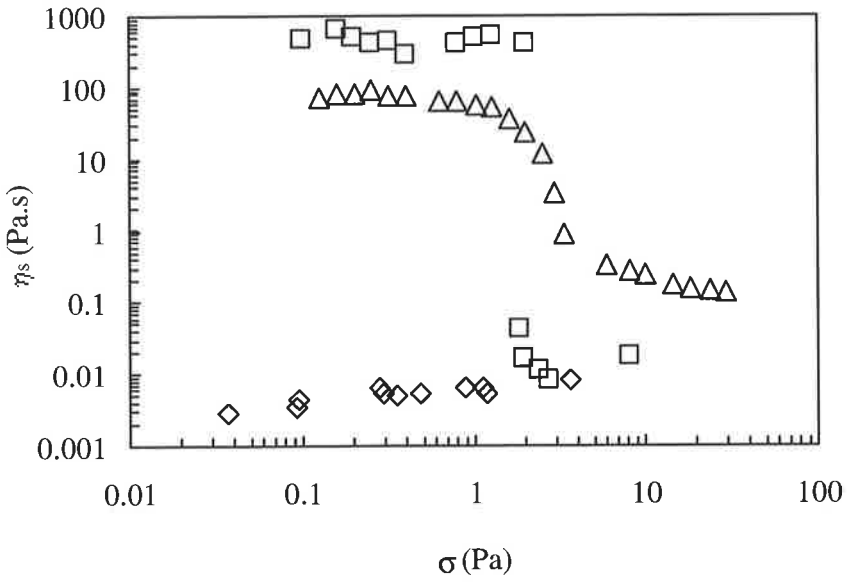

Figure 5.53: Viscosity as a function of stress at 50°C for the emulsions (ϕ_o = 0.3) containing 0.1 (◇), 3.5 (□), and 10 wt% (Δ) P2.

The steady state rheological data for the samples were described in terms of the power law model [Equation (5.6)]. The power law index and consistency parameter were determined from the linear region of $\ln\eta_s$ as a function of $\ln(d\gamma/dt)$ plots (not shown). The data are plotted in Figures 5.54 and 5.55. As in the case with varying the oil volume fraction (Section 5.6.2), the shear thinning behaviour ($n_{pl} < 1$) becomes more significant as temperature increases. This is due to the formation of copolymer chain networks trapping the droplets and resisting flow. Once a critical shear stress has been exceeded, these networks are broken up and the droplets and chains move with the flow of the liquid. This is manifested by the shear thinning behaviour exhibited by the emulsions as the shear stress increases.

The increase in A_c at 50°C may be ascribed to network formation resulting in a highly structured system. Interestingly, the value of $A_c \sim 0$ at all temperatures for the emulsion containing 0.1 wt% P2 indicates the absence of a highly structured system. In other words, no network is formed at this copolymer concentration. It should be noted that the decrease in n_{pl} with temperature for this sample may be attributed to the relative ease of the droplets and copolymer chains moving with the flow of the liquid upon shear due to increased thermal energy (Brownian motion).

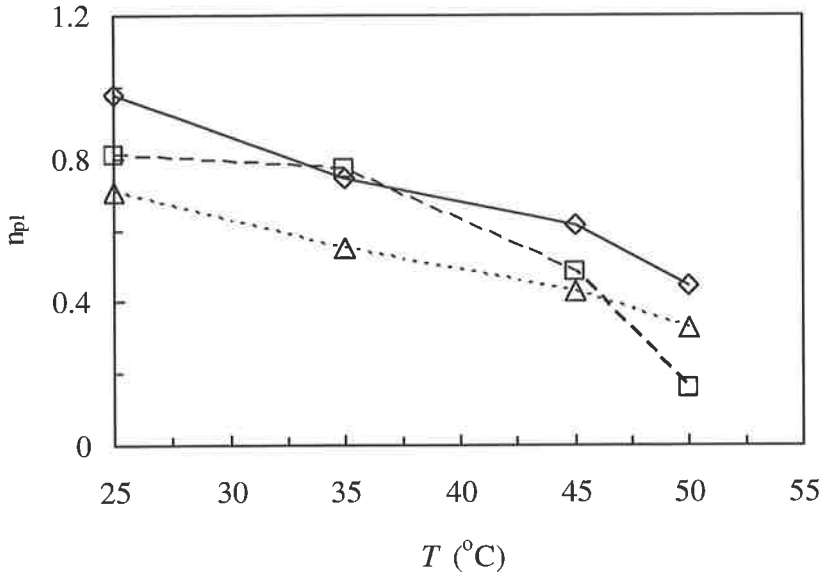

Figure 5.54: Plot of n_{pl} vs. T obtained from fitting the power law model to the $\ln\eta_s$ vs. $\ln(d\gamma/dt)$ data (not shown) for the emulsions containing 0.1 (◇), 3.5 (□) and 10 wt% (Δ) P2.

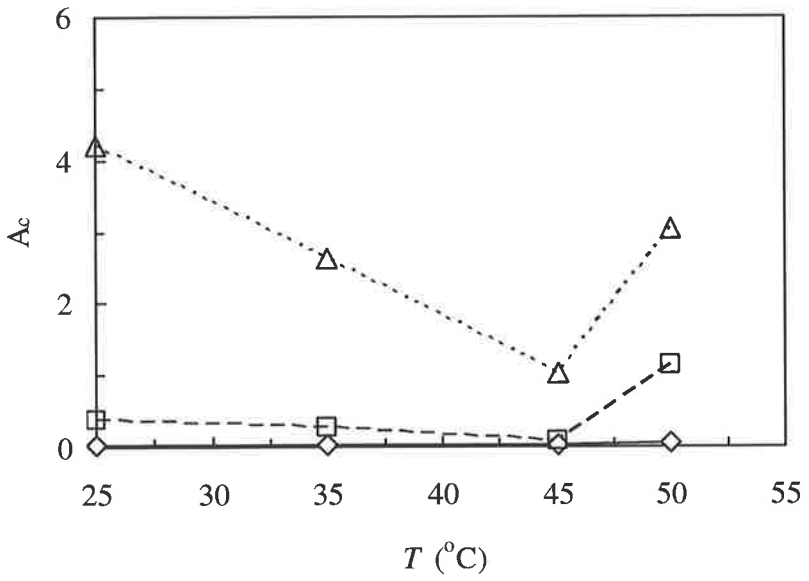

Figure 5.55: Plot of A_c vs. T obtained from fitting the power law model to the $\ln\eta_s$ vs. $\ln(d\gamma/dt)$ data (not shown) for the emulsions containing 0.1 (◇), 3.5 (□) and 10 wt% (Δ) P2.

5.6.3.2 Oscillatory Shear Measurements

The viscoelastic behaviour of the emulsions was investigated using oscillatory measurements (σ =0.1 Pa). The variation in the elastic and viscous moduli as a function of applied frequency is shown in Figures 5.56 to 5.63. Except for the emulsions containing 3.5 and 10 wt% P2 at 50°C, the samples exhibited viscous behaviour (G' < G") at low f and elastic behaviour (G' > G") dominates at high f across the temperature range investigated. This is expected since the viscous response for a material dominates at long times (low frequency) and the elastic response dominates at short time (high frequency). The emulsions containing 3.5 and 10 wt% P2 at 50°C showed elastic behaviour across the frequency range. This is characteristic of concentrated dispersions and gels.[139] Increasing the copolymer concentration (for a given ϕ_o) increases the proportion of chains which adsorbs on the droplets. At T > LCST, the increased number of copolymer chains that can participate in temperature-induced association increases ϕ_{eff} of the droplets. Evidence of this can be seen from the G' values for the 10 wt% sample being greater than that for the 0.1 wt% sample at all temperatures. The presence of oil droplets has the same rheological effect as increasing the copolymer concentration for the pure copolymer solutions. This is apparent from the higher G' value at 50°C for the emulsion containing 10 wt% P2 (Figure 5.62) compared to the pure copolymer solution (Figure 5.17).

The G' vs. f curves at 35 and 45°C for the emulsion containing 3.5 wt% P2 resemble that for the 10 wt% sample at the same temperatures, whilst G' increases slowly with f for the 0.1 wt% sample at all high temperatures. The values for G' for the 3.5 and 10 wt% samples at 50°C were near independent of the frequency indicating the presence of highly structured emulsions, *i.e.*, emulsion gels. This was a result of temperature-induced association of the chains which led

to thermothickening of the emulsions. Note that the decrease in G' at high frequencies at 50°C for the 10 wt% sample is due to the disruption of the gelled system.

The higher G' values across the stress range at 50°C for the emulsion containing 3.5 wt% P2 (Figure 5.62) compared to the data for similar emulsion shown in Figure 5.45 ($\phi_o = 0.3$) may be attributed to the type of oil used. The higher mass per unit volume, *i.e.*, density, of perfluorodecalin (used in the former) allows the oil to behave in a more elastic fashion since more of the material is able to store energy when deformation takes place, *e.g.*, when a high enough shear is applied. In contrast, when shear force is applied, most of the energy dissipates, *i.e.*, viscous flow, in the case of the 1-bromohexadecane oil (used in the latter) as it is less dense than perfluorodecalin. In addition, differences in the total surface area and surface excess concentration of the copolymer for each emulsion could vary its rheological properties. It is expected that the elastic behaviour of the emulsion will be more pronounced with increasing concentration of adsorbed copolymer.

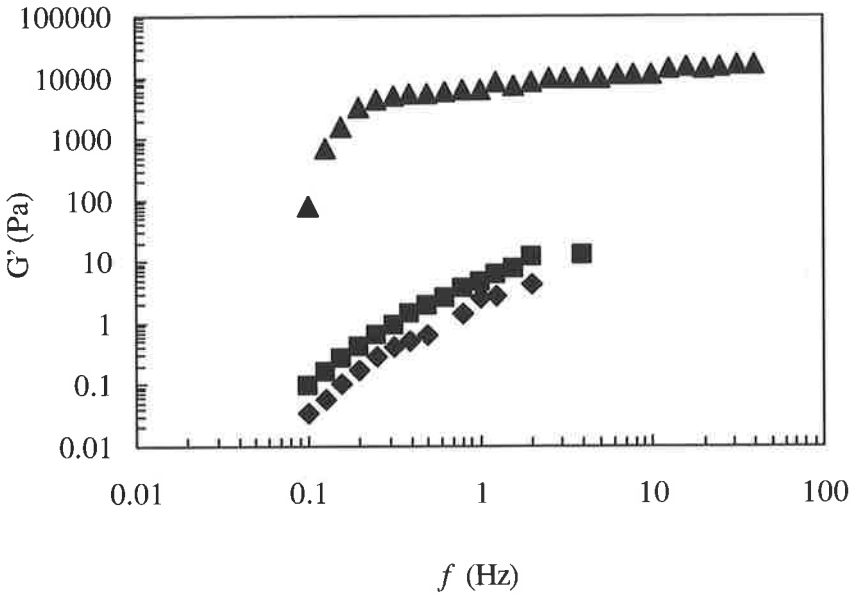

Figure 5.56: The elastic modulus as a function of frequency at 25°C for the emulsions (ϕ_o = 0.3) containing 0.1 (◆), 3.5 (■), and 10 wt% (▲) P2.

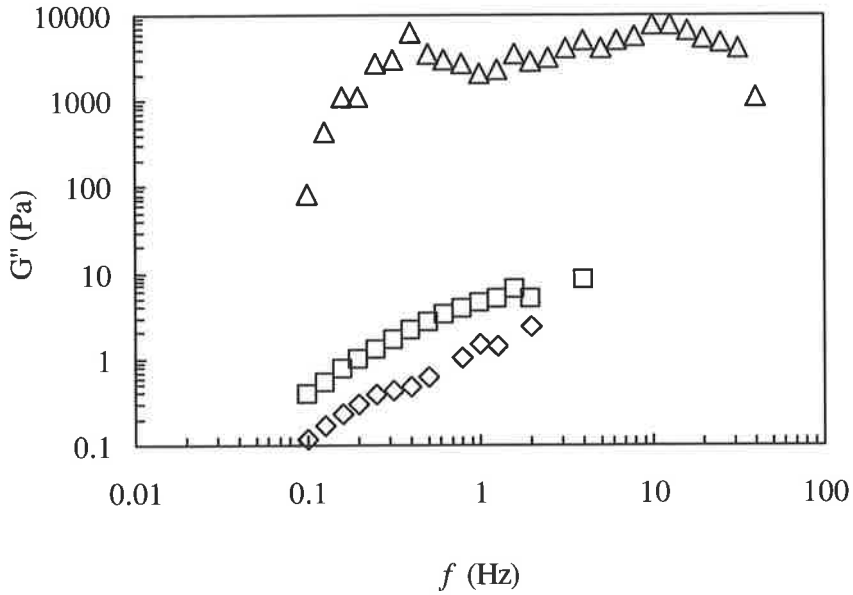

Figure 5.57: The viscous modulus as a function of frequency at 25°C for the emulsions (ϕ_o = 0.3) containing 0.1 (◇), 3.5 (□), and 10 wt% (Δ) P2.

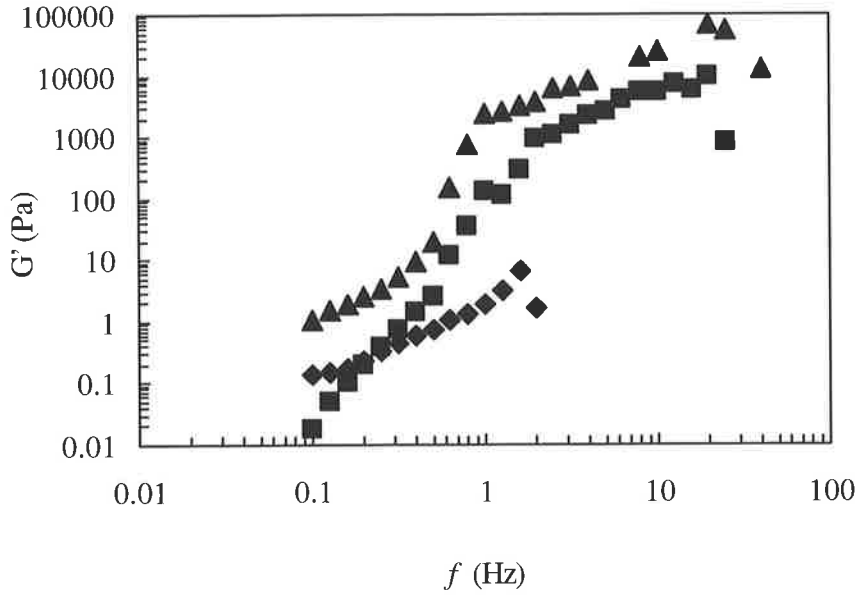

Figure 5.58: The elastic modulus as a function of frequency at 35°C for the emulsions (ϕ_o = 0.3) containing 0.1 (◆), 3.5 (■), and 10 wt% (▲) P2.

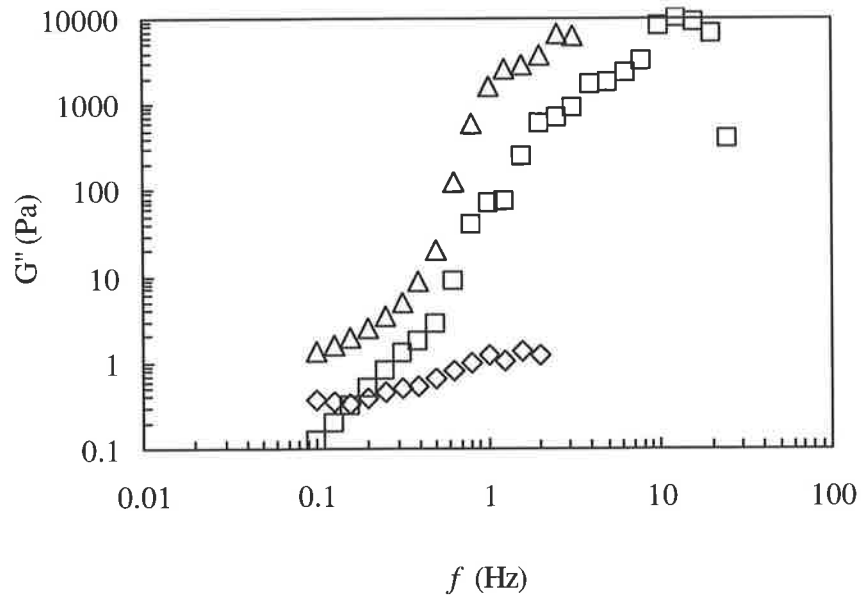

Figure 5.59: The viscous modulus as a function of frequency at 35°C for the emulsions (ϕ_o = 0.3) containing 0.1 (◇), 3.5 (□), and 10 wt% (Δ) P2.

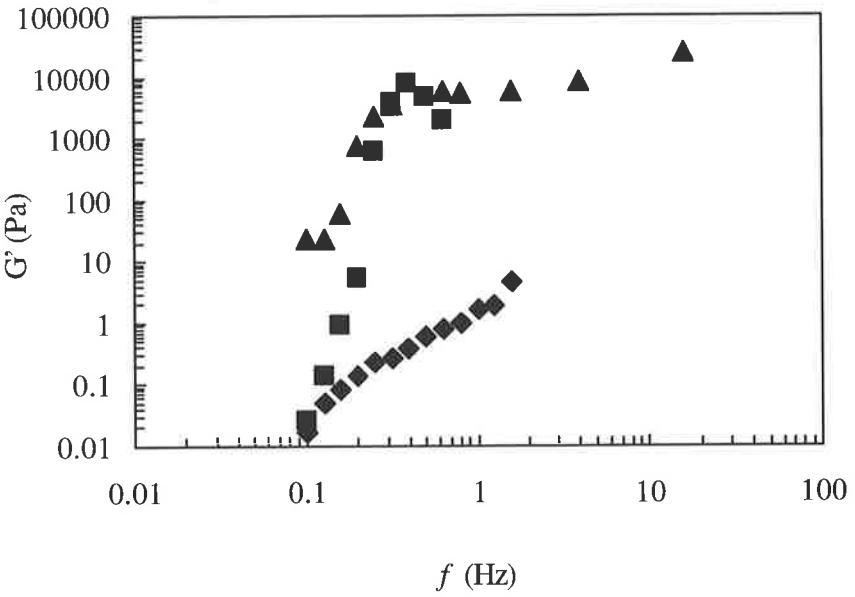

Figure 5.60: The elastic modulus as a function of frequency at 45°C for the emulsions (ϕ_o = 0.3) containing 0.1 (◆), 3.5 (■), and 10 wt% (▲) P2.

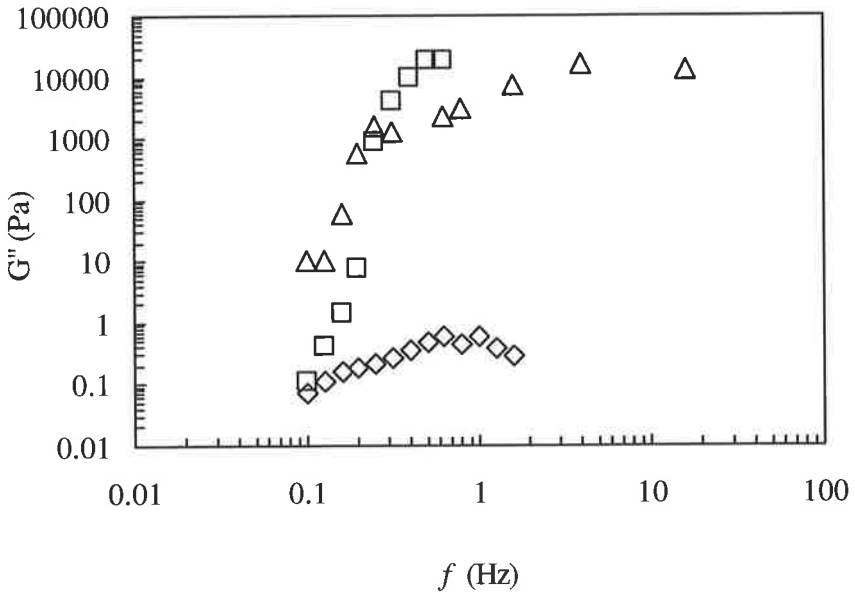

Figure 5.61: The viscous modulus as a function of frequency at 45°C for the emulsions (ϕ_o = 0.3) containing 0.1 (◇), 3.5 (□), and 10 wt% (Δ) P2.

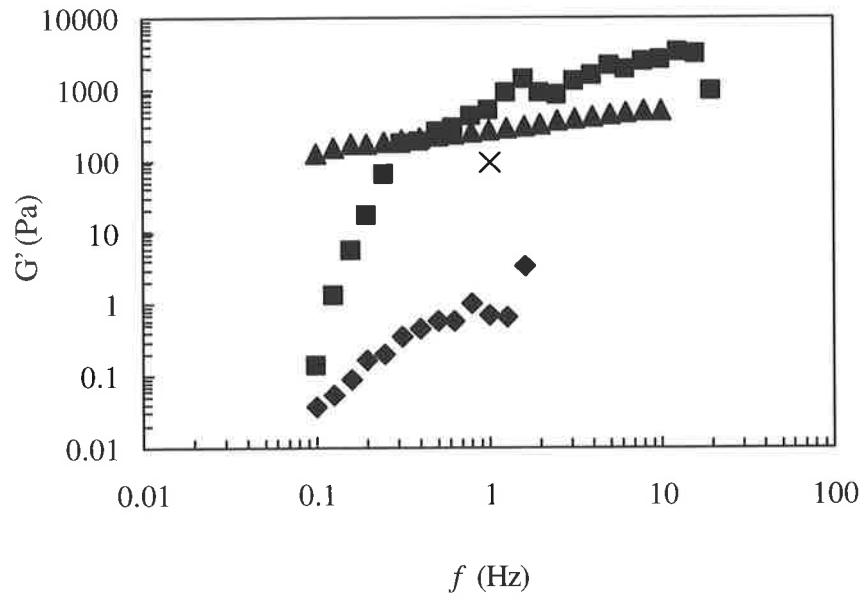

Figure 5.62: G' vs. f at 50°C for the emulsions (ϕ_o = 0.3) containing 0.1 (◆), 3.5 (■), and 10 wt% (▲) P2. The 10 wt% P2 solution is shown by (x) (data from Figure 5.17).

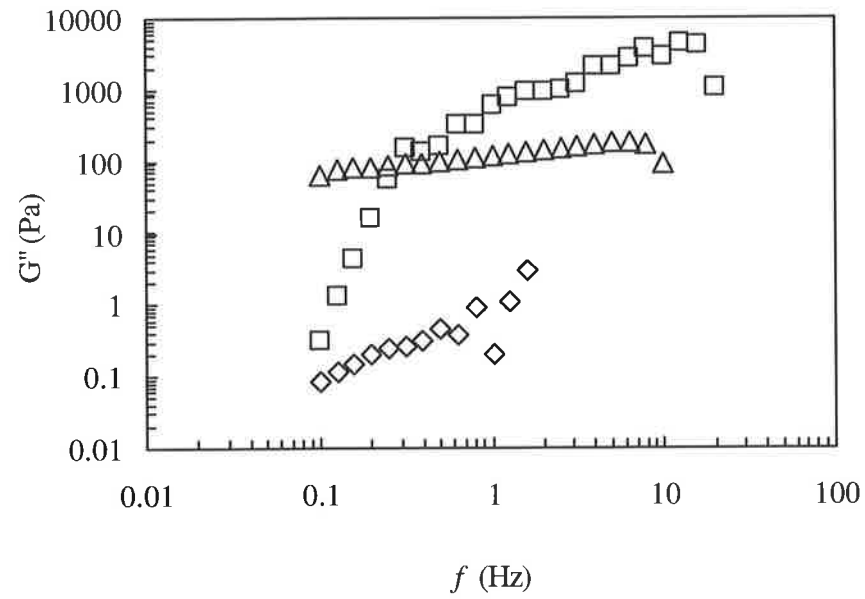

Figure 5.63: The viscous modulus as a function of frequency at 50°C for the emulsions (ϕ_o = 0.3) containing 0.1 (◇), 3.5 (□), and 10 wt% (Δ) P2.

The gelation temperature for the emulsions was obtained by plotting the loss tangent as a function of temperature for various frequencies. The plots are shown in Figures 5.64 to 5.66. The point where $\tan\delta_p$ is independent of frequency is the gel point, *i.e.*, Winter-Chambon criterion. It was found that the frequency lines for both the 3.5 and 10 wt% samples have common intersection at *ca.* 50°C, implying that the systems follow the Winter-Chambon[143,143] criterion. Very different behaviour can be seen for the 0.1 wt% sample, where $\tan\delta_p$ was dependent on the applied frequency at all temperatures. This shows absence of emulsion gelation for this system.

These results indicate that c_{gel}: $0.1 < c_{gel} < 3.5$ wt% for emulsions containing $\phi_o = 0.3$. This is consistent with the data presented in Figure 4.15, where using the tube inversion method, c_{gel} was found to be *ca.* 1 wt% for emulsions containing $\phi_o = 0.3$. However, T_{gel} from the oscillatory data for the sample containing 10 wt% P2 is 5°C higher than the value of 45°C reported from the preliminary viscometry studies (data shown in Figure 4.15). This can be attributed to the same reasons stated before (Section 5.6.2.2), where different methods and criteria were used for assessing the gelation behaviour of the samples.

Qualitatively, increasing the copolymer concentration has the same rheological effect as increasing the oil volume fraction. This is evident by the decrease in T_{gel} of the emulsions with increasing oil volume fraction (Figures 5.47 to 5.49) and/copolymer concentration (Figures 6.64 to 6.66). This has been attributed to an increased number of droplets and/copolymer chains (in the case of emulsions) that can participate in temperature-induced association at $T >$ LCST of the copolymer. Extensive aggregation leads to thermothickening and in more concentrated systems, *e.g.*, emulsion containing $\phi_o = 0.3$ and $c_p = 3.5$ wt%, gelation results.

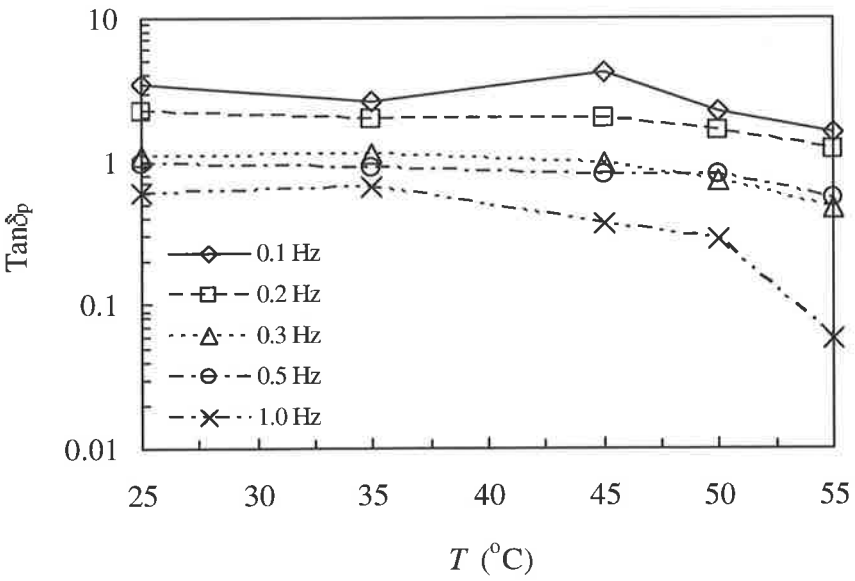

Figure 5.64: Loss tangent as a function of temperature for the various frequencies for the emulsion containing 0.1 wt% P2.

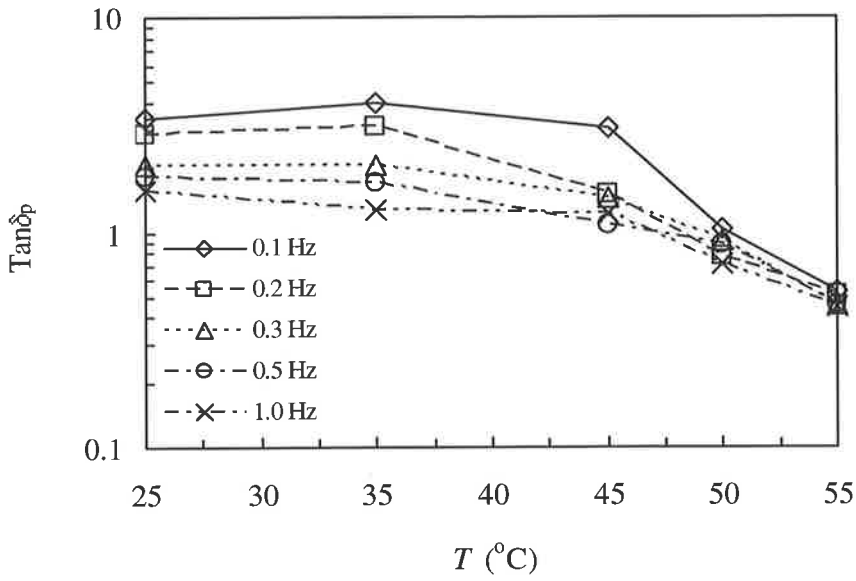

Figure 5.65: Loss tangent as a function of temperature for the various frequencies for the emulsion containing 3.5 wt% P2.

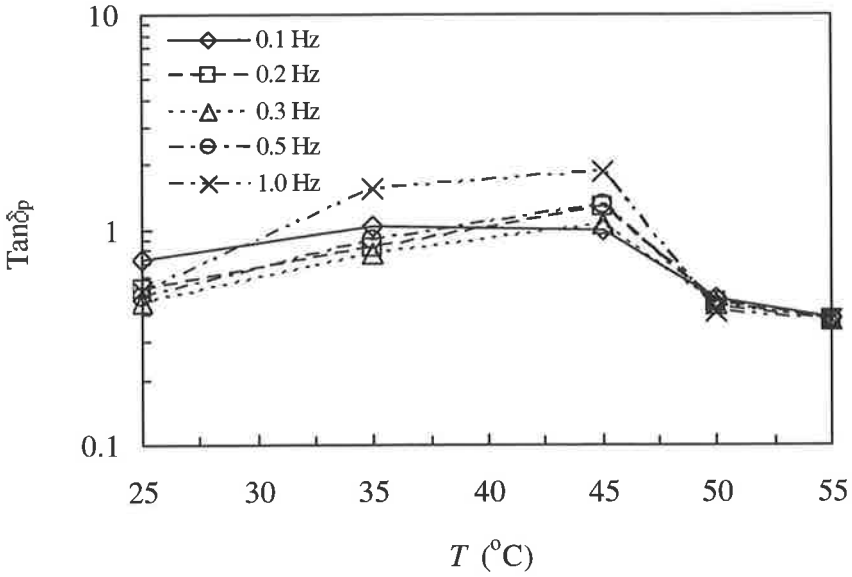

Figure 5.66: Loss tangent as a function of temperature for the various frequencies for the emulsion containing 10 wt% P2.

5.6.4 Effect of Heating/Cooling Cycles on Rheology

Rheological studies can provide an indirect means of identifying changes in emulsion properties.[150] Thermally accelerated stability testing was conducted to allow changes in the physical and chemical properties of the emulsions upon undergoing a number of heating/cooling cycles to be ascertained. Figure 5.67 shows the viscosity vs. stress curves for the emulsion (ϕ_o = 0.3) containing 3.5 wt% P2 after undergoing a number of heating/cooling cycles. The emulsion was heated to 50°C for 5 min. and left at that temperature over the same period of time. The sample was then allowed to cool. The time taken for the sample to cool and equilibrate at 25°C was 5 min. each. The heating/cooling cycle was repeated in succession for five times. The similarity in the trend of the plots at a given temperature suggests that the rheological properties of the emulsion are not significantly affected by cycles of temperature-induced gelation.

A photomicrograph of the emulsion (Figure 5.68) revealed that the droplets were slightly flocculated after undergoing the heating/cooling cycles. This result is consistent with the photomicrograph shown in Section 4.5.2.2 (Figure 4.18) and supports the view that the physical and chemical properties of the emulsion are not significantly affected by temperature-induced gelation cycles. Note that prolonged storage at elevated temperatures on the stability of the emulsions was not investigated in this work. It is possible that pronounced coalescence of the oil droplets may occur.

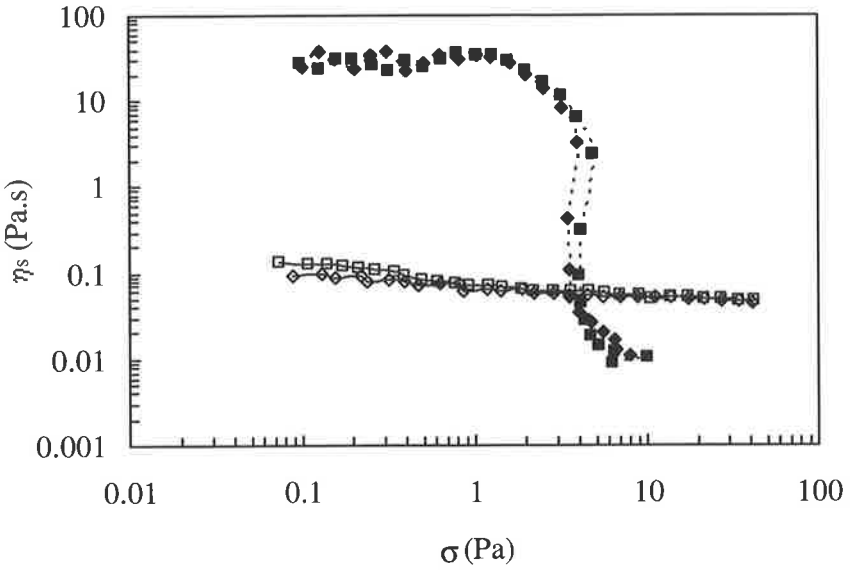

Figure 5.67: Viscosity as a function of shear stress after a number of temperature-induced gelation cycles for the emulsion (ϕ_o = 0.3) containing 3.5 wt% P2. The cycles at 25 and 50°C are represented by the open and closed symbols, respectively. The number of heating/cooling cycles carried out was 1 (diamonds) and 5 (squares).

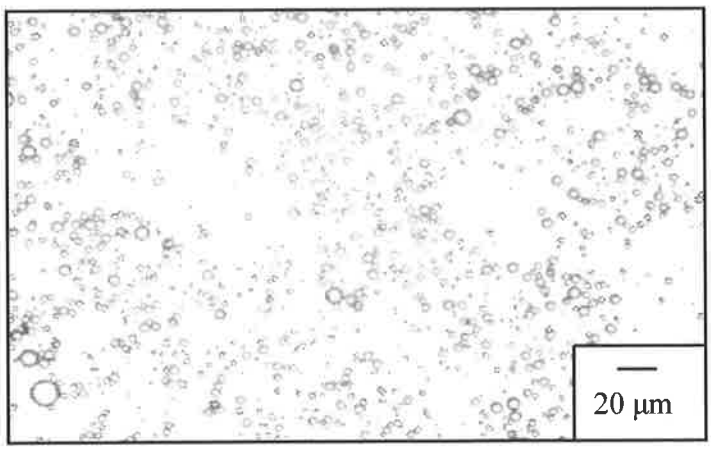

Figure 5.68: Optical micrograph of the emulsion containing P2 (3.5 wt%) after five heating/cooling cycles (diluted to ϕ_o = 0.1). The average droplet size is *ca.* 10.0 μm (*cf.* Figure 4.2).

5.6.5 Temperature-induced Emulsion Gelation: Role of the Droplets

The rheological data may provide additional information about the mechanism for temperature-induced emulsion gelation presented in Section 4.5.3. The mechanism involves the surface of oil droplets acting as anchoring sites for the copolymer chains for the formation of network at high temperatures. Thus, increasing the oil volume fraction in the emulsion is expected to increase the number of cross-links, N_c. The relative shear modulus, G_r, is given by:[7]

$$G_r = \frac{G_E}{G_N} \tag{5.11}$$

where G_E is the elastic modulus and G_N is the network modulus. The elastic modulus is governed by the volume fraction and polydispersity of the oil droplets as described by:

$$G_E = G_N\left(1-\frac{\phi_o}{\phi_{max}}\right)^{-2.5\phi_{max}} \tag{5.12}$$

where ϕ_{max} is the maximum concentration that the droplets can achieve. Note that for monodisperse spherical droplets, ϕ_{max} = 0.64. The network modulus[7] can be expressed in terms of the copolymer concentration and the molar mass between entanglements, M_e:

$$G_N = c_p \frac{N_A}{M_e} kT \tag{5.13}$$

Equation (5.13) indicates that G_N is the product of the thermal energy and the number of copolymer chains that are entangled, *i.e.*, cross-links. The relative shear modulus is related to the

number density of additional network links, N_L, (in this case due to the presence of oil droplets) as given by:[7]

$$G_r = \left(1 + \frac{N_L}{N_I}\right)\left(1 - \frac{\phi_o}{0.64}\right)^{-1.6} \tag{5.14}$$

where N_I is the number density of initial cross-links present. The variation of G' with *f* for the emulsion containing 10 wt% P2 is shown in Figure 5.62. Equivalent data are shown in Figure 5.69 for the 10% copolymer solution. The frequency independence of $\tan\delta_p$ is indicative of a temperature-induced association effect, *i.e.*, gelation, for the copolymer solution. Using the G' values at f = 2.5 Hz and Equations (5.11) and (5.14), G_r = 51 and N_L/N_I = 18. Note that the possible variation in the value of N_L/N_I exists, due to the slight variation in G' across *f*. However, the analysis of the results remains the same, in that $N_L/N_I > 1$ across the frequency range. The calculations show that the oil droplets act as anchoring sites for the copolymer (*i.e.*, as an interacting filler[7]), increasing the number density of network links. The droplets have the same qualitative effect as a substantial increase in the copolymer concentration. This supports the observation of temperature-induced gelation for emulsions containing a continuous phase copolymer concentration less than that required for gelation of the parent copolymer concentration. Note that droplets acting as junction points for the formation of three-dimensional networks by associative thickeners has been reported in the literature.[136,151] Thus, the gelled emulsion network contains two different types of cross-link points, namely, micelle-like aggregates of the copolymer chains in the continuous phase and oil droplets with copolymer adsorbed at the surface with one of their terminal groups, the other terminal group extending in the solution. The latter has a stronger effect on the elastic properties of the network.

Increasing the volume fraction of oil and/copolymer concentration decreases the gelation temperature and increases the gel strength, *i.e.*, high yield stress, since a higher proportion of droplets and/copolymer chains are able to participate in the gelation process as temperature increases above the LCST, allowing a more extensive (and stronger) network to be formed. This results in pronounced shear thinning behaviour at high stresses due to the oil droplets and/copolymer chains restricting the flow of the liquid upon shear.

The relative high degree of reversibility for the gelation transition (Section 5.6.4) may be explained as follows. Strongly flocculated emulsions invariably consist of aggregates containing considerable entrapped continuous phase (water).[152] The flocculated droplets will form a three-dimensional network provided that a critical oil volume fraction is exceeded, such that chains of droplets can achieve a sufficient degree of connectivity throughout the emulsion. As temperature decreases, the collapsed copolymer chains begin to expand (as now water becomes a good solvent). This causes the network to break-up and the flocculated droplets that once formed the three-dimensional network, to redisperse.

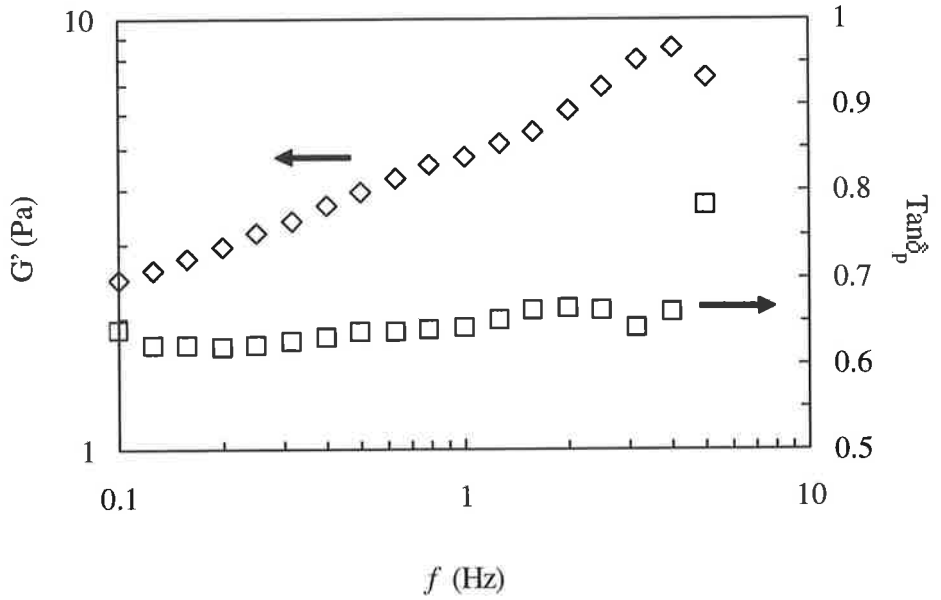

Figure 5.69: Plot of the elastic modulus (◇) and loss tangent (□) as a function of frequency for the 10 wt% P2 at 50°C.

5.7 Conclusions

The gelation concentration for the copolymer P2 has been found to be *ca.* 10 wt% from steady shear measurements. Temperature-induced association behavior of the copolymers was observed and found to be shear rate dependent, in that at high shear rates the sample viscosity is less than that at temperatures less than the LCST. The shear thinning profile was well described in terms of the power law model. Increasing the temperature and/copolymer concentration, which effectively increased the number of chains available for aggregation and copolymer network formation, led to a more pronounced shear thinning behaviour. Oscillatory shear measurements revealed that the elastic modulus is considerable greater than the viscous modulus at temperatures greater than the LCST. At room temperature, the samples behaved as viscous liquids, but became more elastic as temperature was increased.

Steady shear measurements showed that the emulsion containing P2 exhibited thermothickening behaviour, *i.e.*, increased viscosity with temperature, at low shear rates once the temperature exceeded the LCST of P2 at *ca.* 35°C. The dispersed phase droplets appeared to have the same qualitative effect on the rheological properties as a substantial increase in the copolymer concentration. Increasing the temperature increased the number of copolymer chains and the amount of time that junctions remained in hydrophobic clusters. This resulted in a stronger gel to be formed and a greater shear stress was required to disrupt the junctions.

Increasing the oil volume fraction of the emulsion not only increased the low shear viscosity, but also a higher stress was required before shear thinning was observed at high temperatures. The 3.5 wt% copolymer solution, *i.e.*, $\phi_o = 0$, did not show temperature-induced gelation across the temperature range examined, which supported the finding from preliminary experiments (Section 4.5.1.2). The lower elastic behaviour for this sample was attributed to the

absence of interdroplet interactions, since networks were solely formed by aggregated copolymer chains at T > LCST. In contrast, the relatively high and independent values of G' across the frequency range at high temperatures for the more concentrated samples suggests the presence of highly structured systems, *i.e.*, emulsion gels. Using the Winter-Chambon gel point criteria, ϕ_o = 0.3 and 0.5 had T_{gel} of *ca.* 50°C.

Increasing the copolymer concentration resulted in a higher yield stress in the emulsions due to increased number of junctions formed. This led to the number of elastically effective links between the chains to rise, resulting in stronger network formation and gel strength. At 50°C, the G' values for the 3.5 and 10 wt% samples were effectively independent of the frequency, indicating that the emulsions have gelled. More importantly, the emulsion containing 0.1 wt% copolymer showed no signs of gelation across the temperature range studied. This indicates that a critical copolymer concentration was required for emulsion gelation to occur. Preliminary studies (Section 4.5.1.3) indicated c_{gel} to be *ca.* 1 wt% for emulsions containing ϕ_o = 0.3. Heating/cooling cycles showed that the rheological properties of the emulsions were not significantly affected by temperature-induced gelation.

CHAPTER 6 REVIEW

6.1 Conclusions

Poly(NIPAM-*co*-PEGMA) copolymers have been successfully synthesised using free-radical polymerisation. The copolymers were shown to have different chemical properties, *e.g.*, LCST and polydispersity, depending on the reaction conditions used. The value for c_p^* of the copolymer was found to be *ca.* 1 wt% from viscosity measurements. Increasing the proportion of PEGMA resulted in an increase in the LCST of the copolymer due to the PEGMA segments inhibiting the collapse of the chains more extensively as temperature was increased. By means of the Lewis-Mayo method, the monomer reactivity ratios were found to be 1.05 and 0.63 for NIPAM and PEGMA, respectively. A drift of the copolymer composition with monomer conversion was predicted due to the reactivity ratio of the monomers being different and the synthetic method employed. The conditions used in this work were to synthesise copolymers having asymmetric compositions. This was necessary since conditions designed to promote symmetric compositions yielded copolymers that would not stabilise and/or promote emulsion gelation.

Analysis of the SANS data revealed that the copolymer chains of poly(NIPAM-*co*-PEGMA) contained three structural features at temperatures between 25 and 50°C, namely, rods, coils and particles This is shown in Figures 6.1(a) to (c). At room temperature, there were evidence of coils (R_g = 8 nm) and rods (R_r = 1 nm). As temperature increased, only coils were present and the chains aggregated to form micelles. This temperature-induced aggregation was accompanied by an increase in the radius of gyration to *ca.* 17 nm. At 50°C, particles rich in

NIPAM segments were formed. The size of the particles were estimated to be 120 nm in diameter.

Poly(NIPAM-*co*-PEGMA) copolymers have been shown to emulsify and stabilise O/W emulsions [Figures 6.1(d)]. The homopolymers did not stabilise emulsions of oil and water due to the absence of either a stabilising (hydrophilic) or anchoring (hydrophobic) chains. The absence of gelation behaviour for the emulsion containing copolymer with a low proportion of NIPAM was attributed to insufficient NIPAM units required for inter-layer aggregation to occur. The lack of a significant number of stabilising units, *i.e.*, EO segments, for steric stabilisation to operate, could have caused the phase separation behaviour to be observed for the emulsion containing copolymer with a high mol% NIPAM. Steric stabilisation was found to be the primary mechanism of stability for the emulsions containing the copolymers. Viscosity studies showed a decrease in emulsion viscosity as temperature was increased but above the gel point, *ca.* 45°C, the viscosity increased dramatically. Visual inspection of the sample revealed the viscosity increased to such an extent that the emulsion had gelled above this temperature [Figures 6.1(e)]. The phase diagrams showed that for temperature-induced emulsion gelation to be observed, $\phi_o \geq 0.1$ and $c_p \geq 1$ wt%.

From rheological measurements, the critical gelation concentration for poly(NIPAM-*co*-PEGMA) copolymers in solution was found to be *ca.* 10 wt% [Figures 6.1(f)]. Temperature-induced association behavior of the copolymers was observed and found to be shear rate dependent. At high shear rates, the sample viscosity was less than that at temperatures less than the LCST. At room temperature the samples behaved as viscous liquids, but became more elastic as temperature was increased. Steady shear measurements showed that the emulsions containing P2 exhibited thermothickening behaviour once the temperature exceeded the LCST of the

copolymer at *ca.* 35°C. The dispersed phase droplets appeared to have the same qualitative effect on the rheological properties as a substantial increase in the copolymer concentration. Increasing the temperature increased the number of copolymer chains and the amount of time that junctions remained in hydrophobic clusters. This resulted in the formation of a strong gel ~~a stronger gel to be formed~~ and a greater shear stress was required to disrupt the junctions. Increasing the oil volume fraction/copolymer concentration of the emulsion not only increased the zero shear viscosity, but also a higher stress was required before shear thinning was observed at high temperatures. Using the Winter-Chambon gel point criteria, the 3.5 wt% copolymer solution, *i.e.*, $\phi_o = 0$, did not show temperature-induced gelation across the temperature range examined, whilst the $\phi_o = 0.3$ and 0.5 samples had T_{gel} of *ca.* 50°C [Figure 6.1(g)]. At 50°C, the G' values for the 3.5 and 10 wt% samples ($\phi_o = 0.3$) were effectively independent of the frequency, indicating that the emulsions have gelled. More importantly, the emulsion containing 0.1 wt% copolymer showed no signs of gelation across the temperature range studied [Figure 6.1(h)]. Heating/cooling cycles showed that the rheological properties of the emulsions were not significantly affected by temperature-induced gelation.

The gelation mechanism postulated is similar to bridging flocculation observed in colloidal systems containing high molecular mass polymers. The surface of the emulsion droplets are extensively covered by adsorbed copolymer. The steric interaction which keeps the oil droplets from flocculating becomes less significant as temperature increases, due to the reduction in the adsorbed layer thickness [Figure 6.1(i)]. The copolymer chains at one droplet surface may attach to other chains which are adsorbed on a second droplet. Bridging flocculation occurs due to the attractive nature of inter-chain interactions at $T >$ LCST [Figure 6.1(j)]. Gelation results when a critical concentration of oil droplets is exceeded which allows formation

of the network [Figure 6.1(g)], or a high enough copolymer concentration is present which spans the entire system [Figure 6.1(h)]. The oil droplets act as anchoring sites for the copolymer and increase the number density of network links, *i.e.*, the droplets have the same qualitative effect as a substantial increase in the copolymer concentration. Only copolymer adsorbed at the droplet surface need be involved in formation of the connected droplet network and gelation. Entanglement meshes of copolymer chains existing throughout the aqueous phase are considered to play a minimal role for emulsion gelation. The network contains two different types of cross-link points, namely, micelle-like aggregates of the copolymer chains in the continuous phase and oil droplets with copolymer adsorbed at the surface with one of their terminal groups, the other terminal group extending in the solution. Although the number of junctions decreases with increasing temperature, larger ones appear in the form of particulate phase, which is NIPAM-rich, and are connected through the PEGMA-rich coils [Figure 6.1(c)]. Increasing the temperature increases the number of polymer chains and the amount of time that junctions remain in hydrophobic clusters. This results in ~~a stronger gel to be formed~~ the formation of a stronger gel, *i.e.*, higher G', and a greater shear stress is required to disrupt the junctions.

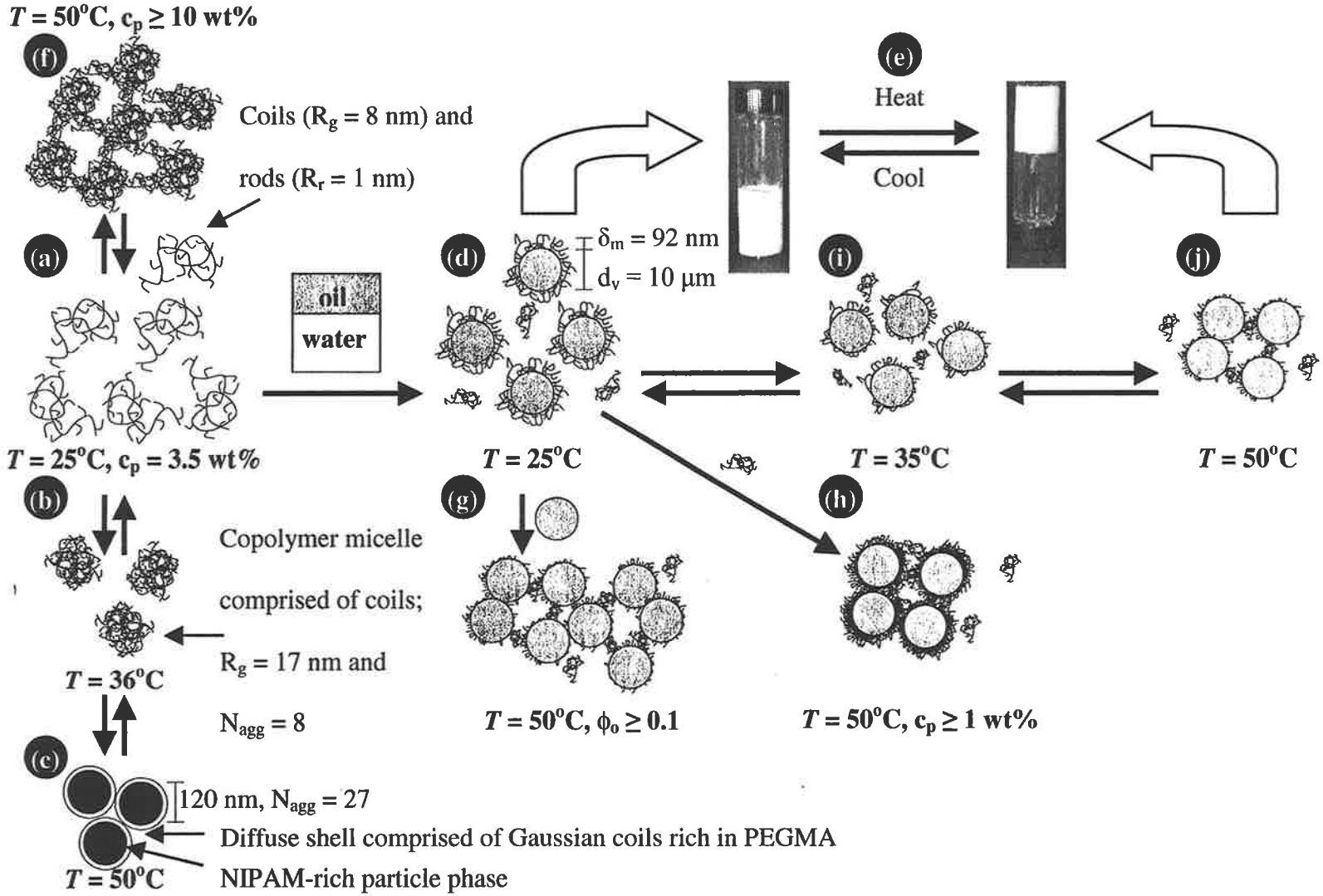

Figure 6.1: Phase behaviour of the temperature-responsive copolymers and emulsions investigated in this work at temperatures between 25 and 50°C. See text for explanation.

6.2 Applications

The temperature-induced association behaviour of poly(NIPAM-*co*-PEGMA) copolymers is of great interest for various reasons. Some of these are as follow. This thermothickening behaviour may provide the solution to problems found in industrial applications where water-based emulsions are subjected to heating during applications, *e.g.*, cooking processes in food industry. The copolymer may be of use in the control of the rheology of drilling fluids, *e.g.*, fluid to gel transition, in subterranean formation.[17] Also, it has potential applications in the medical field, *e.g.*, drug delivery[40] and skin care. Recently, Scherlund *et al.*[153] incorporated PEO-PPO-PEO block copolymers in their local anaesthetic formulations for use in the periodontal cavity. The formulations, containing an oil phase, the block copolymer and a surfactant (which stabilises the oil droplets), remained as a low viscosity fluid at room temperature, but turned to a rigid elastic gel at body temperature. The temperature sensitive behaviour of the copolymer may be used in separation of substances from aqueous solutions. As the chains start to collapse when the temperature approaches the LCST, the polymer may adsorb substances, *e*.g., non-ionic surfactants, through hydrophobic interactions. The polymer with the substance may then be recovered by desorption on cooling below the LCST. This technology may provide an alternative to traditional methods of waste water treatment. The thermothickening behaviour requires reversibility; thus, allowing the property to be turned on or off when required. From a theoretical point of view, the hydrophobic association of the copolymer chains at temperatures greater than the LCST and the formation of gels at concentrations higher than c_{gel}, may provide a model for the formation of micelles and be used to verify the percolation theory[154] which is based on associative systems.

The reversible gelation process may be of technological importance in pharmaceutical and agricultural controlled release formulations. It is possible the emulsions might provide water insoluble coatings at one temperature, thereby preventing drug (in which it is encapsulated in) diffusion and release. Altering the temperature will lead to the emulsions breaking up or becoming water soluble, resulting in drug delivery. This is possible when the emulsions are heated for long periods of time, resulting in extensive droplet coalescence and phase separation. In addition, this reversible behaviour would allow emulsions to be broken or formed at will for ease of cleanup, phase separation and reuse.[41] In the case of thickeners, thermally-induced response will allow emulsions to be in a liquid state at one temperature but of higher viscosity (gelation) at other temperatures. More importantly, gelation will result in emulsions to be stable over long periods, since droplet movement is restricted by the viscous continuous phase, *i.e.*, flocculation and creaming/sedimentation of droplets can be reduced. Removal of the heat will result in the gel becoming a fluid emulsion again. This might be beneficial to the emulsion industry, where the transported emulsion may remain unaltered, *i.e.*, remain stable, when it is converted to a gel. In addition, it will be much easier to handle the gelled emulsion compared to its liquid state. In all of these applications, there is a need for the emulsions to behave in a reversible fashion, rather than permanent.

6.3 Future Work

The goal of this work was to synthesise copolymers which could stabilise emulsions at room temperature, whilst achieving gelation at high temperatures. Poly(NIPAM-*co*-PEGMA) copolymers was found to meet the criteria. In the presence of electrolyte, AMPS and PMMA show responsive behaviour, *e.g.*, increase in the radius of gyration due to ionisation of the polymer chain resulting in repulsive interactions, which extends the conformation of the polymer backbone.[22,155] It would be interesting, therefore, to determine how the responsive behaviour of these systems compares to that of poly(NIPAM-*co*-PEGMA) copolymer.

The monomer reactivity ratios were determined from compositions of the copolymers formed at low conversions, in a series of copolymerisations performed using known initial comonomer compositions. By performing the reaction via the NIPAM-feed method (since this is the method used for the preparation of P2) a more accurate determination of the monomer reactivity ratios can be obtained. Knowing the monomer reactivity ratios will allow tailoring of the microstructure for desired physical and chemical characteristics. Investigation of the change in composition with reaction time for the various synthesis methods, *e.g.*, dual-feed and NIPAM-feed, would indicate the efficiency, *i.e.*, yield of product with reaction time, of the synthesis routes employed. More importantly, it allows a more accurate copolymerisation composition simulation to be performed.

Analysis of the SANS data revealed that the copolymer chains of poly(NIPAM-*co*-PEGMA) contained three structural features at temperatures between 25 and 50°C, namely, rods, coils and particles. In the case of the emulsions, information regarding the structural features of the oil and water interface can be obtained when the dispersed phase is contrast matched and the scattering pattern of the sample is compared to that of the copolymer solution. The proportion of

adsorbed copolymer may be obtained by comparing the scattering of the copolymer solution to that of the supernatant of the emulsion.

Interactions between polymers and surfactants have been extensively studied.[127,156,157] The interaction between surfactants and poly(NIPAM-*co*-PEGMA) copolymers, especially at interfaces, could be an interesting field of study. The temperature dependence of the overall hydrophobicity for poly(NIPAM-*co*-PEGMA) copolymers may provide the opportunity to vary the segment-segment interaction strengths without changing the composition. This could have important implications for interparticle interactions, in that, when incorporated in emulsions, the polymer and surfactant mixture will impart steric and electrostatic interactions, enhancing the stability of the emulsion.

REFERENCES

1. Young, R. J. and Lovell, P. A. *Introduction to Polymers*, 2nd Ed. Chapman and Hall: London, New York, 1991.
2. Campbell, I. M. *Introduction to Synthetic Polymers*, 2nd Ed. Oxford University Press: New York, 2000.
3. Hasan, E.; Jankova, K.; Samichkov, V.; Ivanov, Y.; Tsvetanov, Ch. B. *Macromol. Symp.* **2002**, 177, 125.
4. Hunter, R. J. *Foundations of Colloids Science*, Vol. 1, Oxford University Press: New York, 1989.
5. Cowie, J. M. G. *Polymers*: *Chemistry and Physics of Modern Materials* 2nd Ed. Blackie: Glasgow, 1997.
6. Mayo, F. R. and Lewis, F. M. *J. Am. Chem. Soc.* **1944**, 66, 1594.
7. Goodwin, J. M. and Hughes, R. W. *Rheology for Chemist*: *An Introduction*, Royal Society of Chemistry: Cambridge, 1999.
8. Fleer, G. J.; Cohen Stuart, M. A.; Scheutjens, J. M. H. M.; Cosgrove, T.; Vincent, B. *Polymers at Interfaces*, Chapman and Hall: London, 1993.
9. Schild, H. G. and Tirrell, D. A. *J. Phys. Chem.* **1990**, 94, 4352.
10. Snowden, M. J.; Murray, M. J.; Chowdry, B. Z. *Chem. Ind.* **1996**, 14, 531.
11. Napper, D. H. *Polymeric Stabilization of Colloidal Dispersions*, Academic Press: New York, 1983.
12. Wagner, P.; Brochard-Wyart, F.; Hervet, H.; de Gennes, P.-G. *Coll. Polym. Sci.* **1993**, 271, 621.

13. Zhu, P. W. and Napper, D. H. *J. Colloid Interface Sci.* **1996**, 177, 343.

14. Rubinstein, M. and Semenov, A. N. *Macromolecules* **1998**, 31, 1386.

15. Durand, A.; Herve, M.; Hourdet, D. in *Stimuli-responsive Water Soluble and Amphiphilic Polymers*, ACS Symposium Series, 780, McCormick, C. L. Ed.; American Chemical Society: Washington D. C., 2000.

16. L'Alloret, F.; Maroy, P.; Hourdet, D.; Audebert, R. *Rev. Inst. Fr. Pet.* **1997**, 52, 117.

17. Durand, A. and Hourdet, D. *Polymer*, **1999**, 40, 4941.

18. Green, M. S. and Tobolsky, A. V. *J. Chem. Phys.* **1946**, 14, 80.

19. Tanaka, F. and Edwards, S. F. *Macromolecules* **1992**, 25, 1516.

20. Tanaka, F. and Ishida, M. *Macromolecules* **1996**, 29, 7571.

21. Annable, T.; Buscall, R.; Ettelaie, R. *Coll. and Surf. A: Physicochem. Eng. Aspects* **1996**, 112, 97.

22. Lowe, A. W. and McCormick, C. L. in *Stimuli-responsive Water Soluble and Amphiphilic Polymers*, ACS Symposium Series, 780, McCormick, C. L. Ed.; American Chemical Society: Washington D. C., 2000.

23. Koh, A. Y. C. and Saunders, B. *Chem. Commun.* **2000**, 24, 2461.

24. **It's OK to be left on the shelf**, *New Scientist* **2000**, 168, 2266, 20.

25. Koh, A. Y. C.; Prestidge, C.; Ametov, I.; Saunders, B. R. *Phys. Chem. Chem. Phys.* **2002**, 4, 96.

26. Bokias, G.; Hourdet, D.; Iliopoulos, I. *Macromolecules* **2000**, 33, 2929.

27. Hourdet, D.; L'Alloret, F.; Durand, A.; Lafuma, F.; Audebert, R.; Cotton, J.-P. *Macromolecules* **1998**, 31, 5323.

28. Hourdet, D.; L'Alloret, F.; Audebert, R. *Polymer* **1994**, 35, 2624.

29. **New oil-in-water Emulsions**, *Adv. Mater.* **2001**, 13, 858.

30. Virtanen, J.; Baron, C.; Tenhu, H. *Macromolecules* **2000**, 33, 336.

31. Virtanen, J. and Tenhu, H. *Macromolecules* **2000**, 33, 5970.

32. Virtanen, J.; Lemmetyinen, H.; Tenhu, H. *Polymer* **2001**, 42, 9487.

33. Berlinova, I. V.; Dimitrov, I. V.; Vladimirov, N. G.; Samichkov, V.; Ivanov, Ya. *Polymer* **2001**, 42, 5963.

34. L'Alloret, F.; Hourdet, D.; Audebert, R. *Coll. Polym. Sci.* **1995**, 273, 1163.

35. Mi, K. Y.; Yong, K. S.; Chong, S. C.; Young, M. L. *Polymer* **1997**, 38, 2759.

36. Mi, K. Y.; Yong, K. S.; Young, M. L.; Chong, S. C. *Polymer* **1998**, 39, 3703.

37. Chang, K. W.; and You, H. B. *Polymer* **1998**, 39, 2809.

38. Qiu, X. and Wu, C. *Polymer* **1998**, 39, 1749.

39. Bokias, G.; Staikos, G.; Iliopoulos, I. *Polymer* **2000**, 41, 7399.

40. Chen, G. and Hoffman, A. S. *Nature* **1995**, 373, 49.

41. Porcar, I.; Perrin, P. Tribet, C. *Langmuir* **2001**, 17, 6905.

42. Binks, B. P. in *Modern Aspects of Emulsion Science*, Binks, B. P. Ed.; RSC: Cambridge, 1998.

43. Tadros, Th. F. *Adv. Colloid Interface Sci.* **1993**, 46, 1.

44. Aveyard, R. and Vincent, B. *Progr. Surface Sci.* **1977**, 8, 59.

45. Walstra, P. in *Encyclopedia of Emulsion Technology, Vol. 1, Basic Theory*, Becher, P. Ed.; Marcel Dekker: New York, 1983.

46. Shaw, D. J. *Introduction to Colloid and Surfaces Chemistry*, 4th Ed. Ellis Horwood/PTR Prentice Hall: New Jersey, 1993.

47. Stein, H. N. *The Preparation of Dispersions in Liquids*, *Surfactant Science Series*, *Vol. 58*, Marcel Dekker: New York, 1996.

48. Becher, P. and Schick, M. J. in *Non Ionic Surfactants*: *Physical Chemistry*, *Surfactant Science Series*, *Vol. 23*, Schick, M. J. Ed.; Marcel Dekker: New York, 1987.

49. Davies, J. T. and Rideal, E. K. *Interfacial Phenomena*, Academic Press: New York, 1961.

50. Perrin, P. and Lafuma, F. *J. Colloid Interface Sci.* **1998**, 197, 317.

51. Perrin, P.; Monfreux, N.; Lafuma F. *Coll. Polym. Sci.* **1999**, 277, 89.

52. Groeneweg, F.; van Dieren, F.; Agterof, W. G. M. *Coll. and Surf. A*: *Physicochem. Eng. Aspects* **1994**, 91, 207.

53. Becher, P. *Emulsions*: *Theory and Practice*, American Chemical Society Monograph Series, Reinhold Publishing Corporation: New York, 1957.

54. Salager, J. L. in *Encyclopedia of Emulsion Technology*, *Vol. 3*, *Basic Theory, Measurement, Applications*, Becher, P. Ed.; Marcel Dekker: New York, 1983.

55. Shinoda, K. and Kunieda, H. in *Encyclopedia of Emulsion Technology*, *Vol. 1*, *Basic Theory*, Becher, P. Ed.; Marcel Dekker: New York, 1983.

56. Vaessen, G. E. J.; Visschers, M.; Stein, H. N. *Langmuir* **1996**, 12, 875.

57. Groeneweg, F.; Agterof, W. G. M.; Jaeger, P.; Janssen, J. J. M.; Wieringa, J. A.; Klahn, J. K. *Trans IchemE* **1998**, 76, 55.

58. Brooks, B. W. and Richmond, H. N. *Chem. Eng. Sci.* **1994**, 49, 1053.

59. Brooks, B. W. and Richmond, H. N. *Chem. Eng. Sci.* **1994**, 49, 1075.

60. Brooks, B. W. and Richmond, H. N. *Chem. Eng. Sci.* **1994**, 49, 1843.

61. Umbanhowar, P. B.; Prasad, V.; Weitz, D. A. *Langmuir* **2000**, 16, 347.

62. Bibette, J. *J. Colloid Interface Sci.* **1991**, 147, 474.

63. Bibette, J.; Calderon, F. L.; Poulin, P. *Rep. Prog. Phys.* **1999**, 62, 969.

64. Mabille, C.; Schmitt, V.; Gorria, P.; Calderon, F. L.; Faye, V.; Deminiere, B. Bibette, J. *Langmuir* **2000**, 16, 422.

65. Tadros, T. F. and Vincent, B. in *Encyclopedia of Emulsion Technology, Vol. 1, Basic Theory*, Becher, P. Ed.; Marcel Dekker: New York, 1983.

66. Smet, Y. De.; Deriemaeker, L.; Parloo, E.; Finsy, R. *Langmuir* **1999**, 15, 2327.

67. Weers, J. G. in *Modern Aspects of Emulsion Science*, Binks, B. P. Ed.; RSC: Cambridge, 1998.

68. Danov, K. D.; Petsev, D. N.; Denkov, N. D.; Borwankar, R. *J. Chem. Phys.* **1993**, 99, 7179.

69. Mathur, A. M.; Drescher, B.; Scranton, A. B.; Klier, J. *Nature* **1998**, 392, 367.

70. Philip, J.; Poirier, J. E.; Bibette, J.; Leal-Calderon, F. *Langmuir* **2001**, 17, 3545.

71. Winnik, F. M. *Macromolecules* **1990**, 23, 233.

72. Shibayama, M. and Tanaka, T. *J. Chem. Phys.* **1995**, 102, 9392.

73. Williams, D. H. and Fleming, I. *Spectroscopic methods in Organic Chemistry*, 5th Ed. McGraw-Hill: London, New York, 1995.

74. Everett, D. H. *Basic Principles of Colloid Science*, Royal Society of Chemistry: London, 1994.

75. Atkins, P. W. *Physical Chemistry*, 4th Ed. Oxford University Press: Oxford, 1990.

76. Long, J. A.; Osmond, D. W. J.; Vincent, B. *J. Colloid Interface Sci.* **1973**, 42, 545.

77. Everett, D. H. *Basic Principles of Colloid Science*, RSC: Cambridge, 1998.

78. Zeng, F.; Tong, Z.; Feng, H. *Polymers* **1997**, 38, 5539.

79. Drescher, B.; Scranton, A. B.; Klier, J. *Polymer* **2001**, 42, 49.

80. Qiu, X. and Wu, C. *Macromolecules* **1997**, 30, 7921.

81. Ganachaud, F.; Monteiro, M. J.; Gilbert, R. G.; Dourges, M.-A.; Thang, S. H.; Rizzardo, E. *Macromolecules* **2000**, 33, 6738.

82. Wu, X. Y.; Pelton, R. H.; Tam, K. C.; Woods, D. R.; Hamielec, A. E. *J. Polym. Sci.: Part A* **1993** 31, 957.

83. Xue, W.; Champ, S.; Huglin, M. B. *Polymer* **2000**, 41, 7575.

84. Idziak, I.; Avoce, D.; Lessard, D.; Gravel, D.; Zhu, X. X. *Macromolecules* **1999**, 32, 1260.

85. Tudos, F.; Kelen, T.; Foldes-Berezsnich, T.; Turcsanyi, B. *J. Macromol. Sci. Chem.* **1975**, 10, 1513.

86. Buback, M.; Feldermann, A.; Barner-Kowollik, C. *Macromolecules* **2001**, 34, 5439.

87. Ito, H.; Dalby, C.; Pomerantz, A.; Sherwood, M.; Sato, R.; Sooriyakumaran, R.; Guy, K.; Breyta, G. *Macromolecules* **2000**, 33, 5080.

88. Skeist, I. *J. Am. Chem. Soc.* **1946**, 68, 1781.

89. Meyer, V. E. and Lowry, G. G. *J. Polym. Sci.*: Part A **1965**, A3, 2843.

90. Lide, D. R. *CRC Handbook of Chemistry and Physics*, 76th Ed. CRC Press: Boca Raton, 1995.

91. Larsson, A.; Kuckling, D.; Schönhoff, M. *Coll. and Surf. A*: *Physicochem. Eng. Aspects* **2001**, 190, 185.

92. King, S. M. in *Experimental Methods in Polymer Characterisation, Vol. 1*, Pethrick, R. A. and Dawkins J. V. Eds.; Wiley: Chichester, 1999.

93. Shibayama, M.; Tanaka, T.; Han, C. C. *J. Chem. Phys.* **1992**, 97, 6842.

94. Auvray, L. and Cotton, J. P. *Macromolecules* **1987**, 20, 202.

95. Francois, J.; Maitre, S.; Rawiso, M.; Sarazin, D.; Beinert, G.; Isel, F. *Coll. and Surf. A: Physicochem. Eng. Aspects* **1996**, 112, 251.

96. Mao, G.; Sukumaran, S.; Beaucage, G.; Saboungi, M.-L.; Thiyagarajan, P. *Macromolecules* **2001**, 34, 552.

97. Gladman, J. M.; Crowley, T. L.; Schofield, J. D.; Eaglesham, A. *Physica Scripta.* **1995**, T57, 146.

98. Washington, C.; King, S. M.; Heenan, R. K. *J. Phys. Chem.* **1996**, 100, 7603.

99. Washington, C. and King, S. M. *Langmuir* **1997**, 13, 4545.

100. Barnes, T. J. and Prestidge, C. A. *Langmuir* **2000**, 16, 4116.

101. Staples, E.; Penfold, J.; Tucker, I. *J. Phys. Chem. B* **2000**, 104, 606.

102. Hatto, N.; Cosgrove, T.; Snowden, M. J. *Polymer* **2000**, 41, 7133.

103. Higgins, J. S. and Benoit, H. C. *Polymers and Neutron Scattering*, Clarendon Press: Oxford, 1996.

104. Heenan, R. K.; Penfold, J.; King, S. M. *J. Appl. Cryst.* **1997**, 30, 1140.

105. King, S. M. *Using COLETTE*, ISIS Facility, Rutherford Appleton Laboratory, Chilton, England, 2000.

106. Tirell, M. in *Interactions of Surfactants with Polymers and Proteins*, Goddard, E. D. and Ananthapadmanabhan, K. P. Eds.; CRC Press: Florida, 1993.

107. Koh, A. Y. C.; Heenan, R. K.; Saunders, B. R. *Phys. Chem. Chem. Phys.* **2003**, 5, 2417.

108. Seelenmeyer, S.; Deike, I.; Rosenfeldt, S.; Norhausen, Ch.; Dingenouts, N.; Ballauff, M.; Narayanan, T.; Lindner, P. *J. Chem. Phys.* **2001**, 114, 10471.

109. Su, T. J.; Lu, J. R.; Cui, Z. F.; Thomas, R. K.; Heenan, R. K. *Langmuir* **1998**, 14, 5517.

110. Heenan, R. *The FISH fitting program*, ISIS Facility, Rutherford Appleton Laboratory, Chilton, England.

111. Choi, S.; Briber, R. M.; Bauer, B. J.; Topp, A.; Gauthier, M.; Tichagwa, L. *Macromolecules* **1999**, 32, 7879.

112. Mears, S. J.; Deng, Y.; Cosgrove, T.; Pelton, R. *Langmuir* **1997**, 13, 1901.

113. Koh, A.; Gillies, G.; Gore, J.; Saunders, B. R. *J. Colloid Interface Sci.* **2000**, 227, 390.

114. Binks, B. P.; Cho, W.-G.; Fletcher, P. D. I.; Petsev, D. N. *Langmuir*, **2000**, 16, 1025.

115. Chanamai, R. and McClements, D. J. *J. Colloid Interface Sci.* **2000**, 225, 214.

116. Dickinson, E. and Ritzoulis, C. *J. Colloid Interface Sci.* **2000**, 224, 148.

117. Avranas, A.; Stalidis, G.; Ritzoulis, G. *Coll. Polym. Sci.* **1988**, 266, 937.

118. Stachurski, J. and Michalek, M. *J. Colloid Interface Sci.* **1996**, 184, 433.

119. Koenig, A.; Hébraud, P.; Perrin, P. *Langmuir* **2002**, 18, 6458.

120. Bibette, J.; Mason, T. G.; Gang, H.; Weitz, D. A. *Phys. Rev. Lett.* **1992**, 69, 981.

121. Solans, C.; Pons, R.; Kunieda, H. in *Modern Aspects of Emulsion Science*, Binks, B. P. Ed.; RSC: Cambridge, 1998.

122. Cardenas-Valera, A. E. and Bailey, A. I. *Coll. and Surf. A: Physicochem. Eng. Aspects* **1995**, 97, 1.

123. Washington, C.; King, S. M.; Attwood, D.; Booth, C.; Mai, S.-M.; Yang, Y.-W.; Cosgrove, T. *Macromolecules* **2000**, 33, 1289.

124. Kikuchi, A. and Nose T. *Macromolecules* **1996**, 29, 6770.

125. Richardson, R. M.; Pelton, R.; Cosgrove, T.; Zhang, J. *Macromolecules* **2000**, 33, 6269.

126. Shriver, D. F.; Atkins, P. W.; Langford, C. H. *Inorganic Chemistry* 2nd Ed. Oxford University Press: Oxford, 1994.

127. Zhu, P. W. and Napper, D. H. *J. Colloid Interface Sci.* **1994**, 164, 489.

128. Barnes, H. A.; Hutton, J. F.; Walter, K. *An Introduction to Rheology*, Elsevier: Amsterdam; New York, 1989.

129. Senff, H. and Richtering, W. *J. Chem. Phys.* **1999**, 111, 1705.

130. Dickinson, E. in *Modern Aspects of Emulsion Science*, Binks, B. P. Ed.; RSC: Cambridge, 1998.

131. English, R. J.; Gulati, H. S.; Jenkins, R. D.; Khan, S. A. *J. Rheol.* **1997**, 41, 427.

132. Kwon, K.-W.; Park, M. J.; Bae, Y. H.; Kim, H. D.; Char, K. *Polymer* **2002**, 43, 3353.

133. Desbrières, J.; Hirrien, M.; Ross-Murphy, S. B. *Polymer* **2000**, 41, 2451.

134. Sarkar, N. *J. Appl. Polym. Sci.* **1979**, 24, 1073.

135. Huldén, M. *Coll. and Surf. A: Physicochem. Eng. Aspects* **1994**, 82, 263.

136. Huldén, M. *Coll. and Surf. A: Physicochem. Eng. Aspects* **1994**, 88, 207.

137. Quintana, J. R.; Hernáez, E.; Katime, I. *Polymer* **2002**, 43, 3217.

138. Luckham P. F. and Ukeje, M. A. *J. Colloid Interface Sci.* **1999**, 220, 337.

139. Barnes, H. A. *A Handbook of Elementary Rheology*, University of Wales Institute of Non-Newtonian Fluid Mechanics: Aberystwyth, 2000.

140. Mortimer, S.; Ryan, A. J.; Stanford, J. L. *Macromolecules* **2001**, 34, 2973.

141. Li, L.; Thangamathesvaran, P. M.; Yue, C. Y.; Tam, K. C.; Hu, X.; Lam, Y. C. *Langmuir* **2001**, 17, 8062.

142. Winter, H. H. and Chambon, F. *J. Rheol.* **1986**, 30, 367.

143. Chambon, F. and Winter, H. H. *Polym. Bull.* **1985**, 13, 499.

144. Manoj, P.; Watson, A. D.; Hibberd, D. J.; Fillery-Travis, A. J.; Robins, M. M. *J. Colloid Interface Sci.* **1998**, 207, 294.

145. Hirata, Y. and Ozaki, T. *Mater. Lett.* **1992**, 15, 31.

146. Hirata, Y. and Kawabata, M. *Mater. Lett.* **1993**, 16, 175.

147. Shay, J. S.; Raghavan, S. R.; Khan, S. A. *J. Rheol.* **2001**, 45, 913.

148. Tung, C.-Y. M. and Dynes, P. J. *J. Polym. Sci.* **1982**, 27, 569.

149. Tanodekaew, S.; Godward, J.; Heatley, F.; Booth, C. *Macromol. Chem. Phys.* **1997**, 198, 3385.

150. Thurston, G. B. and Davis, S. S. *J. Colloid Interface Sci.* **1979**, 69, 199.

151. Jenkins, R. D.; Durali, M.; Silebi, C. A.; El-Aasser, M. S. *J. Colloid Interface Sci.* **1992**, 154, 502.

152. Princen, H. M.; Aronson, M. P.; Moser, J. C. *J. Colloid Interface Sci.* **1980**, 75, 246.

153. Scherlund, M.; Malmsten, M.; Brodin, A. *Int. J. Pharm.* **1998**, 173, 103.

154. Stauffer, D.; Coniglio, A.; Adam, M. *Adv. Polym. Sci.* **1982**, 44, 105.

155. Lu, T.; Vesterinen, E.; Tenhu, H. *Polymer* **1998**, 39, 641.

156. Zhu, P. W. and Napper, D. H. *Langmuir* **1996**, 12, 5992.

157. Goddard, E. D. in *Interactions of Surfactants with Polymers and Proteins*, Goddard, E. D. and Ananthapadmanabhan, K. P. Eds.; CRC Press: Florida, 1993.

158. Deryagin, B.V. and Landau, L. Acta Phys. Chim. URSS 1941, 14, 633.

159. Verwey, E. J.W. and Overbeek, J. Th. G. Theory of the Stability of Lyophobic Colloids, Elsevier; 1948

LIST OF PUBLICATIONS

(i) **Thermally Induced Gelation of an Oil-in-water Emulsion Stabilised by a Graft Copolymer**, Koh, A. Y. C. and Saunders, B. *Chem. Commun.* **2000**, 24, 2461.

(ii) **It's OK to be left on the shelf**, *New Scientist* **2000**, 168, 2266, 20.

(iii) **New oil-in-water Emulsions**, *Adv. Mater.* **2001**, 13, 858.

(iv) **Temperature-induced Gelation of Emulsions Stabilised by Responsive Copolymers: A Rheological Study**, Koh, A. Y. C.; Prestidge, C.; Ametov, I.; Saunders, B. R. *Phys. Chem. Chem. Phys.* **2002**, 4, 96.

(v) **A Study of Temperature-induced Aggregation of Responsive Comb Copolymers in Aqueous Solution**, Koh, A. Y. C.; Heenan, R. K.; Saunders, B. R. *Phys. Chem. Chem. Phys.* **2003**, 5, 2417.

ChemComm

Thermally induced gelation of an oil-in-water emulsion stabilised by a graft copolymer

Andrew Y. C. Koh and Brian R. Saunders*

Colloid and Polymer Chemistry Research Group, Department of Chemistry, University of Adelaide, Adelaide, SA, 5005, Australia. E-mail: brian.saunders@adelaide.edu.au

Received (in Cambridge, UK) 16th October 2000, Accepted 7th November 2000
First published as an Advance Article on the web

Oil-in-water (O/W) emulsions exhibiting reversible thermally induced gelation have been prepared using a graft (comb) copolymer containing poly(*N*-isopropylacrylamide) [poly(NIPAM)] as the backbone and poly(ethylene glycol) methacrylate as the side chains.

Emulsions are dispersions of one immiscible liquid in another. They occupy a significant position in colloid science and occur as products (or during processing stages) in a number of areas including the paint, food and agrochemical industries.[1] The majority of emulsions studied or produced commercially are prepared using short-chain surfactants. The properties of these systems are reasonably well understood.[1,2] In recent years copolymers have been employed as macrosurfactants to prepare emulsions.[3,4] One of the advantages of using macrosurfactants for emulsion preparation is the large degree of architectural control that can be exerted in order to explore and optimise copolymer structure—emulsion property relationships. Water-soluble copolymers can be prepared which exhibit solvent–polymer interactions that are thermally responsive. This compositional control thus allows fine control over the lower critical solution temperature of the copolymer.[5] The preparation of emulsions using thermally responsive copolymers is a new area of research and is the subject of this communication.

The objective of the present study was to prepare emulsions with stabilities which are responsive to environmental conditions (*e.g.* temperature). We reasoned that the use of copolymers based on poly(*N*-isopropylacrylamide) [poly(NIPAM)] would provide gross conformational changes at the oil-in-water (O/W) interface at temperatures lower than the cloud point of short-chain ethylene-oxide based surfactants. Perrin *et al.*[3,6] have used hydrophobically modified poly(sodium acrylate) copolymers in order to prepare emulsions the stability of which are sensitive to pH and ionic strength. Mathur *et al.*[7] employed pH sensitive poly(acrylic acid)-g-poly(ethyleneoxide) copolymers in order to break emulsions. Our interest in the use of poly(NIPAM) copolymers to prepare emulsions follows from our earlier work involving swellable poly(NIPAM) microgel particles,[8] linear poly(NIPAM) chains adsorbed at latex particle interfaces[9] and depletion flocculation of emulsions.[10,11] The use of copolymers based on poly(NIPAM) to prepare emulsions was expected to provide large and reversible changes in emulsion properties (*e.g.* viscosity) as the temperature approaches the lower critical solution temperature (LCST). The results presented below show that this is indeed the case.

The copolymer comprised of poly(NIPAM) and poly(ethylene glycol methacrylate) (PEGMa); the latter having a number average molecular weight of 360. AIBN and *tert*-butyl alcohol were used, as the initiator and solvent, respectively, during the free radical copolymerisation stage.[12] Proton NMR data revealed that there was on average one PEGMa group per six NIPAM units in the copolymer. Fig. 1 shows how the turbidity and viscosity vary with temperature for poly(NIPAM–PEGMa) in water. The LCST of the copolymer is taken as *ca.* 34 °C from the turbidity data. This is *ca.* 2 °C higher than that of poly(NIPAM) homopolymer, which is attributed to the hydrophilic nature of the PEGMa in the copolymer.[13] The O/W

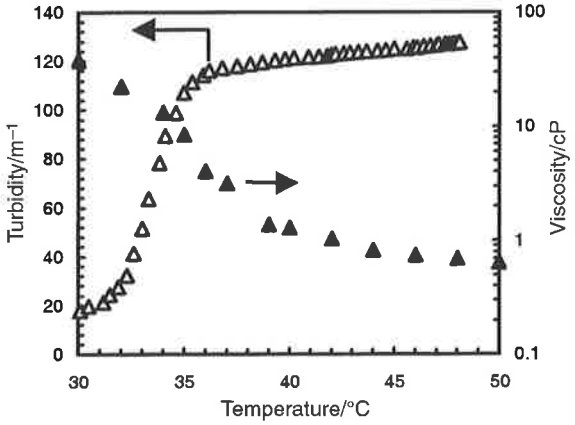

Fig. 1 Variation of the turbidity (Δ) and viscosity (▲) of poly(NIPAM–MPEGMa) solution as a function of temperature. The concentration of copolymer used was 2.5 wt%.

emulsions were prepared by first dissolving the copolymer in water (5 wt%). 1-bromohexadecane was then added to the copolymer solution, before the mixture was sheared using a Silverson SL2T laboratory mixer operating at *ca.* 7500 rpm. A control emulsion was prepared using the short-chain surfactant $Me(CH_2)_8(OCH_2CH_2)_6OH$, ($C_9E_6$) for comparison.

Fig. 2 shows the variation of viscosity with temperature for the emulsions prepared using poly(NIPAM–PEGMa) and C_9E_6. The viscosity data were measured using an Ostwald capillary viscometer. The viscosity for the emulsion prepared using poly(NIPAM–PEGMa) decreases with increasing temperature and reaches a minimum at 44 °C. A dramatic increase in viscosity occurs above 48 °C. The viscosity increased to such an extent that gelation of the emulsion occurred (see Fig. 3). As

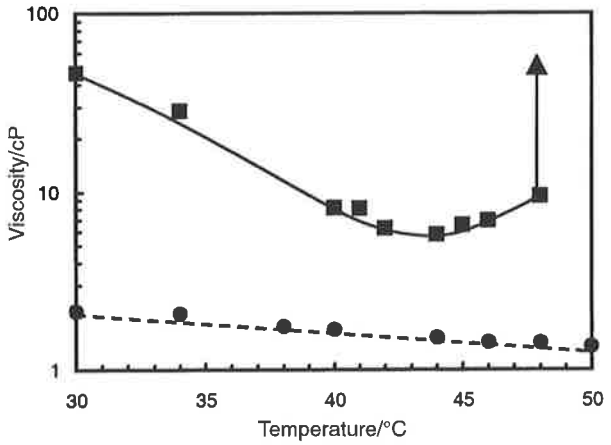

Fig. 2. Effect of temperature on the viscosity of emulsions prepared using poly(NIPAM–MPEGMa) (■) and C_9E_6 (●). The volume average diameters were 9.6 and 4.9 μm, respectively. The volume fraction of the dispersed phase was 0.30. The concentration of copolymer or C_9E_6 present was 2.5 wt% with respect to the total emulsion.

DOI: 10.1039/b008334h

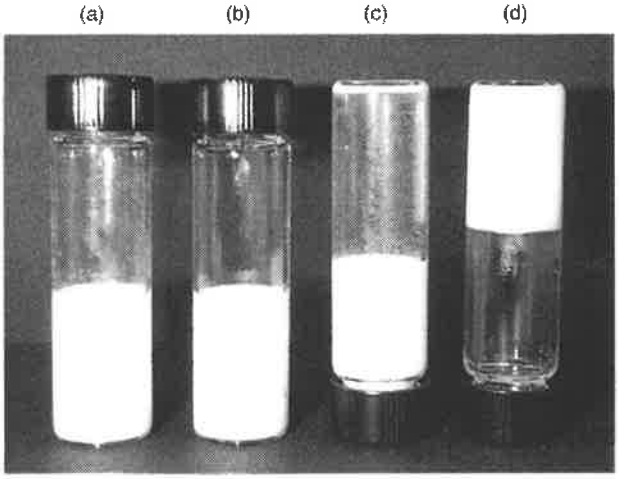

Fig. 3 Emulsions prepared using C_9E_6 (a) at RT and (c) at 50 °C and poly(NIPAM–MPEGMa) (b) at RT and (d) at 50 °C. Note that tubes (c) and (d) have been inverted.

expected, the emulsion prepared using C_9E_6 exhibited a slight decrease in viscosity over the whole experimental temperature range. It should be noted that the rheological behaviour observed for the emulsion prepared using the copolymer is opposite to what is observed for concentrated poly(NIPAM) microgel dispersions, which form gels at room temperature and flow when the temperature exceeds the LCST. It was found that emulsion gelation could be reversed by agitation at 50 °C or cooling to room temperature in the absence of agitation. The emulsions did not break as a result of gelation reversal, although there was evidence of a slight increase in droplet size. Optical microscopy revealed residual flocs were present in the emulsions after one heating/cooling cycle. The emulsion viscosity measured at 30 °C increased by *ca.* 5% as a result of one heating/cooling cycle.

The data shown here demonstrate that it is possible to reversibly gel our O/W emulsion using temperature variation alone. The mechanism by which this occurs is of interest to both the polymer and emulsion science communities. The fact that the gelation temperature is significantly greater than the LCST of the copolymer in solution suggests that the onset of gelation is not solely due to the collapse of the copolymer in the aqueous phase. The viscosity data for the copolymer (Fig. 1) show a decrease in viscosity with increasing temperature and rules out any contribution from temperature-induced continuous phase thickening (*e.g.* associated with the copolymer chains in solution) to emulsion gelation. The zeta potential for the droplets was measured at *ca.* 5 mV, which indicates that electrostatic stabilisation of the emulsions is not significant. The LCST of poly(NIPAM) chains adsorbed at highly charged surfaces is known to increase to values above that for the solution polymer.[14] However, this effect is not likely to occur in the present system due to the low charge of the droplets.

The stability of the emulsions arises primarily from steric stabilisation afforded by the adsorbed copolymer. The mechanism tentatively suggested for emulsion gelation involves thermally induced flocculation due to collapse of the adsorbed poly(NIPAM–PEGMa) layer at temperatures greater than the solution LCST. The depth of the secondary minimum would increase with increasing temperature (decreasing copolymer layer thickness) leading to stronger flocculation at higher temperatures. At 45 °C the minimum is sufficiently greater than kT to provide strong gelation *via* adhesive droplets. The collapse of the adsorbed layer presumably results in a rigid interface which opposes coalescence of flocculated droplets. It is likely that interpenetration and entanglement of interfacial copolymer chains contributes to the limits of residual flocculation observed upon cooling. Note that this good degree of reversibility for the copolymer stabilised emulsions is distinctly different to the behaviour of emulsions stabilised by short-chain ethylene oxide surfactants (*e.g.* C_9E_6) when heated to above the phase inversion temperature. For the latter emulsion breaking results from heating to the phase inversion temperature in absence of shear.

The work described above has shown that the use of poly(NIPAM–MPEGMa) graft copolymers allows the reversible gelation of O/W emulsions. This could have significant technological importance in the field of emulsion stability as the thermally induced gelation results in reversible transformation of a liquid emulsion into a highly viscous gel within a short period of time upon application of modest heating. Copolymers based on NIPAM can be prepared that have a range of LCST values. These ratios can be carefully controlled *via* copolymer architecture modification during synthesis. This versatility should allow the gelation temperature to be finely tuned to suit specific applications. The mechanism by which gelation occurs will be further investigated using light scattering, rheological and small-angle neutron scattering measurements and the results of these stuides will be published in due course.

We acknowledge the Department of Chemical Engineering for access to the PCS instrument.

Notes and references

1 B. Binks, in *Modern Aspects of Emulsion Science*, ed. B. P. Binks, RSC, Cambridge, 1998.
2 T. F. Tadros and B. Vincent, in *Encylopedia of Emulsion Technology*, ed. P. Becher, Marcel Dekker, New York, 1983.
3 P. Perrin, *Langmuir*, 2000, **16**, 881.
4 A. E. Cárdenas-Valera and A. I. Bailey, *Colloids Surf. A*, 1995, **97**, 1.
5 M. Hahn, E. Görnitz and H. Dautzenberg, *Macromolecules*, 1998, **31**, 5616.
6 P. Perrin, N. Monfreux, A. L. Dufour and F. Lafuma, *Colloid Polym. Sci.*, 1998, **276**, 945.
7 A. M. Mathur, B. Drescher, A. B. Scranton and J. Klier, *Nature*, 1998, **392**, 367.
8 B. R. Saunders and B. Vincent, *Adv. Colloid Interface Sci.*, 1999, **80**, 1.
9 B. R. Saunders, J. M. Saunders, J. Mrkic and E. H. Dunlop, *Phys. Chem. Chem. Phys.*, 1999, **1**, 1562.
10 A. Koh, G. Gillies, J. Gore and B. R. Saunders, *J. Colloid Interf. Sci.*, 2000, **227**, 390.
11 M. Shields and B. R. Saunders, *Colloids Surf. A*, in press.
12 A. Koh and B. R. Saunders, manuscript in preparation.
13 J. Virtanen and H. Tenhu, *Macromolecules*, 2000, **33**, 5970.
14 P. W. Zhu and D. H. Napper, *J. Colloid Interf. Sci.*, 1994, **164**, 489.

PCCP

Temperature-induced gelation of emulsions stabilised by responsive copolymers: A rheological study

Andrew Y. C. Koh,[a] Clive Prestidge,[b] Igor Ametov[b] and Brian R. Saunders*[a]

[a] *Colloid and Polymer Chemistry Research Group, Department of Chemistry, University of Adelaide, SA, 5005, Australia*
[b] *Ian Wark Research Institute, University of South Australia, Mawson Lakes, SA, 5095, Australia*

Received 5th July 2001, Accepted 1st November 2001
First published as an Advance Article on the web 18th December 2001

The steady-state and dynamic rheological properties of 1-bromohexadecane-in-water emulsions stabilised by responsive poly(*N*-isopropylacrylamide)-co-poly(ethyleneglycol methacrylate) (poly(NIPAM-co-PEGMa)) copolymer have been investigated. The data were compared to measurements performed using dilute and concentrated poly(NIPAM-co-PEGMa) copolymer solutions. These solutions exhibit viscosities that decrease and increase, respectively, with increasing temperature. The increase in viscosity for the concentrated solution is attributed to transient network formation. The presence of dispersed oil droplets (volume fraction = 0.30) in the emulsion causes temperature-induced gelation even though the copolymer concentration in the aqueous phase is such that transient network formation due to overlapping copolymer chains throughout the aqueous phase does not occur. Dynamic rheological data confirmed gelation for the emulsions at elevated temperatures. Emulsion gelation is attributed to flocculation between neighbouring droplets. The adhesive droplets form a network that entraps the aqueous phase. The strength of the network increased with increasing temperature. To our knowledge these data represent the first comprehensive rheological investigation of reversible, temperature-induced gelation for an oil-in-water emulsion.

Introduction

Koh and Saunders recently reported that oil-in-water (O/W) emulsions stabilised by responsive copolymers of poly(*N*-isopropylacrylamide)-co-poly(ethyleneglycol methacrylate) (poly(NIPAM-co-PEGMa)) exhibited reversible, temperature-induced gelation.[1] This behaviour is unusual for O/W emulsions since it is more common for these emulsions to phase separate upon heating.[2] The report by Koh and Saunders used capillary viscometry. In the present study we extend the preliminary work and use steady-state and dynamic rheological measurements to investigate the temperature-induced gelation.

The phenomenon of gelation for thermally responsive polymer solutions above the critical overlap concentration has received significant attention in recent years.[3-6] The common structural element for the copolymers is a hydrophilic portion, which can be caused to become hydrophobic by increasing the temperature. One of the earliest reports of this phenomenon was by L'Alloret *et al.*[7] who investigated the temperature dependent viscosity of poly(AMPS-g-PEO) copolymers in the presence of salt (AMPS and PEO are 2-acrylamido-2-methylpropoane sulfonic acid and poly(ethylene oxide), respectively). The viscosity enhancement observed with increasing temperature was attributed to hydrophobic microdomain formation. Related data have been reported in the absence of salt for poly(acrylic acid-co-AMPS)[3] and also poly(acrylic acid-co-AMPS-co-PEO).[4] More recently Durand and Hourdet[5] have shown that the behaviour of the graft copolymer poly(acrylic acid-g-*N*-isopropylacrylamide) can be attributed to poly(NIPAM) microdomains connected through the highly soluble poly(acrylic acid) chains into a physical three-dimensional network.

Transient network theory has been invoked to explain the qualitative features of thermally induced gelation of concentrated responsive copolymer solutions.[4,5] The theory was originally devised by Green and Tobolsky[8] and has been more recently developed by Tanaka *et al.*[9,10] Transient network theory envisages a model network made up of polymer chains with "sticky" end groups. The associative cross-links are hydrophobic clusters (junctions). An effective chain results when both ends of the chain are embedded within a junction that is connected to at least two other junctions. The steady shear viscosity is proportional to the number of elastically effective chains and the mean time the chain ends spend within a junction.

Several workers have reported studies on emulsions that are sensitive to the environmental conditions. Perrin *et al.*[11,12] have investigated emulsions stabilised by amphiphilic copolymers based on poly(acrylic acid). The emulsion stability was found to be strongly dependent on the balance of hydrophilic and hydrophobic moieties within the copolymer as well as the ionic strength. Barnes and Prestidge[13] have shown that the adsorbed layer thickness of PEO–PPO–PEO copolymers at the PDMS emulsion droplet interface is dependent on the extent of droplet cross-linking, *i.e.* the droplet rheology, which is temperature dependent. There has been a report of food emulsions stabilised by proteins, which undergo irreversible gelation upon heating.[14] In addition, Philip *et al.* induced gelation of asphalt-in-water emulsions by addition of NaOH at room temperature.[15] The gel phase for their emulsions exhibited strong volume contraction after formation. We are not aware of any reports of emulsions stabilised by responsive poly(NIPAM) copolymers. Furthermore, the observation of reversible, temperature-induced gelation for O/W emulsions based on these copolymers appears to be a new phenomenon.

 DOI: 10.1039/b105990b

In the present work, the synthesis of a thermally sensitive copolymer, poly(NIPAM-co-PEGMa), and its use in the preparation of thermally responsive emulsions are presented. The rheological properties of the emulsions are systematically investigated using steady-state and dynamic shear measurements as a function of temperature. The data are compared with those obtained for dilute and concentrated poly(NIPAM-co-PEGMa) solutions. The data show significant differences that reveal an important role for the dispersed droplets in emulsion gelation. More importantly, these rheological studies allow gel properties (*e.g.* onset of gelation and gel strength) to be determined and a gelation mechanism in emulsions and concentrated copolymer solutions at elevated temperatures to be proposed.

Experimental

Reagents

N-isopropylacrylamide (NIPAM, Acros Organics, 99%), poly(ethylene glycol methacrylate) (PEGMa, molecular weight = 360, Aldrich) and azobis(isobutyronitrile) (AIBN) were used as received. Reagent grade solvents were used without further purification and water was Millipore Milli-Q quality. 1-Bromohexadecane employed as the oil phase in the preparation of the emulsion was obtained from B.D.H.

Copolymer synthesis

Xue *et al.*[16] have shown that the NIPAM has a strong tendency for homopolymerisation in the presence of other comonomers. The conditions used for the preparation of poly(NIPAM-co-PEGMa) were specifically designed to promote copolymerisation through an excess of PEG macromonomer at the onset of copolymerisation.[17] A representative preparation for poly(NIPAM-co-PEGMa) is as follows. PEGMa (1.73 g) and *tert*-butyl alcohol (37.5 ml) were added to a nitrogen-purged five-necked 250 ml reaction kettle equipped with a burette, Teflon stirrer blade, condenser, thermometer and nitrogen inlet. The stirred monomer solution was allowed to degas for 30 min before the mixture was heated to 80 °C under nitrogen. NIPAM (3.27 g) and AIBN (0.03 g) in *tert*-butyl alcohol (12.5 ml) were added dropwise with stirring over 1 h. The solution was refluxed for a further 4.5 h before it was allowed to cool and then added dropwise to 2.5 l of diethyl ether with constant vigorous stirring. The white solid that precipitated was filtered, washed, dissolved in milli-Q quality water (5 wt.%), extensively dialysed, before freeze-drying the sample, which gave a white powder (yield was around 50%). For comparison, poly(NIPAM) homopolymer was prepared according to the method by Winnik *et al.*[18]

Emulsion preparation

Sufficient time (1 day) was allowed for the copolymer to dissolve in water to ensure complete dissolution. 3.5 ml of the copolymer solution (3.6 wt.% copolymer) was placed in a 10 ml beaker before the addition of 1.5 ml of 1-bromohexadecane. The mixture was homogenised using a Silverson SL2T laboratory mixer for 5 min at 8000 rpm at room temperature. Dilution tests confirmed that the emulsion was of oil-in-water (O/W) type, *i.e.* the dispersed phase is 1-bromohexadecane.

Physical measurements

The composition of both the homopolymer and copolymer was determined by ^{1}H NMR in $CDCl_3$ using a Varian (300 MHz) spectrometer using methods reported elsewhere.[19,20] The polydispersity index of the samples was obtained from GPC using Waters Styragel columns. THF was used as the eluent and the columns were calibrated with polystyrene standards. Phase transitions were monitored by the absorbance at 600 nm through a 1 cm sample cell referenced against milli-Q water, using a Cary 2200 UV–Vis. spectrophotometer. Samples (0.5 wt.%) were heated at a rate of 0.5 °C min^{-1} in the thermally controlled cell holder. Photomicrographs of the emulsion were obtained using an optical microscope (Olympus, H30). The images were acquired using digital image-processing software and stored on a computer. Steady-state and dynamic rheological measurements were carried out using a stress-controlled rheometer (Rheometrics SR-5000). A concentric cylinder measurement cell (inner cylinder diameter 32.0 mm and outer cylinder diameter 29.5 mm) was used for the copolymer solutions and parallel plate geometry (43 mm diameter) used for the emulsion samples. Sample temperatures during rheological analysis were controlled to ± 0.1 °C, through a combination of a Peltier element and an oil bath. Dynamic measurements involved the determination of the elastic (G') and viscous moduli (G'') as a function of applied stress at an oscillation frequency of 1 Hz. G' and G'' are linked by the phase angle (δ), *i.e.* $\tan\delta = G''/G'$.

Results and discussion

Copolymer preparation and characterization

A range of poly(NIPAM-co-PEGMa) copolymer compositions were screened prior to deciding upon the optimum copolymer composition for this work. A key criterion for assessing the suitability of the copolymer was its ability to stabilise O/W emulsions at room temperature whilst achieving thermally induced gelation. Poly(NIPAM) and poly(PEGMa) homopolymers did not stabilise O/W emulsions at any temperature. Poly(NIPAM-co-PEGMa) copolymers containing *ca.* 25, 50 and 75 mol% of PEG were synthesised and evaluated. The poly(NIPAM-co-PEGMa) copolymer containing *ca.* 50 mol% PEG yielded emulsions with optimum stability at room temperature whilst exhibiting thermally induced gelation behaviour.

Table 1 shows characterisation data for the poly(NIPAM-co-PEGMa) copolymer used in this work. Data for a reference poly(NIPAM) homopolymer are also shown for comparison. Obtaining good quality GPC data is challenging for poly(NIPAM) polymers. These polymers may exhibit filtration problems prior to GPC as a result of chain entanglement.[21] This problem has led some workers[22] to claim that GPC cannot be used to obtain molecular weight data for poly(NIPAM) polymers. As can be seen from Table 1, the poly(NIPAM-co-PEGMa) copolymer has a high polydispersity. A repeat synthesis yielded a poly(NIPAM-co-PEGMa) copolymer with the same composition and comparable M_n (44 600 g mol^{-1}) but a lower polydispersity (2.9). Both copolymers behaved similarly with respect to their ability to confer thermally induced gelation on oil-in-water emulsions. The polydispersity of poly(NIPAM-co-PEGMa) copolymers prepared by the synthetic method used in this work does not

Table 1 Characterisation data for the polymers used

Polymer	M_n/g mol^{-1}	PD	PEG[a] (mol%)	LCST/°C[b]
poly(NIPAM)	41 700	2.3	0	31
poly(NIPAM-co-PEG)	39 100	5.2	52.0	35

[a] Based on ^{1}H NMR data. [b] Based on turbidity–wavelength measurements (see text).

significantly affect emulsion behaviour. The data discussed in the remainder of the work concerns the poly(NIPAM-co-PEGMa) copolymer identified in Table 1.

Investigation of responsive copolymer solutions

Fig. 1 shows the variation of the turbidity (τ) with temperature for poly(NIPAM) and poly(NIPAM-co-PEGMa) solutions (0.5 wt.%). Values for the lower critical solution temperature (LCST) (Table 1) were taken as the point of inflection on the curves in Fig. 1, *i.e.*, the point at which $d^2\tau/dT^2 = 0$. The LCST for poly(NIPAM-co-PEGMa) is *ca.* 4.0 °C higher than the value for poly(NIPAM) and is in accord with other work for related copolymers.[23] It is well established that an increase in the hydrophilicity of the repeat unit by structural modification increases the LCST of poly-(acrylamide)s. The fact that the LCST for poly(NIPAM- co-PEGMa) is higher than that for poly(NIPAM) supports the view that the PEG macromonomer units are well dispersed along the copolymer chains. A block of poly(NIPAM-b-PEG) copolymer would be expected to have a significantly sharper LCST with a value closer to that for poly(NIPAM).

Fig. 2(a) and (b) show the variation of the viscosity (at three different shear rates) with temperature for poly(NIPAM-co-PEGMa) solutions containing, respectively, 5 and 20 wt.% copolymer. At 5 wt.% copolymer the viscosity decreases with increasing temperature; this result is expected for polymer coils below the critical overlap concentration. Temperature-induced coil collapse occurs resulting in a decrease in the disperse phase volume fraction.

In contrast, at 20 wt.% copolymer there is evidence of temperature induced thickening between 25 and 40 °C. This is attributed to temperature-induced network formation[4] and is an indication that the copolymer chains overlap throughout the solution (*i.e.*, polymer concentration greater than c^*). The effect of increasing the temperature is to increase the number of elastically effective chains and also the time over which junctions containing two (or more) chains exist. There is evidence for a decrease in viscosity at temperatures greater than 40 °C. This type of behaviour has been reported elsewhere[4] for related copolymer solutions.

The effect of shear stress on the viscosity of 10 and 20 wt.% copolymer solutions is shown in Fig. 3(a) and (b), respectively. (5 wt.% copolymer solutions exhibited viscosities less than 0.0050 Pa s with poor signal-to-noise ratios and are not presented here). The data indicate a temperature-induced association effect is operative above the LCST. An increase in the temperature increases the number and longevity for elastically effective chains. The effect becomes more pronounced at increasing polymer concentration because of a greater proportion of elastically effective chains.

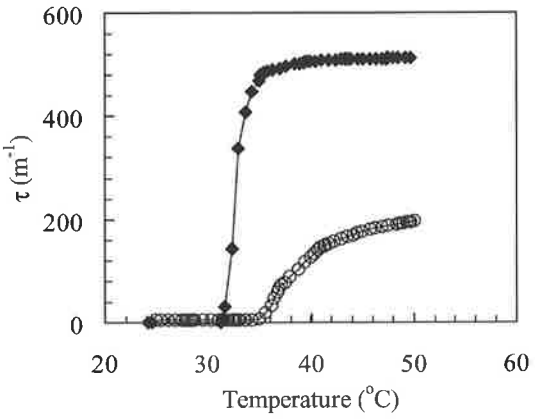

Fig. 1 Variation of the turbidity with temperature for poly(NIPAM) (◆) and poly(NIPAM-co-MPEG) (○).

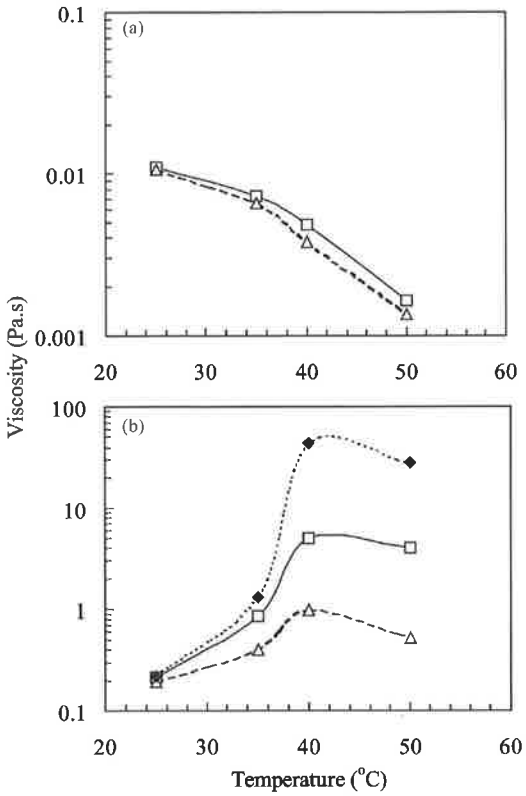

Fig. 2 The effect of temperature on the viscosity of poly(NIPAM-co-PEGMa) copolymer solutions. The concentrations employed were 5 (a) and 20 wt.% (b). The three shear rates used were 1 (◆), 10 (□) and 100 s^{-1} (△).

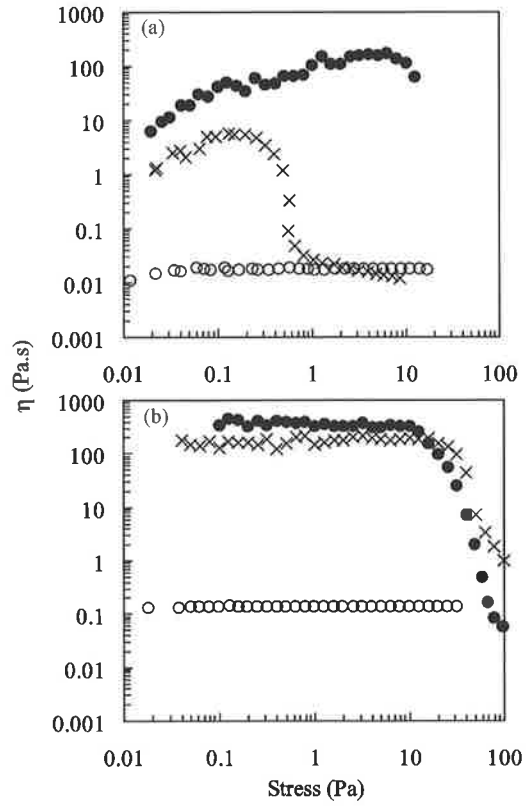

Fig. 3 Viscosity as a function of shear stress for poly(NIPAM-co-PEGMa) copolymer solutions. The copolymer concentrations employed were 10 (a) and 20 wt.% (b). The temperatures investigated were 25 (○), 40 (×) and 50 °C (●).

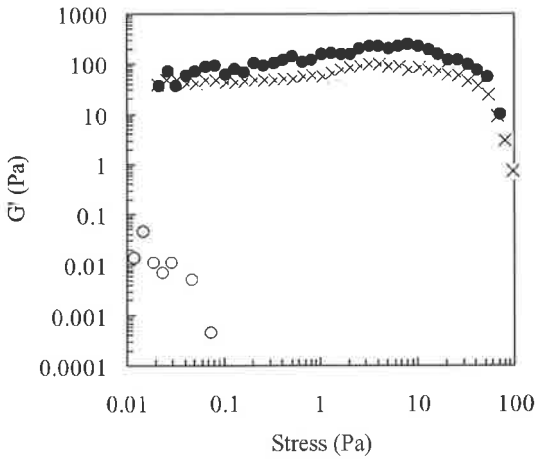

Fig. 4 The storage modulus (G') as a function of shear stress for a 20 wt.% poly(NIPAM-co-PEGMa) copolymer solution. The temperatures investigated were 25 (○), 40 (×) and 50 °C (●).

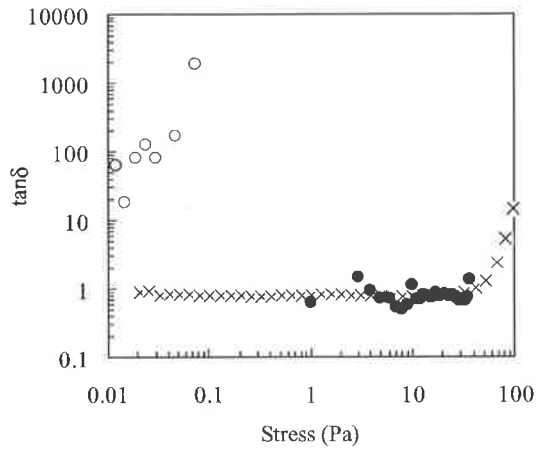

Fig. 5 Tan δ as a function of shear stress for a 20 wt.% poly(NIPAM-co-PEGMa) copolymer solution. The temperatures investigated were 25 (○), 40 (×) and 50 °C (●).

Fig. 4 and 5 show dynamic rheological data for a 20 wt.% copolymer solution measured at different temperatures. Both the elastic modulus (G') values and the range of linear viscoelasticity (*i.e.* stress range where G' is independent of stress) are considerably greater at temperatures higher than the LCST, supporting the view that an increase in temperature produces a viscoelastic network. Fig. 5 indicates that the phase angle (δ) approaches 45° (*i.e.* $G' = G''$) at elevated temperatures, which again supports gelation. (At 25 °C the solution behaves as a viscous liquid ($G' \ll G''$)). It is noted that the term gelation is used here to describe the reversible formation of non-covalent, associative, bonds. The primary modes of attraction for the groups involved are van der Waals and hydrophobic forces. This differs considerably from the covalently bonded networks studied by Mortimer *et al.*[24] The polymer concentration required for a significant temperature-induced gelation effect is ~10 wt.% for the copolymer solutions investigated in this work.

Investigation of responsive emulsions

Poly(NIPAM-co-PEGMa) copolymer was found to be an effective O/W emulsifier for 1-bromohexadecane-in-water emulsions. Fig. 6 shows representative optical micrographs for an emulsion prepared using an oil phase volume fraction (ϕ_0)

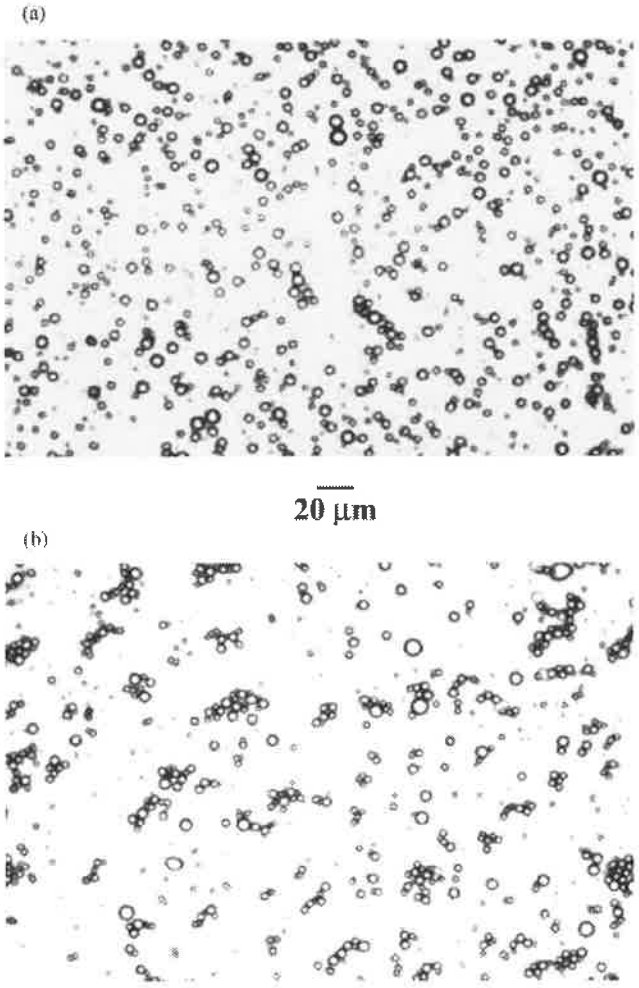

Fig. 6 Optical micrograph of the emulsion at room temperature: before (a) and after (b) gelation.

of 0.30. These were obtained prior to (Fig. 6(a)) and after (Fig. 6(b)) one temperature-induced gelation cycle, *i.e.*, heating from room temperature to 50 °C and holding at the temperature for *ca.* 30 min and then cooling to room temperature. It is evident that the droplets are reasonably polydisperse and weakly flocculated. A droplet size distribution was obtained from the data shown in Fig. 6(a) and fitted to log-normal distribution[25] profile. The values for the peak diameter and broadness parameter were 7.2 μm and 0.42, respectively. These data for the emulsion together with its weakly flocculated nature (prior to gelation) are typical of emulsions stabilised by macro-surfactants.[11] The values for the peak diameter and broadness parameter were 9.6 μm and 0.39, respectively, for the emulsion shown in Fig. 6(b). The effect of temperature on the storage stability of the emulsions will be the subject of a future publication. It is important to note that the flocs observed at room temperature in Fig. 6(a) could be broken up with gentle agitation. Electrophoresis measurements on the droplets at room temperature revealed a zeta potential values less than 5 mV. This low value suggests that the emulsion stability at room temperature is due to steric rather than electrostatic interaction. The extent of steric stabilisation will diminish as the solution temperature approaches the LCST (and θ-temperature) of the copolymer.[26] Kapsabelis and Prestidge[27] revealed that the adsorbed layer thickness for cellulose-based polymers was highly temperature sensitive, but that adsorbed layer contraction was dependent on a balance of the segment–solution, segment–segment and segment–surface interaction parameters.

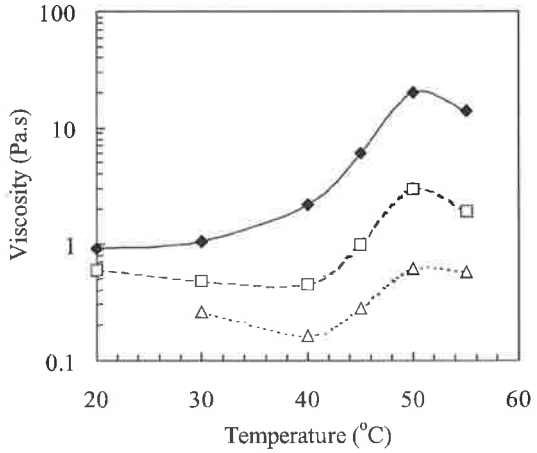

Fig. 7 The effect of temperature on the viscosity of a 1-bromohexadecane-in-water emulsions prepared using poly(NIPAM-co-PEGMa). The three shear rates used were 1 (◆), 10 (□) and 100 s^{-1} (△).

Fig. 7 shows the variation of emulsion viscosity with temperature, as determined at shear rates of 1, 10 and 100 s^{-1}. The viscosity data at the higher shear rate (100 s^{-1}) are in agreement with data measured for related emulsions using capillary viscometry.[1] The variation of the emulsion viscosity with temperature in Fig. 7 for the lowest shear rate (1 s^{-1}) shows similar behaviour to the equivalent data shown in Fig. 2(b) for the concentrated copolymer solution. Thus, pronounced thickening of the emulsion occurs at low shear rates once the temperature exceeds the LCST. Sample tubes containing the emulsion can be inverted at 50 °C with the gelled emulsion remaining in its original position.[1] Overall, the dispersed droplets appear to have the same qualitative effect on the rheological properties as a substantial increase in the copolymer concentration, *i.e.*, addition of the oil phase results in a thermally-induced gelation which would have otherwise been absent at that temperature.

Fig. 8 shows the effect of shear stress and temperature on the viscosity of the emulsion. The emulsion exhibits weak shear-thinning behaviour at 25 °C. This may be ascribed to droplet deformation, which is a well-known phenomenon for emulsions under shear[28] and the disruption of weak flocs. Upon increasing the temperature a significant increase is observed in the low stress viscosity and the stress required for the onset of thinning (*i.e.* the apparent yield stress). This rheological behaviour is indicative of the formation of a transient network

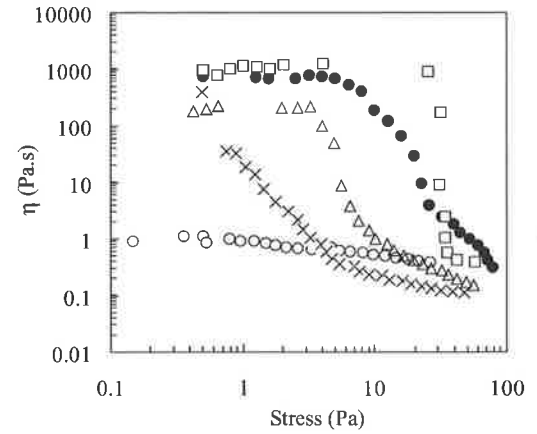

Fig. 8 The effect of shear stress on the viscosity of 1-bromohexadecane-in-water emulsions prepared using poly(NIPAM-co-PEGMa). The measurement temperatures were 20 (○), 40 (×), 45 (△), 50 (●) and 60 °C (□).

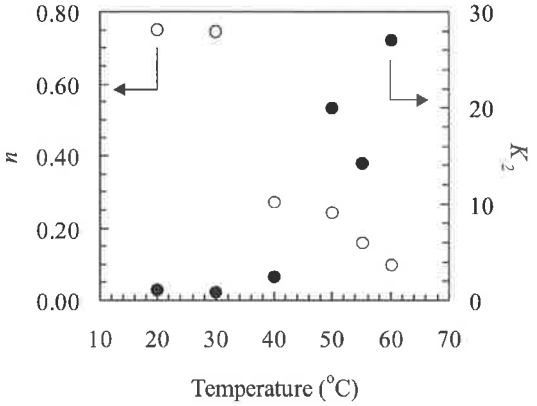

Fig. 9 The effect of temperature on the values of n (○) and K_2 (●) obtained from fitting the power-law model (eqn. (1)) to the viscosity *vs.* shear rate data for the emulsion.

upon heating. The number of effective chains and the amount of time that junctions remain in hydrophobic clusters will increase with temperature, *i.e.* a temperature increase results in a stronger network. The network is considered to be based upon flocculated emulsion droplets, where the droplets are held together by attractive hydrophobic interactions between clusters of copolymer segments at the interface, as well as van der Waals attraction between the droplets themselves. Increasing the temperature results in a stronger hydrophobic attraction and therefore a greater shear stress is required to disrupt the junctions.

The steady state rheological data for the emulsion (*e.g.* Fig. 8) may also be considered in terms of viscosity (η) *vs.* shear rate ($d\gamma/dt$) and, in the shear-dependent regime, can be described in terms of a power-law model:[29]

$$\eta = K_2(d\gamma/dt)^{n-1} \quad (1)$$

where n and K_2 are power-law index and consistency factor, respectively. Values for n and K_2 were determined from the linear region of $\ln\eta$ *vs.* $\ln(d\gamma/dt)$ plots (*i.e.* where the viscosity was significantly less than the zero shear viscosity) and are plotted against temperature in Fig. 9 (R^2 values for the fits were greater than 0.994). The values for n are less than unity and are consistent with shear thinning. The K_2 values relate directly to the structure of the emulsion droplet network and exhibit a pronounced increase above the LCST for the copolymer. A concomitant decrease in n is observed; this reflects a greater extent of shear thinning for the more highly structured emulsions.

The dynamic rheological properties of the emulsion were also determined as a function of temperature: Fig. 10 and 11 show, respectively, the variation of G' and $\tan\delta$ with shear stress. The observed increase in G' with temperature is indicative of an increased elasticity of the emulsion[29] and is consistent with network formation. The values for $\tan\delta$ decrease with increasing temperature, which further supports the transformation from a viscous fluid to an elastic, gel-like structure. It should also be noted that $\tan\delta$ values for the emulsion are less than that for the equivalent copolymer solution, again reflecting differences in microstructure and gel properties.

Proposed mechanism for temperature-induced emulsion gelation

The mechanism for the observed temperature-induced gelation of the emulsion is of considerable interest. There are several key experimental observations that must be accounted for: (a)

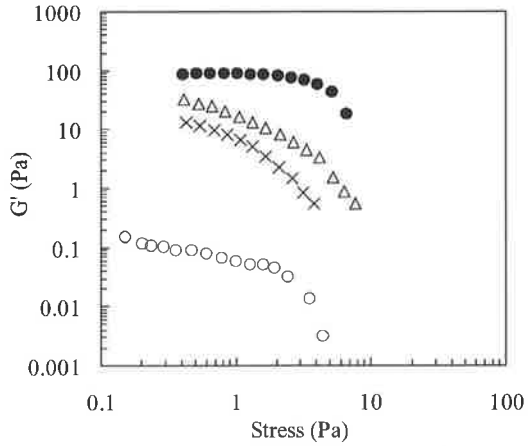

Fig. 10 The storage modulus (G') as a function of shear stress for a 1-bromohexadecane-in-water emulsions prepared using poly(NIPAM-co-PEGMa). The temperatures were 20 (○), 40 (×), 45 (△), 50 °C (●).

The prevention of phase separation as a consequence of gelation. (b) The relatively high degree of reversibility for the gelation transition, and (c) The observation of temperature-induced gelation for emulsions containing a continuous phase copolymer concentration less than that required for gelation of the parent copolymer solution.

The consequence of increasing the temperature to above the LCST for the emulsion is considered to be a change from repulsive to attractive inter-coil interactions.[26] This will necessarily cause droplet–droplet interactions to become attractive, resulting in flocculation. The adsorbed copolymer chains will also collapse leading to a more rigid interfacial layer to oppose coalescence. This would account for the prevention of phase separation upon gelation and increase in elastic structure. It follows that a finite contact angle should emerge between droplet pairs as the temperature increases. This aspect will be investigated in future work.

Strongly flocculated emulsions invariably consist of aggregates containing considerable entrapped solvent.[30] The flocculated droplets will form a three-dimensional network provided that a critical ϕ_0 is exceeded such that chains of droplets can achieve a sufficient degree of connectivity throughout the emulsion volume. As the temperature decreases, the collapsed polymer chains begin to expand (as now water becomes a good solvent). This causes the network to break-up and the flocculated droplets that once formed the three-dimensional network, to redisperse.

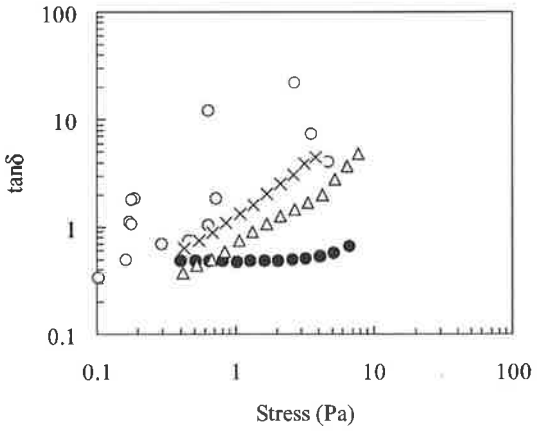

Fig. 11 Variation of tan δ as a function of shear stress for a 1-bromohexadecane-in-water emulsions prepared using poly(NIPAM-co-PEGMa). The temperatures were 20 (○), 40 (×), 45 (△), 50 °C (●). Note that the variability of the data measured at 20 °C is due to the low values of G' and G''.

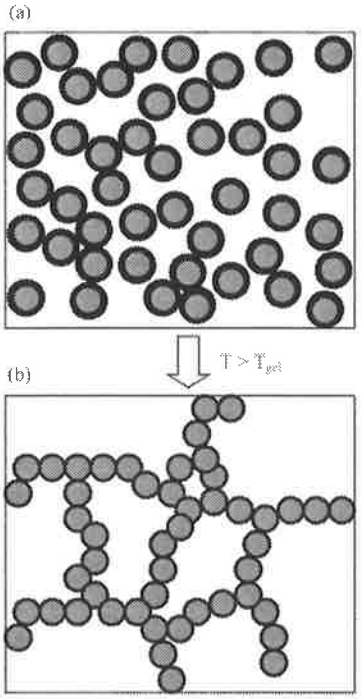

Fig. 12 Diagram depicting the proposed mechanism for thermally-induced gelation for an O/W emulsion. The oil droplets (grey) contain an adsorbed layer of copolymer (black) in each case. At room temperature (a) the layer is expanded and at elevated temperature (b, above the LCST) it is collapsed and the emulsion gels.

It is appropriate to comment on the complex form of the attractive interactions that are believed to maintain the gelled state for the emulsions. The three-dimensional droplet network structure would consist of droplet chains held together by overlapping copolymer chains adsorbed at the emulsion interface. (A schematic representation is given in Fig. 12). These interfacial copolymer chains form their own transient network, which acts as the "glue" for the droplet network. Thus, only copolymer adsorbed at the droplet surface need be involved in formation of the connected droplet network and gelation. An attractive feature of this model is that a gelled network can result in the presence of a lower copolymer concentration than the critical overlap concentration. An entangled mesh of copolymer chains existing throughout the aqueous phase is not required for emulsion gelation.

Conclusions

This work has provided a detailed rheological investigation into a new type of emulsion behaviour: temperature-induced emulsion gelation. It has been clearly shown that the presence of a dispersed oil phase ($\phi_0 = 0.30$) within a dilute copolymer solution results in temperature-dependent rheological properties that are significantly different to that of the parent copolymer solution. The emulsion exhibits temperature-induced gelation that is mostly reversible, whereas, the viscosity of the dilute copolymer solution decreases with increasing temperature. The gelled emulsions are sensitive to shear and the gel-to-fluid transition results at modest shear stresses (< 100 N m^{-2}). The mechanism proposed to explain the temperature-induced gelation envisages bridging flocculation as a consequence of an increase in the polymer–solvent interaction parameter (to greater than 0.5) for the stabilising copolymer chains with increasing temperature. Above the LCST, the copolymer–copolymer interactions become attractive resulting in transient network formation between neighbouring droplets and creation of networks of flocculated droplets.

It is important to note that reversible, temperature-induced gelation is a general effect for emulsions stabilised by poly(-NIPAM-co-PEGMa). We have observed equivalent behaviour for a range of oil phases including toluene, poly(-dimethylsiloxane) and perfluorodecalin. This reversible gelation process may be of great technological importance in the emulsion field because it allows the transformation of a fluid emulsion into a gel in a short time using temperature alone as the trigger.

Acknowledgements

The authors would like to thank the University of Adelaide for providing an international scholarship to A.K. We also thank Dulux Australia for providing the GPC data. A University of Adelaide Grant is acknowledged. C.P. and I.A. acknowledge funding from the Australian Research Council's Special Research Centre for Particle and Material Interfaces.

References

1 A. Koh and B. R. Saunders, *Chem. Commun.*, 2000, 2461.
2 B. P. Binks and S. O. Lumsdon, *Langmuir*, 2000, **16**, 2539.
3 A. Durand and D. Hourdet, *Macromol. Chem. Phys.*, 2000, **201**, 858.
4 F. L'Alloret, P. Maroy, D. Hourdet and R. Audebert, *Rev. Inst. Fr. Pet.*, 1997, **52**, 117.
5 A. Durand and D. Hourdet, *Polymer*, 1999, **40**, 4941.
6 A. M. Mathur, B. Drescher, A. B. Sevanton and J. Klier, *Nature*, 1998, **392**, 367.
7 F. L'Alloret, D. Hourdet and R. Audebert, *Colloid Polym. Sci.*, 1995, **273**, 1163.
8 M. S. Green and A. V. Tobolsky, *J. Chem. Phys.*, 1946, **14**, 80.
9 F. Tanaka and S. F. Edwards, *Macromolecules*, 1992, **25**, 1516.
10 F. Tanaka and M. Ishida, *Macromolecules*, 1996, **29**, 7571.
11 P. Perrin and F. Lafuma, *J. Colloid Interface Sci.*, 1998, **197**, 317.
12 P. Perrin, N. Monfreux and F. Lafuma, *Colloid Polym. Sci.*, 1999, **277**, 89.
13 T. J. Barnes and C. A. Prestidge, *Langmuir*, 2000, **16**, 4116.
14 E. Dickinson and S.-T. Hong, *Colloids Surf. A*, 1997, **127**, 1.
15 J. Philip, L. Bonakdar, P. Poulin, J. Bibette and F. Leal-Calderon, *Phys. Rev. Lett.*, 2000, **84**, 2018.
16 W. Xue, S. Champ and M. B. Huglin, *Polymer*, 2000, **41**, 7575.
17 A. E. Cardenas-Valera, A. I. Bailey and A. Doroszkowski, *Colloids Surf. A*, 1995, **96**, 53.
18 F. M. Winnik, *Macromolecules*, 1990, **23**, 233.
19 X. Qiu and C. Wu, *Macromolecules*, 1997, **30**, 7921.
20 F. Zeng, Z. Tong and H. Feng, *Polymer*, 1997, **38**, 5539.
21 F. Ganachaud, M. J. Monteiro, R. G. Gilbert, M.-A. Dourges, S. H. Thang and E. Rizzardo, *Macromolecules*, 2000, **33**, 6738.
22 X. Y. Wu, R. H. Pelton, K. C. Tam, D. R. Woods and A. E. Hamielec, *J. Polym. Sci., Part A*, 1993, **31**, 957.
23 J. Virtanen and H. Tenhu, *Macromolecules*, 2000, **33**, 5970.
24 S. Mortimer, A. J. Ryan and J. L. Stanford, *Macromolecules*, 2001, **34**, 2973.
25 Y. De Smet, D. Danino, L. Deriemaeker, Y. Talmon and R. Finsy, *Langmuir*, 2000, **16**, 961.
26 D. H. Napper, *Polymeric Stabilization of Colloidal Dispersions*, Academic Press, New York, 1983.
27 S. Kapsabelis and C. A. Prestidge, *J. Colloid Interface Sci.*, 2000, **228**, 297.
28 P. Manoj, A. D. Watson, D. J. Hibberd, A. J. Filler-Travis and M. M. Robins, *J. Colloid Interface Sci.*, 1998, **207**, 294.
29 H. A. Barnes, J. F. Hutton and K. Walters, An Introduction to Rheology, Elsevier, Amsterdam, 1989.
30 H. M. Princen, M. P. Aronson and J. C. Moser, *J. Colloid Interface Sci.*, 1980, **75**, 246.

PCCP

A study of temperature-induced aggregation of responsive comb copolymers in aqueous solution

Andrew Y. C. Koh,[a] Richard K. Heenan[b] and Brian R. Saunders*[c]

[a] *Department of Chemistry, University of Adelaide, S. A. 5005, Australia*
[b] *ISIS Facility, Rutherford Appleton Laboratory, Chilton, Didcot, UK OX11 0QX*
[c] *Manchester Materials Science Centre, UMIST and University of Manchester, Grosvenor St., Manchester, UK M1 7HS*

Received 15th November 2002, Accepted 10th April 2003
First published as an Advance Article on the web 23rd April 2003

Responsive copolymers can be used to confer temperature-responsiveness to emulsions in the form of temperature-induced gelation triggered by conformational changes of the copolymer. In this study the structural changes of a responsive comb copolymer, poly(NIPAM-*co*-PEGMa) (N-isopropylacrylamide and poly(ethyleneglycol methacrylate), respectively) in D_2O are studied using small-angle neutron scattering (SANS) as well as complementary turbidity measurements. The copolymer was synthesised under conditions that favoured a compositionally asymmetric ("blocky") structure. Scattering data obtained for the poly(NIPAM) and poly(PEGMa) homopolymers at 25 °C are also presented. The scattering profiles for the copolymer in aqueous solution are strongly temperature-dependent. At temperatures less than or equal to 32 °C the scattering profiles have contributions from q^{-1} and q^{-2} scattering terms (rods and Gaussian coils, respectively); whereas, at 36 and 40 °C the profiles are dominated by scattering from Gaussian coils. At 50 °C the contributions to the scattering are from q^{-2} and q^{-4} (Gaussian coils and Porod scattering from an interface, respectively). The data were fitted successfully using models that combined these contributions. The radius of gyration (R_g) and aggregation number (N_{agg}) for poly(NIPAM-*co*-PEGMa) increased, respectively, from 76 Å and $N_{agg} = 1$ at 25 °C to 257 Å and $N_{agg} = 27$ at 50 °C. Rods were present (although in a minority) at temperatures less than 36 °C with an average radius of 11 Å. The rods disappeared once the temperature increased to around 36 °C, which is similar to the LCST measured for the copolymer in D_2O. At 50 °C the data were fitted with a model containing a Porod scattering term and the results indicated the presence of particles with a diffuse layer thickness of 60 Å. The average size of the particles was estimated as 1200 Å. The insights gained from the data help to explain the temperature-induced gelation observed for solutions and emulsions containing poly(NIPAM-*co*-PEGMa).

Introduction

Responsive polymers are polymers that undergo a conformation change in response to an environmental stimuli. The stimulii may include[1,2] temperature or pH. Poly(NIPAM) (NIPAM = N-isopropylacrylamide) is a well known temperature-responsive polymer. The properties of poly(NIPAM) have been studied in the form of linear polymer,[3] copolymer[4] and microgel particles.[5,6] Poly(NIPAM) exhibits a coil-to-globule transition as a consequence of the temperature-induced disruption of hydrogen bonding between the water and the polymer. Poly(NIPAM) has a lower critical solution temperature[3] of 32 °C in H_2O. NIPAM can be copolymerised with other monomers to yield responsive copolymers. Recently, Koh and Saunders[7,8] copolymerised NIPAM with poly(ethylene glycol) methacrylate (PEGMa) to produce a responsive comb copolymer, poly(NIPAM-*co*-PEGMa). The responsive copolymer stabilised oil-in-water emulsions at room temperature. Interestingly, at temperatures exceeding the LCST the emulsion exhibited a fluid-to-gel transition, which was reversible and has potential for improving the shelf-life of emulsions. This novel behaviour for emulsions most likely relies upon reversible temperature-induced bridging flocculation. Attractive hydrophobic interactions dominate segment–segment interactions resulting in junctions of physically crosslinked chains that support the network. Emulsion stabilisation at room temperature and temperature-induced gelation at higher temperature were only observed if the copolymer was synthesised in a manner that favoured "blockiness". Compositionally symmetric poly(NIPAM-*co*-PEGMa) copolymers failed to satisfy these criteria. In order to obtain an improved understanding of the mechanism for this phenomenon a comprehensive study of the behaviour of the poly(NIPAM-*co*-PEGMa) copolymers in solution as a function of temperature was undertaken. In this work small-angle neutron scattering (SANS) is used to study the temperature-induced structural changes of poly(NIPAM-*co*-PEGMa) copolymers in aqueous solution as a function of temperature.

SANS is a powerful technique for studying structural detail of polymers[9,10] on the scale 10–1000 Å. The general equation that describes the scattered intensity, $I(q)$ for dilute particles is:

$$I(q) = \phi V(\Delta\rho)^2 P(q) S(q) \quad (1)$$

where ϕ and V are the volume fraction and volume of the scattering species, respectively. The contrast term is $\Delta\rho$, whilst the form factor is $P(q)$. The inter-particle structure factor $S(q)$ approaches unity for dilute solutions and this is assumed to be the case in the present work. The contrast term ($\Delta\rho$) gives the difference in scattering length densities of the polymer (ρ_2) and solvent (ρ_1). In this work the hydrogenous polymer is studied in D_2O solutions in order to

DOI: 10.1039/b211294a

maximise $\Delta\rho$. For a SANS experiment the scattered intensity is measured as a function of the scattering vector (q), which is given by:

$$q = \frac{4\pi}{\lambda}\sin\left(\frac{\theta}{2}\right) \quad (2)$$

The dimension for q is reciprocal distance and for a Bragg scatterer it is related to the distance scale probed (d) by $d = 2\pi/q$. The SANS experiment provides a scattering profile consisting of the scattered intensity, $I(q)$ *vs.* q.

SANS has not been previously used to study responsive poly(NIPAM) *copolymers* in solution. Mao *et al.*[11] used SANS to study the temperature-induced conformational changes of PEO-PPO-PEO block copolymer micelles in aqueous solution. The amphiphilic copolymers were found to comprise Gaussian coils and rods. The temperature dependent behaviour was accentuated in the presence of added electrolyte. (The structural transformations that occur at the LCST for pluronics are less pronounced compared to poly(NIPAM) copolymers.) A related system was investigated by Washington and King[12] where the behaviour of the copolymer at the surface of emulsions was investigated. Hatto *et al.*[13] studied the temperature responsive behaviour of poly(NIPAM) adsorbed to silica particles using SANS. They found a surface layer contraction as a result of temperature increase.

In the present work SANS is used to investigate the behaviour of poly(NIPAM-co-PEGMa) copolymers in aqueous solution as a function of temperature.

Experimental section

Materials

NIPAM (Acros Organics, 99%), PEGMa, (molecular weight = 360 g mol^{-1}, Aldrich) and azobis(isobutyronitrile) (AIBN) were used as received. Deuterium oxide (Aldrich, 99.9%) was also used as received. Water was of Milli-Q quality.

Copolymer synthesis

Xue *et al.*[14] have shown that NIPAM has a strong tendency for homopolymerisation in the presence of other co-monomers. The conditions used for the preparation of poly(NIPAM-co-PEGMa) were specifically designed to promote a composition gradient of NIPAM and PEGMa within poly(NIPAM-*co*-PEGMa). A representative preparation for poly(NIPAM-co-PEGMa) is as follows. PEGMa (1.73 g) and *tert*-butyl alcohol (37.5 ml) were added to a nitrogen purged five-necked 250 ml reaction kettle equipped with a burette, Teflon stirrer blade, condenser, thermometer and nitrogen inlet. The stirred monomer solution was allowed to degas for 30 min before the mixture was heated to 80 °C under nitrogen. NIPAM (3.27 g) and AIBN (0.03 g) in *tert*-butyl alcohol (12.5 ml) were added dropwise with stirring to the PEGMa solution over 1 h. The solution was refluxed for a further 4.5 h before it was allowed to cool and then added dropwise to diethyl ether with constant vigorous stirring. The white solid precipitant was filtered, washed, dissolved in milli-Q quality water (5 wt.%), extensively dialysed, before freeze-drying the sample. Poly(NIPAM) and poly(PEGMa) homopolymers were prepared according to the method by Winnik *et al.*[15]

Physical measurements

Turbidity measurements were performed using D_2O as the solvent. The details of the equipment and conditions are given elsewhere.[8] The SANS experiments were performed using LOQ at the ISIS facility (Rutherford Appleton Laboratory, Didcot, UK). The SANS samples were prepared by freeze-drying the copolymer followed by re-dispersion in D_2O. The samples were measured in quartz cuvettes (Hellma) of 2 mm pathlength and a concentration of 3.5% w/w. The SANS measurements were conducted with LOQ running at 50 Hz. The effective q-range of the instrument was 0.009–1.6 Å^{-1}, although there was negligible signal from the samples at $q > 0.25$ Å^{-1}. The scattered intensity data was corrected for the wavelength dependence of the sample transmission, detector efficiency and background scattering (*e.g.*, cuvette containing D_2O) using the instrument specific software. These corrected data were then placed on an absolute scale by reference to the scattering from a partially-deuterated polystyrene blend of known composition and molecular weight in accordance with established procedures.

The incoherent background level for each sample was determined in the following manner. The scattering exponent for the high q contribution (*e.g.*, q^{-n}) was determined from an initial investigation of $d\ln I(q)/d\ln q$ *vs.* q. In every case (except poly(NIPAM-*co*-PEGMa) at 50 °C where $n = 4$) the value of n was 2 for the $I(q)$ data for q values greater than a minimum value (q_2). A plot of $I(q)$ *vs.* q^{-2} was then constructed for $q > q_2$. The gradient was then used to calculate a value for A_2 using $I(q) = A_2q^{-2} + B_{inc}$, where B_{inc} is the incoherent background. Subtraction of each value for A_2q^{-2} from I(q) (for a given $q > q_2$) gave a value for B_{inc}. The values for B_{inc} for each $q > q_2$ were then averaged to give an average value for B_{inc}. The advantage of this method is that the value for A_2 was calculated using linear regression which is inherently biased to the high range of $I(q)$ and q^{-2} which corresponds to values with least relative error for $I(q)$. The average value for B_{inc} was subtracted from the scattering data, enabling the coherent scattering for the poly(NIPAM) microgel particles to be determined. The value for B_{inc} for poly(NIPAM-*co*-PEGMa) at 50 °C was determined using the method of Auvray and Cotton,[16] *i.e.*, from the gradient of a plot of $I(q)q^4$ *vs.* q^4.

Results and discussion

Copolymer characterisation and solution studies using light scattering

The poly(NIPAM-*co*-PEGMa) copolymer investigated in this study had a number average molecular weight of 44.6 k and a polydispersity of 2.9 (*i.e.*, M_w/M_n). The copolymer composition was investigated using NMR and found to contain 86 mol% NIPAM. (This corresponds to 66% w/w NIPAM.) The copolymer was prepared by a semi-batch polymerisation method. In this method the NIPAM was fed into a PEGMa monomer solution. This method of copolymerisation was selected due to our discovery that poly(NIPAM-*co*-PEGMa) copolymers prepared using conditions that favoured compositional symmetry gave unstable oil-in-water emulsions at room temperature which exhibited phase separation on heating (*cf.* temperature-induced gelation[8]). It appears that "blockiness" of the poly(NIPAM-PEGMa) is a requirement for conferring temperature-induced emulsion gelation. Consequently, here we have investigated the solution behaviour of these blocky poly(NIPAM-*co*-PEGMa) copolymers. We have measured the reactivity ratios for NIPAM and PEGMa and found them to be 1.1 and 0.6, respectively (data not shown). Consequently, the copolymer chains that formed first were PEGMa-rich, whilst those that formed last were NIPAM-rich. Fig. 1 shows turbidity *vs.* temperature data for poly(NIPAM-*co*-PEGMa) measured in D_2O. The data show a significant increase in turbidity at temperatures greater than 35 °C. Although the transition is broad, analysis of the $d^2\tau/dT^2$ indicates a major

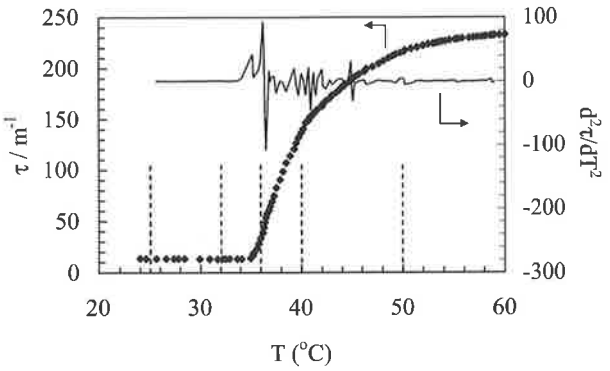

Fig. 1 Turbidity of poly(NIPAM-*co*-PEGMa) solution in D_2O as a function of temperature. The second derivative ($d^2\tau/dT^2$) is also shown. The key temperatures 25, 32, 36, 40 and 50 °C are highlighted.

inflection point for τ *vs.* T at 36.5 ± 0.5 °C.† The data indicate the presence of a range of LCSTs within the copolymer. This is consistent with an asymmetric incorporation of NIPAM into the copolymer chains. The LCST of poly(NIPAM-*co*-PEGMa) in H_2O was found to be 34 °C in earlier work.[8]

It should be noted poly(NIPAM-*co*-PEGMa) does not phase separate from solution when heated above the LCST at the concentrations used in this work (3.5 wt.%). Here, colloidal dispersions form that are kinetically stable. The turbidity-temperature profiles for a given concentration were not significantly affected by heating rate. For example, the turbidity *vs.* temperature profiles obtained at heating rates of 0.05 and 0.5 °C min^{-1} (data not shown) were very similar attesting to a similar aggregate size and particle density. In our experience with these copolymers the main variables that affect the dispersion structure and properties are copolymer concentration and temperature. At very high concentrations (greater than 10%) the dispersions form gels at above the LCST which indicates substantial aggregation.[8]

Identification of scattering exponents for the SANS data

Fig. 2 shows the scattering profiles for poly(NIPAM), poly(MPEGa) and poly(NIPAM-*co*-PEGMa) solutions at 25 °C. The data for the copolymer were most similar in shape to those of poly(PEGMa) (*cf.* poly(NIPAM)) especially at low and medium q ranges. This qualitative comparison suggests that the copolymer is structurally similar to the poly(PEGMa) comb copolymer. A more detailed discussion follows.

Fig. 3 shows the scattering profiles for poly(NIPAM-PEGMa) in solution as a function of temperature. Data were also obtained at 40 °C. These data were very similar to those obtained at 36 °C and are not shown for clarity. The data show that the scattered intensity at low q increases with increasing temperature. At 50 °C a substantial increase in the magnitude of the gradient at low q has occurred. This is analysed more rigorously in Fig. 4 which shows the instantaneous gradients ($d\ln I(q)/d\ln q$) for the data shown in Fig. 3 in the region of $0.007 \leq q \leq 0.10$ Å^{-1}. This method of plotting the data provides a clear illustration of the variation of the instantaneous scattering exponent (n) as a function of q, where $I(q) = A_n q^{-n}$ (A_n is a constant). These data show the presence of scattering exponents of $n = -1$ and -2, respectively, at low and medium q for data obtained at 25 °C. At higher temperature (50 °C) the low q data shows a significant increase in the magnitude of n to

† The second derivative is used here to identify the LCST because it represents the point at which the rate of turbidity change passes through a maximum value. This is a more powerful method for assessing LCST variation within a sample than using other methods, such as onset of turbidity change which only detect the polymer chains with the lowest LCST.

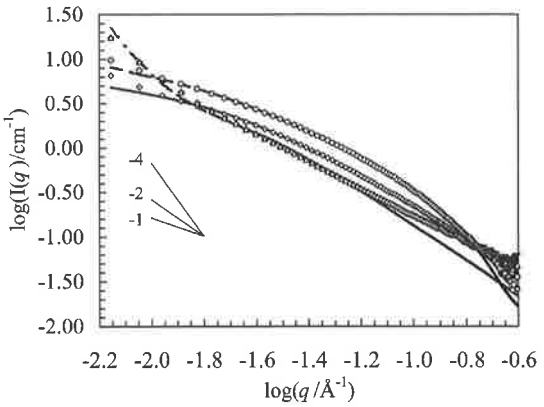

Fig. 2 Scattering profiles for poly(NIPAM) (△), poly(PEGMa) (○) and poly(NIPAM-*co*-PEGMa) (◇) measured at 25 °C. The fits to the data are also shown (see text).

the vicinity of -4 or steeper, which is consistent with Porod scattering from a sharp or even diffuse interface. Therefore, the data shown in Fig. 4 suggest the following scattering functions for poly(NIPAM-*co*-PEGMa):

$$\text{(a) for } T \leq 32\,^\circ\text{C} \quad I(q) = A_1 q^{-1} + A_2 q^{-2} \tag{3}$$

$$\text{(b) for 36 and 40 °C} \quad I(q) = A_2 q^{-2} \tag{4}$$

$$\text{(c) for } T = 50\,^\circ\text{C} \quad I(q) = A_2 q^{-2} + A_4 q^{-4} \tag{5}$$

where A_1, A_2 and A_4 are constants for a given temperature. The q ranges over which each scattering exponent contributes has not been established thus far. A plot of $I(q)q^2$ *vs.* q is an effective way for probing this further because the presence q^{-1} and q^{-2} scattering will be evident from a linear relationship and zero gradient, respectively. It can be seen from Fig. 5 that extended linearity is present at low q (for the data measured at 25 and 32 °C) while zero gradients are evident at higher q for all temperatures. The zero gradient region extends to lower q values with increasing temperature. This is exactly what is expected for a Gaussian coil model in which the radius of gyration increases with increasing temperature (see below). The linearity evident for the low q data at temperatures less than or equal to 32 °C indicates contributions from both q^{-1} and q^{-2} scattering.

The data for the copolymer obtained at 50 °C are plotted as $I(q)q^4$ *vs.* q^2 in Fig. 6 in order to establish the region over which eqn. (5) applies. Linearity is observed. This indicates contributions from q^{-2} over the entire q range.

In this study the concentration of polymer employed was 3.5 wt.%. The discussion given above has assumed that the

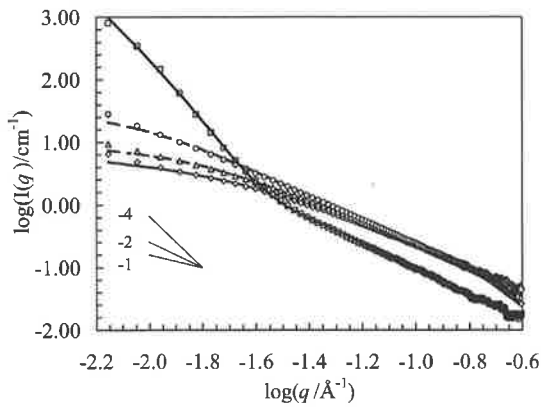

Fig. 3 Scattering profiles for poly(NIPAM-*co*-PEGMa) in D_2O measured at 25 (◇), 32 (△), 36 (○) and 50 (□) °C. The fits to the data are also shown (see text).

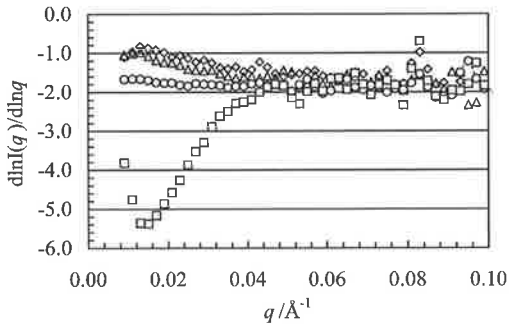

Fig. 4 Plot of $d\ln I(q)/d\ln q$ as a function of q for poly(NIPAM-*co*-PEGMa) measured at 25 (◇), 32 (△), 36 (○) and 50 °C (□).

interparticle structure factor, $S(q) = 1$. Our intrinsic viscosity measurements for poly(NIPAM-*co*-PEGMa) at 25 °C (not shown) yielded an intrinsic viscosity $[\eta]$ of about 0.01 cm^3 g^{-1}. An overlap concentration (c^*) of 1 wt.% could be estimated if it were assumed that $c^* = 1/[\eta]$. This approximation is sometimes used for linear polymers.[17] However, $c^* = 1/[\eta]$ is not a reasonable approximation in the case of poly(NIPAM-*co*-PEGMa) because the segment concentration is significantly higher for branched copolymers than for linear polymers.[17] This would increase the calculated value for c^*. In addition, we consider $S(q) = 1$ to be reasonable approximation for the overwhelming majority of the data considered here because:

(a) The copolymer chains are uncharged. Strong repulsive interactions from neighbouring chains that may cause structure factors not equal to unity are unlikely.

(b) Neutrons are scattered most effectively from segment dense regions close to the polymer coil centres. This means that the effective size of the coils that scatter neutrons at 25 °C is less than the hydrodynamic coil size[18] measured by viscosity measurements.

(c) In the case of the data measured at higher temperature (*e.g.*, 50 °C) the separation between the aggregates will be sufficiently large that a structure term due to inter-aggregate interference is unlikely. This has been verified using our data obtained using higher polymer concentrations (not shown).

(d) The scattering exponent at low q ($q \geq 0.01$ Å^{-1}) for the copolymer solutions at 25 °C is -1 from the data shown in Figs. 4 and 5. This is consistent with rods and has been observed elsewhere for related systems.[11]

In summary, contributions from $S(q)$ not being equal to unity are only likely to occur at the smallest q values (*e.g.* <0.01 Å^{-1}) for the data obtained at 25 and 32 °C.

Model fitting of the SANS data

The analysis given above has shown strong evidence for the scattering contributions given generally by eqns. (3)–(5). The

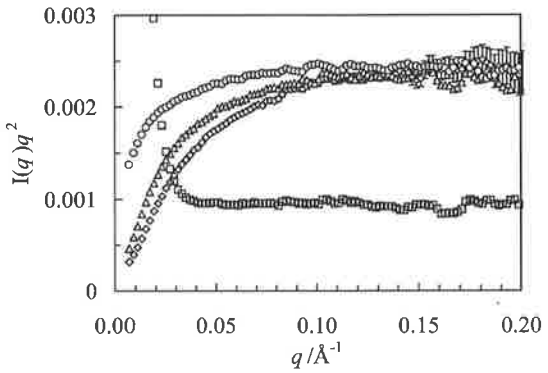

Fig. 5 The variation of $I(q)q^2$ as a function of q for poly(NIPAM-*co*-PEGMa) measured at 25 (◇), 32 (△), 36 (○) and 50 °C (□).

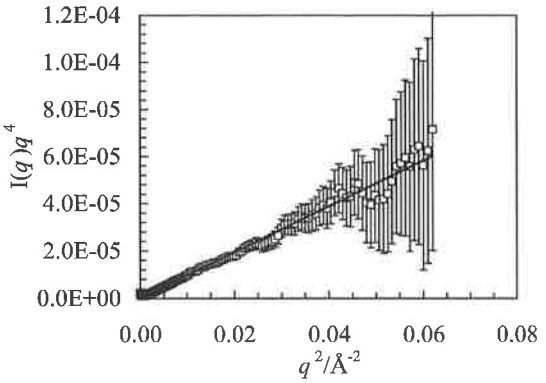

Fig. 6 Kratky plot of $I(q)q^4$ as a function of q^2 for poly(NIPAM-*co*-PEGMa) measured at 50 °C. Error bars based the error of $I(q)$ are shown for this plot.

presence of q^{-1} is taken to be indicative of long thin rods,[9] whilst the presence of q^{-4} scattering is taken to be due to Porod scattering from a sharp interface of large particles.[19] The q^{-2} portion is attributed to scattering from Gaussian chains[11] though may rarely also appear for thin, rigid, sheets. It should be noted that Mao *et al.*[11] also found evidence of rods in their study of PEO-PPO-PEO block copolymers in aqueous electrolyte solutions at elevated temperature. The scattering intensity for rods is given by:

$$I_r(q) = \phi_r(\pi R^2 L)(\Delta\rho_r)^2 P_r(q) \quad (6)$$

where L and R are the length and radius of the rods, respectively. $P_r(q)$ is the form factor for rods.[20]

The scattering function for Gaussian chains is given by:

$$I_c(q) = \phi_c N_{agg}\left(\frac{M}{d_2 N_A}\right)(\Delta\rho_c)^2 \; P_c(q) \quad (7)$$

where N_{agg}, M and d_2 are the aggregation number, molecular weight of the individual chains and the bulk density of the polymer, respectively. $P_c(q)$ is the form factor for Gaussian chains,[9] which includes the radius of gyration (R_g). Eqn. (7) can be reduced to the following as q approaches zero:

$$I_c(0) = \lim_{q->0} I_c(q) = \phi_c N_{agg}\left(\frac{M}{d_2 N_A}\right)(\Delta\rho_c)^2 \quad (8)$$

where N_A is Avagadro's number. The scattered intensity for the coils is then: $I_c(q) = I_c(0)P_c(q)$.

The scattering for the large particles (*cf.* $1/q$) with a diffuse interface is modulated by an $\exp(-\sigma^2 q^2)$ term,[19] which generates gradients steeper than q^{-4} for $\sigma > 0$:

$$I_p(q) = \frac{2\pi S_T \Delta\rho^2 \exp(-\sigma^2 q^2)}{q^4} \quad (9)$$

where the total surface area per unit volume is given by $S_T = 4\pi R_p^2 N$ and N is the number density of particles.

The scattering data for all the polymers and copolymer solutions were fitted using the following combinations of eqns. (6), (7) and (9):

$$I(q) = I_c(q) + I_r(q) \quad (10)$$

was used for poly(PEGMa) and poly(NIPAM-*co*-PEGMa) at T: $25 \leq T \leq 32$ °C, whereas

$$I(q) = I_c(q) + I_p(q) \quad (11)$$

was used for poly(NIPAM) at 25 °C and poly(NIPAM-*co*-PEGMa) at 50 °C. Eqn. (7) was used to fit the data measured at 36 and 40 °C. The fitted scattering profiles are shown in Figs. 2 and 3, and the fitted parameters appear in Table 1.

The fits for the homopolymers at 25 °C are reasonable over much of the q range (Fig. 2). The exceptions are for the

Table 1 Fitting parameters for Gaussian coil plus Rods model[a]

System	Temp./°C	$I(0)_{c,T}$/cm^{-1}	R_g/Å	$\psi_{r,T}$[b]/cm^{-4}	R/Å	$2\pi S_T\Delta\rho_p^2$/cm^{-5}	σ/Å	$N_{agg,T}$[c]	$\phi_{c,T}$	$\phi_{r,T}$
Copolymer	25	2.78	75.8	1.70×10^{19}	10.3	—	—	1.0	0.024	0.011
Copolymer	32	6.35	99.6	1.18×10^{19}	11.5	—	—	2.1	0.027	0.008
Copolymer[d]	36	31.6	169	—	—	—	—	8.0	0.035	0
Copolymer[d]	40	33.3	172	—	—	—	—	8.4	0.035	0
Copolymer[e]	50	30.8	257	—	—	2.80×10^{26}	59.6	27[f]	0.01[f]	0
Poly(PEGMa)	25	3.09	77.6	—	14.4	—	—	—	—	—
Poly(NIPAM)[e]	25	2.86	65.8	—	—	4.80×10^{24}	31.7		—	—

[a] Data were obtained using a total volume fraction of polymer of 0.035. Columns 3–8 show fitting parameters obtained from the FISH program. Columns 9–11 are variables calculated using the fitting parameters (see text). [b] $\psi_{r,T} = \phi_{r,T}\Delta\rho_r^2$. [c] Calculated using eqn. (12). [d] Gaussian coil model. [e] Coil plus spherical particle model. [f] Values calculated by assuming that all of the NIPAM segments had collapsed at 50 °C.

lowest q value (0.007 Å^{-1}, log$q$ = −2.15) for each material and the high q range for poly(NIPAM) ($q > 0.079$ Å^{-1}, log$q \geq -1.1$). The source of the error for the fits for the lowest q values is not clear. However, a contribution from intra-particle interference (*i.e.*, $S(q)$ not equal to unity) is possible at this temperature and concentration at $q \leq 0.007$ Å^{-1}. The model used to fit the scattering data for poly(NIPAM) at 25 °C assumes the presence of particles with a diffuse interface. SANS scattering profiles for poly(NIPAM) at room temperature have been previously fitted using only q^{-2} contributions.[21] The present analysis is congruent with recent work[22] that indicated the presence of aggregates in linear poly(NIPAM) solutions. (Porod scattering does *not* appear to be significant for poly(NIPAM-*co*-PEGMa) solutions at temperatures less than the LCST based on the scattering profiles—see below.) The poor fit for the poly(NIPAM) scattering data at high q values is not considered significant from the viewpoint of interpretation. This system was the most weakly scattering of all systems investigated. Consequently, these high q data are most susceptible to error. The fits for the scattering data were dominated by the range of $q \leq$ 0.079 Å^{-1} (*i.e.*, log$q \leq -1.1$).

The scattering profiles and fits obtained for poly(NIPAM-*co*-PEGMa) as a function of temperature are shown in Fig. 3. The fits are very good over the q range ≥0.009 Å (log$q \geq -2.04$) at all temperatures investigated. The tabulated data allow a number of the parameters to be considered in detail (below).

Analysis of the scattering data for the polymers at 25 °C

The values of R_g (Table 1) for poly(NIPAM), poly(PEGMa) and poly(NIPAM-*co*-PEGMa) at 25 °C are in the range 66–78 Å. These values are consistent with Gaussian chains of polymer with a molecular weight of 10^4–10^5 g mol^{-1}. The fit for the poly(PEGMa) included contributions from rods with a value for R of 14 Å. The identity of the species responsible for the rods is of interest. The rods are also evident from the scattering data of the copolymer at 25 °C, but not for those of poly(NIPAM). Scattering from rod-like species became insignificant for the copolymers when the scattering profiles were measured at 36 °C. Thus, the structural feature is a characteristic of PEGMa-rich polymer segments which must also be present within the copolymer at temperatures less than the LCST.

The value for N_{agg} at 25 °C for poly(NIPAM-*co*-PEGMa) can be calculated from first principles using eqn. (8). The value for $\Delta\rho_c$ can be calculated using $\Delta\rho_c = \rho_1 - \rho_2$. The value for ρ_1 (D_2O) of 6.4×10^{10} cm^{-2} is taken from the literature.[10] The value for ρ_2 (poly(NIPAM-*co*-PEGMa)) of 0.8×10^{10} cm^{-2} was calculated using the copolymer composition, density and literature values for the scattering lengths of the atoms present.[10] Hence, the magnitude of $\Delta\rho_c$ is 5.6×10^{10} cm^{-2}. Values for N_{agg} of 0.33 and 0.67 can be calculated using M_n and M_w, (assuming $\phi_c = 0.035$) respectively. These values are consistent with isolated chains with N_{agg} of 1. This is reasonable given the values of R_g (Table 1) and because water is a good solvent for both poly(PEGMa) and poly(NIPAM) at 25 °C (favouring isolated chains).

It is possible to obtain an experimental value for $\Delta\rho_c$ from the fit obtained at 25 °C. Expressions are required that relate ϕ_c at a given temperature ($\phi_{c,T}$) and $\phi_{r,T}$. To obtain such expressions the following assumptions need to be made: (a) only rods and coils are present for poly(NIPAM-*co*-PEGMa) at 25 and 32 °C; and (b) the species present in the rods and coils have similar compositions (*i.e.*, $\Delta\rho_r = \Delta\rho_c = \Delta\rho$). From eqn. (8):

$$\phi_{c,T} = \frac{I_{c,T}(0)}{N_{agg,T}(\Delta\rho)^2}\left(\frac{d_2 N_A}{M}\right) \quad (12)$$

$$\phi_{c,T} + \phi_{r,T} = 0.035 \quad (13)$$

The FISH fitting programme[23] gives values for $\phi_{r,T}\Delta\rho^2$ which are equated to the parameter, $\psi_{r,T}$ for simplification:

$$\psi_{r,T} = \phi_{r,T}\Delta\rho^2 \quad (14)$$

Using the assumption that $N_{agg} = 1$ at 25 °C and using eqns. (12) to (14):

$$\Delta\rho = \left\{\frac{I_{c,25}(0)}{0.035}\left(\frac{d_2 N_A}{M}\right) + \left(\frac{\psi_{r,25}}{0.035}\right)\right\}^{1/2} \quad (15)$$

Using values of $M_n = 44\,600$ g mol^{-1}, $d_2 = 1.0$ g cm^{-3}, $I_{c,25}(0) =$ 2.78 cm^{-1} and $\psi_{r,25} = 1.7\times10^{19}$ cm^{-4}, a value of $\Delta\rho = 3.9\times10^{10}$ cm^{-2} can be calculated. This value is lower than the value of 5.6×10^{10} cm^{-2} calculated above which may be due to a non-uniform density or blockiness within the polymer chains. In addition, exchange of the OH groups of PEGMa to OD would contribute to a decrease in $\Delta\rho$.

Analysis of the scattering data for poly(NIPAM-*co*-PEGMa) at various temperatures

In order to calculate values for the N_{agg} from the data, values for $\phi_{c,T}$ are required at each temperature. The polymer chains responsible for the Gaussian coil scattering are expected to have a solvent–polymer interaction that is largely temperature-independent. Accordingly, the value for $\Delta\rho$ is taken to be constant. This allows the values for $\phi_{r,T}$ (and hence $\phi_{c,T}$) to be calculated using eqn. (14) and the values of $\psi_{r,T}$ obtained from fitting the data at 25 and 32 °C. These values for $\phi_{c,25}$ and $\phi_{c,32}$ appear in Table 1. At 36 and 40 °C only coils are present and hence $\phi_{c,36} = \phi_{c,40} = 0.035$. A unique value for ϕ_c cannot be determined at 50 °C from the data available. However, if it is assumed that only the PEGMa segments remain as coils at 50 °C then a value for $\phi_{c,50}$ of *ca.* 0.01 can be calculated from the vol.% of PEGMa in the copolymer (34 vol.%) (*i.e.*, $0.035\times0.34 \simeq 0.01$).

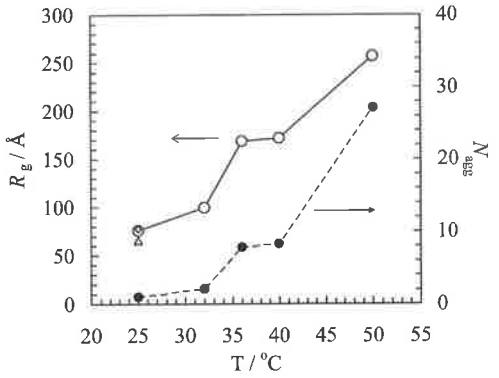

Fig. 7 The effect of temperature on the calculated radii of gyration (○) and aggregation numbers (●) for poly(NIPAM-*co*-PEGMa) as a function of temperature. The radii of gyration for poly(NIPAM) (△) and poly(PEGMa) (◇) at 25 °C are also shown.

Values for N_{agg} can be calculated using eqn. (12) and the values for $\phi_{c,T}$ determined above. The calculated values for N_{agg} appear in Table 1. These values together with the values for R_g are plotted as a function of temperature in Fig. 7. The data support the view that the increase in R_g between 30 and 50 °C is due to aggregation of coils. It appears that further aggregation occurs beyond the primary LCST of 36.5 °C identified from Fig. 1. This is a consequence of the asymmetric copolymer structure which contains NIPAM-poor sequences with local LCST values that are higher than 36.5 °C. The values for N_{agg} at 36 and 50 °C are smaller than those reported for PEO-PPO-PEO copolymers by Mao *et al.*[11] This is in accord with the structural differences of comb and block copolymers. The hydrophilic arms of the former generally offer a greater steric barrier to aggregation.

The scattering data obtained at 50 °C show the emergence of a particulate phase. It is reasonable to assume that the particles are NIPAM-rich. It is possible to estimate the average size of the particles using $S_T = 3\phi_p/R_p$ and the value for $2\pi S_T(\Delta\rho_p)^2$ obtained from the curve fitting (Table 1):

$$R_p = \frac{6\pi\phi_p\left(\Delta\rho_p\right)^2}{\Theta_p} \quad (16)$$

where

$$\Theta_p = 2\pi S_T(\Delta\rho_p)^2 \quad (17)$$

Assuming that $\phi_p = 0.025$ (from $\phi_p + \phi_{c,50} = 0.035$ and $\phi_{c,50} = 0.01$) and that ρ_2 is equal to the experimental value for NIPAM reported by Cosgrove *et al.*[24] of 0.6×10^{10} cm^{-2}, then $\Delta\rho_p = 5.8 \times 10^{10}$ cm^{-2}. A value for R_p of 58 nm can be calculated. Thus, the size of the particles that precipitate at 50 °C can be estimated as *ca.* 120 nm. The minimum q range accessible in our experiments was too high for a maximum to be observed for these particles.

The structural information obtained from the SANS analysis can be used to propose a model for the temperature-induced aggregation of the poly(NIPAM-*co*-PEGMa) copolymer chains in water as a function of temperature. At 25 °C the copolymer chains exist as individual coils with a R_g of *ca.* 8 nm. When the temperature exceeds 36 °C aggregation of the coils occurs to produce copolymer micelles with an aggregate R_g of 17 nm. These aggregates contain *ca.* 8 copolymer coils. The aggregates are held together by attractive interactions between NIPAM-rich segments which become hydrophobic due to the temperature being the same as the local LCST. At 50 °C growth of NIPAM-rich particle phase with a diffuse shell occurs. Gaussian coils that are rich in PEGMa are presumably connected to these particles *via* the diffuse shell. Particle precipitation causes further aggregation of the coils and the R_g increases to 26 nm.

Conclusions

This work has investigated the temperature-induced conformational changes of a temperature-responsive poly(NIPAM-*co*-PEGMa) in solution. The copolymer chains contain three structural features over the temperature range 25 to 50 °C: rods, coils and particles. At room temperature the chains exist as unimers and contain coils and rods. At 36 and 40 °C only coils are evident and the chains aggregate to from copolymer micelles with an aggregation number of *ca.* 8. The temperature-induced aggregation is accompanied by an increase in R_g. At 50 °C, particles which are rich in NIPAM are formed with an estimated diameter of 120 nm. The aggregation number of the PEGMa-rich chains that remain as coils increases to *ca.* 27. It is interesting to note that the form of the scattering profiles and changes that occur with increase in temperature (Fig. 2) are similar to those observed by Choi *et al.*[25] in their study of arborescent polystyrene graft polymers in *d*-cyclohexane solutions as a function of generation and temperature. They observed an increase in R_g with increasing generation in worse than θ-solvency conditions. In their case the increase in R_g was due to increasing molecular weight through successive chemical grafting. In this work the increase in R_g is attributed to an increase in the effective molecular weight through temperature-induced aggregation of coils.

The results of this work have important implications for the mechanism of temperature-induced gelation observed for emulsions stabilised by poly(NIPAM-*co*-PEGMa) as well as for concentrated responsive polymer solutions.[1,5,6] This process relies upon the formation of hydrophobic junctions that act as physical crosslinks. The strength, number density and functionality (*i.e.*, number of effective chains per junction) of these junctions determines the gel strength. At temperatures that are similar to the LCST (*e.g.*, 36 °C) and significantly above it (50 °C) the number of cross-linking junctions probably decreases with increasing temperature. However, the number of effective cross-links per junction must increase as the particulate phase emerges. This is because neighbouring junctions of NIPAM-rich segments aggregate further with increasing temperatures to form particles and these will be interconnected *via* the PEGMa-rich coils. The particulate phase would then be expected to increase the elastic modulus for a network as not only will the total cross-link density have increased, but the strength of each crosslink will have increased. These structural changes explain the increase in the elastic modulus with increasing temperature observed in related work for emulsions stabilised by poly(NIPAM-*co*-PEGMa) and concentrated poly(NIPAM-*co*-PEGMa) solutions.[5,6]

Acknowledgements

The authors acknowledge financial support for the work from ANSTO and AINSE. Access to the FISH computer program is also acknowledged. We would also like to thank Emma Daly for providing assistance during the neutron experiment.

References

1 F. L'Alloret, D. Hourdet and R. Audebert, *Colloid Polym. Sci.*, 1995, **273**, 1163.
2 P. Perrin and F. Lafuma, *J. Colloid Interface Sci.*, 1998, **197**, 317.
3 H. G. Schild and D. A. Tirrell, *J. Phys. Chem.*, 1990, **94**, 4352.
4 J. Virtanen and H. Tenhu, *Macromolecules*, 2000, **33**, 5970.
5 B. R. Saunders and B. Vincent, in *Encyclopedia of Surface and Colloid Science*, ed. A. Hubbard, Marcel Dekker, New York, 2002, p. 4544.
6 B. R. Saunders and B. Vincent, *Adv. Colloid Interface Sci.*, 1999, **80**, 1.

7 A. Koh and B. R. Saunders, *Chem. Commun.*, 2000, 2461.
8 A. Koh, C. Prestidge, I. Ametov and B. R. Saunders, *Phys. Chem. Chem. Phys.*, 2002, **4**, 96.
9 J. S. Higgins and H. C. Benoit, *Polymers and Neutron Scattering*, Clarendon Press, Oxford, 1996.
10 S. M. King, in *Experimental Methods in Polymer Characterization*, ed. R. A. D. J. V. Pethrick, Wiley, 1999.
11 G. Mao, S. Sukumaran, G. Beaucage, M.-L. Saboungi and P. Thiyagarajan, *Macromolecules*, 2001, **34**, 552.
12 C. Washington and S. M. King, *Langmuir*, 1997, **13**, 4545.
13 N. Hatto, T. Cosgrove and M. J. Snowden, *Polymer*, 2000, **41**, 7133.
14 W. Xue, S. Champ and M. B. Huglin, *Polymer*, 2000, **41**, 7575.
15 F. M. Winnik, *Macromolecules*, 1990, **23**, 233.
16 L. Auvray and J. P. Cotton, *Macromolecules*, 1987, **20**, 202.
17 M. Tirrell, *Interactions of surfactants with polymers and proteins*, ed. E. D. Goddard and K. P. Ananthapadmanabhan, 1993, ch. 3.
18 S. Seelenmeyer, I. Deike, S. Rosenfeldt, C. Norhausen, N. Dingenouts, M. Ballauff, T. Narayanan and P. Lindner, *J. Chem. Phys.*, 2001, **114**, 10471.
19 T. J. Su, J. R. Lu, Z. F. Cui, R. K. Thomas and R. K. Heenan, *Langmuir*, 1998, **14**, 5517.
20 R. Heenan, *The FISH reference manual*, ISIS Facility, Rutherford Appleton Laboratory, Chilton, Didcot, (Revision 20/11/2001), p. 28.
21 M. Shibayama, T. Tanaka and J. Han, *J. Chem. Phys.*, 1992, **97**, 6829.
22 F. Ganachaud, M. J. Monteiro, R. G. Gilbert, M.-A. Dourges, S. H. Thang and E. Rizzardo, *Macromolecules*, 2000, **33**, 6738.
23 R. Heenan, *The FISH fitting program*, ISIS Facility, Rutherford Appleton Laboratory, Chilton, Didcot, 2002.
24 S. J. Mears, Y. Deng, T. Cosgrove and R. Pelton, *Langmuir*, 1997, **13**, 1901.
25 S. Choi, R. M. Briber, B. J. Bauer, A. Topp, M. Gauthier and L. Tichagawa, *Macromolecules*, 1999, **32**, 7879.